16 April 2010 | $10

Science

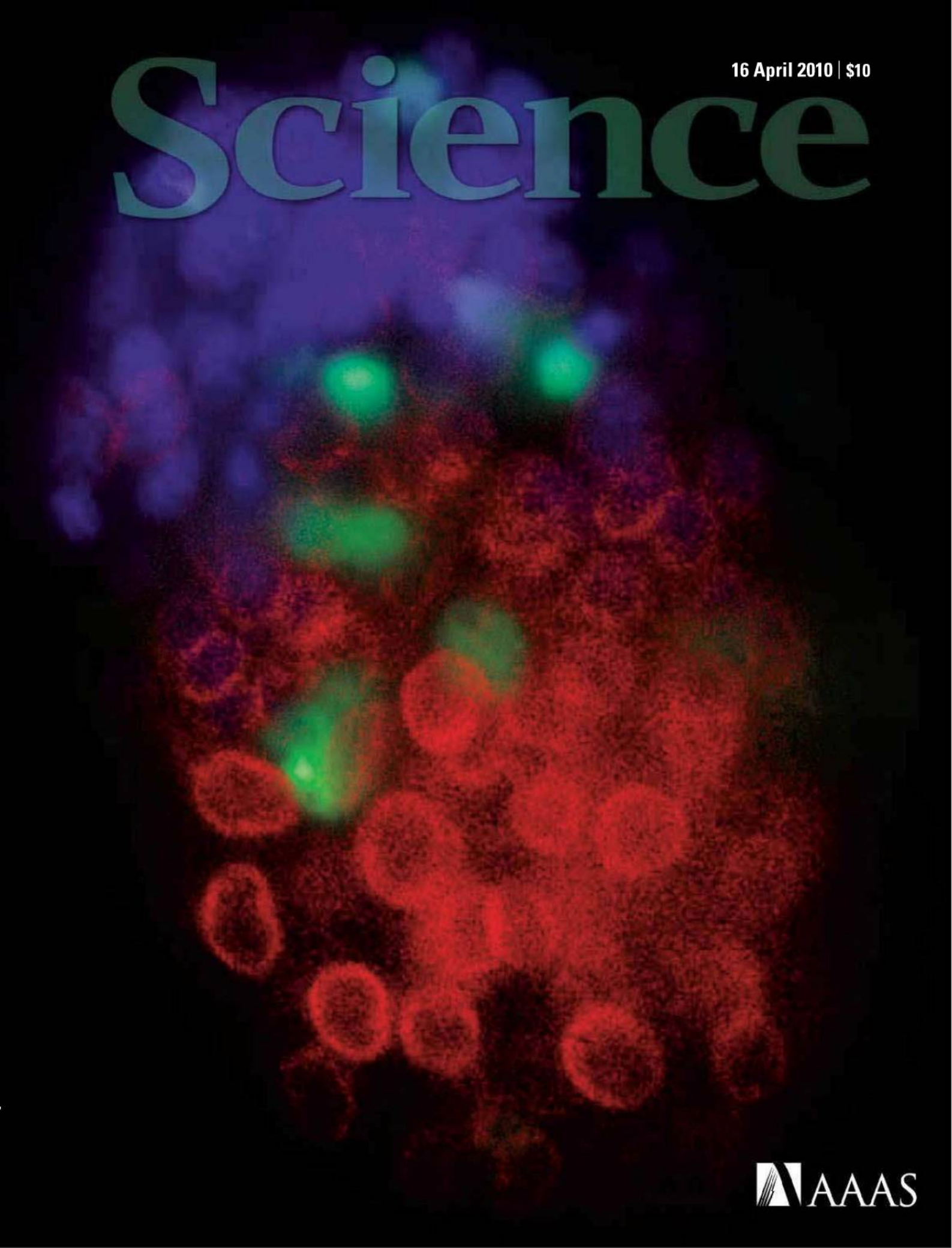

AAAS

Submission deadline August 1

Your name here.

The GE & Science Prize for Young Life Scientists. Because brilliant ideas build better realities.

Imagine standing on the podium at the Grand Hotel in Stockholm, making your acceptance speech for the GE & Science Prize for Young Life Scientists. Imagine having your essay read by your peers around the world. Imagine discussing your work in a seminar with other prize winners and Nobel Laureates. Imagine what you could do with the $25,000 prize money. Now stop imagining. If you were awarded your Ph.D. in molecular biology in 2009, then submit your 1000-word essay by August 1, and you can make it reality.

Want to build a better reality? Go to www.gescienceprize.org

GE & Science
Prize for Young
Life Scientists

imagination at work

Science
AAAS

* For the purpose of this prize, molecular biology is defined as "that part of biology which attempts to interpret biological events in terms of the physico-chemical properties of molecules in a cell".

(McGraw-Hill Dictionary of Scientific and Technical Terms, 4th Edition).

GE Healthcare Bio-Sciences AB,
Björkgatan 30, 751 84 Uppsala, Sweden.
© 2010 General Electric Company
– All rights reserved.

28-9402-06AB

SIGMA-ALDRICH®

Bioselect.

Now offering over 30,000 world-class antibodies, including exclusive Prestige Antibodies® powered by Atlas Antibodies.

Welcome to an antibody portfolio unmatched in scope and quality. With a continuously growing selection, our objective is to supply a highly validated antibody that you can trust to every known protein. Our library includes over 8,300 Prestige Antibodies, each with 700 immunohistochemistry, immunofluorescence and Western blot images available online. Sigma Life Science ensures you'll always have the highest caliber tools to advance your research.

wherebiobegins.com/biomolecules

biomolecules

Prestige Antibodies® Powered by ATLAS

Prestige Antibodies powered by Atlas Antibodies is a registered trademark of Sigma-Aldrich and Sigma-Aldrich Biotechnolgy, LP.


SIGMA Life Science
Where bio begins™

Submission deadline August 1

Your name here.

The GE & Science Prize for Young Life Scientists. Because brilliant ideas build better realities.

Imagine standing on the podium at the Grand Hotel in Stockholm, making your acceptance speech for the GE & Science Prize for Young Life Scientists. Imagine having your essay read by your peers around the world. Imagine discussing your work in a seminar with other prize winners and Nobel Laureates. Imagine what you could do with the $25,000 prize money. Now stop imagining. If you were awarded your Ph.D. in molecular biology in 2009, then submit your 1000-word essay by August 1, and you can make it reality.

Want to build a better reality? Go to www.gescienceprize.org

GE & Science
Prize for Young
Life Scientists

imagination at work

Science
AAAS

* For the purpose of this prize, molecular biology is defined as "that part of biology which attempts to interpret biological events in terms of the physico-chemical properties of molecules in a cell".

(McGraw-Hill Dictionary of Scientific and Technical Terms, 4th Edition).

GE Healthcare Bio-Sciences AB,
Björkgatan 30, 751 84 Uppsala, Sweden.
© 2010 General Electric Company
– All rights reserved.

28-9402-06AB

GE Healthcare
Life Sciences

See more
See beyond

For years, scientists have relied on ImageQuant™ and Typhoon™. Now we can offer a new standard of performance with the Typhoon FLA 9000, Typhoon FLA 7000, ImageQuant 4000, and ImageQuant 4000 mini. Covering the full spectrum of imaging methods including quantitative Westerns, UV, IR, visible fluorescence, phosphorimaging, and 2-D DIGE, the new imagers provide exceptional sensitivity, speed, and versatility.

At GE Healthcare, our focus is on helping scientists achieve more, faster. However simple or complex your imaging needs, you can depend on us for quantitative imaging that's quantifiably better.

To find out more about our new range of imagers, contact us today.
Visit **www.gelifesciences.com/imaging**

I ÄKTA I Amersham I Biacore I IN Cell Analyzer I Whatman I GE Service I

imagination at work

ÄKTA, Amersham, Biacore, ImageQuant, Typhoon and Whatman are trademarks of GE Healthcare companies.
© 2010 General Electric Company – All rights reserved.
GE Healthcare Bio-Sciences AB, Björkgatan 30, 751 84 Uppsala, Sweden
GE01-10. First published January 2010.

EDITORIAL

NEWS OF THE WEEK

NEWS FOCUS

LETTERS

BOOKS *ET AL.*

POLICY FORUM

PERSPECTIVES

CONTENTS continued >>

page 301

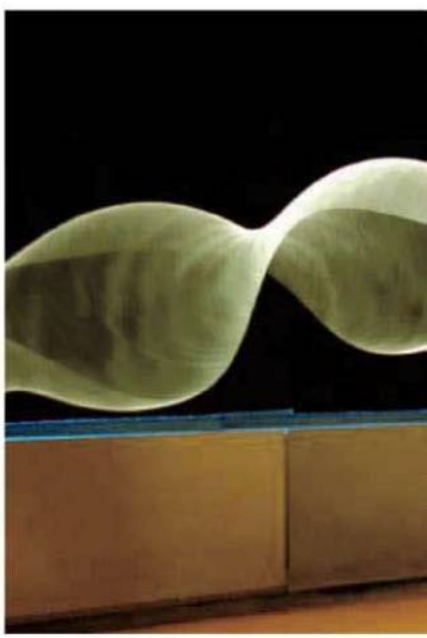

page 311

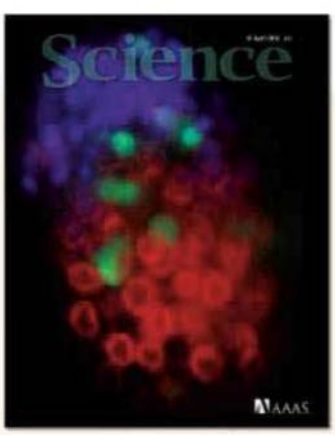

COVER

Fluorescence microscopy image showing fragmentation of chromosomal DNA (green) during programmed cell death or apoptosis in a *Caenorhabditis elegans* embryo. Chromosomes are stained blue and nuclear envelopes red. During apoptosis, the ribonuclease Dicer, known for its role in gene silencing, is converted to a deoxyribonuclease and initiates this DNA fragmentation process. See page 327.

Image: Jay Parrish/University of Colorado

DEPARTMENTS

Choose QIAGEN for detection

Detection platforms, assays, and analysis software by QIAGEN

Use QIAGEN® solutions from sample to result, and benefit from sensitive and reliable detection systems:

- **Quantitative, real-time PCR detection**
- **Automated analysis of DNA fragments and RNA**
- **Pyrosequencing® sequence-based DNA detection and quantification**
- **Optimized, ready-to-use assays and reagents**

Making improvements in life possible — www.qiagen.com

QIAGEN®

Sample & Assay Technologies

AUTODetect01105 1WW

Qs & AAAs

www.sciencedigital.org/subscribe

For just US$99, you can join AAAS TODAY and start receiving *Science* Digital Edition immediately!

Qs & AAAs

www.sciencedigital.org/subscribe

For just US$99, you can join AAAS TODAY and start receiving *Science* Digital Edition immediately!

REVIEW

RESEARCH ARTICLE

REPORTS

CONTENTS continued >>

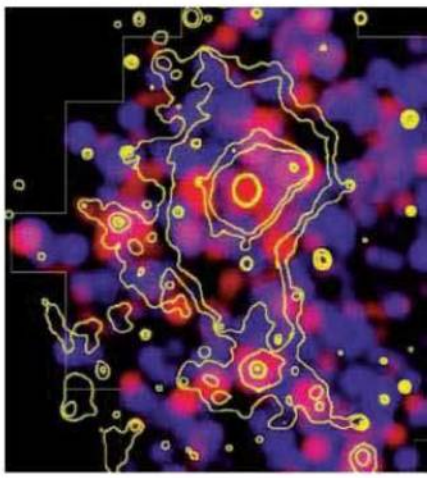

page 334

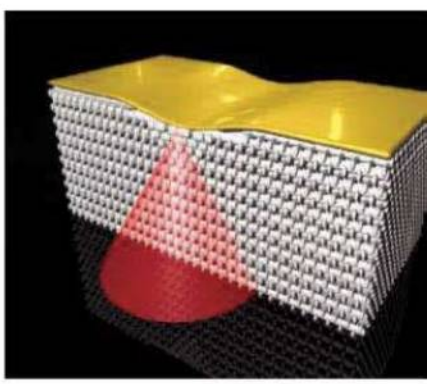

page 337

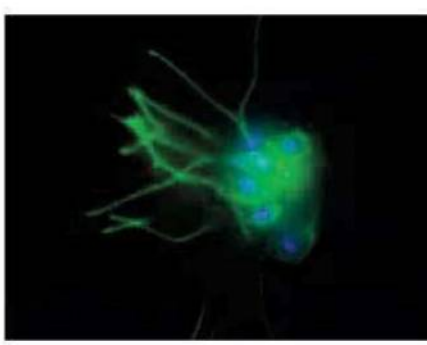

page 351

CREDIT (BOTTOM): JAMES UMEN AND MICHAEL OBERHOLZER/THE SALK INSTITUTE FOR BIOLOGICAL STUDIES

WITHOUT KNOWLEDGE, IT'S JUST DATA

Whether you are working on a dissertation, publishing journal articles or books, collaborating with colleagues or exploring a new research direction, Thomson Reuters can help with integrated information solutions that support your research goals.

- *EndNote*® locates full text for your references, includes *EndNote Web* for sharing your library on the Web and creates instant bibliographies in over 3,700 journal styles.
- *Reference Manager*® *12* features Microsoft® Word 2007 support and much more.
- *ResearcherID*, a global scholarly author community, enables you to identify your published works uniquely, view citation metrics and find collaborators.
- *Web of Knowledge*℠ delivers quality content such as the *Web of Science*® that provides you with crucial research data back to the 1900's as well as a unique look at citation impact.

Visit booth #325 at Experimental Biology 2010 and continue your quest for knowledge.
You may even win your own bibliographic software program.

thomsonreuters.com/science

THOMSON REUTERS™

SCIENCEONLINE

SCIENCEXPRESS
www.sciencexpress.org

pH Sensing by Intracellular *Salmonella* Induces Effector Translocation
X.-J. Yu et al.

Intravacuolar *Salmonella* senses host cytosolic pH, resulting in degradation of a regulatory complex and effector translocation.
10.1126/science.1189000

Genome-Wide Evolutionary Analysis of Eukaryotic DNA Methylation
A. Zemach et al.

Analysis of DNA methylation in 17 species suggests a path for the evolution of this epigenetic mark.
10.1126/science.1186366

Structural Insights into the Assembly and Function of the SAGA Deubiquitinating Module
N. L. Samara et al.

Structures give insight into how a regulator of eukaryotic gene expression achieves one of its chromatin-modifying functions.
10.1126/science.1190049

The Equation of State of a Low-Temperature Fermi Gas with Tunable Interactions
N. Navon et al.

A Fermi gas is characterized along the crossover regime between its weak and strongly interacting limits.
10.1126/science.1187582

Lopsided Growth of Earth's Inner Core
M. Monnereau et al.

The asymmetry of the inner core is explained by iron crystallization on one side and melting on the other.
10.1126/science.1186212

Regional Variation of Inner-Core Anisotropy from Seismic Normal-Mode Observations
A. Deuss et al.

Seismic data from the inner core reveal that anisotropic regions overlap with gravitational anomalies.
10.1126/science.1188596

TECHNICALCOMMENTS

Comment on "Modafinil Shifts Human Locus Coeruleus to Low-Tonic, High-Phasic Activity During Functional MRI" and "Homeostatic Sleep Pressure and Responses to Sustained Attention in the Suprachiasmatic Area"
S. V. Astafiev et al.

full text at www.sciencemag.org/cgi/content/full/328/5976/309-a

Response to Comment on "Modafinil Shifts Human Locus Coeruleus to Low-Tonic, High-Phasic Activity During Functional MRI"
M. J. Minzenberg et al.

full text at www.sciencemag.org/cgi/content/full/328/5976/309-b

Response to Comment on "Homeostatic Sleep Pressure and Responses to Sustained Attention in the Suprachiasmatic Area"
C. Schmidt et al.

full text at www.sciencemag.org/cgi/content/full/328/5976/309-c

SCIENCENOW
www.sciencenow.org
Highlights From Our Daily News Coverage

Earth-Like Planets May Abound in the Milky Way
Dying stars reveal the chemical signatures of rocky worlds.

Cholesterol Genetically Linked to Eye Disease
Scientists uncover connection between age-related macular degeneration and a gene that regulates good cholesterol.

When Social Fear Disappears, So Does Racism
Children with genetic disorder shed light on the roots of racial prejudice.

SCIENCESIGNALING
www.sciencesignaling.org
The Signal Transduction Knowledge Environment

RESEARCH ARTICLE: Identification of the *miR-106b~25* microRNA Cluster as a Proto-Oncogenic *PTEN*-Targeting Intron That Cooperates with its Host Gene *MCM7* in Transformation
L. Poliseno et al.

A microRNA network regulates the tumor suppressor PTEN in prostate cancer.

PERSPECTIVE: Not Lost in Space—Trafficking in the Hedgehog Signaling Pathway
L. Milenkovic and M. P. Scott

Protein kinase A orchestrates Hedgehog signaling from the base of the primary cilium.

SCIENCECAREERS
www.sciencecareers.org/career_magazine
Free Career Resources for Scientists

Conventions of Scientific Authorship
V. Venkatraman

The rules and conventions of authorship are ever-changing and rarely clear.

Adding Humanitarian Value to Mathematics
E. Pain

Begoña Vitoriano Villanueva uses her math skills to help aid organizations respond to disasters.

Tooling Up: Clear and Succinct Rules the Day
D. Jensen

The job search is immeasurably aided by good, transparent writing.

SCIENCEINSIDER
news.sciencemag.org/scienceinsider
Science Policy News and Analysis

SCIENCETRANSLATIONAL MEDICINE
www.sciencetranslationalmedicine.org
Integrating Medicine and Science

PERSPECTIVE: Optimal Control of Blood Glucose—The Diabetic Patient or the Machine?
L. Brown and E. R. Edelman

Diabetic patients may benefit from a device that uses a computer algorithm to deliver proper amounts of insulin and glucagon.

PERSPECTIVE: Challenges in Using Stem Cells for Cardiac Repair
C. L. Mummery et al.

Stem cell–derived cardiomyocytes offer promise for treating damage caused by heart attacks.

RESEARCH: A Bi-Hormonal Closed-Loop Artificial Pancreas for Type 1 Diabetes
F. H. El-Khatib et al.

An algorithm continuously delivers appropriate insulin and glucagon doses to diabetic patients, maintaining their blood glucose at normal values, even after high-carbohydrate meals.

REVIEW: Exploring New Routes for Neuroprotective Drug Development in Traumatic Brain Injury
T. Janowitz and D. K. Menon

The methods and devices used in the clinical management of neurological patients can provide data to facilitate progress in treating brain trauma.

SCIENCEPODCAST
www.sciencemag.org/multimedia/podcast
Free Weekly Show

Download the 16 April *Science* Podcast to hear about how the brain pursues concurrent goals, testing and treatment for rare genetic diseases, telescopes in rural Senegal, and more.

SCIENCEONLINE FEATURE
www.sciencemag.org/sciext/gonzoscientist/

THE GONZO SCIENTIST
The Gonzo Scientist travels to Senegal with an astrophysicist to deliver the universe to remote villagers.

SCIENCE (ISSN 0036-8075) is published weekly on Friday, except the last week in December, by the American Association for the Advancement of Science, 1200 New York Avenue, NW, Washington, DC 20005. Periodicals Mail postage (publication No. 484460) paid at Washington, DC, and additional mailing offices. Copyright © 2010 by the American Association for the Advancement of Science. The title SCIENCE is a registered trademark of the AAAS. Domestic individual membership and subscription (51 issues): $146 ($74 allocated to subscription). Domestic institutional subscription (51 issues): $910; Foreign postage extra: Mexico, Caribbean (surface mail) $55; other countries (air assist delivery) $85. First class, airmail, student, and emeritus rates on request. Canadian rates with GST available upon request, GST #1254 88122. Publications Mail Agreement Number 1069624. **Printed in the U.S.A.**

Change of address: Allow 4 weeks, giving old and new addresses and 8-digit account number. **Postmaster:** Send change of address to AAAS, P.O. Box 96178, Washington, DC 20090–6178. **Single-copy sales:** $10.00 current issue, $15.00 back issue prepaid includes surface postage; bulk rates on request. **Authorization to photocopy** material for internal or personal use under circumstances not falling within the fair use provisions of the Copyright Act is granted by AAAS to libraries and other users registered with the Copyright Clearance Center (CCC) Transactional Reporting Service, provided that $20.00 per article is paid directly to CCC, 222 Rosewood Drive, Danvers, MA 01923. The identification code for *Science* is 0036-8075. *Science* is indexed in the *Reader's Guide to Periodical Literature* and in several specialized indexes.

AAAS
ADVANCING SCIENCE, SERVING SOCIETY

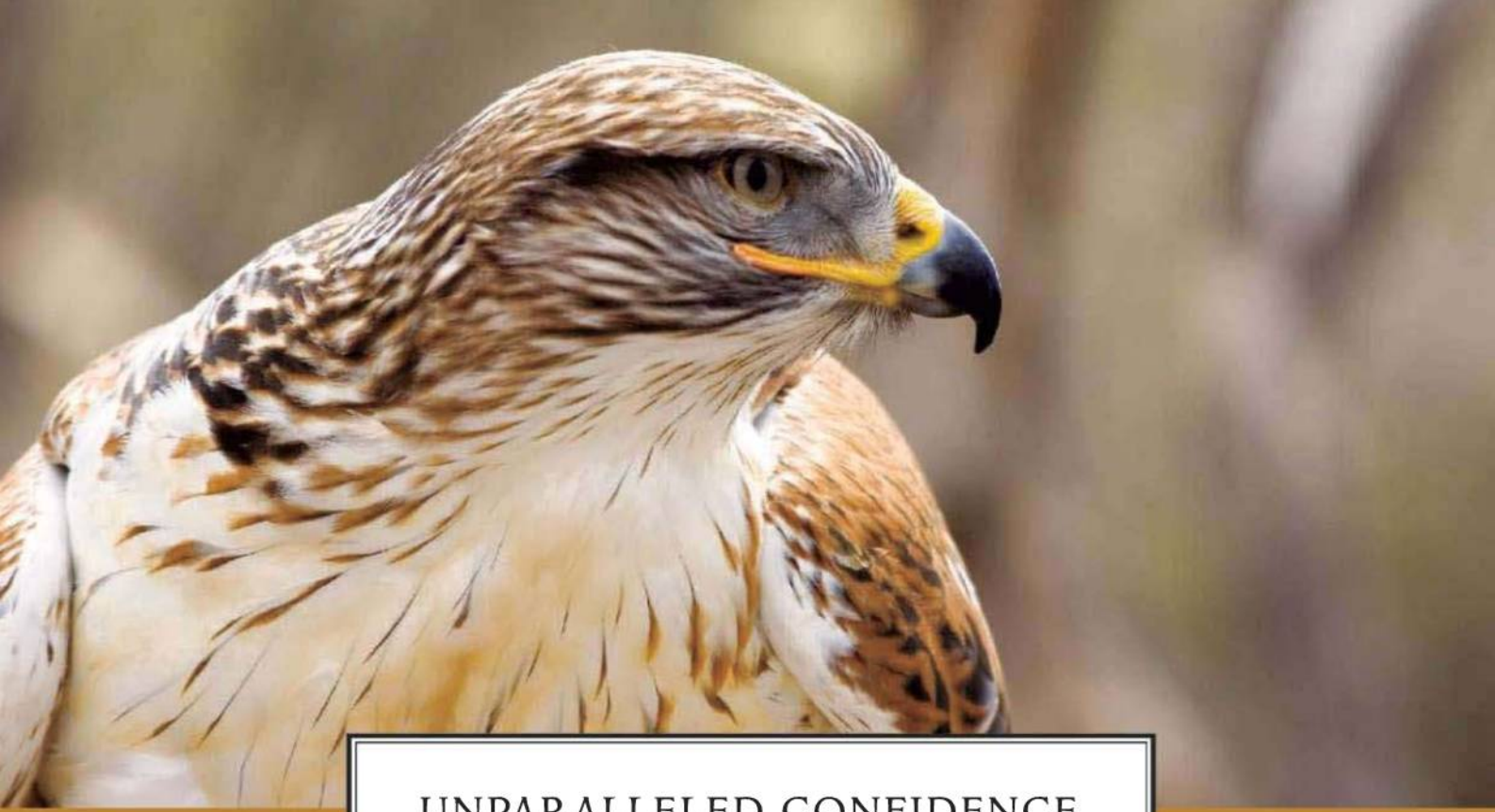

UNPARALLELED CONFIDENCE

PCR Reagents

There are already enough variables in PCR, don't let polymerase performance be one of them. Choose from one of the largest selections of polymerases for PCR applications from the leader in enzyme technology and bring unparalleled confidence to your experiments.

Not all PCR polymerases are created equal

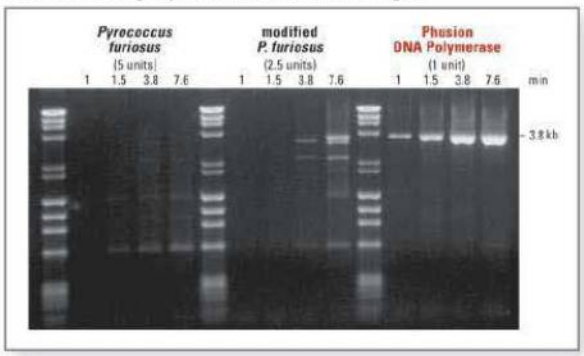

Amplification of a 3.8 kb fragment from human beta globin gene clearly illustrates the extreme speed and robustness offered by using Phusion DNA Polymerase.

Phusion is a registered tradenark of Finnzymes Oy.

NEB has the polymerase for your application:

- **Routine**
- **Hot start**
- **Fast**
- **High-fidelity**
- **Long or difficult templates**
- **High throughput**
- **Extraction-free PCR**
- **Master Mixes**

Visit confidentPCR.com to learn more, and to find PCR-related special offers.

CELEBRATING 35 YEARS

NEW ENGLAND BioLabs Inc.
enabling technologies in the life sciences

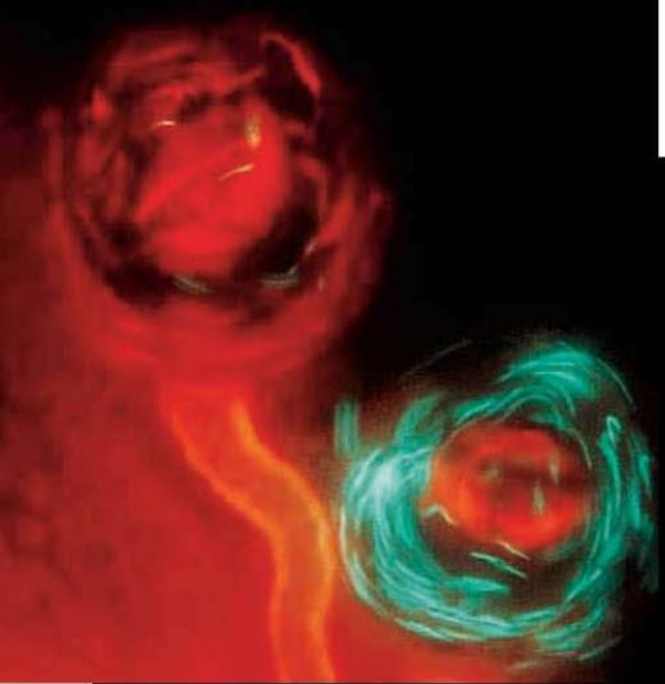

<< Battle of the Sperm

In insects, sperm from multiple matings are stored and retained, and are thought to compete for ova within a female's reproductive tract. **Manier *et al.*** (p. 354, published online 18 March) visualized sperm from fruit flies transgenically tagged with green or red fluorescent protein within the reproductive tracts of female flies. Sperm showed more mobility within the female storage organs than expected, with those from the most recent copulation displacing sperm from previous males; however, sperm viability remained consistent over long-term storage and each male's sperm was equally competitive in fertilizing the female's eggs.

Eat Less, Live Long

Studies in several model organisms have shown that dietary restriction without malnutrition, or manipulation of nutrient-sensing pathways through mutations or drugs, can increase life span and reduce age-related disease. **Fontana *et al.*** (p. 321) review the ways in which nutrient-sensing pathways are central to aging. Studies of yeast, worms, rodents, and primates show that these pathways are conserved during evolution. Although data on the effects of dietary restriction in primates are very limited, in humans, the protective effects of dietary restriction against cancer, cardiovascular disease, and diabetes must be judged against potentially negative long-term effects. More work is needed to determine whether dietary restriction and the modulation of anti-aging pathways through drugs can extend life span and reduce pathologies in humans.

Deadly Diced DNA

Mammalian cells undergoing programmed cell death, or apoptosis, destroy DNA with the deoxyribonuclease known as DFF40. Cells of the worm *Caenorhabditis elegans* also undergo cell death but they do so without a DFF40 enzyme. **Nakagawa *et al.*** (p. 327; see the Perspective by **Liu and Paroo**; see the cover) searched for other nucleases that might be involved in worm apoptosis by systematically depleting nucleases with interfering RNA. They found the ribonuclease Dicer, known for its role in sequence-specific silencing of gene expression, was cleaved by a protease that changed Dicer's catalytic activity. The remaining C-terminal fragment switched from being a ribonuclease to a deoxyribonuclease. Thus, caspase activation leads to DNA degradation in the worm as well.

Bulking Up Water Oxidation

Storing solar energy by water oxidation, in a process akin to photosynthesis, is a promising approach for building a renewable energy infrastructure. Unfortunately, many of the most active synthetic catalysts for this process fall prey to degradation by the generated oxygen. **Yin *et al.*** (p. 342, published online 11 March; see the Perspective by **Hurst**) used bulky polyoxometalate ligands to protect a catalytic cobalt center from this fate. The full complex was easily prepared by mixing proper ratios of inexpensive tungsten, cobalt, and phosphate salts in boiling water. After isolating and redissolving the catalyst in slightly basic aqueous solution, rapid oxygen generation was observed with a ruthenium-based oxidant.

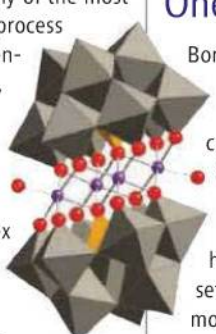

Cluster Within Virgo

Globular clusters are gravitationally bound systems within galaxies containing hundreds of thousands of stars. Using data from the Sloan Digital Sky Survey of the thousands of galaxies that constitute the Virgo cluster, **Lee *et al.*** (p. 334, published online 11 March) fulfilled a prediction made almost 60 years ago and found globular clusters outside galaxies. In Virgo the clusters are found far from the center and are concentrated in several substructures much larger than galaxies. Possibly they were stripped off from low-mass dwarf galaxies, and potentially trace the dark matter distribution within the Virgo cluster.

Aromatic Lead

The bond stabilization, or aromaticity, observed in cyclic carbon molecules, such as benzene, relies on delocalization of electrons around the ring. Although electron distributions in heavier elements can complicate this arrangement, **Saito *et al.*** (p. 339) show that even lead, one of the heaviest metals, is able to participate in an otherwise carbon-based aromatic network. In an analog of the well-studied cyclopentadienyl anion, one carbon atom was replaced with lead, and the framework stabilized by appending phenyl groups to the other four carbons. Crystallography revealed a planar structure, which together with spectroscopic data and theoretical calculations confirmed the aromatic character of the product.

One B, One O

Boron has a tendency to share electrons with multiple different atoms, hence exhibiting a rich cluster chemistry, in contrast to the more traditional two-center, two-electron bonds prevailing in the compounds of most other light elements. **Braunschweig *et al.*** (p. 345) have coaxed boron into a more confined setting and made a boron analog of carbon monoxide as a triply bonded BO anion that was stabilized by coordination to a platinum center. The product formed easily in room temperature solution from a precursor substituted with a silyl group on the oxygen and a bromide on the boron and exhibited surprising stability toward heating and photolysis. The BO anion is a fundamental binary material, isoelectronic with CO, CN-, and NO+, which have been the key binary ligands in organometallic and coordination chemistry for more than 50 years.

Continued on page 285

CREDITS (TOP TO BOTTOM): MOLLIE MANIER AND SCOTT PITNICK; YIN *ET AL.*

Science Careers in Translation

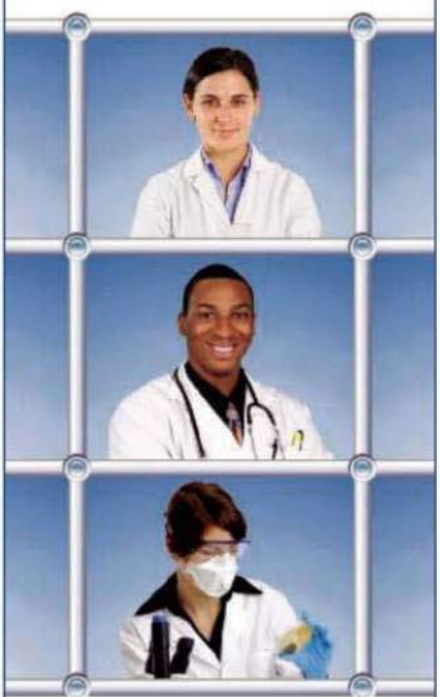

Want to build relationships with clinical or basic scientists? Get advice on the best way to conduct a clinical and translational science career? There's no better place to explore these ideas, and to build new scientific relationships, than CTSciNet, the new online community from *Science*, *Science* Careers, and AAAS made possible by the Burroughs Wellcome Fund.

There's no charge for joining, and you'll enjoy access to:

- Practical and specific information on navigating a career in clinical or translational research
- Opportunities to connect with other scientists including peers, mentors, and mentees
- Access to the resources of the world's leading multidisciplinary professional society and those of our partner organizations

Connect with CTSciNet now at:
Community.ScienceCareers.org/CTSciNet

CTSciNet
Clinical and Translational Science Network

Presented by

AAAS

Science | Science Careers

Continued from page 283

Less Old Martian Meteorite

The oldest Martian meteorite known, ALH84001, was thought to be a remnant of primordial martian crust formed during solidification of an early magma ocean. Using isotope data, **Lapen *et al.*** (p. 347) revised the crystallization age of this meteorite from 4.51 billion years to 4.09 billion years ago, meaning that this rock cannot be a fragment of primordial crust that escaped the period of intense bombardment that occurred between 4.25 and 4.10 billion years ago. The revised age also suggests that magmatism was ongoing in Mars for a large part of its history and that ALH84001 was actually formed during the heavy bombardment period, just before the martian core dynamo stopped and the planetary magnetic field was lost.

Revealing *Volvox*

Female and male gametes of the green alga, ***Volvox***, significantly differ in size. Those of *Chlamydomonas*, another green algae from a lineage that separated from *Volvox* some 200 million years ago, are the same size. We know sex in *Chlamydomonas* is governed by a sex-determining locus called *MT*. In a detailed comparison of the *MT* loci of *Volvox* and *Chlamydomonas*, **Ferris *et al.*** (p. 351) found that although *MT* has retained some similarity in gene order, its composition has greatly changed between the two species. In *Volvox*, new genes have been coopted into this locus and show sex-specific expression.

Swine Flu Neutralized

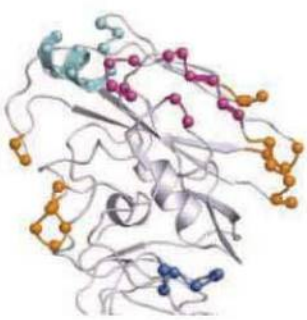

The 2009 H1N1 flu virus had an unusually low infection rate in elderly people. An antibody isolated from survivors of the 1918 flu pandemic was recently shown to cross-neutralize 2009 H1N1 viruses. **Xu *et al.*** (p. 357, published online 25 March) report crystal structures of the virus envelope protein, hemagglutinin (HA) from 2009 H1N1 and of 1918 H1 HA in complex with a neutralizing antibody that cross-reacts with both pandemic viruses. These studies reveal an epitope that is conserved in the pandemic viruses, but divergent in other known H1 HAs, from the 1930s to the present. This antigenic similarity explains the age-related immunity to the 2009 H1N1 influenza.

Domain Swaps to Phenotype Shifts

For natural selection there must be mechanisms that create phenotypic diversity, presumably from relatively simple molecular changes in an organism. **Peisajovich *et al.*** (p. 368) tested the extent to which changes in phenotype can occur by systematic swapping of protein domains in the components of the biochemical signaling pathway that controls mating in yeast. Such changes decreased or increased responsiveness to yeast mating pheromone, and some translated into changes in mating efficiency. The authors propose that shuffling of modular protein domains may be an important source of phenotypic diversity in evolution and may also be a useful strategy for the engineering of biological systems.

Yin-Yang T Cell Signaling

Immune responses are kept in check by $CD4^+$ regulatory T cells (T_{reg}) that suppress other immune cells, including $CD4^+$ effector T cells (T_{eff}). T_{reg} and T_{eff} cells have many signaling components in common, yet triggering through their T cell receptors (TCRs) leads to very different outcomes. **Zanin-Zhorov *et al.*** (p. 372, published online 25 March) compared the recruitment of signaling molecules to the immunological synapse after TCR triggering in T_{reg} and T_{eff} cells. Although T_{reg} cells do form synapses, signaling molecules that promote T_{eff} activation, such as protein kinase C-θ (PKC-θ), were not recruited. Inhibition or depletion of PKC-θ in T_{reg} cells led to suppressive activity against T_{eff} cells, whereas costimulation enhanced PKC-θ recruitment and less suppression. Together, this suggests that PKC-θ is inflammatory in both T_{reg} and T_{eff} cells; however, by excluding it from the synapse, T_{reg} cells are able to maintain suppression in the face of TCR signaling.

CREDIT: XU *ET AL.*

Philip Daro is the director of the Strategic Education Research Partnership, San Francisco, CA. E-mail: pdaro@berkeley.edu

William McCallum is head of the Department of Mathematics, University of Arizona, Tucson, AZ.

Jason Zimba is a professor in the Departments of Physics and Mathematics, Bennington College, Bennington, VT.

Common U.S. Math Standards

THE UNITED STATES HAS NEVER HAD NATIONAL STANDARDS OR CURRICULA FOR MATHEMATICS. Instead, each state decides, for example, what version of high-school algebra should be taught and how to assess whether students have learned it. In March 2010, the National Governors Association and the Council of Chief State School Officers released Common Core State Standards (CCSS) for English language arts and mathematics (www.corestandards.org). The goal is to have all states adopt these as their standards, making more uniform the knowledge and skills expectations for students in preparation for success in college and careers.

The mathematics standards were drafted by teachers, mathematicians, statisticians, mathematics educators, and cognitive scientists, with input from many educational organizations.* Reconciliation of the perspectives of this wide spectrum of participants has relied on research evidence and the curricula of countries that perform better than the United States in mathematics. Research studies such as the Trends in International Mathematics and Science Study (TIMSS) have shown that U.S. mathematics performance is compromised by a lack of focus and coherence in the curriculum. For example, Hong Kong students outscore U.S. students on the grade 4 TIMSS assessment, even though the Hong Kong curriculum covers about half of the tested topics, whereas the U.S. grade 4 curriculum covers over 80% of the tested topics. Higher-performing countries (the U.S. ranks 11th in 4th-grade mathematics, according to TIMSS) teach central topics more coherently and in greater depth. Thus, the proposed new standards differ substantially from today's typical state standards by focusing on key topics and building a coherent progression of learning.

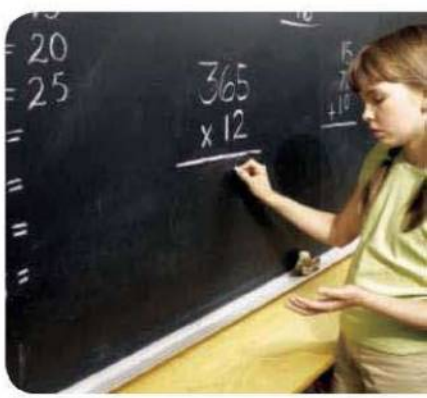

The political push for common standards comes with a push for higher standards. "Higher standards" means covering fewer topics at each grade level but in greater depth, so that students learn them well. It also means covering topics at the appropriate grade level, when students are well prepared for them. In Singapore, division of fractions is not taught until grade 6, whereas in the United States, it is often taught in grade 4 or 5. In top-performing countries, mathematics standards are high for what students actually learn. In contrast, U.S. state standards often tell teachers what to cover, whether students learn it well or not. The CCSS are designed to help teachers know when to devote the necessary time to mathematical ideas that are worth careful study. Cognitive research suggests that conceptual understanding intertwines with procedural skill to develop mathematics achievement. To make solid progress, students need not only skills to tackle mathematics problems but also the mathematical concepts that give coherence and substance to the subject. The CCSS delineate both skills to master and concepts to understand.

Common standards can benefit the education field, just as other fields (such as engineering and medicine) have benefited when common standards have been introduced. And common standards can improve textbooks and other teaching tools. Currently, publishers include every topic that any given state might want to see; as a result, U.S. mathematics textbooks typically have five times as many pages as international texts. By aggregating demand, common standards can make the education market less fragmented, and R&D can focus on creating better and innovative products and services.

Yet by themselves, common standards will accomplish little. They are part of a larger system of tools, organizations, and practices. This raises questions about what else states can share to support effective instruction, such as common training for teachers. Consortia of states are already organizing a common assessment system for student achievement. The promise of an improved education system is thrilling. But people, especially teachers and those who support them, will decide what difference common standards will make.

– Philip Daro, William McCallum, Jason Zimba

10.1126/science.1190309

*The authors are members of the CCSS for Mathematics working group.

CREDIT: HEMERA TECHNOLOGIES/GETTY IMAGES/THINKSTOCK

BIOTECHNOLOGY

Homeostatic Engineering

Not so many years ago, adding a heterologous set of enzymes in order to augment the biosynthetic capacity of a microbe was acknowledged as a remarkable feat of rational design. Apart from the important technical concerns of efficiency and stability, attention then turned to the greater challenge of repairing metabolic dysfunction; the goal here was not only to restore the biochemical reactions but also to place them under endogenous regulation. Kemmer *et al.* demonstrate how this might be achieved in mice suffering from excess uric acid, which in humans can lead to the condition commonly known as gout. Uric acid is the product of purine catabolism, and in mice, urate oxidase converts it to allantoin, which is excreted. Excess uric acid can precipitate as the sodium salt, and humans, who lack urate oxidase, cannot tolerate too much of it. Conversely, uric acid can scavenge free radicals, and a moderate amount is deemed to be beneficial. Stitching together a mini-circuit comprising a *Deinococcus* transcriptional repressor and promoter as well as *Aspergillus* urate oxidase enabled these authors to maintain serum uric acid concentration in urate oxidase–deficient mice at normal physiologic levels. — GJC

Nat. Biotechnol. **28**, 10.1038/nbt.1617 (2010).

EVOLUTION

Sowing the Seeds of Spherulites

The evolution of hard calcified structures such as shells and skeletons gave their bearers a selection advantage over older soft-bodied organisms. Most organisms equipped with such hard structures synthesize enzymes or other biomolecules to serve as sites for controlled crystal growth. The modern sponge *Astrosclera willeyana*—a living fossil related to some of the most primitive sponges—may form its simple calcite spheres via another mechanism. Within the organic matrix of these spherulites, Jackson *et al.* found biomarkers exclusive to the biomolecules of bacteria. This finding suggests that *A. willeyana* degrades the bacteria that enter its much larger cells and then uses the degradation products, rather than its own biomolecules, to nucleate calcite crystals. Bacteria on their own can form large calcified structures such as stromatolites, and did so billions of years ago; however, if sponge-like organisms ~300 million years ago did not have the full suite of genetic machinery to direct biocalcification themselves, the harvesting of bacteria to jump-start the process would have served as an efficient evolutionary shortcut. The appearance of more sophisticated mineralization pathways, which allowed species related to modern corals to outcompete the ancient sponges that previously dominated ocean reefs, may have occurred much later. — NW

Geobiology **8**, 10.1111/j.1472-4669.2010.00236.x (2010).

MOLECULAR BIOLOGY

Read-Only Access

To squeeze eukaryotic genomes into the cramped confines of the cell nucleus, DNA is packaged into nucleosomes, which are composed of octamers of histone proteins: two dimers of histones H3 and H4 and two dimers of H2A and H2B. Accessing the information stored in the genome requires that the nucleosomes be removed or shuffled out of the way and then later replaced. Assembly occurs via the interaction of dimers of H3-H4 with DNA to form a $(H3\text{-}H4)_2$–DNA complex (the tetrasome), and then by the addition of two H2A-H2B dimers. Andrews *et al.* have studied the mechanism by which nucleosome assembly protein 1 (Nap1) acts to promote assembly and find that Nap1 does not affect tetrasome formation but instead binds to the H2A-H2B dimer and reduces its affinity for DNA. This is critical because histones are basic proteins and have a strong propensity for nonproductively interacting with DNA. Deletion of Nap1 in yeast results in increased levels of H2A and H2B in chromatin, without a corresponding increase in H3, supporting the

CREDIT: TITIAAN/LAMBERT SUSTRIS, 1548

idea that Nap1 protects against H2A-H2B dimers binding to DNA disobediently. The derangement of normal chromatin structure in the absence of Nap1 results in the misregulation of transcription, indicating that Nap1 chaperone activity is critical for the correct readout of information. — GR

Mol. Cell **37**, 834 (2010).

MOLECULAR BIOLOGY

Remote Enhancement

The temporal and cell type–specific regulation of gene expression relies in part on enhancers, which are noncoding regions of the genome that control tissue-specific expression of a gene sometimes located hundreds of kilobases away. Enhancers recruit regulatory proteins to decondense chromatin and promote the assembly of transcription machinery at genes. Swanson *et al.* have dissected the 350-bp *sparkling* (*spa*) enhancer that controls expression of the *dPax2* gene, which specifies cone cell fate in the developing *Drosophila* eye. The *spa* enhancer has been shown to consist of 12 binding sites that recruit four regulatory proteins, the combination of which was thought to be sufficient to activate gene expression. By analyzing mutated versions of a synthetic *spa* enhancer in vivo, the authors have identified additional regulatory regions that are required for gene expression. One of these regions was required only when the enhancer was located 846 bp upstream of the promoter, but not at 121 bp, which suggests that other enhancers may contain similar hidden remote-control regions that work at a distance. Rearranging the regulatory elements in *spa* switched its cell-type specificity. Thus, both distance and the order of regulatory regions enable enhancers to fine-tune gene expression, revealing more levels of complexity than previously appreciated. — HP

Rescuing *spa* function by moving it closer.

Dev. Cell **18**, 359 (2010).

CHEMISTRY

A Precatalytic Cycle

When metal particles are deposited or formed on oxides for catalytic applications, the goal is to create small clusters that expose as many surface atoms as possible. One method of limiting surface adsorption is atomic layer deposition, which restricts deposition by requiring the system to undergo cycles of stoichiometric reactions. For the formation of palladium (Pd) particles on silica gel supports, Lu and Stair report a cycle of three reactions that occur at low temperatures (below 110°C) and yield highly uniform particles with an average size of 1 nm. Pd is deposited on a limited number of surface sites as an ion complex, coordinated by hexafluoroacetylacetonate ligands. A second step deposits an alumina or titania precursor, and a third step adsorbs water in order to form the oxides. This cycle is repeated over as many as 15 cycles, and then the protective Pd ligands are removed by reaction with formalin at 200°C. CO chemisorption studies showed that successive cycles do not interfere with the accessibility of the Pd clusters to reactants. — PDS

Angew. Chem. Int. Ed. **49**, 2547 (2010).

CELL BIOLOGY

Natural Skin Care

The skin acts as one of our primary defenses, protecting our organs and tissues from a dry and often hostile environment. During development, fibroblast growth factors (FGFs) and their receptors (FGFRs) help to produce and maintain a robust epidermis. Yang *et al.* generated mutant mice that lacked FGFR1, FGFR2, or both. Mice lacking keratinocyte FGFR1 appeared normal throughout development; those lacking keratinocyte FGFR2, however, had a reduced number of hairs and no sebaceous glands. Mice lacking both receptors displayed a more severe phenotype: As they aged, hair was lost, and the outer layer of the skin—the dermis—underwent fibrosis as a consequence of an increased inflammatory response. The tight junctions that hold skin cells together were also down-regulated in the mutant mice, which correlated with an impairment of epidermal barrier function. — SMH

J. Cell Biol. **188,** 935 (2010).

CLIMATE SCIENCE

A Long Slow March

Among the most important responses to rising temperatures is accelerating rates of melting of the world's ice sheets and glaciers. Nowhere has that melting been more evident than in southern Greenland, where for the past decade or more, ice mass loss has occurred at an increasing rate. Now the mass loss so apparent in the south is spreading up the northwest coast, as would be expected. Khan *et al.* use two independent techniques—gravity measurements from the GRACE satellites and GPS measurements of bedrock elevations adjacent to the ice sheet—to construct a self-consistent record which shows that ice mass loss in northwest Greenland probably began to pick up speed in 2005. Detailed pictures of the evolution of ice sheets should lead to better predictions of other phenomena such as sea-level rise. — HJS

Geophys. Res. Lett. **37**, L06501 (2010).

CREDIT: SWANSON *ET AL.*, *DEV. CELL* **18**, 359 (2010)

Proven Science.
Experienced People.
Trusted Results.

Preclinical, GLP-compliant Toxicology Studies

- Small molecules, biologics, nutraceuticals, and botanical extracts
- Standard species and specialized models
- Standard and specialized routes of administration
- Acute, subchronic, chronic study durations
- Clinical pathology, anatomic pathology, ADME/PK, immunotoxicology

Bioanalytical Services

- Method feasibility, development, and validation
- Formulation and bioanalysis
- *In vitro* metabolism
- qPCR and RT-PCR

Efficacy Models

- Cancer
- Angiogenesis
- Infectious diseases, including virology and bacteriology
- CNS diseases

SOUTHERN RESEARCH
Legendary Discoveries. Leading Innovation.

(888) 322-1166 • 001 (205) 581-2830
BusDev@SouthernResearch.org

www.SouthernResearch.org

www.sciencemag.org

Science

1200 New York Avenue, NW
Washington, DC 20005
Editorial: 202-326-6550, FAX 202-289-7562
News: 202-326-6581, FAX 202-371-9227
Bateman House, 82-88 Hills Road
Cambridge, UK CB2 1LQ
+44 (0) 1223 326500, FAX +44 (0) 1223 326501

Subscription Services For change of address, missing issues, new orders and renewals, and payment questions: 866-434-AAAS (2227) or 202-326-6417, FAX 202-842-1065. Mailing addresses: AAAS, P.O. Box 96178, Washington, DC 20090-6178 or AAAS Member Services, 1200 New York Avenue, NW, Washington, DC 20005

Institutional Site Licenses please call 202-326-6755 for any questions or information

Reprints: Author Inquiries 800-635-7181
Commercial Inquiries 803-359-4578

Permissions 202-326-7074, FAX 202-682-0816

Member Benefits AAAS/Barnes&Noble.com bookstore www.aaas.org/bn; AAAS Online Store www.apisource.com/aaas/ code MKB6; AAAS Travels: Betchart Expeditions 800-252-4910; Apple Store www.apple.com/eppstore/aaas; Bank of America MasterCard 1-800-833-6262 priority code FAA3YU; Cold Spring Harbor Laboratory Press Publications www.cshlpress.com/affiliates/aaas.htm; GEICO Auto Insurance www.geico.com/landingpage/go51.htm?logo=17624; Hertz 800-654-2200 CDP#343457; Office Depot https://bsd.officedepot.com/portalLogin.do; Seabury & Smith Life Insurance 800-424-9883; Subaru VIP Program 202-326-6417; VIP Moving Services www.vipmayflower.com/domestic/index.html; Other Benefits: AAAS Member Services 202-326-6417 or www.aaasmember.org.

science_editors@aaas.org	(for general editorial queries)
science_letters@aaas.org	(for queries about letters)
science_reviews@aaas.org	(for returning manuscript reviews)
science_bookrevs@aaas.org	(for book review queries)

Published by the American Association for the Advancement of Science (AAAS), *Science* serves its readers as a forum for the presentation and discussion of important issues related to the advancement of science, including the presentation of minority or conflicting points of view, rather than by publishing only material on which a consensus has been reached. Accordingly, all articles published in *Science*—including editorials, news and comment, and book reviews—are signed and reflect the individual views of the authors and not official points of view adopted by AAAS or the institutions with which the authors are affiliated.

AAAS was founded in 1848 and incorporated in 1874. Its mission is to advance science, engineering, and innovation throughout the world for the benefit of all people. The goals of the association are to: enhance communication among scientists, engineers, and the public; promote and defend the integrity of science and its use; strengthen support for the science and technology enterprise; provide a voice for science on societal issues; promote the responsible use of science in public policy; strengthen and diversify the science and technology workforce; foster education in science and technology for everyone; increase public engagement with science and technology; and advance international cooperation in science.

Information for Authors
See pages 352 and 353 of the 15 January 2010 issue or access www.sciencemag.org/about/authors

EDITOR-IN-CHIEF **Bruce Alberts**
EXECUTIVE EDITOR **Monica M. Bradford** NEWS EDITOR **Colin Norman**
MANAGING EDITOR, RESEARCH JOURNALS **Katrina L. Kelner**
DEPUTY EDITORS **R. Brooks Hanson, Barbara R. Jasny, Andrew M. Sugden**

Editorial senior editors/commentary Lisa D. Chong, Brad Wible; **senior editors** Gilbert J. Chin, Pamela J. Hines, Paula A. Kiberstis (Boston), Marc S. Lavine (Toronto), Beverly A. Purnell, L. Bryan Ray, Guy Riddihough, H. Jesse Smith, Phillip D. Szuromi (Tennessee), Valda Vinson, Jake S. Yeston; **associate editors** Kristen L. Mueller, Jelena Stajic, Nicholas S. Wigginton, Laura M. Zahn; **research associate** Alexis Wynne Mogul; **book review editor** Sherman J. Suter; **associate letters editor** Jennifer Sills; **editorial manager** Cara Tate; **senior copy editors** Jeffrey E. Cook, Cynthia Howe, Harry Jach, Lauren Kmec, Barbara P. Ordway, Trista Wagoner; **copy editor** Chris Filiatreau; **editorial coordinators** Carolyn Kyle, Beverly Shields; **publications assistants** Ramatoulaye Diop, Joi S. Granger, Emily Guise, Jeffrey Hearn, Michael Hicks, Lisa Johnson, Scott Miller, Jerry Richardson, Jennifer A. Seibert, Brian White, Anita Wynn; **editorial assistants** Emily C. Horton, Patricia M. Moore, Miriam Weinberg; **executive assistants** Alison Crawford; **administrative support** Maryrose Madrid; **editorial fellow** Melissa R. McCartney

Editorial director, web & new media Stewart Wills; **senior web editor** Tara S. Marathe; **web editor** Robert Frederick; **web development manager** Martyn Green; **web developer** Andrew Whitesell

News deputy news editors Robert Coontz, Eliot Marshall, Jeffrey Mervis, Leslie Roberts; **contributing editors** Elizabeth Culotta, Polly Shulman; **news writers** Yudhijit Bhattacharjee, Adrian Cho, Jennifer Couzin, David Grimm, Constance Holden, Jocelyn Kaiser, Richard A. Kerr, Eli Kintisch, Greg Miller, Elizabeth Pennisi, Robert F. Service (Pacific NW), Erik Stokstad, Jue Wang; **intern** Lauren Schenkman; **contributing correspondents** Jon Cohen (San Diego, CA), Daniel Ferber, Ann Gibbons, Sam Kean, Robert Koenig, Andrew Lawler, Mitch Leslie, Charles C. Mann, Virginia Morell, Gary Taubes; **copy editors** Linda B. Felaco, Melvin Gatling, Melissa Raimondi; **administrative support** Scherraine Mack; **bureaus** San Diego, CA: 760-942-3252, FAX 760-942-4979; Pacific Northwest: 503-963-1940

Production director James Landry; **senior manager** Wendy K. Shank; **assistant manager** Rebecca Doshi; **senior specialists** Steve Forrester, Chris Redwood, Anthony Rosen; **Preflight director** David M. Tompkins; **manager** Marcus Spiegler; **specialist** Jason Hillman

Art director Yael Kats; **associate art director** Laura Creveling; **senior illustrators** Chris Bickel, Katharine Sutliff; **illustrator** Yana Greenman; **senior art associates** Holly Bishop, Preston Huey, Nayomi Kevitiyagala; **art associates** Kay Engman, Matthew Twombly; **photo editor** Leslie Blizard

***Science* International**

Europe (science@science-int.co.uk) **editorial: international managing editor** Andrew M. Sugden; **senior editor/commentary** Julia Fahrenkamp-Uppenbrink; **senior editors** Caroline Ash, Stella M. Hurtley, Ian S. Osborne, Peter Stern; **associate editor** Maria Cruz; **locum editor** Helen Pickersgill; **editorial support** Deborah Dennison, Rachel Roberts, Alice Whaley; **administrative support** John Cannell, Janet Clements, Louise Hartwell; **news: europe news editor** John Travis; **deputy news editor** Daniel Clery; **contributing correspondents** Michael Balter (Paris), John Bohannon (Vienna), Martin Enserink (Amsterdam and Paris), Gretchen Vogel (Berlin); **intern** Tim Wogan

Latin America contributing correspondent Antonio Regalado

Asia Japan Office: Asca Corporation, Tomoko Furusawa, Rustic Bldg. 7F, 77 Tenjin-cho, Shinjuku-ku, Tokyo 162-0808, Japan; +81 3 6802 4616, FAX +81 3 6802 4615, inquiry@sciencemag.jp; **asia news editor** Richard Stone (Beijing: rstone@aaas.org); **contributing correspondents** Dennis Normile [Japan: +81 (0) 3 3391 0630, FAX +81 (0) 3 5936 3531; dnormile@gol.com]; Hao Xin [China: +86 (0) 10 6307 4439 or 6307 3676, FAX +86 (0) 10 6307 4358; cindyhao@gmail.com]; Pallava Bagla [South Asia: +91 (0) 11 2271 2896; pbagla@vsnl.com]

EXECUTIVE PUBLISHER **Alan I. Leshner**
PUBLISHER **Beth Rosner**

Fulfillment Systems and Operations (membership@aaas.org); **director** Waylon Butler; **customer service supervisor** Pat Butler; **specialists** Latoya Casteel, LaVonda Crawford, Vicki Linton, April Marshall; **data entry supervisor** Cynthia Johnson; **specialists** Shirlene Hall, Tarrika Hill, William Jones

Business Operations and Administration director Deborah Rivera-Wienhold; **business systems and financial analysis director** Randy Yi; **manager, business analysis** Eric Knott; **manager, business operations** Jessica Tierney; **financial analysts** Priti Pamnani, Celeste Troxler; **rights and permissions: administrator** Emilie David; **associate** Elizabeth Sandler; **marketing director** Ian King; **marketing managers** Allison Pritchard, Alison Chandler, Julianne Wielga; **marketing associates** Aimee Aponte, Mary Ellen Crowley, Wendy Wise; **senior marketing executive** Jennifer Reeves; **director, site licensing** Tom Ryan; **director, corporate relations** Eileen Bernadette Moran; **publisher relations, eresources specialist** Kiki Forsythe; **senior publisher relations specialist** Catherine Holland; **publisher relations, east coast** Phillip Smith; **publisher relations, west coast** Philip Tsolakidis; **fulfillment supervisor** Iquo Edim; **fulfillment coordinator** Carrie MacDonald; **marketing manager** Christina Schlecht; **electronic media: manager** Lizabeth Harman; **project manager** Trista Snyder; **assistant manager** Lisa Stanford; **senior production specialists** Ryan Atkins, Christopher Coleman, **computer specialist** Walter Jones; **production specialists** Nichele Johnston, Kimberly Oster; **director, web and new media** Will Collins

advertising director, worldwide ad sales Bill Moran
commercial editor Sean Sanders: 202-326-6430
project director, outreach Brianna Blaser

Product (science_advertising@aaas.org); **midwest** Rick Bongiovanni: 330-405-7080, FAX 330-405-7081; **east coast/e. canada** Laurie Faraday: 508-747-9395, FAX 617-507-8189; **west coast/w. canada** Lynne Stickrod: 415-931-9782, FAX 415-520-6940; **uk/europe/asia** Roger Goncalves: TEL/FAX +41 43 243 1358; **japan** ASCA Corporation, Nanako Ide +81 (0) 3 6802 4616, FAX +81 (0) 3 6802 4615; ads@sciencemag.jp; **senior traffic associate** Deiandra Simms

worldwide associate director of *Science* Careers Tracy Holmes: +44 (0) 1223 326525, FAX +44 (0) 1223 326532

Classified (advertise@sciencecareers.org); **u.s.: midwest/east coast** Tina Burks: 202-326-6577; **west/south central** Nicholas Hintibidze: 202-326-6533; **sales coordinators** Rohan Edmonson, Shirley Young; **europe/row sales:** Susanne Kharraz, Dan Pennington, Alex Palmer; **sales assistant** Lisa Patterson; **japan** ASCA Corporation, Jie Chin +81 (0) 3 6802 4616, FAX +81 (0) 3 6802 4615; careerads@sciencemag.jp; **advertising support manager** Karen Foote: 202-326-6740; **advertising production operations manager** Deborah Tompkins; **senior production specialist/graphic designer** Amy Hardcastle; **senior production specialist** Robert Buck; **senior traffic associate** Christine Hall

AAAS Board of Directors retiring president, chair Peter C. Agre; **president** Alice Huang; **president-elect** Nina Fedoroff; **treasurer** David E. Shaw; **chief executive officer** Alan I. Leshner; **board** Linda P. B. Katehi, Nancy Knowlton, Stephen Mayo, Cherry A. Murray, Julia M. Phillips, David D. Sabatini, Thomas A. Woolsey

AAAS
ADVANCING SCIENCE, SERVING SOCIETY

SENIOR EDITORIAL BOARD

John I. Brauman, *Chair, Stanford Univ.*
Richard Losick, *Harvard Univ.*
Linda Partridge, *Univ. College London*
Michael S. Turner, *University of Chicago*

BOARD OF REVIEWING EDITORS

Adriano Aguzzi, *Univ. Hospital Zürich*
Takuzo Aida, *Univ. of Tokyo.*
Sonia Altizer, *Univ. of Georgia*
David Altshuler, *Broad Institute*
Arturo Alvarez-Buylla, *Univ. of California, San Francisco*
Richard Amasino, *Univ. of Wisconsin, Madison*
Angelika Amon, *MIT*
Kathryn Anderson, *Memorial Sloan-Kettering Cancer Center*
Siv G. E. Andersson, *Uppsala Univ.*
Peter Andolfatto, *Princeton Univ.*
Meinrat O. Andreae, *Max Planck Inst., Mainz*
John A. Bargh, *Yale Univ.*
Ben Barres, *Stanford Medical School*
Marisa Bartolomei, *Univ. of Penn. School of Med.*
Jordi Bascompte, *Estación Biológica de Doñana, CSIC*
Facundo Batista, *London Research Inst.*
Ray H. Baughman, *Univ. of Texas, Dallas*
Yasmine Belkaid, *NIAID, NIH*
Stephen J. Benkovic, *Penn State Univ.*
Gregory C. Beroza, *Stanford Univ.*
Ton Bisseling, *Wageningen Univ.*
Mina Bissell, *Lawrence Berkeley National Lab*
Peer Bork, *EMBL*
Robert W. Boyd, *Univ. of Rochester*
Paul M. Brakefield, *Leiden Univ.*
Christian Büchel, *Universitätsklinikum Hamburg-Eppendorf*
Joseph A. Burns, *Cornell Univ.*
William P. Butz, *Population Reference Bureau*
Mats Carlsson, *Univ. of Oslo*
Mildred Cho, *Stanford Univ.*
David Clapham, *Children's Hospital, Boston*
David Clary, *Oxford University*
J. M. Claverie, *CNRS, Marseille*
Jonathan D. Cohen, *Princeton Univ.*
Andrew Cossins, *Univ. of Liverpool*
Robert H. Crabtree, *Yale Univ.*
Wolfgang Cramer, *Potsdam Inst. for Climate Impact Research*
F. Fleming Crim, *Univ. of Wisconsin*
William Cumberland, *Univ. of California, Los Angeles*
Jeff L. Dangl, *Univ. of North Carolina*
Stanislas Dehaene, *Collège de France*
Edward DeLong, *MIT*
Emmanouil T. Dermitzakis, *Univ. of Geneva Medical School*
Robert Desimone, *MIT*
Claude Desplan, *New York Univ.*
Dennis Discher, *Univ. of Pennsylvania*
Scott C. Doney, *Woods Hole Oceanographic Inst.*
Jennifer A. Doudna, *Univ. of California, Berkeley*
Julian Downward, *Cancer Research UK*
Bruce Dunn, *Univ. of California, Los Angeles*
Christopher Dye, *WHO*
Michael B. Elowitz, *Calif. Inst. of Technology*
Gerhard Ertl, *Fritz-Haber-Institut, Berlin*
Mark Estelle, *Indiana Univ.*
Barry Everitt, *Univ. of Cambridge*
Paul G. Falkowski, *Rutgers Univ.*
Ernst Fehr, *Univ. of Zurich*
Tom Fenchel, *Univ. of Copenhagen*
Alain Fischer, *INSERM*
Wulfram Gerstner, *EPFL Lausanne*
Charles Godfray, *Univ. of Oxford*
Diane Griffin, *Johns Hopkins Bloomberg School of Public Health*
Christian Haass, *Ludwig Maximilians Univ.*
Steven Hahn, *Fred Hutchinson Cancer Research Center*
Gregory J. Hannon, *Cold Spring Harbor Lab.*
Niels Hansen, *Technical Univ. of Denmark*
Dennis L. Hartmann, *Univ. of Washington*
Chris Hawkesworth, *Univ. of St Andrews*
Martin Heimann, *Max Planck Inst., Jena*
James A. Hendler, *Rensselaer Polytechnic Inst.*
Janet G. Hering, *Swiss Fed. Inst. of Aquatic Science & Technology*
Ray Hilborn, *Univ. of Washington*
Michael E. Himmel, *National Renewable Energy Lab.*
Kei Hirose, *Tokyo Inst. of Technology*
Ove Hoegh-Guldberg, *Univ. of Queensland*
Ronald R. Hoy, *Cornell Univ.*
Jeffrey A. Hubbell, *EPFL Lausanne*
Steven Jacobsen, *Univ. of California, Los Angeles*
Peter Jonas, *Universität Freiburg*
Barbara B. Kahn, *Harvard Medical School*
Daniel Kahne, *Harvard Univ.*
Bernhard Keimer, *Max Planck Inst., Stuttgart*
Robert Kingston, *Harvard Medical School*
Hanna Kokko, *Univ. of Helsinki*
Alberto R. Kornblihtt, *Univ. of Buenos Aires*
Lee Kump, *Penn State Univ.*
Mitchell A. Lazar, *Univ. of Pennsylvania*
David Lazer, *Harvard Univ.*
Virginia Lee, *Univ. of Pennsylvania*
Julian Lewis, *Cancer Research UK*
Olle Lindvall, *Univ. Hospital, Lund*
Marcia C. Linn, *Univ. of California, Berkeley*
John Lis, *Cornell Univ.*
Richard Losick, *Harvard Univ.*
Ke Lu, *Chinese Acad. of Sciences*
Laura Machesky, *CRUK Beatson Inst. for Cancer Research*
Andrew P. MacKenzie, *Univ. of St Andrews*
Anne Magurran, *Univ. of St Andrews*
Oscar Marin, *CSIC & Univ. Miguel Hernández*
Charles Marshall, *Univ. of California, Berkeley*
Martin M. Matzuk, *Baylor College of Medicine*
Virginia Miller, *Washington Univ.*
Yasushi Miyashita, *Univ. of Tokyo*
Richard Morris, *Univ. of Edinburgh*
Edvard Moser, *Norwegian Univ. of Science and Technology*
Sean Munro, *MRC Lab. of Molecular Biology*
Naoto Nagaosa, *Univ. of Tokyo*
James Nelson, *Stanford Univ. School of Med.*
Timothy W. Nilsen, *Case Western Reserve Univ.*
Pär Nordlund, *Karolinska Inst.*
Helga Nowotny, *European Research Advisory Board*
Stuart H. Orkin, *Dana-Farber Cancer Inst.*
Christine Ortiz, *MIT*
Elinor Ostrom, *Indiana Univ.*
Andrew Oswald, *Univ. of Warwick*
Jonathan T. Overpeck, *Univ. of Arizona*
P. David Pearson, *Univ. of California, Berkeley*
John Pendry, *Imperial College*
Reginald M. Penner, *Univ. of California, Irvine*
John H. J. Petrini, *Memorial Sloan-Kettering Cancer Center*
Simon Phillpot, *Univ. of Florida*
Philippe Poulin, *CNRS*
Colin Renfrew, *Univ. of Cambridge*
Trevor Robbins, *Univ. of Cambridge*
Barbara A. Romanowicz, *Univ. of California, Berkeley*
Jens Rostrup-Nielsen, *Haldor Topsoe*
Edward M. Rubin, *Lawrence Berkeley National Lab*
Shimon Sakaguchi, *Kyoto Univ.*
Michael J. Sanderson, *Univ. of Arizona*
Jürgen Sandkühler, *Medical Univ. of Vienna*
Randy Seeley, *Univ. of Cincinnati*
Christine Seidman, *Harvard Medical School*
David Sibley, *Washington Univ*
Joseph Silk, *Univ. of Oxford*
Montgomery Slatkin, *Univ. of California, Berkeley*
Davor Solter, *Inst. of Medical Biology, Singapore*
Allan C. Spradling, *Carnegie Institution of Washington*
Elsbeth Stern, *ETH Zürich*
Yoshiko Takahashi, *Nara Inst. of Science and Technology*
Jurg Tschopp, *Univ. of Lausanne*
Bert Vogelstein, *Johns Hopkins Univ.*
Bruce D. Walker, *Harvard Medical School*
Christopher A. Walsh, *Harvard Medical School*
David A. Wardle, *Swedish Univ. of Agric Sciences*
Colin Watts, *Univ. of Dundee*
Detlef Weigel, *Max Planck Inst., Tübingen*
Jonathan Weissman, *Univ. of California, San Francisco*
Sue Wessler, *Univ. of Georgia*
Ian A. Wilson, *The Scripps Res. Inst.*
Xiaoliang Sunney Xie, *Harvard Univ.*
John R. Yates III, *The Scripps Res. Inst.*
Jan Zaanen, *Leiden Univ.*
Huda Zoghbi, *Baylor College of Medicine*
Maria Zuber, *MIT*

BOOK REVIEW BOARD

John Aldrich, *Duke Univ.*
David Bloom, *Harvard Univ.*
Angela Creager, *Princeton Univ.*
Richard Shweder, *Univ. of Chicago*
Ed Wasserman, *DuPont*
Lewis Wolpert, *Univ. College London*


Sick old Douglas firs look like bottle brushes.

Fungus Slows Fir

A tree fungus that used to be a minor nuisance is now causing a major loss of growth in Douglas firs, a staple of the timber industry in the Pacific Northwest. Swiss needle cast disease has "become an epidemic" in some coastal regions and has significantly lowered productivity, says Bryan Black, a forest ecologist at Oregon State University in Newport and co-author of a study appearing this month in *Forest Ecology and Management*. The blight is being exacerbated by warmer springs and wetter summers, the scientists say.

Scientists used to think the disease, which causes needles to yellow and fall off, affected only young, fast-growing trees. But Black's team spotted severe growth declines in mature trees after taking tree-ring cores from 100-year-old stands on the Oregon coast. Compared with cores from western hemlock, the fir trees' growth rate has been stunted by more than 80% in the past quarter-century. The cores show the trees growing steadily until 1983, then "hitting a brick wall and shutting down," says Black. Alan Kanaskie, a forest pathologist at the Oregon Department of Forestry in Salem, says "this is the first study to rigorously show the decline in mature Douglas fir growth and link it to this disease."

HOW ABOUT 'WON'T I'?

The way individuals talk to themselves may influence their future behaviors. Volunteers solved more anagrams if they prepared for the task by asking themselves whether they would work on anagrams as opposed to declaring they would. In follow-up experiments, merely writing "Will I" 20 times (as part of a supposed unrelated handwriting task) resulted in better performance on solving anagrams and stronger intentions to exercise than writing "I Will" 20 times, suggesting that priming an interrogative structure of self-talk may be enough to motivate goal-directed behavior.

—Summary of a paper published online last month in *Psychological Science*

In Memoriam

Constance Holden, who has edited this page with her singular wit and style since it was launched 20 years ago, was tragically killed on 12 April in a traffic accident. Tancy, as she was fondly known to her many friends and colleagues, was struck by a military vehicle, part of the security forces for the nuclear summit being held in Washington, D.C., as she left the *Science* offices on her bicycle.

Tancy was an accomplished writer and editor for *Science* for almost 40 years. She covered the social and behavioral sciences, bioethics, and stem cell research, delving into the genetics of behavior long before it was fashionable. She was a true original—warm, funny, curious, direct, and always willing to challenge the conventional wisdom. She was also a talented artist and pianist. Her oil paintings grace colleagues' offices and the corridors of the AAAS building. The self-portrait above provides a unique view of a distinctive personality who has left her mark on this magazine. She will be deeply missed.

Jurassic Mark

The Jurassic era—heyday of big dinosaurs, cycad ferns, and certain marine invertebrates—may soon have an official starting point. Geologists are gearing up to decide whether a sequence of 200-million-year-old rocks (see arrow) about 50 kilometers north of Innsbruck in Austria will serve as the "type section" or "global boundary stratotype section," whose fossils define the beginning of the era for researchers worldwide.

Geologists have been arguing for years about the best spot to mark the Triassic-Jurassic boundary. "Formally defining the beginning of the Jurassic would be the same as defining the beginning of the Renaissance," says Stan Finney of California State University, Long Beach, chair of the International Commission on Stratigraphy, which recommends type sections for the International Union of Geological Sciences (IUGS).

The traditional identifying fossil for the Jurassic has been whorl-shelled sea creatures called ammonites. But they are hard to find in buried strata, and many rocks from the era have been washed away by sea-level changes or subducted in ocean crust, now deep inside the earth. Ammonites are sprinkled in potential type sections in British Columbia, Canada; the United Kingdom; and the United States, including Nevada's New York Canyon site. But the commission's preferred candidate is Tyrol's Kuhjoch section in the Karwendel Mountains, which has other tiny Jurassic fossils such as pollen and algal diatoms.

IUGS is expected to hold an official vote on the matter this summer.


Ammonite.

CREDITS (TOP TO BOTTOM): DAVE SHAW/OREGON STATE UNIVERSITY; CONSTANCE HOLDEN, COURTESY OF JOHN BUTTERS; W.M. KERSCHNER. (INSET) LEOPOLD KRYSTYN/UNIV. OF VIENNA

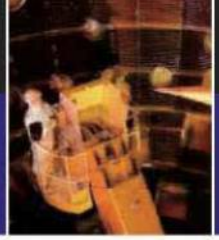

Bringing astronomy to the people 293

The evolution of an educator 294

NUCLEAR PHYSICS

Discovery of 'Missing' Element 117 Hints at Stable Isotopes to Come

Russia strikes again. In the past decade, the Joint Institute for Nuclear Research in Dubna, Russia, has bagged new elements 113, 114, 115, 116, and 118 by firing up a fantastically intense beam of neutron-heavy calcium-48 isotopes and blasting away at the periodic table's radioactive actinide elements. Last week in *Physical Review Letters*, a multi-institution team there announced that it had filled a gap by making element 117 as well.

"They devoted very, very long beam times and very hard work," says nuclear chemist Heino Nitsche, who leads the heavy-element group at Lawrence Berkeley National Laboratory in Berkeley, California. At other labs, Nitsche says, heavy-element scientists vie with other experimenters for beam time, but Dubna physicists enjoy a cyclotron largely dedicated to element-hunting. "You won't find that anywhere else in the world," he says.

For decades, the new-element sweepstakes has been a three-way race. Beginning in 1940, the Berkeley lab dominated the field, claiming or sharing credit for all elements except for one from 93 through 106. In 1981, the GSI Helmholtz Centre for Heavy Ion Research in Darmstadt, Germany, pulled ahead, planting flags on elements 107 through 112, the recently named copernicum.

Even with stretches of beam time available at Dubna, going after 117 required "experimentally, an enormous tour de force," says nuclear physicist Konrad Gelbke, director of the National Superconducting Cyclotron Laboratory (NSCL) at Michigan State University in East Lansing. To get to 117 protons from calcium's 20, Dubna physicists needed the 97 protons in the devilishly-hard-to-synthesize element berkelium. Nuclear chemists at the world's most intense neutron source, the High Flux Isotope Reactor at Oak Ridge National Laboratory in Tennessee, spent 250 days scraping together 22.2 milligrams of the stuff—about the size of a fingernail paring—and another 90 days purifying it to one part in 10 million. Then the clock began to tick: Berkelium's half-life is 320 days.

The hot material's next stop was Russia's Research Institute of Atomic Reactors in Dimitrovgrad, where scientists deposited it on a thin film of titanium. Then it went on to Dubna, where physicists pummeled the target with 7 trillion calcium-48 ions per second, day and night for 5 months. A gas-filled separation chamber diverted atoms blasted off the target into an array of detectors. From thousands of potentially interesting events, the physicists pinned down just six atoms of element 117.

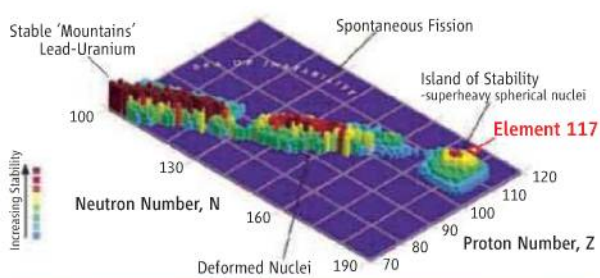

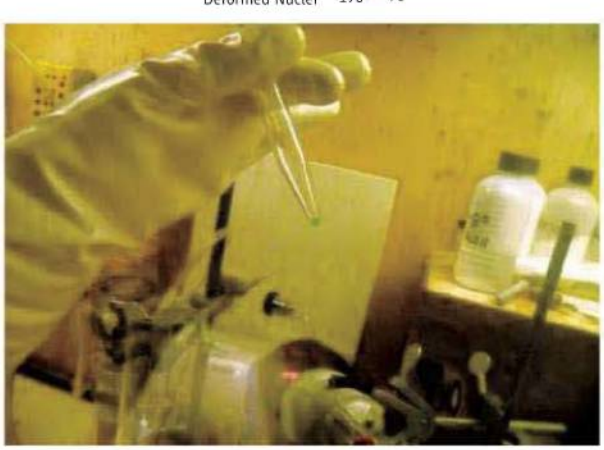

Gotcha. Physicists nabbed element 117 by firing calcium-48 ions at berkelium (*bottom*). The results bolster predictions of an "island of stability" (*top*), a group of long-lived superheavy isotopes.

To do so, they looked at the chains of other elements produced as the radioactive atoms decayed toward stability. An isotope of 117 with 177 neutrons, for example, spits out alpha particles to metamorphose first into daughter nucleus 115 and later into dubnium (105) before fissioning. The elements in this chain—115, 113, 111, and so on—had all been made before. But the new versions had more neutrons than earlier ones did and were strikingly longer-lived—6000 times as long, in the case of one isotope of element 111.

Those results fit with theorists' current picture of heavy-element nuclei, says Witold Nazarewicz, a theoretical physicist at Oak Ridge and the University of Tennessee, Knoxville. The theory predicts that certain so-called magic numbers of protons and neutrons confer extra stability to a nucleus. A magic number at 184 neutrons, for example, ought to anchor an "island of stability," a still-to-be-discovered group of long-lived superheavy isotopes that hold together for days, years, or even millennia. (In contrast, superheavy elements made so far have half-lives of fractions of a second.) The new Dubna results showing that added neutrons increase the stability of heavy elements "suggest that the theory knows what it's doing," Nazarewicz says. "It's encouraging."

Physicists at all three facilities agree that the way to reach the island of stability is by producing heavier isotopes of known elements. That will require superb beams of radioactive elements unlike any now achievable, says Sigurd Hofmann, the head of heavy-element research at Darmstadt. Such beams may become available at labs like NSCL's planned Facility for Rare Isotope Beams, currently in the conceptual design phase, but they are still decades away, Hofmann says.

Meanwhile, Nazarewicz says, efforts to create new elements will help theorists test their models of nuclear structure. But Dubna's spurt of contributions may just have come to an end: Researchers say the lab has run out of useful actinide targets for its calcium beam. To get element 119 would require working with einsteinium, "a very complex task" that Dubna likely won't attempt, says Dubna's director, nuclear physicist Yuri Oganessian. Element 120 is definitely out of range, he says.

That opens the door to other approaches. The Darmstadt group plans to confirm 116

CREDITS (TOP TO BOTTOM): ADAPTED FROM XANTHINE/WIKIPEDIA; U.S. DEPARTMENT OF ENERGY, OAK RIDGE NATIONAL LABORATORY

When success means almost no new patients
298

Engineering the apple
301

this summer by training a calcium beam on a radioactive curium target, says Hofmann; the technique could lay the groundwork for creating 120 from curium with a chromium beam. The Berkeley team, which was devastated in 2002 when it had to withdraw its claim on element 118 after critical data turned out to have been fabricated (*Science*, 19 July 2002, p. 313), is back in the game, recently confirming Dubna's element 114 with a calcium beam and plutonium target. And a newcomer—the superheavy element lab at the Institute of Physical and Chemical Research (RIKEN) in Japan—has been instrumental in confirming some of Darmstadt's finds.

Confirmation is key to the discovery process: Under international rules, a lab may not name a new element until a competitor repeats the finding. That could take years for element 117, says Dubna team member Dawn Shaughnessy, a nuclear chemist at Lawrence Livermore National Lab in Livermore, California. "It's hard for someone to go to their management and say, 'I want to do this long experiment just to verify this person's discovery,' " she says. Still, confirmation will come. "There may be rivalry, … but we all have to work together if anyone wants credit."

–LAUREN SCHENKMAN

U.S. SCIENCE POLICY

Obama Picks Pragmatists for New Bioethics Panel

President Barack Obama named the members of his bioethics commission—headed by two university presidents—last week. The 12-member group, selected more for practical advice than for philosophizing, as the last one was prone to, will hold its first meeting in Washington, D.C., in July.

Headed by Amy Gutmann, president of the University of Pennsylvania (Penn), the new Presidential Commission for the Study of Bioethical Issues succeeds the old President's Council on Bioethics, disbanded last June. Gutmann and her vice chair, Emory University President James Wagner, were named in November. Although the label is longer, the group itself is leaner, with a dozen members instead of the 18 under President George W. Bush.

"Previous commissions have been somewhat too philosophically oriented," presidential science adviser John Holdren said last week. Bush's council, headed successively by bioethicists Leon Kass of the University of Chicago and Edmund Pellegrino of Georgetown University, produced lengthy reports on topics such as "Being Human." The new commission, in contrast, is expected to offer concrete policy and legislative advice. Says White House aide Rick Weiss: "The hope is this will be perhaps a little more nimble." He also says the commission is probably "unique historically" for including several federal employees. Because the president wants practical advice, he wanted people "close to the ground" who understand the government's labyrinthine ways, Weiss says.

Gutmann, 60, is a prolific scholar and has an impressive reputation as a philosopher and political scientist. Prior to going to Penn in July 2004, she served as dean and then provost at Princeton University. She'll preside over an eclectic group of physicians (including a Franciscan friar), scientists, philosophers, and lawyers, as well as a patient advocate—the wife of boxing great and Parkinson's victim Muhammad Ali.

Gutmann is one of four commission members who are also fellows at the Hastings Center in Garrison, New York. She's "a fascinating choice as chair," says Hastings President Thomas Murray, who calls her "brilliant, … delightful, … a great leader." Her vice chair, Wagner, is an engineer and former medical devices researcher who has "championed the role of ethics" in Emory's mission, according to a White House statement.

"To me, it's a very highly qualified, middle-of-the-road panel," says Penn bioethicist Arthur Caplan. Although some criticized the Bush bioethics council for being stacked with conservatives, conservatives don't seem inclined to attack the Obama selections. "I don't like the politics of most of them, but the records of achievement are great," Bush council member Robert George, a Catholic legal scholar at Princeton, told the Christian news magazine *World*.

It's not known what the commission will tackle first, but as Caplan points out, the newly passed health care legislation offers much food for discussion on matters relating to privacy, limits of coverage, and "the much-despised word 'rationing.' " And that raises a crucial issue in the opinion of bioethicist Norman Fost of the University of Wisconsin, Madison. Fost observes that for all their expertise on cloning, bioterror, underserved groups, or the rights of research subjects, none of the commission members is deeply conversant with the economic issues surrounding health care financing, cost control, or rationing of care. Yet, he says, "the overwhelmingly most serious issue in health … is costs." **–CONSTANCE HOLDEN**

BIOETHICS COMMISSION MEMBERS

Amy Gutmann	President	University of Pennsylvania
James Wagner	President	Emory University
Lonnie Ali		Muhammad Ali Enterprises
Anita Allen	Lawyer/bioethicist	University of Pennsylvania
Barbara Atkinson	Vice chancellor	University of Kansas Medical Center
Nita Farahany	Lawyer	Vanderbilt University
Alexander Garza	Chief medical officer	Department of Homeland Security
Christine Grady	Nurse/bioethicist	National Institutes of Health
Stephen Hauser	Neurologist	University of California, San Francisco
Raju Kucherlapati	Geneticist	Harvard Medical School
Nelson Michael	Retrovirologist	Walter Reed Army Institute of Research
Daniel Sulmasy	Bioethicist	University of Chicago

Practical advice. Gutmann and Wagner will chair a streamlined presidential commission.

CREDIT (TOP TO BOTTOM): UNIVERSITY OF PENNSYLVANIA; ANN BORDEN/EMORY UNIVERSITY

- **Manual dispensing**

- **Electronic dispensing**

- **Positive displacement tips**

Over 30 years of experience

eppendorf®, Multipette®, Repeater® and Combitips plus® are registered trademarks of Eppendorf AG.
All rights reserved, incl. graphics and images. Copyright © 2010 by Eppendorf AG. *US product name of the Multipette.

Performing for excellence

Serial dispensing at its best: Multipette®/Repeater®*

The Eppendorf Multipette/Repeater handheld dispensing system offers an outstanding range of benefits:

Together with Combitips plus®, both the electronic and manual hand dispenser, offers automatic tip recognition combined with an automatic volume calculation.
The positive displacement system ensures high-precision dispensing for all kinds of liquids including volatile and viscous solutions. 9 different sizes of tips offer a volume-range from 1 µL – 50 mL.

Easy volume setting

- Multipette/Repeater plus: 1 µL – 10 mL
- stream/Xstream: 1 µL – 50 mL

Up to 100 dispensing steps without stopping

- Multipette/Repeater plus:
  20 different adjustable volumes per tip
- stream/Xstream:
  1,000 different adjustable volumes per tip

For more information visit **www.eppendorf.com/mpplus**
or **www.eppendorf.com/mpxstream**

eppendorf
In touch with life

Your local distributor www.eppendorf.com/worldwide · **Application Support** E-mail: support@eppendorf.com
Eppendorf AG · Hamburg · Germany · Tel: +49 40 538 01-0 · Eppendorf North America, Inc. · USA · Tel: +1 800 645 3050 menu option 2

Blast off. A new U.S. audit criticizes the most energetic laser ever built.

CREDITS (TOP TO BOTTOM): LAWRENCE LIVERMORE NATIONAL LABORATORY; WIKIPEDIA

FUSION SCIENCE

Report Calls for Improvements At Livermore's Giant Laser

Will the world's biggest laser—designed to simulate the nuclear fusion that occurs in stars and thermonuclear weapons—ever work as advertised? A new U.S. government audit of the National Ignition Facility (NIF) at Lawrence Livermore National Laboratory in California says the $4 billion behemoth faces "scientific and technical challenges and management weaknesses." But scientists associated with the project believe that the machine will do great science if Congress gives it a chance to flex its muscles.

NIF's 192 lasers focus on a thimble-sized target in which various types of hydrogen atoms, under incredible heat and pressure, are meant to undergo fusion. That accomplishment, called ignition, would allow researchers to better monitor aging nuclear weapons, understand processes in the cores of stars and planets, and point the way toward clean, cheap energy. The project has encountered repeated delays since construction began in 1997, however, and its cost has more than doubled. Last year, it was formally dedicated (*Science*, 17 April 2009, p. 326) with the hope of performing ignition experiments sometime in 2010.

But the path to ignition still has some bumps, says the Government Accountability Office (GAO) in a report issued last week.* Although GAO said the project had "made progress," among the serious problems it identified was the machine's capability to shoot at full energy. Congress funded NIF to fire at 1.8 megajoules (MJ). But GAO found that problems with laser optics that were identified years ago have continued to limit the machine's 192-beam shots to 1.3 MJ or less.

That shortfall is serious because higher energies improve NIF's chances of success. (At the same time, the laser's optical equipment is more prone to damage at higher energies, and NIF is utilizing a 4-month pause to work on the problem.) Indeed, said GAO, experts "are concerned" that energy losses or damaged optics would doom ignition experiments, undermining NIF's value in weapons science.

GAO also said that the Department of Energy's National Nuclear Security Administration (NNSA), which funds the project, had failed to manage it properly. One major example: NNSA took 4 years to appoint a standing review committee after outside advisers recommended the need for independent oversight.

Raymond Jeanloz, a physicist at the University of California, Berkeley, thinks government auditors have given the project a bum rap. In the past 5 years, scientists at NIF developed new means of examining and repairing glass optics without replacing them, says Jeanloz, who hopes to use the machine to study processes in the interior of planets. The changes give NIF a fighting chance of achieving its 1.8-MJ goal. NIF officials also say that it may be possible to achieve ignition at lower energy. Even at 1.3 MJ, Jeanloz points out, the laser is roughly 40 times more energetic as any other such machine. "You want the best value for the taxpayer, of course, … but we really don't know what will work at these energies."

NIF officials defend their management decisions. And they face little heat from federal lawmakers, who can do little to influence the project at this point short of shutting it down. So Jeanloz says it's time to let the scientists "do cutting-edge science" and then "see what happens." **–ELI KINTISCH**

*www.gao.gov/new.items/d10488.pdf

ScienceNOW

From Science's Online Daily News Site

When Social Fear Disappears, So Does Racism

Children with a genetic condition that quells their fear of strangers don't stereotype based on race, according to a new study. The findings support the idea that prejudice stems from fear of people from different social groups, although some researchers question how well the new study supports that conclusion. http://bit.ly/socialfear

Cholesterol Genetically Linked To Eye Disease

Two genetic studies involving thousands of participants suggest that age-related macular degeneration, an eye disease common among the elderly, is tied to a gene that helps regulate "good" cholesterol. The studies present the first genetic evidence of a link between cholesterol and the disease, and they may lead scientists to identify new targets for therapy. http://bit.ly/eyedisease

Does Our Universe Live Inside A Wormhole?

A long time ago, in a universe much larger than our own, a giant star collapsed. Its implosion crammed so much mass and energy together that it created a wormhole to another universe. And inside this wormhole, our own universe was born. It may seem fantastic, but a theoretical physicist claims that such a scenario could help answer some of the most perplexing questions in cosmology. http://bit.ly/wormholes

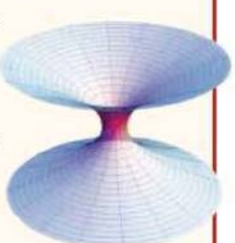

Earth-Like Planets May Abound In Milky Way

Observations of formerly sunlike stars called white dwarfs suggest that the overwhelming majority of them once harbored at least one rocky world. And because sunlike stars could account for up to half of the Milky Way's population of several hundred billion suns, that means thousands or even millions of civilizations might inhabit our galaxy. http://bit.ly/earth-like

For the full postings and more, go to **news.sciencemag.org/sciencenow**.

NEWSMAKER INTERVIEW

Sean Carroll and the Evolution of an Education Maven

With a paper last week in *Nature*, Sean Carroll would seem to be at the top of his game as a researcher. Yet his career is about to take a new tack: The day before the paper appeared, Carroll, a molecular biologist at the University of Wisconsin, Madison, was named vice president for science education at the Howard Hughes Medical Institute. HHMI President Robert Tjian says it's a tribute to his wide-ranging interests and to the success Carroll has enjoyed in both arenas. "He most closely matched the totality of attributes that we were searching for," says Tjian.

A member of the U.S. National Academy of Sciences, the 49-year-old Carroll is a pioneer in the field of evolutionary development. (His most recent paper describes how the polka dots on a fruit fly wing were patterned according to the distribution of a molecule involved earlier in the fly's development.) He has become increasingly engaged with public education over the past 6 years. His *Remarkable Creatures: Epic Adventures in the Origins of Species* was a 2009 National Book Award finalist, and last fall he began writing a monthly column for *The New York Times*. Last month, he received the 2010 Stephen Jay Gould Prize for his outreach efforts. Already a longtime HHMI investigator, Carroll this fall will succeed Peter Bruns as head of the institute's $75 million education portfolio.

Science educator Toby Horn of the Carnegie Institution for Science in Washington, D.C., is thrilled with Carroll's new job. "He's really there for teachers," she says. And biologist Susan Wessler of the University of Georgia, Athens, who has had HHMI support for her undergraduate teaching but was worried because HHMI has recently reduced support for that program, is also pleased. "It sends a very strong message that they are serious about science education. For those of us who had concerns, we are assuaged."

Science caught up with Carroll last week to ask him about his new job.

–ELIZABETH PENNISI

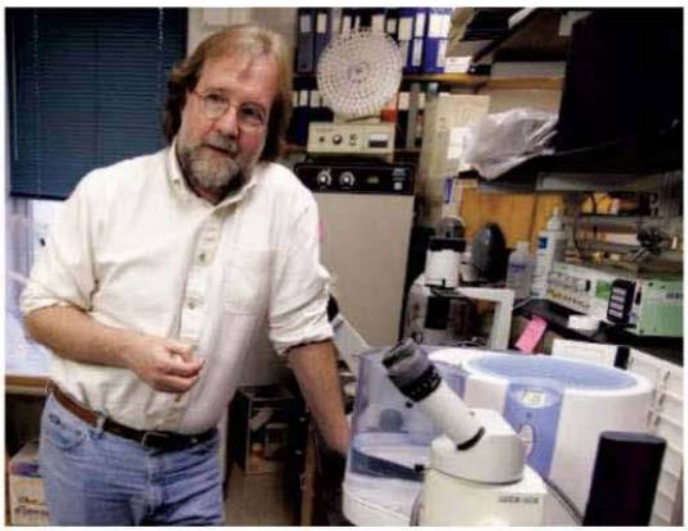

Career shift. Sean Carroll will be spending less time in the lab and more time on science education.

Q: What's the most effective way to do science education?

S.C.: It's a big landscape. There's a continuum there, which is young kids that you want to inspire to have a curiosity about science, slightly older kids that if they are curious about science, you want to encourage them on that path, and then kids who are committing to paths in science, [making sure] that they get inspiring and effective instruction, mentoring, hands-on research experience, et cetera. That's why Hughes is doing lots of different things, as is the National Science Foundation [NSF], as are other organizations.

Q: How does NSF's mission differ from what HHMI is trying to do?

S.C.: HHMI research funding operates on a fundamentally different principle from government funding by backing people, not specific projects. And HHMI explicitly encourages major risk-taking. On the education front, HHMI has the same latitude. Think of HHMI as a venture capitalist. We and our grantees can try a lot of different ideas and approaches.

Q: What has been your most rewarding science education experience?

S.C.: I think the most rewarding for me has been contact with teachers. Now that's probably mostly high school teachers. I think they are a really important and valuable constituency.

Q: What are their biggest concerns?

S.C.: Well, we probably were brought together over the teaching of evolution. That was issue [number] one, … because biology without evolution is kind of like physics without gravity. It's also sort of a canary in the coal mine for the state of science education. There's so much propaganda against evolution, but you see the same sort of techniques being used against climate science or stem cells or whatever it might be.

Q: What are your plans for Hughes?

S.C.: I would say one of the most obvious differences, I think, between the research community that I'm part of and the education community is that in the research community, when anyone has a new tool, a new widget, it often spreads like wildfire. But I think in education, it's a little different. I think campuses have a more local focus. And yet, when it comes to teaching, obviously, what works in Alaska can work in Arkansas and can work in Pennsylvania. I think Hughes can play a role in disseminating good ways of doing things. One of my interests is general public science education, so I think we'll be looking for ways to expand our presence there.

Q: Has the amount of time you've actually spent doing research changed in the last 5 years, and will it change again in this new job?

S.C.: I'm going to spend 80% of my time in the science education role with Hughes. I'll maintain a lab, but I know there's a clear delineation of where my effort's going to be. The University of Wisconsin has released me from teaching. So I'm not going to be in the classroom here.

Q: Why would a master educator abandon the classroom but remain active in the lab?

S.C.: It is not a matter of abandoning [the classroom], it is really a matter of scheduling. It is not realistic to carry out this job and to teach on a typical Monday, Wednesday, Friday schedule. Moreover, it is very important to recognize that classroom teaching is not the only way to contribute to undergraduate education; in my case books and textbooks, articles, DVDs, TV programs, and public lectures all reach undergraduates here at Wisconsin and beyond. So, no, it is not a matter of valuing research over teaching, it is a matter of managing a breadth of activities in the time available.

CREDIT: JEFF MILLER/UNIVERSITY OF WISCONSIN, MADISON

AGRICULTURE

Biotech Crops Good for Farmers and Environment, Academy Finds

Fourteen years after genetically engineered crops began to take off in the United States, the overall benefits to farmers are clear, according to a new report from the National Research Council (NRC) of the National Academies. The shift from conventionally grown crops has paid off economically and environmentally, says the panel. "We can stop arguing about whether the environmental and economic impacts are significant," says agricultural economist Nicholas Kalaitzandonakes of the University of Missouri, Columbia, who was not on the panel.

The debate about impacts of genetically engineered crops on farms has been driven in part by the variability of agriculture. Whether a study shows that a farmer benefits from going biotech can depend on the particular crop, location, and factors such as the abundance of pests. In the past, some researchers and advocates have cherry-picked data to back their views about whether or how much the technology helps farmers, Kalaitzandonakes says.

Going green. Rather than plowing, farmers can control weeds by spraying biotech crops with herbicides, which lessens soil erosion and reduces fuel costs.

CREDIT: BILL BARKSDALE/AGSTOCK IMAGES/CORBIS

The NRC panel sifted through the peer-reviewed literature before coming to its main conclusion. Most of the impacts are relatively straightforward, at least in principle. When corn is enhanced with a bacterial gene for a toxin that kills insects, for example, farmers can spray less of dangerous insecticides, which is good for their bottom line and for wildlife. Another common approach—soybeans outfitted with a gene that renders them immune to the herbicide glyphosate—reduces the need to till fields to control weeds, resulting in less soil erosion. The overall amount of herbicide used has increased because glyphosate-resistant biotech crops can be sprayed with impunity, but glyphosate has generally replaced more toxic herbicides.

Still, many effects need to be better studied. Reduced tillage could offer the "largest single environmental benefit of GE crops," the panel found, because it should mean less sediment, fertilizer, and pesticides washing into streams. But this hasn't been proven, so the panel recommends that the U.S. Geological Survey investigate the impact of reduced tillage on water quality.

The panel also warns that existing gains aren't guaranteed. For instance, insect or weed resistance could render genetically engineered crops ineffective and force farmers to resume using more toxic chemicals (*Science*, 25 May 2007, p. 1114). Economist Paul Mitchell of the University of Wisconsin, Madison, agrees that more needs to be done to slow the evolution of resistant weeds, such as spraying more than one kind of chemical. "Glyphosate is a once-in-a-century herbicide," Mitchell says, referring to its relatively benign side effects. The risk of losing it is a major worry, he says, although new kinds of crops could help thwart resistance.

Another concern is that industry mergers and the dominance of a few players might stifle competition, an issue the Department of Justice is examining. "If we're going to spur innovation, we need a very competitive industry," says economist David Ervin of Portland State University in Oregon, who chaired the panel.

Biotech corn, soy, and cotton are firmly entrenched in the United States, but the report could help win support for other engineered crops, such as wheat and potatoes, observers say. And it could help inform policymakers in countries trying to weigh environmental benefits and risks of biotech crops. "Most of these countries around the world are looking at us in terms of resolving the debate," Kalaitzandonakes says.

–ERIK STOKSTAD

**The Impact of Genetically Engineered Crops on Farm Sustainability in the United States*. The National Academies Press, 2010.

*Science*Insider

From the *Science* Policy Blog

Prominent Old Testament scholar Bruce Waltke has been forced to resign from the Reformed Theological Seminary, an evangelical seminary with a branch in Oviedo, Florida, after saying evangelical Christianity is going to be sidelined as a "cult" if it denies evolution. A video of the talk was made during a workshop at the BioLogos Foundation. http://bit.ly/bBGIPn

Ethiopia has launched its first science academy. The independent **Ethiopian Academy of Sciences** in Addis Adaba will provide advice to the government and promote science, technology, and science education. Demissie Habte, a pediatrician, has been elected president. http://bit.ly/anrAli

The United States has forsworn nuclear attack against nonnuclear countries as long as they comply with their nonproliferation commitments under different international treaties. The new policy, part of a long-awaited **Nuclear Posture Review**, would preclude launching a nuclear offensive against any country in retaliation to a chemical or biological attack. http://bit.ly/amLIRy

A resounding majority of members of the London-based **Royal Institution** have voted to retain its current governing council. The vote quashes an effort to turn back the council's recent dismissal of controversial director Susan Greenfield. http://bit.ly/9WM99l

U.S. Energy Secretary Steven Chu said he plans to proceed with the termination of Nevada's **Yucca Mountain nuclear waste repository** despite congressional opposition. "We believe we do have the legal authority to do this," Chu said. http://bit.ly/desnkv

After *Science*Insider asked readers for ideas, blog commenters proposed the following **names for newly discovered element 117**, among others: StevenColbertium, Perelmanium (after the mathematician Grigori Perelman), Dubnaium (after the town in Russia where the element was discovered), and Chrysanthemum. http://bit.ly/dqUYbK

For the full postings and more, go to **news.sciencemag.org/scienceinsider.**

ASTRONOMY EDUCATION

Telescopes for the People

The International Year of Astronomy (IYA) 2009 has come and gone, but Rick Fienberg is still catching his breath. As leader of the Galileoscope project, one of the most ambitious parts of the global IYA campaign, his work was supposed to be wrapped up by now. The original goal was to put telescopes in the hands of the millions of people attending IYA events. But then the global financial crisis hit. The scientists on Fienberg's team were forced to become instant entrepreneurs to keep the Galileoscope project alive. One "insane" year later, they've pulled it off. "It has had a truly global impact," says Pedro Russo, the coordinator of the IYA based in Garching, Germany.

The ultimate aim of the IYA was "to help the citizens of the world rediscover their place in the universe." What better way to do that than give them their own telescopes? Fienberg says that when he proposed the idea at an astronomy meeting 3 years ago, "it was immediately embraced." And as the longtime editor of *Sky & Telescope* magazine, Fienberg had all the right connections to make it happen. The plan was to use "start-up money from a major donation," he says, and then partner with "an existing commercial telescope manufacturer so we could take advantage of their distribution network."

The device had to be powerful enough for people to see what Galileo first saw 400 years ago—the lunar landscape, the rings of Saturn, the moons of Jupiter—but also cheap enough to distribute, says Fienberg, "especially in developing countries." He was joined by Stephen Pompea, an astronomer at the U.S. National Optical Astronomy Observatory in Tucson, Arizona, and Douglas Arion, an astronomer at Carthage College in Kenosha, Wisconsin.

Because seeing the innards of the telescope would be as important for education as viewing celestial objects, the instrument would be taken apart and put back together on a daily basis—and yet it must cost no more than $30. (Charitable support would drive the price of the telescopes below $10.) The solution was a plastic clamshell design with the lenses locked in place by internal slots. Engineering by their manufacturing partner, Thomas Smith, the owner of U.S. company Merit Models, proved crucial, says Arion, ensuring that "all the tolerances were met [and] the parts fit together well."

The final instrument was far more powerful than Galileo's telescope. Rather than a 20-fold magnified view of 10 arc minutes of sky—far narrower than the face of the moon—the Galileoscope was designed to magnify as many as 50 times and comfortably take in the full moon in a single view.

Stargazing. Middle school students peer through Galileoscopes at the Arizona state capital in March.

The lenses of the Galileoscope also correct for distortions called chromatic aberrations that Galileo's original telescope produced.

By late 2008, they had a prototype Galileoscope ready to go. And that's when the financial floor fell out from under them. In the wake of the financial crisis, says Fienberg, "the donation didn't materialize, and telescope manufacturers lost interest in working with us on a project that wasn't designed to make any real money." At that point, they might have thrown in the towel, but the Galileoscopes were already locked in as a "cornerstone project" of the IYA, says Fienberg. "So three of us formed our own new company, Galileoscope LLC."

The business faced a daunting challenge. "We had no cash, no capital, and with no profit to be made and no assets, no realistic way to raise funds," says Arion. So the trio spent a significant amount of their own money to create the tooling to manufacture the Galileoscopes. They built a Web site that could handle orders, "and then we bootstrapped from there," using funds from orders to pay for inventory, says Arion. "That's the primary reason why the delivery schedule has been, shall we say, sporadic." Fienberg, Pompea, and Arion prefer not to disclose how much money they each "loaned" the Galileoscope project, but they hope "to get it back out" in the near future.

By the time the IYA launched in January 2009 with global fanfare, the Galileoscopes were far from ready. The first orders weren't met until July. Some of the gap was filled by parallel efforts in the United Kingdom and Japan, which distributed an existing telescope kit to schools in Asia and Africa.

After the summer, huge waves of Galileoscopes finally went out around the globe. Norway bought 15,000 of them. Brazil bought 20,000. By the end of last year, 140,000 Galileoscopes were delivered. Orders for another 40,000 will be fulfilled in the coming weeks, pushing the total to 180,000. "Pretty good considering the late start we got," says Fienberg. And because most of the telescopes went to "schools, planetariums, and science museums, they'll be used by dozens or hundreds of people each," he adds.

The Galileoscopes are already taking on a life of their own. "This spring, 15,000 telescopes will be distributed to teachers nationwide," says Pompea, with workshops organized through the National Earth Science Teachers Association. Meanwhile, Chi-kwan Chan, an astrophysicist at Harvard University, is preparing to take a Galileoscope across North America by bicycle. He'll be teaching astronomy, measuring light pollution, and sharing astronomical photographs on a live blog (www.bikexus.blogspot.com). "Yes, I am a geek," says Chan.

But the future of the Galileoscope project is uncertain. The hope is to keep producing the telescopes, "but we can't maintain the level of volunteer effort we've put in during the past year," says Fienberg, who is now director of outreach for the American Astronomical Society. The team is hunting for an organization or company willing to take over their labor of love. So far, no takers.

–JOHN BOHANNON

Online
gonzoscientist.org
Introducing villagers to telescopes in Senegal.

CREDIT: ROBERT SPARKS (NOAO)

NEUROSCIENCE

New Guidelines Aim to Improve Studies of Traumatic Brain Injury

It's still dark outside as neurosurgeon Geoffrey Manley greets a visitor in the lobby of San Francisco General Hospital. "It's been a busy night," Manley says. An overnight rain has made the roads slick. "We just got a guy who was ejected from the back seat of a car," Manley says. "He wasn't wearing a seat belt."

The U.S. Centers for Disease Control and Prevention estimates that 1.7 million Americans suffer a traumatic brain injury (TBI) each year in car accidents, falls, or other mishaps. Unfortunately, the doctors who treat them have limited options. Despite promising leads from animal research, dozens of drugs intended to protect the brain after injury have failed in clinical trials.

Manley thinks part of the problem is an outdated system used to classify TBI patients for trials. (For a perspective on obstacles to drug development, see the 14 April issue of *Science Translational Medicine*). Manley has been a leading force in an initiative to improve the way TBI patients are characterized for clinical trials and other studies. A rough draft of new guidelines was released on 1 April by one of the project's sponsors, the National Institute of Neurological Disorders and Stroke,* and they will be described in detail later this year in a special issue of the *Archives of Physical Medicine and Rehabilitation*. Manley, who co-directs the Brain and Spinal Injury Center at the University of California, San Francisco, recently received a $4.1 million Grand Opportunities Grant from NINDS to study at four U.S. medical centers whether it's feasible to collect up to 500 pieces of information on individual TBI patients and to standardize brain scans and other measurements so they can be compared across centers. If it succeeds, the project's leaders hope the methodology will be widely adopted.

One of the primary tools now used to assess TBI patients, the Glasgow Coma Scale (GCS), has been in use since the 1970s. It rates patients' eye movements, limb movements, and speech. Scores range from 3 (comatose) to 15 (fully awake and responsive). Doctors describe patients' injuries as mild (13 or above), moderate (9 to 12), or severe (8 or below), and researchers use these groupings in clinical trials and observational studies. Sorting patients by their GCS scores makes sense when you're triaging patients in the emergency room at 3:00 a.m., says Manley, but it's an awfully coarse tool for research: "We're taking one of the most complex, heterogeneous disorders in the most complex organ in body and dumbing it down to mild, moderate, and severe."

Two people with the same GCS score can have very different brain injuries, Manley says. One patient, for example, might have a subdural hematoma, an expanding pool of blood between the protective layers surrounding the brain, whereas another might suffer from diffuse axonal injury: extensive damage to the white matter tracts that convey signals from one brain region to another. Grouping together two such patients in a drug trial may dilute any therapeutic effects, because a drug that helps patients with subdural hematoma would likely have a mechanism very different from one that helps patients with diffuse axonal injury.

Several types of TBI can easily be distinguished by CT scans, which have become routine in the decades since the GCS was developed. Although the scans are often used to diagnose patients in the hospital, they're rarely used to sort patients for clinical trials or other studies, says Manley, who would like to change that. This can be tough to do retrospectively, but part of the goal of his pilot study is to standardize CT scans and other measurements taken shortly after an injury so that they can be used to sort patients for research.

Deciding which data are most useful for characterizing patients is one goal of the NINDS "common data elements" project, which is also sponsored by four other agencies, including branches of the Department of Defense and the Department of Veterans Affairs, whose interest in TBI has surged with the tide of soldiers returning home from Iraq and Afghanistan with head injuries. The first draft contains checklists for collecting several categories of patient information, from demographic details to neurological symptoms and CT results.

Andrew Maas, a neurosurgeon at University Hospital Antwerp in Belgium, helped draft the new guidelines and hopes they can be applied globally to make it easier to compare findings across studies. He and colleagues recently analyzed data sets for 11 large TBI observational studies and clinical trials in Europe and North America. It was far more work than his team imagined because the studies differed in which variables they measured, how they measured them, and how they were coded in their database. "It took 10 person-years just to transform the data into a format we could work with," he says.

Still, the utility of the guidelines will depend on how they're used, says John Whyte of Moss Rehab, a rehabilitation center in Elkin Park, Pennsylvania. There needs to be a balance between standardizing data collection and bogging down researchers with long lists of data elements that may or may not be relevant for a given study, Whyte says.

Meanwhile, as Manley leads a cluster of medical residents on rounds, each patient they visit illustrates how a life can be altered in an instant by a fall, a crash, or even a punch to the head. Some are likely to recover; others aren't. For all of them, better science can't come soon enough. **–GREG MILLER**

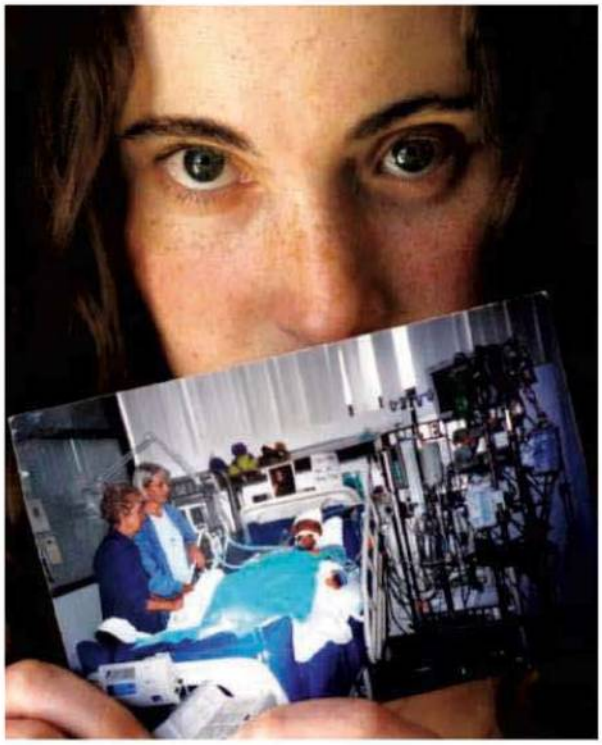

A good outcome. Linda Sparks of Huntington Beach, California, holds a photograph of herself unconscious in the hospital with a TBI caused by a car accident.

CREDIT: LEONARD ORTIZ/ ZUMAWIREWESTPHOTOS/NEWSCOM

*www.ninds commondataelements.org/TBI.aspx

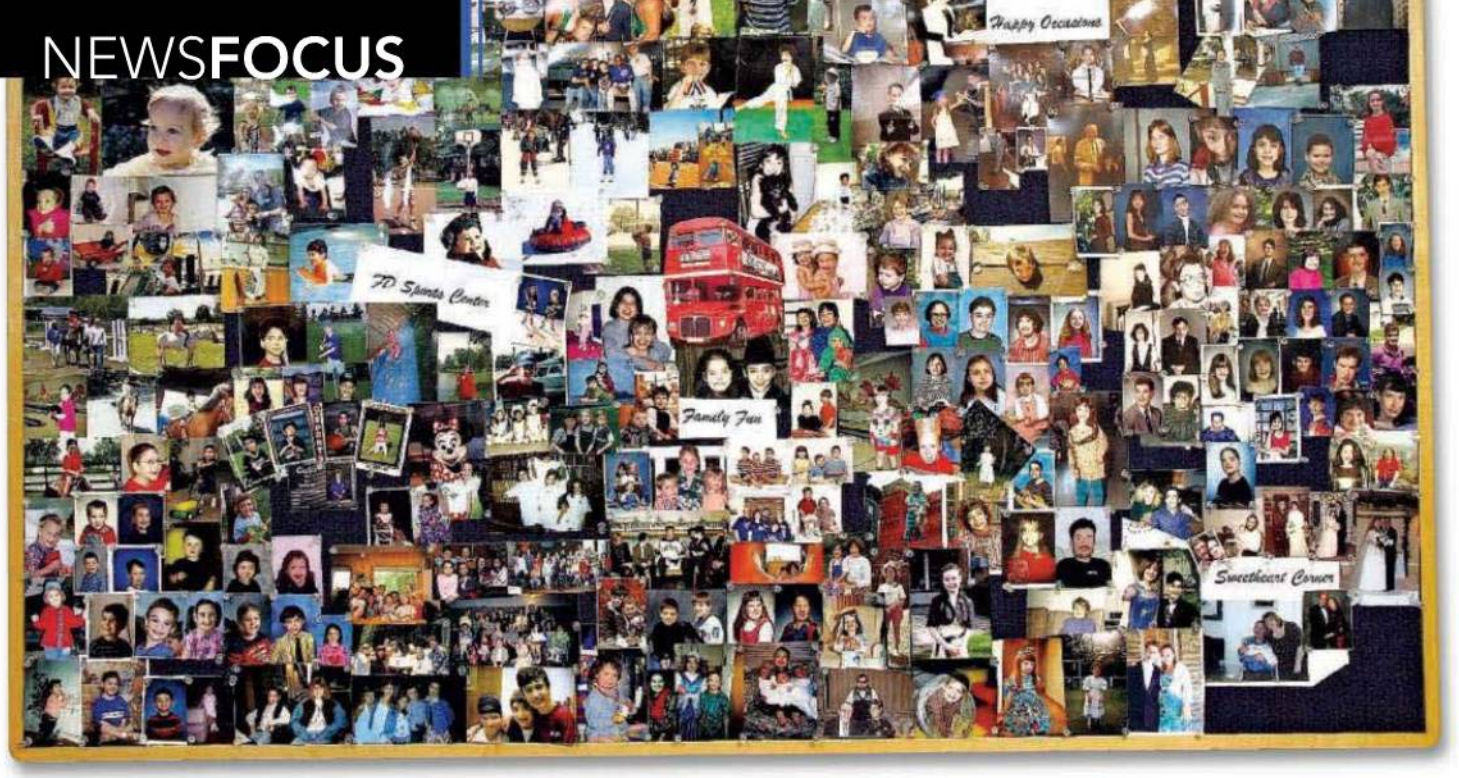

Chasing a Disease To the Vanishing Point

Genetic testing is making a rare disease, familial dysautonomia, even rarer. At the same time, more tools than ever are available to study it

NEW YORK, NEW YORK—When suite 9Q in the neurology department emptied out a few years ago, Felicia Axelrod knew that this cluster of offices and exam rooms was destined to be hers. "I had to have it," says Axelrod, a pediatrician at New York University Langone Medical Center in New York City, whose diminutive stature belies her resolve. She met with the neurology chair to press for a move from the third floor. "I was a pit bull," she says. Axelrod was soon ensconced in 9Q—making her perhaps the only physician in the country whose office address is the same as the address of the gene for a disease that's consumed all 40 years of her career: familial dysautonomia, located on chromosome 9Q31.

Familial dysautonomia (FD) brutalizes the autonomic and sensory nervous systems. Patients have difficulty swallowing, speaking, coughing, and walking; they lack sensitivity to pain, leaving them at risk of burns and broken bones; and their blood pressure swings from extreme highs to faint-inducing lows. As one researcher puts it, patients with FD are "at the mercy of their emotions" because their blood pressure and heart rate are improperly regulated. Excitement about a birthday party, or anxiety about a school test, can send them into paroxysms of retching, drooling, nausea, and soaring blood pressure, a state known as crisis. "The first crisis I saw, I got so scared," says Horacio Kaufmann, a neurologist who works with Axelrod. "I thought the patient was going to explode."

Most physicians have never seen a person with FD. That's because nearly all of them find their way to Axelrod, who opened her FD clinic back in 1970. But there's another reason FD patients don't show up in waiting rooms: The rare disease has gotten even rarer, thanks to widespread genetic testing that has led prospective parents with the gene to avoid or terminate affected pregnancies. FD is almost exclusive to the Ashkenazi Jewish community. The FD gene was reported in January 2001, and within months the push for carrier testing began. The result: In 2009, only five new FD cases were diagnosed in the world, down from about 15 or 20 a year in the 1990s.

FD is just one of a rapidly expanding set of diseases for which carrier testing is available or soon will be (see sidebar, p. 300). In 2001, the American College of Obstetricians and Gynecologists recommended that before having a child all couples be offered carrier testing for cystic fibrosis, the first such push to make carrier testing available to everyone. Last year, a California company called Counsyl began selling a genetic test for $349 that screens for mutations for more than 100 genetic diseases. Technology has advanced to the point that once an individual is being tested for one gene mutation, it's easy to include dozens more. Some of these diseases will become extraordinarily rare—as FD has—though they may never vanish completely.

What does this mean for patients and families living with these conditions, and for physicians and researchers who have dedicated their careers to them? The communities are better off but shrinking at the same time. "We're entering the era of rare disease research and treatment," says Steven Walkley, a neuroscientist at Albert Einstein College of Medicine in New York City who has studied Tay-Sachs disease and related conditions. In August, the U.S. National Institutes of Health (NIH) awarded a consortium $3.5 million to develop gene therapy for Tay-Sachs. Last year, approximately 11 children in the United States were diagnosed with the disease, down from about 100 per year before prenatal testing began.

The same trend affects FD. In Axelrod's waiting room, a toy wooden kangaroo and plastic stacking cups still sit on a miniature

Online
sciencemag.org
Podcast interview with author Jennifer Couzin-Frankel.

CREDIT: FELECIA AXELROD

Memories. These days, few new faces are added to a waiting room collage of familial dysautonomia patients.

table with chairs, but few young children come through the door these days. The average age of patients is now 17. The Dysautonomia Foundation, the advocacy group in New York City that has funded Axelrod's clinic from the start, is struggling to raise money. At the same time, in the past 3 years the clinic has expanded, hiring Kaufmann and his wife, Lucy Norcliffe-Kaufmann, both of whom study autonomic syndromes, and filling a room with high-tech equipment. The group belongs to a newly minted NIH-funded consortium studying rare autonomic diseases and recently scored a grant from the U.S. Food and Drug Administration (FDA) to test a 40-year-old drug for Parkinson's disease in their patients. The irony is that the expanded resources serve a dwindling pool of FD patients.

Untilled terrain

When Axelrod began working on FD, half of her patients died by the age of 5; now half make it to 40. She and her husband, an obstetrician who delivered the first baby born to a woman with FD, in the late 1970s, have always lived across the street from the hospital, in an apartment complex Axelrod looks onto from her office window. Her oldest patient is now 65. "She's the only pediatrician who has patients who have gone through menopause," says David Brenner, executive director of the Dysautonomia Foundation, "because she's had them since they were little kids, and she won't give them up." Axelrod diagnosed Brenner's 22-year-old son Michael with FD when he was 2 years old.

But after going it alone for so long, Axelrod concluded a few years ago that she needed help. Although the number of new FD cases had shrunk to close to zero, she was still treating several hundred teenagers and adults to whom she felt overwhelming responsibility. Meanwhile, the nature of the disease was shifting in ways she didn't understand. Patients were developing kidney failure, which Axelrod hadn't seen before. (Three have had transplants.) Some died suddenly of cardiac arrest, including, last month, a 28-year-old vacationing in Amsterdam with his parents. Axelrod wanted to find a physician with expertise in treating autonomic disease in adults.

"A lot of people would say, 'You're out of your mind because you're betting your career on a disease that's disappearing,' " says Kaufmann, an Argentinean with close-cropped gray hair and blue eyes who came to the United States in 1981. He had what he describes as a cushy job in an endowed chair at Mount Sinai Medical Center on the posh Upper East Side of Manhattan. He left it 2½ years ago, he says, after much "wining and dining" by the determined Axelrod, who persuaded him to throw himself into FD research.

Like so many others who end up devoting themselves to rare diseases, Kaufmann was quickly hooked. FD was like nothing he'd seen before, and the untilled tract of medicine captured his imagination. He recruited 50 of Axelrod's patients—by far the largest FD cohort in a research study—for a battery of tests to better define the disease.

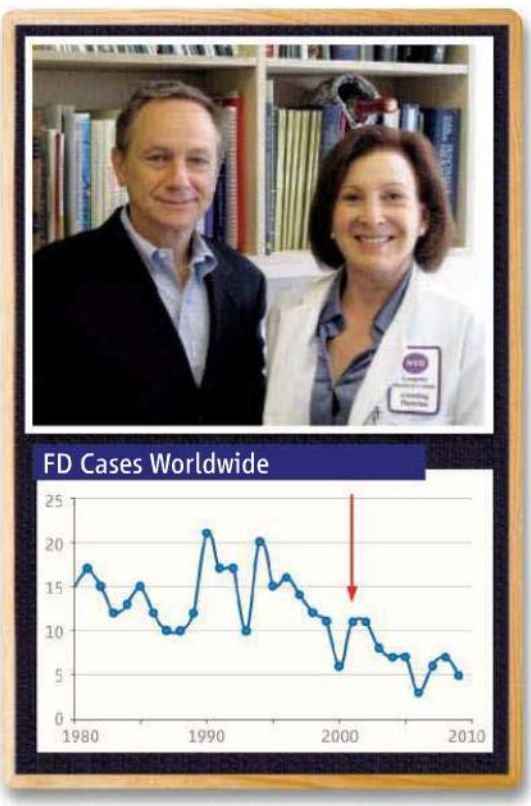

Intensified focus. Felicia Axelrod recruited Horatio Kaufmann to step up work on FD; cases, meanwhile, have declined since carrier testing began (red arrow).

Kaufmann presented his findings this week at a neurology meeting in Toronto, Canada. Among other things, Kaufmann says he discovered that FD patients in crisis produce large amounts of dopamine—something also seen in Parkinson's patients given levodopa, a drug that is converted to the neurotransmitter dopamine. Although extra dopamine counters the effects of Parkinson's, it also causes constant vomiting; Parkinson's patients get a drug called carbidopa to block the production of dopamine from levodopa outside the brain. Carbidopa is never given alone, but Kaufmann wondered if it should be in those with FD. The center received almost $200,000 from FDA to find out, and it will begin testing the drug this month.

Deciding where to focus funding for a disease like FD is difficult. Does it make sense to invest in better managing it in young adults, as Kaufmann wants to do with carbidopa, or to focus on a cure in younger patients, who are healthier but are so few? "You can't pick," says Axelrod. "It's like saying which child do you love more," the 3-year-old or the 23-year-old?

Brenner at the Dysautonomia Foundation agrees. "As long as there's one new baby born, you want to find a therapy that will stop the disease in its tracks," he says. But already, with so few FD births, the Dysautonomia Foundation is finding it tougher and tougher to sustain interest in FD. "This is a real challenge," Brenner says. "Raising money is easier when you have more patients, and when those patients are very sick, young children. It's hard to resist giving money to help children survive." Furthermore, as science has advanced, the research needs—drug development and animal work—have grown more expensive.

The foundation has tried to be more creative about its fundraisers, arranging bowlathons and cycling tours, and it is still raising between $1 million and $2 million a year.

Although winning grants remains an uphill battle, diseases like FD are receiving more government support, even as they grow rarer. If peer reviewers back a proposal, "we do fund them," says Danilo Tagle, the program director in neurogenetics at the National Institute of Neurological Disorders and Stroke in Bethesda, Maryland. His portfolio includes Tay-Sachs, for which the institute last summer awarded $3.5 million over 4 years for a new gene-therapy effort. "Knowledge of this disease will contribute to any number of disorders," says Tagle, explaining why the agency would pour so much money into a disease whose caseload has dropped so much and which is preventable with genetic testing.

Those working in rare diseases are frustrated by talk of their disappearance. That's because, they say, diseases like FD are unlikely to vanish, and studying them holds much value. It "tells us a lot about development and basic biology," says Susan Slaugenhaupt of Massachusetts General

CREDITS (TOP TO BOTTOM): JENNIFER COUZIN-FRANKEL; FELECIA AXELROD

Screening Disease Away

For familial dysautonomia (FD), the goal of screening potential carriers has always been clear: prevent new cases. "I can't imagine an FD parent saying there's a good reason" to have more babies born with the disease, says Amelia Peck, a curator at the Metropolitan Museum of Art in New York City whose 18-year-old daughter, Alice Altshuler, has FD.

When it comes to genetic diseases, deciding who to screen can be difficult. Many early programs targeted specific populations whose members are more likely to carry the disease mutations. In the early 1980s, for example, with broad community support, the government of Cyprus launched an unusual mandatory screening program for the blood disease beta-thalassemia, which was so prevalent that 1 in 150 babies were being born with it on the island. With screening, the disease virtually disappeared. The Jewish community began aggressive enzyme testing for Tay-Sachs in the early 1970s, and that disease has almost vanished among Jews.

But Tay-Sachs shows up in non-Jews as well. While about 1 in 27 Ashkenazis are carriers, about 1 in 250 in the general population are. Most new cases of Tay-Sachs are now in non-Jews, whose physicians don't think to offer them carrier testing or consider it cost-effective.

In the United States, where carrier screening is more available and more accepted than in virtually any other country, "none of us is a purebreed, if you will," says Wendy Chung, who directs the clinical genetics program at Columbia University. "We're literally a melting pot, [and] it's difficult to know what you should screen for" in any given individual.

"I think everyone" should be screened for FD, says David Brenner. "Not everyone is so in tune with their ancestry" that they're aware they may be at risk. Brenner is executive director of the Dysautonomia Foundation in New York City, which has partnered with the California company Counsyl to help it spread the word about carrier screening. It's holding events that bring together dozens of adults who can take Counsyl's carrier test for more than 100 genetic diseases; the company picks up the balance if insurance doesn't cover the full cost.

But as carrier testing expands, its goals are changing. In the past, they were unequivocal: cut down on new cases of a disease. But these days, there is a "reframing," says Wylie Burke, a geneticist and bioethicist at the University of Washington, Seattle. Screening is presented vaguely as "providing options," she says, or offering reassurance to noncarriers. Partly, she believes, that's due to discomfort with aborting affected pregnancies. Screening before pregnancy—the approach Counsyl advocates—rarely happens. Implanting embryos unaffected by disease genes is expensive and "available only to a narrow stripe of people," Burke notes.

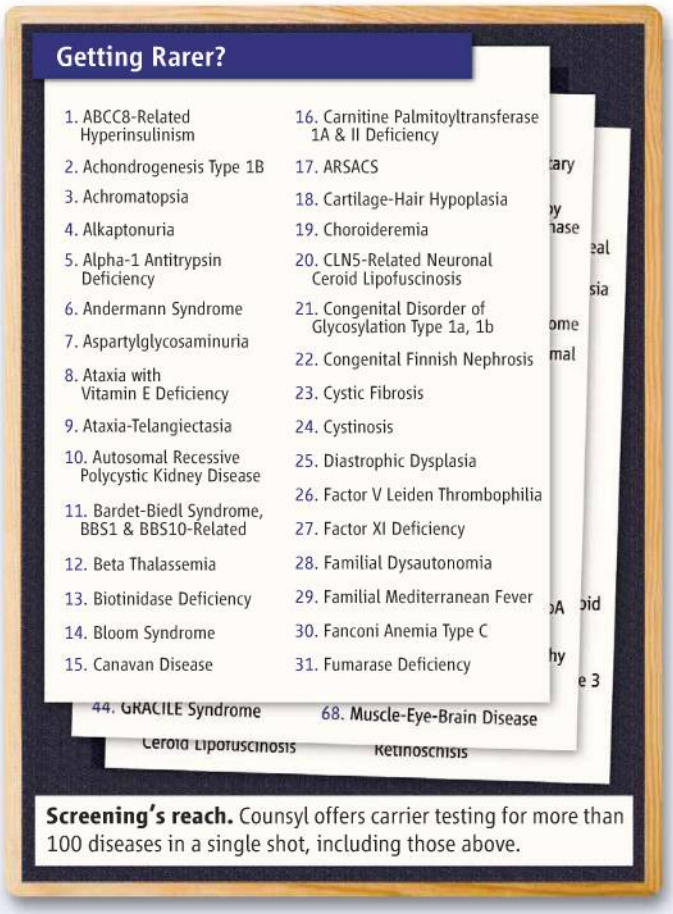

Screening's reach. Counsyl offers carrier testing for more than 100 diseases in a single shot, including those above.

Another reason for ambivalence about screening is that many diseases for which it is available are considered less severe. Canada came out against universal screening for cystic fibrosis (CF) carriers in 2002, rejecting the U.S. policy. In part, that's because its health care system would have had to pay, says Anne-Marie Laberge, a medical geneticist at CHU Sainte-Justine in Montreal, Canada, but also because patients with CF now experience an "improved quality of life." That said, a study of 23 couples in California who learned through prenatal testing that their fetus had CF found that 20 terminated the pregnancy. **–J.C-F.**

Hospital in Boston, who found the FD gene and has since shifted toward developing new treatments. One challenge, she says, is balancing an exclusive focus on the disease with the "big picture": the general implications often needed to justify a grant. The FD team is finding some intriguing details about the disease. For example, says Norcliffe-Kaufmann, they are learning which emotions produce a physiologic response. Excitement often sends the autonomic nervous system, which controls blood pressure and heart rate, into overdrive in an FD patient, but embarrassment doesn't have much effect. Why is that, and what might it tell us about broader connections between blood pressure and emotion? No ones knows.

Sustaining curiosity

It's the morning after the first night of Passover, raining hard, and Axelrod's office is quiet. ("When you work in a Jewish genetic disease, patients don't come in today," she says.) One wall is decorated with dozens of photos of her patients—in karate uniforms, at their bar mitzvahs, with children of their own. She knows them all. Is she worried that others will perceive a now-preventable disease like FD, with only 350 surviving patients worldwide who are slowly dying, as undeserving of money and attention? "Absolutely," she says. Kaufmann, munching on leftovers from Axelrod's seder the night before, explains his efforts to make FD sound "sexy" to other researchers, in hopes of drumming up attention, by describing the underlying abnormalities in their nervous system as opposed to their symptoms. "When you come out with interesting things, you get other bright minds interested," he says. An Australian researcher visited in early April, carting in equipment to study afferent nerve fibers—the nerve cells that convey signals about pain—in FD patients.

For FD families accustomed to leisurely chats with Axelrod, the shift to more intensive research in which they are asked to participate has been somewhat disconcerting, says Kaufmann. But, say Axelrod, Kaufmann, and others, now is the time to probe this disease as never before—and before its numbers dwindle even further.

–JENNIFER COUZIN-FRANKEL

SOURCE: COUNSYL

Besting Johnny Appleseed

With a few tricks, and a lot of patience, fruit geneticists are undoing the work of an American legend

KEARNEYSVILLE, WEST VIRGINIA—Ask how many fruit trees he's responsible for, and Michael Glenn just laughs. "I have no idea," he says.

Glenn oversees some 120 hectares as director of the Appalachian Fruit Research Station here, and seemingly every road leads to a new orchard. Glenn tramps through one rolling 6-hectare plot on a bright day in March, pruning season. Half the branches of some trees lie discarded. After thinking for a moment, Glenn guesses that 315,000 trees live on the station's acreage in the eastern handlebar of West Virginia. To fit them in, the station plants row after row of ash-brown trees, two meters tall and about as far apart, in military formations. The regularity is deceptive.

Even though all these trees are the same species, *Malus x domestica*, the apple, there's no end to the variety of shapes and postures they assume. Glenn, trim, white-haired, points out that some trees grow vertically like elms, while some droop like willows. Some have branches with elbows and right angles, still others lack a central trunk and sprout stalks like bamboo. And that's only part of the variety he'll see when their fruit arrives in late April. Cross two adult fruit trees—a wild variety resistant to disease, say, and a domesticated one with sweet fruit—and there's almost no telling what you'll get.

As slower-breeding plants, apples are not far removed from their wild ancestors, so they have had fewer chances to shed unwanted genes. And apple trees cannot reproduce with close relatives because special proteins recognize their own or similar pollen and choke off reproduction. Growers get consistent varieties only through clonal propagation, and today 11 cloned varieties make up 90% of the apples sold in the United States. This leaves apples vulnerable to diseases and environmental stress. To "update" a popular variety to withstand those traumas, a breeder must cross it with apples with quite different genes, which can dilute or scatter its good qualities.

This genetic roulette makes for interesting walks through orchards but frustrates scientists who want to develop consistent but hearty apples, plums, and pears. "Stringent, ugly, bitter, tiny fruit, squishy, doesn't store well—anything you can think of that will be bad in a fruit—it happens," says Cameron Peace, an apple and cherry geneticist at Washington State University, Pullman.

Traditional breeding, part of what Glenn calls "cultural practices," requires crossing two lines of apples, each with one or a few good traits. The result: anonymous brown pips. Once, the only way to sort the duds from sweet and hearty varieties was to plant them all, an expensive and laborious job. And because first crosses rarely meet supermarket standards, breeders improve them by recrossing the best fruit of each generation with other varieties, up to five times.

A faster approach would be tweaking apple DNA directly with the tools of molecular genetics. But until recently, geneticists, their skills honed on *Arabidopsis* and other quick-breeding flora, avoided fruit-tree research like a blight. Of the 11,000 U.S. field tests on plants with transgenic genes between 1987 and 2004, just 1% focused on fruit trees. That's partly because of the slow pace. Whereas vegetables like corn might produce two harvests each summer, apple trees need eons—around 5 years—to produce their first fruit, most of which will be disregarded as ugly, bitter, or squishy. Given the odds, 315,000 trees can look tiny.

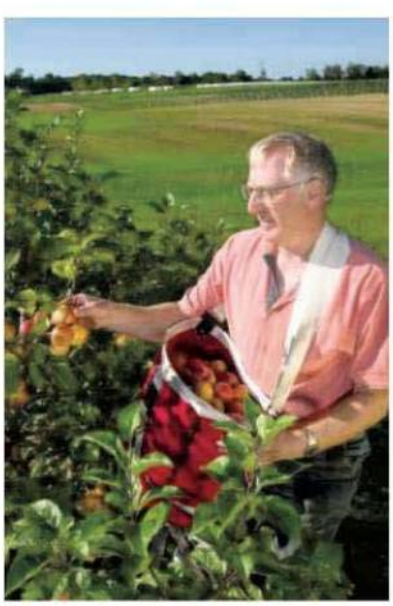

Mr. Appleseed. In New York, USDA's Philip Forsline studies *M. sieversii* (*top*) from wild fruit collected in Kazakhstan.

But everything in apple breeding is about to change. An Italian team plans to publish the decoded apple genome this summer, and scientists at places like Kearneysville, which is run by the U.S. Department of Agriculture (USDA), are starting to single out complex genetic markers for taste and heartiness. In some cases the scientists even plan, by inserting genes from other species, to eliminate the barren juvenile

CREDIT (TOP TO BOTTOM): HELENE BOZZY/ SEPPIA GROUP; PEGGY GREB/USDA

stage and push fruit trees to mature rapidly, greatly reducing generation times. Glenn came of age when someone might spend decades breeding the Johnagold or Fuji. No more. Expectations are changing, and as Glenn says, "The orchards of the future will be driven more by genetics than cultural practices."

Wide variety. Although one species, apples have genes that can change their fruit wildly.

Legends in their times

In the early 1800s, a nomad named John Chapman began wandering through Pennsylvania, Ohio, and beyond, a burlap gunnysack of seeds (as tradition has it) over his shoulder, to spread the apple to the American frontier. That most apple trees he planted gave squishy or crabby fruit didn't make Johnny Appleseed's gifts any less welcome for farmers and hunters eager to make liquors like cider and applejack.

But not all were stringent, and many "dessert" apples with colorful names like Irish Peach, Maiden Blush, and Sops of Wine thrived in America. Unfortunately, Chapman, no geneticist, had drawn on a narrow stock of European apples—itself a narrow selection of wild apples, which are native to Kazakhstan. Other U.S. stocks, spread by pioneers and missionaries, had the same shortcomings, and grafting clones further tapered the line. (Every single Red Delicious traces back to one farm, Jesse Hiatt's, near Peru, Iowa, for example.) Meanwhile, USDA's efforts to breed heartier varieties have proved inefficient and slow.

The foundations for modern apple research were laid in the 1990s. Fittingly, it all started with another trek to the frontier, by another legend among apple breeders. Philip Forsline had already made a name for himself in the 1980s when Cornell University decided to bulldoze its renowned groves of apple trees. Forsline, an apple curator for USDA's Agricultural Research Service, oversaw the transfer of every variety from Cornell in Ithaca, New York, to his USDA research station 70 kilometers away in Geneva, New York, where buds were meticulously grafted onto rootstock.

Even those holdings, however, were genetically narrow, so USDA drew up ambitious collection trips to China and Kazakhstan. Forsline made seven trips to Central Asia in the 1990s, collecting apples from coastlands and inland steppes, from veritable deserts and dense forests where 90% of trees sprouted apples. He saw groves where bears smashed branches to knock apples loose, and among the thousands of shapes he saw a few 8-centimeter beauties "that looked like they could be at the supermarket," he marvels. In all Forsline collected 949 varieties of *Malus sieversii* trees, forerunner to the domesticated apple.

Back in New York state, Forsline recreated the Kazakh and Chinese forests (with humans pruning instead of bears) by planting 1600 seedlings. And as he loves to joke, the work is finally bearing fruit. Over the past dozen years, he and his successor at Geneva, Gennaro Fazio, have monitored which apples could weather cold snaps or dry spells, and which handled "The Gauntlet"—a pestilential greenhouse crawling with pathogens that kills three-quarters or more of all prisoners. After these tests, Forsline and Fazio have identified apples that can withstand nearly any natural evil. The next trick will be identifying the key genes and getting them into the 11 apple varieties Americans covet.

Double trouble

Traditional breeders face two barriers to making better apples, plums, and pears: the staggering inefficiencies and the tedious wait between generations. Genetic work has the potential to eliminate both problems.

As for the inefficiencies, "you can use molecular tools … to screen a large population of seedlings" for genetic markers associated with a desirable trait, explains Gayle Volk, a geneticist at USDA's National Center for Genetic Resources Preservation in Fort Collins, Colorado. If scientists screen for multiple traits, only 10 or so of 1000 seeds may have the right combination, she says, but scientists can focus on those few.

Peace discovered a great example of the potential savings through work on ethylene, a natural hormone that causes fruit to ripen. Breeders want low ethylene levels so that fruit doesn't turn mushy in trucks on the way to stores. Peace has discovered two gene markers for fruit that produce 90% less ethylene, and with his tests, breeders can discard three of every four seeds and possibly save 60% on maintaining groves.

Ultimately, Peace wants to find markers for taste, the most desirable and elusive trait that fruit breeders pursue. Texture and crispness are largely fixed by genes, while all-important sweetness depends heavily on environmental factors, and

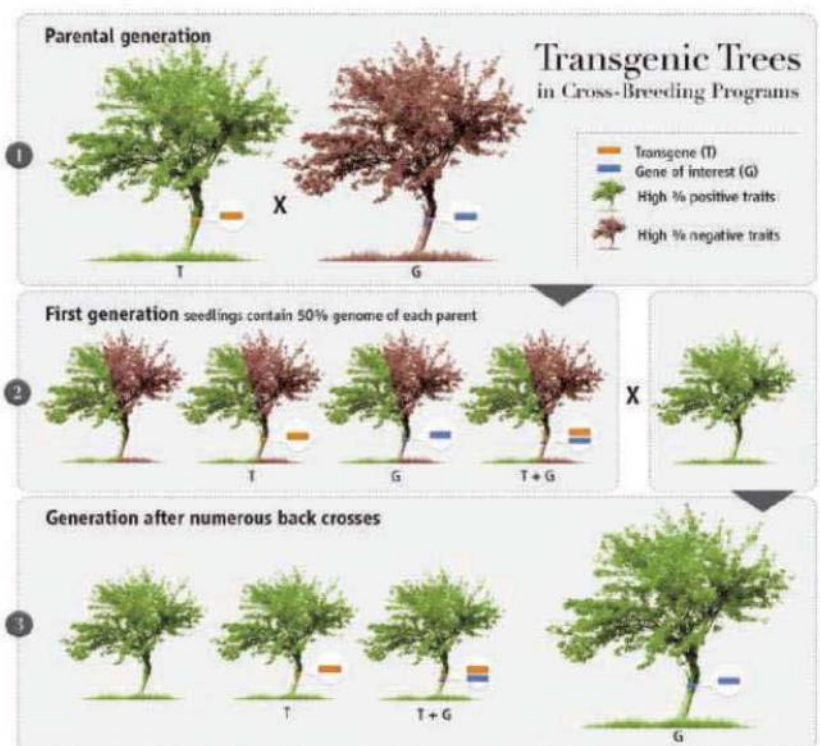

The transgene vanishes. A fast-flowering poplar gene (pink) speeds new fruit varieties. In the middle generations, scientists select for trees with both the poplar gene and a gene of interest (blue). In the last generation, scientists select trees without the poplar gene to avoid the stigma of genetically modified (GM) food.

CREDIT (TOP TO BOTTOM): HELENE BOZZY/ SEPPIA GROUP; (PHOTO CREDIT) ISTOCKPHOTO.COM

scientists don't know the details. But thanks to collaborations like USDA's $14.4 million RosBREED project, Peace thinks geneticists can start finding robust correlations for taste within about 2 years.

Still, even the best screening won't solve the second problem, that fruit trees mature so slowly. But scientists at Kearneysville, in collaboration with scientists at a few universities, may have a shortcut. In the next 6 months or so, Kearneysville geneticist Jay Norelli will begin a project to introduce two alleles for resistance to fire blight, a common apple plague, into dessert apples. Using traditional methods, it would take 20-some years to fix this trait into a supermarket-quality apple. But by introducing a "fast-flowering" gene from a poplar tree, Norelli believes he can cut the generation time down to roughly a year.

The process works like this. First, scientists introduce the fast-flowering gene into the chromosomes of a dessert apple, with traditional genetic engineering tools (such as a bacterium loaded with the fast gene). Scientists then cross this altered apple with a complementary variety that might not taste good but is resistant to disease. After this cross, scientists will, as usual, get many dud seeds. But they can screen their DNA and find varieties likely to taste good, mature quickly, and withstand diseases. They discard the rest. Scientists then cross the best of the new generation with another tasty (but not fast-flowering) apple. And once again, they select the best offspring. With each subsequent cross, they become more like dessert apples, except disease-resistant.

Norelli is confident the poplar transgene shortcut can work because colleagues at the research station, led by horticulturist Ralph Scorza, have used it to create fast-flowering plums, a close relative of the apple.

Control plum trees in the Kearneysville greenhouse, which lack the accelerating gene, have sturdy, woody trunks and stand a good meter tall after 12 months. The controls are also barren—and will be for several years until they reach fruit-bearing age. The experimental, "FasTrack" trees look softer and greener, and they slouch. But that's partly because their branches are bowed down from the weight of plums. Sixty more plum-poplar trees are growing outdoors on a few of Kearneysville's 120 hectares. And like Norelli, Scorza will soon begin introducing new traits into the plums, at speeds that would have seemed miraculous 50 years ago.

To determine how sweet the FasTrack plums are, Scorza's team will chemically test their sugar concentration this summer. But no one will know how they taste for some time. Including a poplar gene makes the trees genetically modified (GM) food, and scientists would need government permission to sample them.

Fast track. Genetically modified in the lab (*inset*) to include a poplar gene, plums grow fruit in less than a year, allowing faster breeding.

What's more, no one knows whether poplar genes in fruit will do something unwanted, like shortening the life of the tree.

But the Kearneysville geneticists have a neat trick to circumvent these concerns. Only a fraction of the offspring in each generation contain the fast-flowering gene. Early in the breeding process, scientists discard the trees that lack it. (They search for the gene by doing PCR on a tissue sample.) But once they have fixed a new trait in the fruit, they select *against* fast-flowering in the final generation. This selection involves no genetic engineering: They simply screen the trees (again, usually with PCR), and toss out the ones with the poplar gene. The leftover trees, which mature normally, are no different than if Scorza's team bred them the traditional way. And as long as any new genes came from wild or semiwild fruit, the trees are, almost magically, no longer GM.

As for potential controversies, Scorza argues that the FasTrack system combines "the latest methods of modern biology with a breeding tradition as old as agriculture." And he thinks it will become valuable with global climate change. "Fifteen, 20 years is no longer good enough" to deliver new fruit varieties to a hungry world, he says.

Still, it's telling that not even FasTrack breeders can eat their fruit—a far cry from the American frontier farmer. And opponents of GM food seem unlikely to accept a "non-GM" label for such varieties. Bill Freese, a science policy analyst at the Center for Food Safety in Washington, D.C., has not studied the new FasTrack program but said, "the genetic engineering process is very disruptive" and often changes surrounding DNA. "Our experience with USDA is that they tend to downplay risks with genetic engineering."

What's next

For the next few years, apple, plum, and peach trees will dominate the grounds of places like Kearneysville. But scientists elsewhere are developing ways to maintain the genetic diversity of fruit with as few trees as possible. In Colorado, Volk has studied cryogenic preservation of dormant buds in liquid nitrogen, and the results show promise for reducing the number of trees that must be kept in dirt. Nitrogen tanks cost $1.50 per year per bud to maintain compared with $50 to $75 per orchard tree. And the germ plasm shows no ill effects.

Even at Kearneysville, breeders spend more and more hours indoors in their labs and fewer in the groves. In fact, Glenn says he's become an anomaly—someone who even prunes on occasion. But most traditional breeders, Glenn included, are eager to eliminate all the tedium and heartache of traditional methods. "Personally, I am nostalgic for the so-called better days, but I think this is the natural progress of science," he says. What's more, in the past 5 years, "the molecular biologists are coming back to the field-oriented scientists to collaborate with them on projects in the field."

So although the informal days of Johnny Appleseed are gone forever, fruit breeders still have a place, and scientists are trembling with excitement at the possibilities. Forsline estimates that his trips to Asia have doubled the known stock of apple genes in the world. Johnny Appleseed may have made the American apple in the 1800s, but as Forsline has written of modern fruit work, "All of this—and forthcoming findings—may one day put the impact of [USDA research] on a par with that of John Chapman's legendary work."

–SAM KEAN

CREDITS: CHRIS DARDICK USDA-ARS; (INSET) RALPH SCORZA USDA-ARS

ENGINEERING

Nanogenerators Tap Waste Energy To Power Ultrasmall Electronics

Tiny devices that convert movements into electricity won't power cities. But they may soon be efficient enough to power arrays of invisible sensors and hand-held electronics

In the corner of a conference center on the main campus of Microsoft in Redmond, Washington, engineers have built a small four-room apartment. Called MS Home, it serves as both a testing ground and a showcase for how the future home may look and, well, behave. In Microsoft's vision, that home will be run by a computer system that turns on lights, controls the heat, and manages the appliances. An array of invisible sensors would do everything from tracking your movements (in order to know when to turn the lights on in the next room) to monitoring whether your plants need water.

Uses of sensor networks have been talked about for years. One stumbling block has been figuring out how to power the devices. Sure, each one could be plied with batteries or wired to the grid. But that is expensive and requires periodic maintenance, which often upends such proposals. Now, however, the rise of a new technology to scavenge power from vibrations and other ambient sources may finally usher this vision of the future into the present.

Power scavengers have actually been around for some time. Companies, for example, already make larger scale devices that harness vibrations to monitor the structural health of buildings and bridges. But over the past few years, researchers have been progressively shrinking these scavengers to nanoscale dimensions in an effort to power everything from minuscule sensors inside the body to arrays of self-powered environmental sensors to monitor things such as air quality and stream flows. This miniaturization push has been aided by the steady progress of microelectronics technology, which now turns out sensors and computing devices small enough and frugal enough with their energy needs that many can be powered with just nanowatts to microwatts of power.

Today, the field "has now reached a critical mass and momentum," says Zhong Lin Wang, a physicist at the Georgia Institute of Technology (Georgia Tech) in Atlanta. "I am confident that with the way things are progressing, this will one day soon impact our daily lives."

Although several technologies are competing to power such devices, most nanogenerators are made from piezoelectric materials that convert mechanical motion into electricity. Piezoelectric materials, such as crystals of the ceramic lead zirconate titanate (PZT), are made of subunits that separate electrical charges. Mechanical strain, such as bending a thin piezoelectric wire, changes this electric polarization of the material and causes positive and negative charges to migrate to opposite faces of the material, creating an electric voltage that can be used to do work. The effect can also be reversed: Applying a voltage across a piezoelectric crystal causes it to move. This effect—first discovered in 1880—is behind decades of technology; sonar detectors, loudspeakers, autofocusing cameras, atomic force microscopes, and many other gadgets.

Today the most widely used piezoelectric material is PZT, as it is the most efficient material at converting mechanical strain to electricity. But PZT has its drawbacks. For starters, it is brittle and breaks easily. It also contains lead, a toxic metal, which makes it a poor choice for powering medical sensors in the body.

Now, researchers may have found a way around PZT's shortcomings. In the 10 February issue of *Nano Letters*, researchers led by Michael McAlpine, a chemist at Princeton University, reported the creation of a flexible PZT nanogenerator encapsulated inside a biocompatible plastic. McAlpine notes that whereas large crystals of PZT are brittle, ultrathin ribbons of the material can bend and flex without breaking. So McAlpine's team grew a thin layer of PZT atop a crystal of magnesium oxide (MgO) and then used a lithographic patterning technique, akin to that used to pattern microchips, to pattern the PZT into an array of long ribbons. They then dissolved the MgO substrate, leaving the ribbons behind, and pressed a rubbery plastic known as PDMS on top, transferring the PZT nanoribbons to the plastic (see bottom figure, p. 305). Several characterization studies showed that the transferred PZT nanoribbons retained their same piezoelectric properties, and they were roughly four times as efficient at transferring mechanical strain to electricity as were competing nanogenerators.

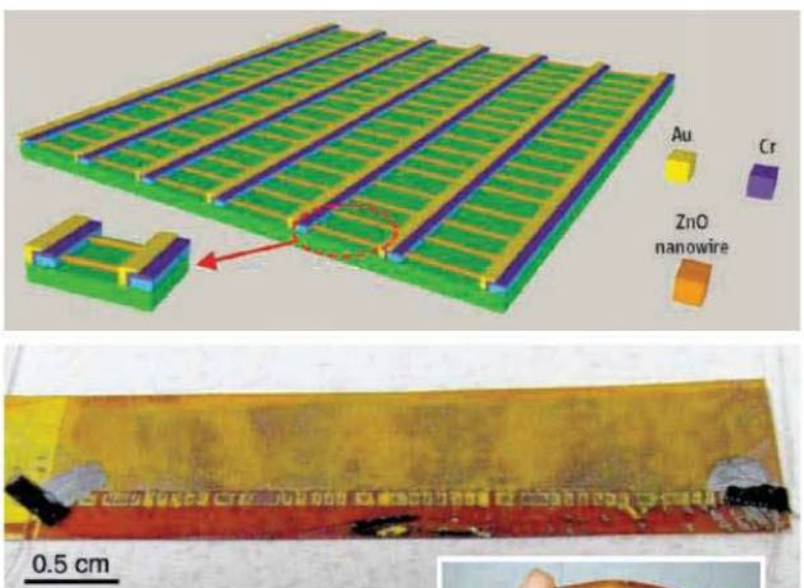

Good vibrations. Zinc oxide (ZnO) nanowires are grown between chromium (Cr) and gold (Au) electrodes (*top*) to make a nanogenerator that produces a high voltage when flexed.

Still, flexible PZT nanoribbons have a way to go before they are ready to power real devices, McAlpine says. Among the steps still needed is to refine the PZT nanowire growth techniques. McAlpine says it should be possible to improve the power output of the devices 10-fold. Also, he says, scaling the technique up to make larger arrays would help to power more types of devices.

If efforts to make PZT nanogenerators more flexible and biocompatible don't succeed, alternatives are moving in to pick up the slack. Wang and his colleagues at Georgia Tech, for example, have pushed nanogenera-

CREDITS: S. XU ET AL., *NATURE NANOTECHNOLOGY* (PUBLISHED ONLINE 28 MARCH 2010) ©2010 MACMILLAN PUBLISHERS LIMITED

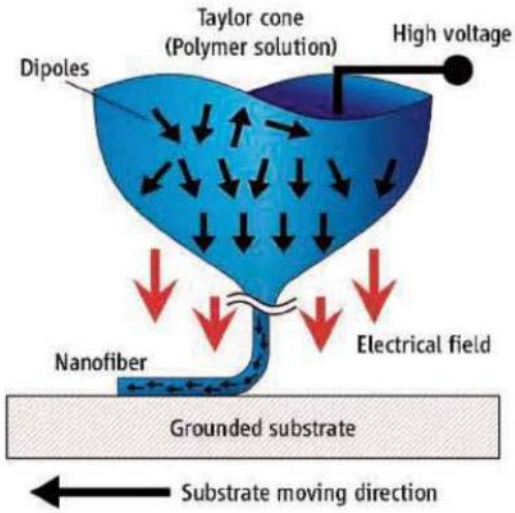

Power threads. A large electric field orients electric dipoles in a polymer being drawn into fibers.

tors made from zinc oxide (ZnO) nanowires considerably further than their PZT cousins. In 2006, Wang and his student Jinhui Song reported in *Science* that they grew arrays of vertical ZnO nanowires that when bent to the side created a small electric voltage (*Science*, 14 April 2006, p. 242). In the years since, Wang's team has developed successive iterations of their ZnO nanogenerators in an effort to increase the power output and robustness.

Last month, they raised the bar to the highest point yet. In a paper posted online in *Nature Nanotechnology* on 28 March, Wang and colleagues reported making two new nanogenerators. One produced the highest voltage of any nanogenerator to date; the other produced a lower voltage but was rigged up to power either a pH sensor or an ultraviolet detector without need for any outside energy. Both nanogenerators were made by growing arrays of long, thin zinc oxide nanowires. In the version wired to the sensors, these nanowire collections resemble a bed of nails with thin electrodes placed on the top and bottom. When the researchers then squeezed their device—thereby bending the nanowires—it produced 0.24 volts, with enough current to run their sensors. "That's pretty cool," says McAlpine, who credits Wang for pioneering several nanogenerator concepts.

One of those was Wang's higher voltage nanogenerator. Pushing the output is important, Wang says, because most devices today need more than one-quarter of a volt to run. Standard AA battery–powered devices, for example, require up to 1.5 volts to operate—well beyond what most nanogenerators can generate.

To make a higher voltage device, Wang and his colleagues needed to find a way to make the voltage output of individual nanowire devices add up. To do so they needed to orient the crystallographic axis of each ZnO nanowire in the same direction so that when force was applied to them all collectively, the polarity of charges on each wire would be aligned, producing a higher output voltage. Wang's team patterned an array of parallel chromium wires atop a substrate. They then grew thousands of ZnO nanowires laterally between these wires, like rungs in a ladder, under conditions that ensured they all grew with the same crystallographic orientation. Finally, they soldered the ZnO nanowires to the chromium by depositing gold at the connection points (see figure, p. 304). The scheme worked. When they flexed their array, it generated 1.26 volts. That's not quite the 1.5 volts of a AA battery, but in the months since their paper was submitted, Wang says his team has upped that output to 2.4 volts. "This enables us to operate true technology," Wang says.

The Georgia Tech group isn't the only one closing in on that goal. At the University of California, Berkeley, another nanogenerator group, headed by mechanical engineer Liwei Lin, is making nanogenerators out of long polymer fibers that one day may be woven into cloth. "This technology could eventually lead to wearable 'smart clothes' that can power hand-held electronics through ordinary body movements," Lin says.

For their nanogenerators, Lin and his colleagues start with a polymer called polyvinylidene fluoride (PVDF) that can be processed to separate electrical charges. Other groups have previously made PVDF generators from thin films of the polymer. But PVDF films are typically inefficient, converting only 1% to 2% of kinetic energy to electricity. Lin and his colleagues also reported in the 10 February issue of *Nano Letters* that when they used a technique called electrospinning to spin PVDF into threadlike fibers as little as 500 nanometers across, the resulting fibers converted 10 times as much kinetic energy to electricity as the thin-film PVDF devices did.

Although Lin and his colleagues are still trying to understand exactly why that is, Lin says part of the explanation probably has to do with the electrospinning technique. The method draws out the polymer fibers in the presence of a large electric field, which seems to orient individual polymer molecules better than the filmmaking techniques do (see figure, left). And once the fibers are formed and solidify, this arrangement is locked in place. The output is high enough, Lin says, that calculations suggest that 1000 or so fiber generators incorporated into the cloth of a shirt would capture enough energy from a person's movements to charge a cell phone or an iPod. Although Lin says he hasn't yet formed a company to commercialize his power-suit material, he's already taking visits from venture capitalists looking to do just that.

If nanogenerators of any sort succeed, could they possibly be scaled up to generate large amounts of power? After all, most of the handwringing about energy these days is about how to generate terawatts, rather than microwatts, of carbon-free power. Lin, Wang, and McAlpine agree that for now that doesn't seem likely. Nanogenerators simply produce too little power to change our civilization. For now, they'll be working on the small scale, which might still be enough to change our lives.

–ROBERT F. SERVICE

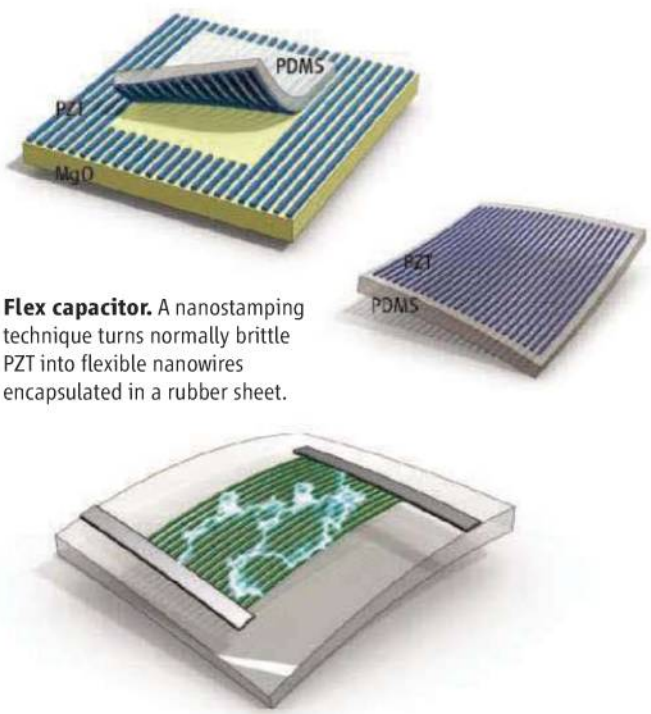

Flex capacitor. A nanostamping technique turns normally brittle PZT into flexible nanowires encapsulated in a rubber sheet.

CREDITS (TOP TO BOTTOM): C. CHANG *ET AL.*, *NANO LETTERS* **10** (25 JANUARY 2010) © 2010 AMERICAN CHEMICAL SOCIETY; Y. QI *ET AL.*, *NANO LETTERS* **10** (26 JANUARY 2010) © 2010 AMERICAN CHEMICAL SOCIETY

ENGINEERING

Nanogenerators Tap Waste Energy To Power Ultrasmall Electronics

Tiny devices that convert movements into electricity won't power cities. But they may soon be efficient enough to power arrays of invisible sensors and hand-held electronics

In the corner of a conference center on the main campus of Microsoft in Redmond, Washington, engineers have built a small four-room apartment. Called MS Home, it serves as both a testing ground and a showcase for how the future home may look and, well, behave. In Microsoft's vision, that home will be run by a computer system that turns on lights, controls the heat, and manages the appliances. An array of invisible sensors would do everything from tracking your movements (in order to know when to turn the lights on in the next room) to monitoring whether your plants need water.

Uses of sensor networks have been talked about for years. One stumbling block has been figuring out how to power the devices. Sure, each one could be plied with batteries or wired to the grid. But that is expensive and requires periodic maintenance, which often upends such proposals. Now, however, the rise of a new technology to scavenge power from vibrations and other ambient sources may finally usher this vision of the future into the present.

Power scavengers have actually been around for some time. Companies, for example, already make larger scale devices that harness vibrations to monitor the structural health of buildings and bridges. But over the past few years, researchers have been progressively shrinking these scavengers to nanoscale dimensions in an effort to power everything from minuscule sensors inside the body to arrays of self-powered environmental sensors to monitor things such as air quality and stream flows. This miniaturization push has been aided by the steady progress of microelectronics technology, which now turns out sensors and computing devices small enough and frugal enough with their energy needs that many can be powered with just nanowatts to microwatts of power.

Today, the field "has now reached a critical mass and momentum," says Zhong Lin Wang, a physicist at the Georgia Institute of Technology (Georgia Tech) in Atlanta. "I am confident that with the way things are progressing, this will one day soon impact our daily lives."

Although several technologies are competing to power such devices, most nanogenerators are made from piezoelectric materials that convert mechanical motion into electricity. Piezoelectric materials, such as crystals of the ceramic lead zirconate titanate (PZT), are made of subunits that separate electrical charges. Mechanical strain, such as bending a thin piezoelectric wire, changes this electric polarization of the material and causes positive and negative charges to migrate to opposite faces of the material, creating an electric voltage that can be used to do work. The effect can also be reversed: Applying a voltage across a piezoelectric crystal causes it to move. This effect—first discovered in 1880—is behind decades of technology; sonar detectors, loudspeakers, autofocusing cameras, atomic force microscopes, and many other gadgets.

Today the most widely used piezoelectric material is PZT, as it is the most efficient material at converting mechanical strain to electricity. But PZT has its drawbacks. For starters, it is brittle and breaks easily. It also contains lead, a toxic metal, which makes it a poor choice for powering medical sensors in the body.

Now, researchers may have found a way around PZT's shortcomings. In the 10 February issue of *Nano Letters*, researchers led by Michael McAlpine, a chemist at Princeton University, reported the creation of a flexible PZT nanogenerator encapsulated inside a biocompatible plastic. McAlpine notes that whereas large crystals of PZT are brittle, ultrathin ribbons of the material can bend and flex without breaking. So McAlpine's team grew a thin layer of PZT atop a crystal of magnesium oxide (MgO) and then used a lithographic patterning technique, akin to that used to pattern microchips, to pattern the PZT into an array of long ribbons. They then dissolved the MgO substrate, leaving the ribbons behind, and pressed a rubbery plastic known as PDMS on top, transferring the PZT nanoribbons to the plastic (see bottom figure, p. 305). Several characterization studies showed that the transferred PZT nanoribbons retained their same piezoelectric properties, and they were roughly four times as efficient at transferring mechanical strain to electricity as were competing nanogenerators.

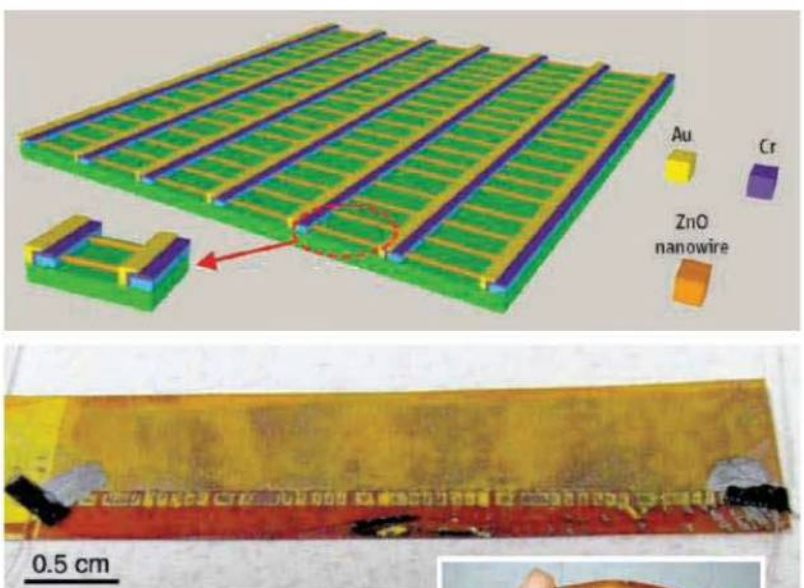

Good vibrations. Zinc oxide (ZnO) nanowires are grown between chromium (Cr) and gold (Au) electrodes (*top*) to make a nanogenerator that produces a high voltage when flexed.

Still, flexible PZT nanoribbons have a way to go before they are ready to power real devices, McAlpine says. Among the steps still needed is to refine the PZT nanowire growth techniques. McAlpine says it should be possible to improve the power output of the devices 10-fold. Also, he says, scaling the technique up to make larger arrays would help to power more types of devices.

If efforts to make PZT nanogenerators more flexible and biocompatible don't succeed, alternatives are moving in to pick up the slack. Wang and his colleagues at Georgia Tech, for example, have pushed nanogenera-

CREDITS: S. XU ET AL., *NATURE NANOTECHNOLOGY* (PUBLISHED ONLINE 28 MARCH 2010) ©2010 MACMILLAN PUBLISHERS LIMITED

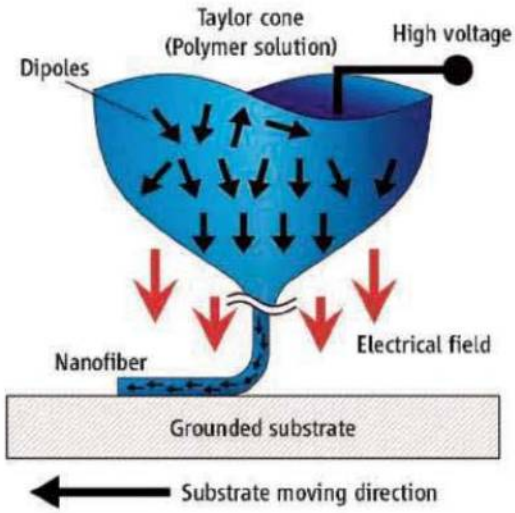

Power threads. A large electric field orients electric dipoles in a polymer being drawn into fibers.

tors made from zinc oxide (ZnO) nanowires considerably further than their PZT cousins. In 2006, Wang and his student Jinhui Song reported in *Science* that they grew arrays of vertical ZnO nanowires that when bent to the side created a small electric voltage (*Science*, 14 April 2006, p. 242). In the years since, Wang's team has developed successive iterations of their ZnO nanogenerators in an effort to increase the power output and robustness.

Last month, they raised the bar to the highest point yet. In a paper posted online in *Nature Nanotechnology* on 28 March, Wang and colleagues reported making two new nanogenerators. One produced the highest voltage of any nanogenerator to date; the other produced a lower voltage but was rigged up to power either a pH sensor or an ultraviolet detector without need for any outside energy. Both nanogenerators were made by growing arrays of long, thin zinc oxide nanowires. In the version wired to the sensors, these nanowire collections resemble a bed of nails with thin electrodes placed on the top and bottom. When the researchers then squeezed their device—thereby bending the nanowires—it produced 0.24 volts, with enough current to run their sensors. "That's pretty cool," says McAlpine, who credits Wang for pioneering several nanogenerator concepts.

One of those was Wang's higher voltage nanogenerator. Pushing the output is important, Wang says, because most devices today need more than one-quarter of a volt to run. Standard AA battery–powered devices, for example, require up to 1.5 volts to operate—well beyond what most nanogenerators can generate.

To make a higher voltage device, Wang and his colleagues needed to find a way to make the voltage output of individual nanowire devices add up. To do so they needed to orient the crystallographic axis of each ZnO nanowire in the same direction so that when force was applied to them all collectively, the polarity of charges on each wire would be aligned, producing a higher output voltage. Wang's team patterned an array of parallel chromium wires atop a substrate. They then grew thousands of ZnO nanowires laterally between these wires, like rungs in a ladder, under conditions that ensured they all grew with the same crystallographic orientation. Finally, they soldered the ZnO nanowires to the chromium by depositing gold at the connection points (see figure, p. 304). The scheme worked. When they flexed their array, it generated 1.26 volts. That's not quite the 1.5 volts of a AA battery, but in the months since their paper was submitted, Wang says his team has upped that output to 2.4 volts. "This enables us to operate true technology," Wang says.

The Georgia Tech group isn't the only one closing in on that goal. At the University of California, Berkeley, another nanogenerator group, headed by mechanical engineer Liwei Lin, is making nanogenerators out of long polymer fibers that one day may be woven into cloth. "This technology could eventually lead to wearable 'smart clothes' that can power hand-held electronics through ordinary body movements," Lin says.

For their nanogenerators, Lin and his colleagues start with a polymer called polyvinylidene fluoride (PVDF) that can be processed to separate electrical charges. Other groups have previously made PVDF generators from thin films of the polymer. But PVDF films are typically inefficient, converting only 1% to 2% of kinetic energy to electricity. Lin and his colleagues also reported in the 10 February issue of *Nano Letters* that when they used a technique called electrospinning to spin PVDF into threadlike fibers as little as 500 nanometers across, the resulting fibers converted 10 times as much kinetic energy to electricity as the thin-film PVDF devices did.

Although Lin and his colleagues are still trying to understand exactly why that is, Lin says part of the explanation probably has to do with the electrospinning technique. The method draws out the polymer fibers in the presence of a large electric field, which seems to orient individual polymer molecules better than the filmmaking techniques do (see figure, left). And once the fibers are formed and solidify, this arrangement is locked in place. The output is high enough, Lin says, that calculations suggest that 1000 or so fiber generators incorporated into the cloth of a shirt would capture enough energy from a person's movements to charge a cell phone or an iPod. Although Lin says he hasn't yet formed a company to commercialize his power-suit material, he's already taking visits from venture capitalists looking to do just that.

If nanogenerators of any sort succeed, could they possibly be scaled up to generate large amounts of power? After all, most of the handwringing about energy these days is about how to generate terawatts, rather than microwatts, of carbon-free power. Lin, Wang, and McAlpine agree that for now that doesn't seem likely. Nanogenerators simply produce too little power to change our civilization. For now, they'll be working on the small scale, which might still be enough to change our lives.

–ROBERT F. SERVICE

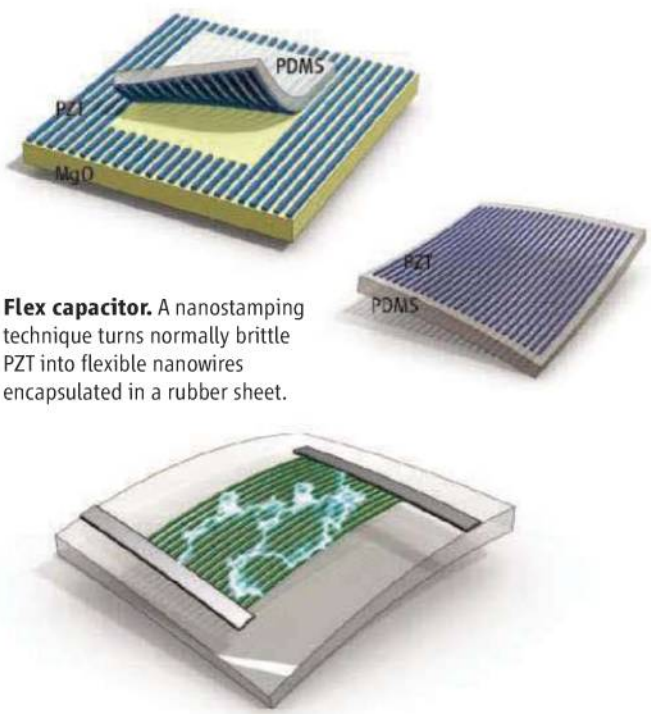

Flex capacitor. A nanostamping technique turns normally brittle PZT into flexible nanowires encapsulated in a rubber sheet.

CREDITS (TOP TO BOTTOM): C. CHANG *ET AL.*, *NANO LETTERS* **10** (25 JANUARY 2010) © 2010 AMERICAN CHEMICAL SOCIETY; Y. QI *ET AL.*, *NANO LETTERS* **10** (26 JANUARY 2010) © 2010 AMERICAN CHEMICAL SOCIETY

Qs & AAAs

www.sciencedigital.org/subscribe

For just US$99, you can join AAAS TODAY and start receiving *Science* Digital Edition immediately!

LETTERS

edited by Jennifer Sills

Finding Animals for Research

CONTRARY TO THE IMPRESSION CONVEYED IN THE NEWS FOCUS STORY "Dog dealers' days may be numbered" (D. Grimm, 26 February, p. 1076), the American Physiological Society endorses the National Academy of Sciences (NAS) recommendation to replace Class B dealers. However, the article cited only half of the key sentence: "It is not necessary to continue to obtain random source dogs and cats from Class B dealers *provided that alternative sources of animals with similar characteristics can continue to be assured*" (emphasis added) [(*1*), p. 95]. The problem is that the alternatives available (donors, pounds, and commercial breeders) cannot currently replace Class B dealers. This is why the NAS panel recommended "that NIH undertake an effort to explore new potential sources of random source dogs and cats to meet important biomedical research needs" [(*1*), p. 7].

Researchers doing translational research in areas such as cardiovascular disease need large, fully mature dogs. This is where the current alternatives fail: Owners donate sick animals, which cannot be used to study other diseases. In most parts of the country, pounds are either prohibited from making unwanted animals available for research or they choose not to do so. Commercial breeders are the most promising option, but they almost exclusively sell young animals. If it were financially feasible, breeders might be willing to sell mature animals. However, this will likely require NIH to provide start-up funds for breeders to expand their facilities and grant supplements so that researchers can buy older animals. Given time to make arrangements and money to implement them, it should be possible to obtain older dogs and cats needed for cardiovascular and other areas of research.

Congress established the Class B system and put the U.S. Department of Agriculture in charge of enforcing the law. The Pet Safety and Protection Act, if approved by Congress, would end Class B dealer sales of dogs and cats after 90 days. Before the system is abolished, there must be a viable alternative. Otherwise, important translational research will falter.

ALICE W. RA'ANAN

Office of Science Policy, American Physiological Society, Bethesda, MD 20817, USA. E-mail: araanan@the-aps.org

Reference

1. National Research Council, *Scientific and Humane Issues in the Use of Random Source Dogs and Cats in Research* (National Academies Press, Washington, DC, 2009).

Promoting Scientific Standards in Germany

WE APPLAUD THE EDITORIAL BY B. ALBERTS emphasizing the continuing need for ethical conduct in research ("Promoting scientific standards," 1 January, p. 12). We believe that efforts should go beyond the elimination of "honorary authorships" and a higher valuation of mentors if we are to "attract and retain individuals of outstanding intellect and character" (*1*), at least in the German academic setting.

The ongoing erosion of our research system can only be efficiently reversed if the key recommendations in the 2005 European Charter for Researchers and Code of Conduct for the Recruitment of Researchers are implemented by our universities on a broad scale. For instance, candidates for university positions should be selected on the basis of their creativity and level of independence, which could be ascertained and even quantified by the number of first and/or corresponding authorships they have accumulated. By contrast, the current selection approach favors the impact factor of the journals in which these individuals have published, often regardless of their actual contribution and the novelty of their findings. In addition, to minimize conflict and scientific misconduct, the frequently found disparity between project originators and grant holders in German academia should be streamlined into one and the same principal investigator, as is the case in the United States.

RAZVAN T. RADULESCU,[1]* KLAUS FISCHER,[2] EDUARD STANGE,[3] JOHANNES SCHULZE[4]

[1]Molecular Concepts Research, Muenster, Germany. [2]Faculty of Philosophy, University of Trier, Trier, Germany. [3]Department of Internal Medicine I, Robert Bosch Hospital, Stuttgart, Germany. [4]University of Frankfurt, Frankfurt am Main, Germany.

*To whom correspondence should be addressed. E-mail: ratura@gmx.net

Reference

1. B. Alberts, K. Shine, *Science* **266**, 1660 (1994).

The Missing Link in Biodiversity Conservation

THE EDITORIAL BY J. MARTON-LEFÈVRE TITLED "Biodiversity is our life" (5 March, p. 1179) does not address the missing link in appeals for biodiversity conservation. Conservationists have two messages for the public: (i) Biodiversity loss is tragic because of the impending extinctions of charismatic species of mammals, birds, amphibians,

CREDIT: ANIMAL WELFARE INSTITUTE

and plants; and (ii) biodiversity is important because it contributes to ecosystem services. Conspicuously missing from these seemingly disparate concepts is the connection between them: the many millions of species within the numerous phyla of microbes and invertebrates, which represent perhaps 95% of total species and genetic biodiversity (*1*). These species are less likely to gain public sympathy than a frog or hawk, yet they are the ones (in addition to plants) that drive agriculture, forestry, and fisheries—the very ecosystem services we strive to protect—by mediating soil chemistry and generating marine food chains (*2*, *3*). Crucially, these species also support the more charismatic ones (*2*). We can connect the dots for the public with a new message, one we would like to label "production biodiversity": By protecting microbes and invertebrates, we also protect the primary industries upon which we all depend.

ANDREW BEATTIE[1]* AND PAUL EHRLICH[2]

[1]Department of Biological Sciences, Macquarie University, NSW 2109, Australia. [2]Center for Conservation Biology, Department of Biological Sciences, Stanford University, Stanford, CA 94305–5020, USA.

*To whom correspondence should be addressed. E-mail: abeattie@bio.mq.edu.au

References

1. L. Margulis, K. V. Schwartz, *Five Kingdoms* (W. H. Freeman, New York, 2000).
2. *Millennium Ecosystem Assessment, Vol. 1, Ecosystems and Human Well-Being* (Island Press, Washington, DC, 2005).
3. G. Daily, K. Ellison, *The New Economy of Nature* (Island Press, Washington, DC, 2002).

Energy Efficiency Merits More Than a Nudge

IN THEIR POLICY FORUM ("BEHAVIOR AND energy policy," 5 March, p. 1204), H. Allcott and S. Mullainathan identify an important opportunity for reducing energy consumption inexpensively by applying behavioral science. Even larger opportunities can be realized, however, by combining behavioral interventions with other policy tools to address a wider range of behaviors.

The field policy experiments cited by the authors use behavioral "nudges" to change home equipment use. The full potential of behavioral interventions comes from inducing people to adopt energy-efficient technology. More than 30 years of social and behavioral science research on household energy consumption demonstrates the power of combining behaviorally sensitive features—such as norms, social influence networks, and attention to convenience and quality assurance in program design—with financial incentives and information (*1*–*4*). This can make a huge difference in effectiveness for efficiency programs. For example, a utility grant program that paid for over 90% of home retrofit costs achieved penetration that ranged from 1.4 to 19.3% per year, depending on how the program was implemented (*5*). The strongest programs have the potential to achieve behavioral plasticity (i.e., the percentage of people who could make a choice who actually do so) of 80 to 90% for adoption of energy-efficient equipment over 10 years (*6*). If implemented across equipment classes and scaled up nationally, such programs could reduce carbon emissions by an estimated 123 million tons of carbon (MtC) (*6*). This is far greater than the national savings of 12.7 MtC estimated for the program in the Policy Forum.

PAUL C. STERN,[1]* THOMAS DIETZ,[2] GERALD T. GARDNER,[3] JONATHAN GILLIGAN,[4] MICHAEL P. VANDENBERGH[5]

[1]Division of Behavioral and Social Sciences and Education, National Research Council, 500 Fifth Street, NW, Washington, DC 20001, USA. [2]Environmental Science and Policy,

MPC-200
Multi-manipulator system

Versatile:	User friendly interface controls up to two manipulators with one controller. Select components to tailor a system to fit your needs.
Expandable:	Daisy chain a second controller and operate up to four manipulators with one input device.
Stable:	Stepper motors and cross-rolled bearings guarantee reliable, drift-free stability.
Doubly Quiet:	Linear stepper-motor drive reduces electrical noise. Thermostatically-controlled cooling fans barely whisper.

Make the right move!

SUTTER INSTRUMENT
PHONE: 415.883.0128 | FAX: 415.883.0572
EMAIL: INFO@SUTTER.COM | WWW.SUTTER.COM

Learn how current events are impacting your work.

***Science*Insider, the new policy blog from the journal *Science*,** is your source for breaking news and instant analysis from the nexus of politics and science.

Produced by an international team of science journalists, *Science*Insider offers hard-hitting coverage on a range of issues including climate change, bioterrorism, research funding, and more.

Before research happens at the bench, science policy is formulated in the halls of government. Make sure you understand how current events are impacting your work. Read *Science*Insider today.

www.ScienceInsider.org

*Science*Insider
Breaking news and analysis from the world of science policy

Science
AAAS

Michigan State University, East Lansing, MI 48824, USA. [3]Department of Behavioral Sciences, University of Michigan, Dearborn, MI 48128, USA. [4]Department of Earth and Environmental Sciences, Vanderbilt University, Nashville, TN 37235, USA. [5]Climate Change Research Network, Vanderbilt University Law School, Nashville, TN 37203, USA.

*To whom correspondence should be addressed. E-mail: pstern@nas.edu

References

1. P. C. Stern, G. T. Gardner, *Am. Psychol.* **36**, 329 (1981).
2. National Research Council (NRC), *Energy Use: The Human Dimension* (Freeman, New York, 1984).
3. NRC, *Energy Efficiency in Buildings: Behavioral Issues* (National Academy Press, Washington, DC, 1985).
4. G. T. Gardner, P. C. Stern, *Environmental Problems and Human Behavior* (Pearson Custom Publishing, Boston, ed. 2, 2002).
5. P. C. Stern *et al.*, *Eval. Rev.* **10**, 147 (1986).
6. T. Dietz *et al.*, *Proc. Natl. Acad. Sci. U.S.A.* **106**, 18452 (2009).

Letters to the Editor

Letters (~300 words) discuss material published in *Science* in the previous 3 months or issues of general interest. They can be submitted through the Web (www.submit2science.org) or by regular mail (1200 New York Ave., NW, Washington, DC 20005, USA). Letters are not acknowledged upon receipt, nor are authors generally consulted before publication. Whether published in full or in part, letters are subject to editing for clarity and space.

TECHNICAL COMMENT ABSTRACTS

Comment on "Modafinil Shifts Human Locus Coeruleus to Low-Tonic, High-Phasic Activity During Functional MRI" and "Homeostatic Sleep Pressure and Responses to Sustained Attention in the Suprachiasmatic Area"

Serguei V. Astafiev, Abraham Z. Snyder, Gordon L. Shulman, Maurizio Corbetta

Minzenberg *et al.* (Reports, 12 December 2008, p. 1700) and Schmidt *et al.* (Reports, 24 April 2009, p. 516) reported blood oxygen level–dependent (BOLD) responses in the human locus coeruleus (LC). Here, we show that these LC responses do not correspond to the anatomical location of the LC and present cautionary data concerning the quality of BOLD signals measured from the LC using standard functional magnetic resonance imaging acquisition parameters.

Full text at www.sciencemag.org/cgi/content/full/328/5976/309-a

Response to Comment on "Modafinil Shifts Human Locus Coeruleus to Low-Tonic, High-Phasic Activity During Functional MRI"

Michael J. Minzenberg, Andrew J. Watrous, Jong H. Yoon, Christian La, Stefan Ursu, Cameron S. Carter

Contrary to the arguments put forth by Astafiev *et al.*, our new analyses and high-resolution replication show that modulation of brain activity by the cognitive enhancing drug modafinil indeed localizes to the locus coeruleus. The authors' critical stance regarding blood oxygen level–dependent imaging in the brainstem does not follow from their data.

Full text at www.sciencemag.org/cgi/content/full/328/5976/309-b

Response to Comment on "Homeostatic Sleep Pressure and Responses to Sustained Attention in the Suprachiasmatic Area"

Christina Schmidt, Philippe Peigneux, Pierre Maquet, Christophe Phillips

Astafiev *et al.* question whether the blood oxygen level–dependent (BOLD) response that we reported in the brainstem was located in the locus coeruleus (LC). Using high-resolution T1-turbo spin echo images (T1-TSE) acquired in an independent group of subjects, we show that the reported task-related BOLD response in the brainstem is actually compatible with the anatomical location of the LC. Full text at www.sciencemag.org/cgi/content/full/328/5976/309-c

Discount amount varies in some states. Discount is not available in all states or in all GEICO companies. One group discount applicable per policy. Coverage is individual. In New York a premium reduction is available. Some discounts, coverages, payment plans and features are not available in all states or companies. Government Employees Insurance Co. • GEICO General Insurance Co. • GEICO Indemnity Co. • GEICO Casualty Co. These companies are subsidiaries of Berkshire Hathaway Inc. GEICO: Washington, DC 20076. GEICO Gecko image © 1999-2010. © 2010 GEICO

EVOLUTION

No Sex, Please

John M. Logsdon, Jr.

> We do not even in the least know the final cause of sexuality; why new beings should be produced by the union of the two sexual elements, instead of by a process of parthenogenesis. –Charles Darwin (*1*)

Why sex? Darwin clearly understood this to be a problem. But 150 years after the publication of *The Origin*, there is still no clear answer to what has been dubbed the "queen of problems in evolutionary biology" (*2*). One fruitful avenue to understanding the evolutionary enigma of sex has been to focus on organisms that are capable of the strategy suggested by Darwin: reproducing asexually, by parthenogenesis (i.e., virgin birth). By shedding light on how and why—or even if—such organisms are "exceptions," it is expected that some "rules" of sexual reproduction might be illuminated.

This is the main premise of the aptly titled *Lost Sex*, which spans intellectual history, theoretical treatments, and empirical studies from a diverse menagerie of asexual systems, either derived by loss from sexual ancestors or also capable of sexual reproduction. Many authors participated in a series of European Science Foundation–funded workshops on the biology of parthenogenesis that looked "at the paradox of sex from an asexual perspective."

One important issue in the field of asexual biology is the divergence between botanists and zoologists in language and, possibly, in conceptual understanding. For example, in animals "apomixis" refers to a particular type of parthenogenesis, whereas in plants parthenogenesis is only a part of apomixis—so it is easy to see how confusing and difficult a synthesis of animal and plant research might be. The editors and authors are to be applauded for their considerable efforts to bridge this divide. Chapters by Peter van Dijk and by Per Stenberg and Anssi Saura together provide much-needed primers on the sometimes obscure terminology and often complex underlying genetic processes. Future progress requires reconciliation of these worlds (and words).

The first 10 chapters highlight introductory and historical themes and develop theoretical and philosophical issues regarding asexual taxa, emphasizing aspects relevant to the evolution of sex. The volume starts with a bang: Bengt Bengtsson's provocative overview both lays out the main issues for understanding asexuality and challenges some conventional notions. He suggests that "any notion of a general evolutionary advantage for asexuality is at best misleading." That point (somewhat contrary to the book's theme) underlies his conclusion: "Asexual biology is interesting, not because of what it says about something else, namely sex, but because of what it says about the organisms under study." The last two introductory chapters consider the key and controversial issues of defining "clone" and "species." Rather than advocate a particular concept of clone, Koen Martens, Hugh Loxdale, and Isa Schön want users to clearly state and cautiously deploy the concept they adopt. Insisting that species concepts can (and should) apply to asexuals, William Birky and Timothy Barraclough prescribe some practical and tenable solutions to accomplish this.

The next 13 chapters present thorough case studies of the natural history and fascinating biology of various asexual taxa. Three cover the star "ancient" asexuals: darwinulid ostracods, oribatid mites, and bdelloid rotifers. The remainder describe a wide cast of other parthenogenetic animal and plant groups, all of which are either closely related to sexuals or can themselves alternate between sexual and asexual reproduction. A theme running through these chapters is that modern, rapidly developing genetic, molecular, and cytological tools place us on the brink of a deeper understanding of these systems—which promises a larger impact on what have been labors of love among a small number of dedicated investigators.

Lost Sex
The Evolutionary Biology of Parthenogenesis
Isa Schön, Koen Martens, and Peter van Dijk, Eds.
Springer, Dordrecht, Netherlands, 2009. 633 pp. $209, £144. ISBN 9789048127696.

Lost Sex concludes with four chapters on applied aspects of asexual reproduction. These cover such topics as infectious diseases, pesticide resistance in insects, the importance of epigenetics to cloning, and the implications of clonality for the stability of crop plants (here, wine grapes—a subject that goes well with discussions of sex).

The chapters are ordered in a logical fashion, and there is some cross-referencing among them. As with many edited volumes, however, there are issues of evenness and repetition. Each chapter can be taken on its own, whereas a cover-to-cover read leads to considerable redundancy. A single glossary would have been more helpful than the several distributed among chapters. Lastly, a more stringent editorial hand would have improved some chapters and generated more consistency throughout.

The lack of coverage of some major groups of organisms largely reflects the field. Some asexual fungi are being studied and could have been included. But very little research is being done on asexuality in protists, even though a number are suspected to have also lost sex. In contrast, the general exclusion of prokaryotes seems appropriate and justifiable: The central questions in the evolution of sex have been centered on the whole-genome reshuffling mode of sex that eukaryotes enjoy via meiosis, whereas bacterial "sex" can be deployed one or a few genes at a time.

Overall, *Lost Sex* is praiseworthy for its conception and execution. The volume will appeal to both general readers and specialists and find a home on desks and bookshelves of faculty and students (for them, given its cost, likely from libraries). It should serve as an unrivaled resource for future studies on asexual organisms.

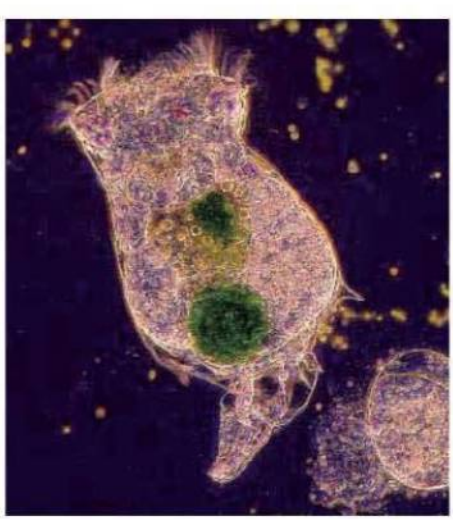

Cyclical parthenogens. Environmental cues trigger sexual reproduction in monogonont rotifers (here, *Brachionus calyciflorus*).

CREDIT: S. J. HANSON/UNIVERSITY OF IOWA

The reviewer is at the Department of Biology, University of Iowa, Iowa City, IA 52242, USA, and the National Evolutionary Synthesis Center (NESCent), Durham, NC 27705, USA. E-mail: john-logsdon@uiowa.edu

References

1. C. Darwin, *J. Proc. Linn. Soc. Bot.* **6**, 77 (1862).
2. G. Bell, *The Masterpiece of Nature: The Evolution and Genetics of Sexuality* (Univ. California Press, Berkeley, 1982).

10.1126/science.1187970

SCIENCE AND THE ARTS

Why Science?

David Edwards

Art + Science Now
by Stephen Wilson
Thames and Hudson, New York, 2010. 208 pp. $50, C$63, £29.95. ISBN 9780500238684.

Science advances by what can seem to be an occasional boom rising over a chorus of mysterious whispers. It remains easier to say what scientists have discovered, or might discover, than to explain how or why, exactly, they discover anything. This difficulty to converse around scientific process short of pointing to startling outcome, or to the rattle of beakers in a lab, is more than a public communication problem. It limits opportunities for scientists to question what they do, or how they do it, and conceivably slows down the advance of science. Fortunately, artists are learning to express an opinion. What these artists do, and sometimes say, is livening up the debate around scientific process, even while it is inevitably erasing some of the convenient, simplifying distinctions we have long made between art and science, artists and scientists, and the distinctive roles and objectives of each.

A few years ago, the Calouste Gulbenkian Foundation's Sian Ede wrote a wise book, *Art and Science* (*1*). It spotlighted the phenomenon of artists—sometimes working with scientists, sometimes working alone, and even sometimes looking like scientists themselves—exploring the meaning of scientific frontiers. Where Ede shows us why, Stephen Wilson's *Art + Science Now* shows us what. Where Ede paints a broad canvas with eloquent and precise prose, Wilson (an art professor at San Francisco State University) shares diverse imagery that marches us past artworks from 2000 through 2007 that were inspired by science and technology.

Some of the works Wilson reviews probe popular and by now familiar questions about the future of biological science. In *Genesis*, a 1999 installation by the Chicago artist Eduardo Kac, we have images of *Escherichia coli* bacteria colonies genetically modified to express in their DNA base pairs the Biblical code. That theme was pursued more provocatively in Kac's subsequent *Alba* (2000), a rabbit modified genetically by French geneticist Louis-Marie Houdebine to express green fluorescent protein and glow in the shine of a blue light. Alexis Rockman's painting *The Farm* (2000) presents a Salvador Dali–like image of a sun-drenched field with farm animals distorted in ways that express a probable bioengineered future. In her installation *Family Portrait* (2002), Marilene Oliver reconstructs three-dimensional sculptures of four members of a family with slices of full-body magnetic resonance imaging (MRI) scans. Certain projects captured in the book explore the meaning of human identity even more obviously than they do the meaning of science—for example, Annie Cattrell's installation *Sense* (2001–3), which presents three-dimensional functional MRI scans of human brain activity associated with specific emotions. That is now part of the permanent collection of London's Wellcome Collection, one of several galleries that have emerged in Europe since 2007 where artists and designers actively explore science frontiers.

Other projects included in *Art + Science Now* invite us to experience worlds accessible only through scientific research. In Evelina Domnitch and Dmitry Gelfand's *Camera Lucida* (2005–6), installed at Nijo Castle in Kyoto (and more recently at the Science Gallery in Dublin, another of the new art and science galleries), viewers could manipulate a musical composition, which was subsequently converted into ultrasound waves at variable frequencies to produce sonoluminescent images in liquid. Jean Dubois and Philippe Jean's *Radicaux Libres* (2006), following Brian Knep's powerful *Healing* installation (2005) at Harvard University's Memorial Hall, produced a temporary site-specific work in which visitors' movements in a space trigger the appearance of light images that form behind their feet. These floor images turn into letters that trail visitors as they continue forward, forming words and expressions for everyone to see—as if invisible virtual worlds might, like the shadow of Peter Pan, suddenly spin away from us, another kind of questioning of identity.

Certain art projects in the book appear closer to scientific research itself. This is the case with New York artist Natalie Jeremijenko's *OneTrees* (1999–2004), in which she planted 80 genetically identical plantlets around San Francisco and monitored the influences of environment (they were significant), in an attempt to explore "our own agency in the world." Massachusetts Institute of Technology–trained computer artist Ben Fry's *Valence* (1999–2002) explored the structural relationship among words in Mark Twain's *Innocents Abroad*. It projected words onto a screen as his program received page after page of text, with more commonly appearing words moving to the periphery of the screen and displacing less commonly used words to the center.

Wilson covers so much ground and writes with such informality that his insights, where they near scientific frontiers, can fall short of helpful explanation. He is occasionally dismissive of scientific aims, as when he writes of the limits of artificial intelligence or of artist fears of bioengineering doom. But the sheer vastness of Wilson's contemporary art exploration of science is fascinating. Artworks today can be as fleeting as the scientific process they often seek to explore. *Art + Science Now* captures and preserves a special moment in the history of artistic practice and positions it within what is the inextricable relationship between science and society.

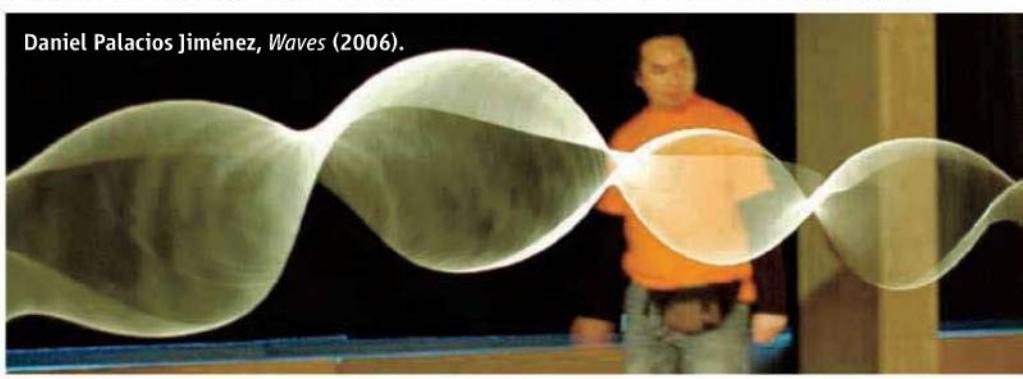

Daniel Palacios Jiménez, *Waves* (2006).

CREDIT: COURTESY THAMES AND HUDSON

The quest to participate in the advance of science through artistic creation and expression goes back to the origins of science and has attracted such prominent scientists and artists as Johannes Kepler, Leonardo da Vinci, Louis Pasteur, and John Cage. If during the technology revolutions of the past two centuries we often lost sight of this broad, autocatalytic, and sometimes self-contradictory dimension of human inquiry, it seems likely that the 21st century is about to put us back on track.

The reviewer is at the School of Engineering and Applied Sciences, Pierce 322, Harvard University, 29 Oxford Street, Cambridge, MA 02138, USA. E-mail: dedwards@seas.harvard.edu

References

1. S. Ede, *Art and Science* (Taurus, London, 2005).

10.1126/science.1187345

LAND USE

Does REDD+ Threaten to Recentralize Forest Governance?

A major new approach to emissions mitigation may interrupt a promising trend toward decentralized forest management.

Jacob Phelps,[1] Edward L. Webb,[1]* Arun Agrawal[2]

Over the past 25 years, developing countries have transitioned toward decentralized forest management that allows local actors increased rights and responsibilities (*1*–*4*), and has helped protect forests in many regions (*5*, *6*). A new approach to mitigating terrestrial emissions associated with climate change, Reducing Emissions from Deforestation and Forest Degradation (REDD+), is poised to interrupt this trend. Given the implications for tropical forest management, REDD+ governance links should be a research priority (*7*).

Decentralization

Decentralized resource management in the developing world has been called "the most significant ... most distinctive and [most] visible shift in national environmental policies since the late 1980s" (*3*). At its most extensive, decentralization allows stakeholders to redefine ownership, use, and management of forests (*4*, *8*). Governments have decentralized forest management for many reasons: to reduce costs and increase efficiency by transferring responsibilities, to respond to local demands for rights and international donor pressures to transfer benefits to users, and in recognition that conservation is possible across diverse tenure regimes (*2*, *3*). Decentralization reforms have primarily targeted low-value forests (*2*, *9*); central governments have mostly reserved control of forests suitable for commercial exploitation (*1*) or biodiversity conservation (*9*).

Outcomes vary, but effective decentralization reforms have increased local actors' benefits and rights in forests (*3*), reduced costs of protection (*5*), and provided opportunities for biodiversity conservation (*10*). A recent analysis of 80 forest commons across 10 countries shows that rule-making autonomy at the local level is associated with greater forest carbon storage and higher livelihood benefits (*11*).

However, when presented with strong incentives, central governments have at times reversed forest policy decentralization (*12*, *13*). Centralized governance can protect forests and enhance regrowth, but it requires costly enforcement (*14*); is isolated to within-park boundaries (*15*); and can result in resentment among excluded users, which undermines conservation goals (*16*).

REDD+

REDD+ is a proposed performance-based mechanism under negotiation through the United Nations Framework Convention on Climate Change (UNFCCC), in which developed country donors, corporations, nongovernmental organizations, and individuals will compensate developing countries for forest emissions reductions, including through market mechanisms (see the chart on page 313) (*17*, *18*). Payments will require demonstrated emissions reductions through improved forest protection, sustainable forest management, and/or enhancement of carbon stocks (*19*). REDD+ will be a key emissions mitigation strategy as evidenced by extensive donor investments to prepare developing countries to implement REDD+, e.g., $4.5B from six developed countries by 2012 (*20*–*22*). By 2020, REDD+ investments may reach $30B a year (*21*).

Under REDD+, recipient governments will devise strategies for national land-use and forest-sector planning, stakeholder negotiations, tenure clarification, carbon brokering, national-level carbon accounting, and provision of funds and services to local actors (see the chart on page 313). A national approach is considered integral to the success of REDD+ projects: It can help avoid leakage (*23*); ensure permanence; and provide reliable monitoring, reporting, and verification (MRV) (*19*). This approach effectively converts national governments into the principal forest stakeholders.

REDD+ Reversing Decentralization Trends

Although there are efforts to promote community involvement in REDD+ (*24*), funding and requirements for REDD+ may undermine decentralization. Generous, long-term REDD+ funding will considerably reduce past financial burdens that motivated decentralization. A conservative market-value estimate of $1.2 billion per year for avoided deforestation (*25*) exceeds current global investment for forest conservation. For example, the market value of avoided deforestation for Indonesia [U.S.$108M per year (*25*)] exceeded the entire 2005 Department of Forestry budget [$102M (*26*)].

REDD+ implementation will place new demands on national forest managers: detailed carbon-oriented forest management plans, reliable baseline data and subsequent quantitative MRV of emissions reductions at the national level, and resources for brokering deals between buyers and sellers (*27*). These demands would impose prohibitive costs for small-scale initiatives (*27*), but a centralized system would benefit from economies of scale, coordination, and standardization (*14*). Communities may participate in collecting forest-specific data, but carbon accounting, a major REDD+ component, will require centralized management.

By monetizing forest carbon, REDD+ will substantially increase the market value of forests, including those previously considered marginal, incentivizing central governments to increase control. Under a performance-based payment mechanism, governments will be pressured to avoid the risk of nonpayment resulting from local-level failures. Evidence suggests that central governments affirm control over forests considered "critical" to national welfare for conservation, protection of ecosystem services, or national economic interests (*16*). With billions of dollars at stake, governments could justify recentralization by portraying them-

CREDIT: PHOTODISC

[1]Department of Biological Sciences, National University of Singapore, Singapore, 117543. [2]School of Natural Resources and Environment, University of Michigan, Ann Arbor, MI 48109, USA.

*Author for correspondence. E-mail: ted.webb@nus.edu.sg

Prospective state-centric REDD+ mechanism. Elements of the figure are based in part on (*18*).

selves as more capable and reliable than local communities at protecting national interest. This could involve imposition of excessive requirements (*1*) or even evictions of local users, as in some national parks (*28*).

Balancing Multiple Incentives of REDD+

Many governments have yet to apply lessons of decentralization to REDD+ strategies. Of the 34 nationally appropriate mitigation actions submitted by developing countries to the UNFCCC, 12 identified centrally coordinated forest-based mitigation actions without mention of decentralization (*29*, *30*). Moreover, a majority of submissions for REDD+ "readiness" funding from the World Bank did not adequately address governance challenges, such as tenure, benefit sharing, and local engagement (*31*). After feedback from donors, some proposals adopted the language of local participation and benefit sharing (*22*). Evidently, the incorporation of decentralized strategies and community participation in REDD+ will depend on concrete incentives. However, individual donor safeguards may not be consistent or rigorous, and the UNFCCC does not currently mandate safeguards, benefit sharing, or local involvement (*19*). Furthermore, carbon markets seeking cheap verifiable credits will have little incentive to create local partnerships. It is therefore urgent that as major REDD+ financial transfers occur, ground-level projects include decentralized strategies; heavily centralized REDD+ implementation can be detrimental to efficiency and equity (*32*).

The Way Forward

Communities should have control over local REDD+ design and implementation. Governments may propose REDD+ sites, support low-emissions rural-development strategies, and deliver payments and/or services as incentives (*33*). Local users should be given authority, information, and support to determine whether they engage with REDD+, to align their management, monitoring, and enforcement with low-emissions objectives, and to negotiate revenue sharing. New research is necessary to optimize REDD+ effectiveness through a combination of decentralized and centralized forest governance. We must better understand trade-offs and synergies between rural livelihood activities (*34*), alternative land uses, and REDD+ goals. Research should also focus on how carbon sequestration varies with differing levels of community engagement and autonomy, and across diverse tenure regimes. Studies of the practicality and acceptability to international markets of low-cost community-based MRV strategies will help determine the feasibility of decentralized MRV.

Abbreviated timelines (*21*, *22*) make it doubtful whether pilot studies will mature before global-scale REDD+ implementation. There is a tension between the urgency to reduce emissions and the need for science-based REDD+ governance that could enhance forest carbon sequestration while benefiting millions of forest-dependent people.

References and Notes

1. J. C. Ribot, A. Agrawal, A. M. Larson, *World Dev.* **34**, 1864 (2006).
2. A. Agrawal, A. Chhatre, R. Hardin, *Science* **320**, 1460 (2008).
3. A. Agrawal, E. Ostrom, in *Decentralization, Forests and Rural Communities: Policy Outcomes in South and Southeast Asia*, E. L. Webb, G. Shivakoti, Eds. (SAGE, New Delhi, 2008), pp. 44–67.
4. C. J. Pierce Colfer, D. Capistrano, Eds., *The Politics of Decentralization: Forests, Power, and People* (Earthscan, London, 2005).
5. E. Somanathan, R. Prabhakar, B. S. Mehta, *Proc. Natl. Acad. Sci. U.S.A.* **106**, 4143 (2009).
6. E. Ostrom, H. Nagendra, *Proc. Natl. Acad. Sci. U.S.A.* **103**, 19224 (2006).
7. W. J. Sutherland *et al.*, *Trends Ecol. Evol.* **25**, 1 (2010).
8. E. L. Webb, G. Shivakoti, Eds., *Decentralization, Forest and Rural Communities: Policy Outcomes in South and Southeast Asia* (SAGE, New Delhi, 2008).
9. H. Nagendra, *Environ. Conserv.* **29**, 530 (2002).
10. R. Chazdon, *Science* **320**, 1458 (2008).
11. A. Chhatre, A. Agrawal, *Proc. Natl. Acad. Sci. U.S.A.* **106**, 17667 (2009).
12. Y. B. Malla, *Environ. Hist.* **6**, 287 (2001).
13. D. A. Wardell, C. Lund, *World Dev.* **34**, 1887 (2006).
14. J. S. Oestreicher *et al.*, *Glob. Environ. Change* **19**, 279 (2009).
15. L. Naughton-Treves, M. B. Holland, K. Brandon, *Annu. Rev. Environ. Resour.* **30**, 219 (2005).
16. N. L. Peluso, P. Vandergeest, *J. Asian Stud.* **60**, 761 (2001).
17. L. Miles, V. Kapos, *Science* **320**, 1454 (2008).
18. A. Angelsen, S. Wertz-Kanounnikoff, in *Moving Ahead with REDD: Issues, Options and Implications*, A. Angelsen, Ed. (Center for International Forestry Research, Bogor, Indonesia, 2008), pp. 11–22.
19. P. A. Minang, D. Murphy, *REDD after Copenhagen: The Way Forward* (World Agroforestry Center, Nairobi, 2010) www.asb.cgiar.org/PDFwebdocs/REDD_After_Copenhagen-EN.pdf.
20. "Meeting on deforestation boosts morale, budget" (Associated Press, 2010). www.npr.org/templates/story/story.php?storyId=124555748.
21. For details, see UN-REDD Programme, www.un-redd.org/.
22. See Forest Carbon Partnership Facility, www.forestcarbonpartnership.org/fcp/.
23. Leakage is when interventions to reduce deforestation or degradation at one site displace pressures and increase emissions elsewhere.
24. S. Wertz-Kanounnikoff, M. K. Kongphan-apirak, "Emerging REDD+: A preliminary survey of demonstration and readiness activities" (Working Paper 46, Center for International Forestry, Bogor, Indonesia, 2009); www.cifor.cgiar.org/publications/pdf_files/WPapers/WP46Wertz-Kanounnikoff.pdf.
25. J. O. Niles *et al.*, *Philos. Trans. R. Soc. London A* **360**, 1621 (2002).
26. Ministry of Finance, Republic of Indonesia, *Budget Statistics 2008–2009* (Bank of Indonesia, Jakarta, Indonesia, 2009); www.bi.go.id/web/en/Publikasi/Investor+Relation+Unit/Policy+Document/Economic+Program/budget+statistic+2008-2009.htm.
27. O. J. Cacho, G. R. Marshall, M. Milne, *Environ. Dev. Econ.* **10**, 597 (2005).
28. D. Brockington, *Fortress Conservation: The Preservation of the Mkomazi Game Reserve, Tanzania* (Indiana Univ. Press, Bloomington, IN, 2002).
29. Party's submissions can be accessed at http://unfccc.int/home/items/5265.php.
30. Twelve do not mention any implementation mechanisms, and 10 make no mention of forests.
31. C. Davis, F. Daviet, S. Nakhooda, A. Thuault, "A review of 25 readiness plan idea notes from the World Bank Forest Carbon Partnership Facility" (World Resources Institute, Washington, DC, 2009).
32. T. Griffiths, *Seeing RED? Avoided deforestation and the rights of indigenous peoples and local communities* (Forest Peoples Programme, Moreton-in-Marsh, UK, 2007).
33. D. Nepstad *et al.*, *Science* **326**, 1350 (2009).
34. Harvest of nontimber forest products, fuel wood, and subsistence-level timber, and agricultural systems, e.g., swidden, agroforestry, forest grazing.

35. Funding provided by the National University of Singapore, Harry S. Truman Foundation, and NSF grant # HSD-0527138 and CNH-0709545.

10.1126/science.1187774

MOLECULAR BIOLOGY

Dicer's Cut and Switch

An enzyme that cleaves RNA is converted to a DNA-cleaving enzyme during programmed cell death in *Caenorhabditis elegans*.

Qinghua Liu and Zain Paroo

Apoptosis is an essential developmental process in which a highly concerted series of biochemical events directs cell disassembly and death. Degradation of chromosomal DNA is a defining characteristic of apoptosis, involving distinct deoxyribonucleases that initiate DNA fragmentation (initiator DNases) and metabolize residual DNA (progressive DNases). On page 327 of this issue, Nakagawa *et al.* (*1*) report an unexpected role in apoptotic DNA degradation for an enzyme that was previously known for its role in RNA interference (RNAi).

The first advance in understanding the mechanistic basis of apoptosis was the identification of *ced-3*, the gene that encodes a cysteine protease (caspase) in the nematode *Caenorhabditis elegans* (*2*, *3*). CED-3 and other caspases function in a cascade to activate a spectrum of effectors for cellular dissolution. Although progressive DNases are common to nematodes and mammals, initiators of DNA cleavage in *C. elegans* have been elusive. In mammals, DNA fragmentation factor (DFF40) [also known as caspase-activated deoxyribonuclease (CAD)] is sequestered in a complex with DFF45 [also called inhibitor of CAD (ICAD)] (*4*, *5*). Upon induction of apoptosis, activated caspases cleave the inhibitory DFF45 subunit, thereby freeing the DFF40 subunit to initiate chromosome cleavage, generating 3′ hydroxyl DNA breaks.

To identify the functional equivalent of mammalian DFF in *C. elegans*, Nakagawa *et al.* conducted a targeted RNAi screen. Candidate initiator DNases were selected through informatics searches and not limited solely to annotated DNases. Surprisingly, a gene (*dcr-1*) encoding a ribonuclease called Dicer was identified as a weak hit in the screen. Dicers are highly conserved RNase III enzymes that function in tandem with double-stranded RNA binding proteins (dsRBPs) in processing dsRNA to small regulatory RNA (*6*, *7*) (see the figure). These small RNAs effect RNAi by programming Argonaute proteins to guide sequence-specific silencing of messenger RNA (*8*).

Recognizing that the targeting of *dcr-1* by RNAi was achieved with low efficiency, Nakagawa *et al.* confirmed the initial finding by examining two different nematode strains lacking the *dcr-1* gene, both of which exhibited a stronger apoptotic phenotype. Historically, loss-of-function experiments that involve RNAi components have been used to infer functional roles for small RNAs (*9*). Given the wide spectrum of biological processes governed by such regulatory RNAs, it seemed plausible that small RNAs might be involved in apoptotic DNA degradation. However, animals defective for other RNAi components did not produce the same phenotype as that of the *dcr-1* mutants, indicating an RNAi-independent role for Dcr-1 in apoptotic DNA fragmentation.

Nakagawa *et al.* postulated that Dcr-1 might be a direct target of the CED-3 caspase because the lack of functional Dcr-1 reduced the number of cell deaths induced by constitutively activated CED-3. Indeed, recombinant CED-3 cleaved Dcr-1 in its RNase IIIa domain, producing a truncated Dcr-1 consisting of only an RNase IIIb domain and a dsRNA binding domain. Because both RNase III domains are required for dsRNA processing (*10*–*12*), this cleavage abolished RNase activity. Remarkably, truncated Dcr-1, but not full-length Dcr-1, exhibited DNase activity, generating 3′ hydroxyl DNA breaks much like initiator DNases in mammalian cells. Moreover, mutation of catalytic RNase residues in full-length Dcr-1 abolished both RNA and DNA cleavage activity. These findings indicate that CED-3 switches Dcr-1 from an RNase to a DNase.

Through a series of elegant genetic experiments, Nakagawa *et al.* further demonstrate that cleavage of Dcr-1 by CED-3 is required for promoting apoptosis. In addition to deficiencies in apoptosis, *dcr-1* mutants exhibit aberrant vulvar anatomy due to defective production of microRNA. In *dcr-1* mutants,

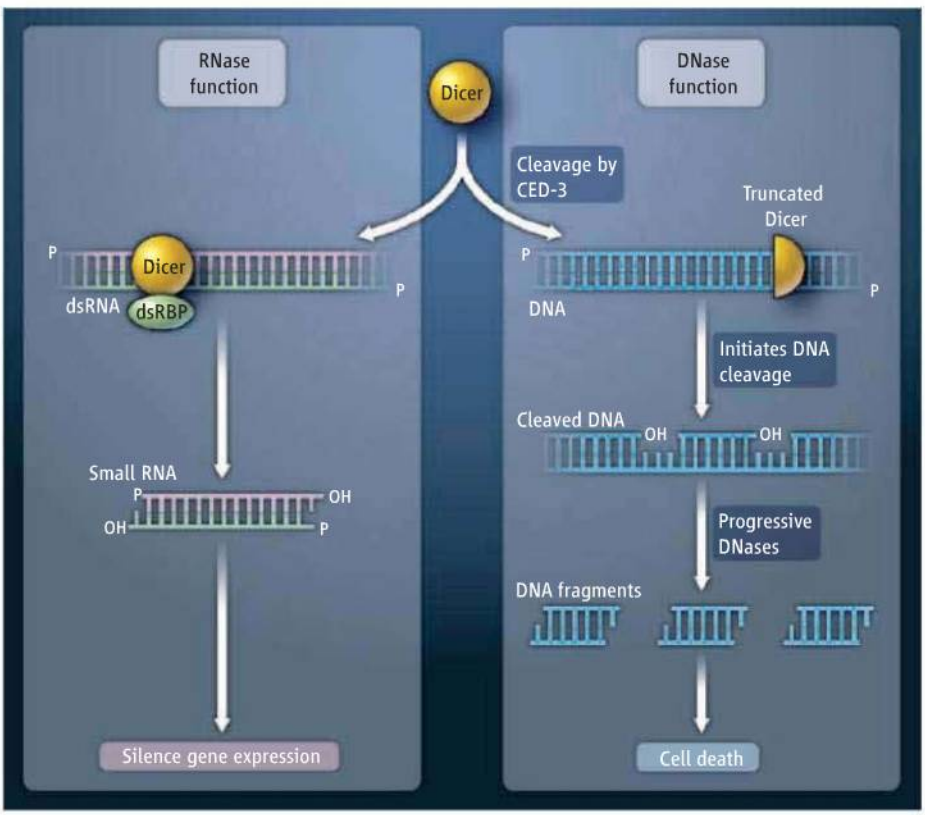

RNA and DNA substrate crossover. The RNase III Dicer functions with a double-stranded RNA binding protein (dsRBP) in processing long double-stranded RNA (dsRNA) to small RNAs. In *C. elegans*, the CED-3 protease cleaves Dicer (or a Dicer-dsRBP complex), which inactivates its RNase function. The truncated Dicer product gains DNase function and initiates breaks on chromosomal DNA. Progressive DNases further metabolize DNA fragments to complete apoptotic DNA degradation.

CREDIT: Y. GREENMAN/SCIENCE

Department of Biochemistry, University of Texas Southwestern Medical Center, Dallas, TX 75390, USA. E-mail: qinghua.liu@utsouthwestern.edu; zain.paroo@utsouthwestern.edu

expression of a *dcr-1* transgene that lacks a cleavage site for CED-3 rescued the developmental (vulva) defect, but not the apoptotic phenotype. Conversely, transgenic expression of the truncated form of Dcr-1 in *dcr-1* mutants rescued apoptosis but not the vulvar phenotype.

This highly unexpected role for Dcr-1 in early apoptotic DNA degradation has numerous important implications. Caspase-mediated activation of DNA degradation now appears conserved from nematodes to mammals. Full-length Dcr-1 (and/or Dcr-1 in complex with a dsRBP) maintains an inactive DNase in a manner similar to the DFF40-DFF45 complex in mammals. Cleavage of Dcr-1 by CED-3 activates a functional DNase that generates 3′ hydroxyl DNA breaks, which are subsequently resolved by progressive DNases. Conservation of this enzymatic switch may mean that Dicer also serves as an apoptotic DNase in higher organisms. The DNase activity of Dicer may also govern other aspects of chromosome dynamics. Thus, it may be prudent to consider RNAi-independent mechanisms underlying the phenotypes of *dicer* mutants. Perhaps most exciting will be determining the extent to which regulators of nucleic acid function exhibit substrate crossover, and the mechanisms through which this switching may occur.

References

1. A. Nakagawa, Y. Shi, E. Kage-Nakadai, S. Mitani, D. Xue, *Science* **328**, 327 (2010); published online 11 March 2010 (10.1126/science.1182374).
2. J. Yuan, S. Shaham, S. Ledoux, H. M. Ellis, H. R. Horvitz, *Cell* **75**, 641 (1993).
3. M. Miura *et al.*, *Cell* **75**, 653 (1993).
4. X. Liu, H. Zou, C. Slaughter, X. Wang, *Cell* **89**, 175 (1997).
5. H. Sakahira, M. Enari, S. Nagata, *Nature* **391**, 96 (1998).
6. E. Bernstein *et al.*, *Nature* **409**, 363 (2001).
7. Q. Liu *et al.*, *Science* **301**, 1921 (2003).
8. J. Liu *et al.*, *Science* **305**, 1437 (2004).
9. E. Bernstein *et al.*, *Nat. Genet.* **35**, 215 (2003).
10. H. Zhang *et al.*, *Cell* **118**, 57 (2004).
11. I. J. MacRae *et al.*, *Science* **311**, 195 (2006).
12. X. Ye, Z. Paroo, Q. Liu, *J. Biol. Chem.* **282**, 28373 (2007).

10.1126/science.1189245

CHEMISTRY

In Pursuit of Water Oxidation Catalysts for Solar Fuel Production

A durable molecular catalyst for water oxidation has been made from readily available and relatively inexpensive materials.

James K. Hurst

Roughly three-fourths of the power generated globally comes from burning fossil fuels. For solar energy to compete directly as a replacement, technologies are needed to capture this energy in a chemical form—as a fuel—so it can be used when sunlight is not available. One bottleneck in the development of practical solar fuels is the water oxidation reaction. Water is the only potential source of electrons capable of reducing protons to H_2 or CO_2 to carbonaceous fuels on a global scale. Thus, while there may be many options for reduction catalysts, redox cycling inevitably requires the coupling of reduction reactions to water oxidation (see the figure, panel A). On page 342 of this issue, Yin *et al.* (*1*) report on a water-soluble water oxidation catalyst that has a reaction center containing four cobalt (Co) atoms. Its surrounding ligands are not organic groups but are polyoxotungstate ($PW_9O_{34}^{9-}$) anions that resemble the solid oxide supports of heterogeneous catalysts. This catalyst weds the best features of extant heterogeneous and homogeneous catalysts while remedying many of their respective disadvantages.

The task of developing a catalyst that meets the diverse criteria for practical applications is daunting. The half-reaction comprising water oxidation, $2H_2O \rightarrow O_2 + 4H^+ + 4e^-$, is a chemist's nightmare, in that it involves multiple bond rearrangements between two molecules that must be carefully synchronized with the removal of protons and electrons if the formation of rate-retarding, high-energy intermediates is to be avoided. Moreover, to be of use in large-scale applications, the catalysts must stay active for extended periods of time or be easily regenerated, and must be made from readily available and inexpensive materials.

Both homogeneous and heterogeneous catalysts have advantages and drawbacks for water oxidation. Homogeneous catalysts permit maximal dispersion of catalytic centers (and hence maximal reactivity), and in most cases, many well-characterized variants can be synthesized with different ligand environments, All of these features foster performance optimization. However, currently available catalysts tend to rapidly lose their catalytic capabilities because they contain heterocyclic organic ligands that easily degrade (*2*–*4*) in the hostile environments required to oxidize water. These catalysts are

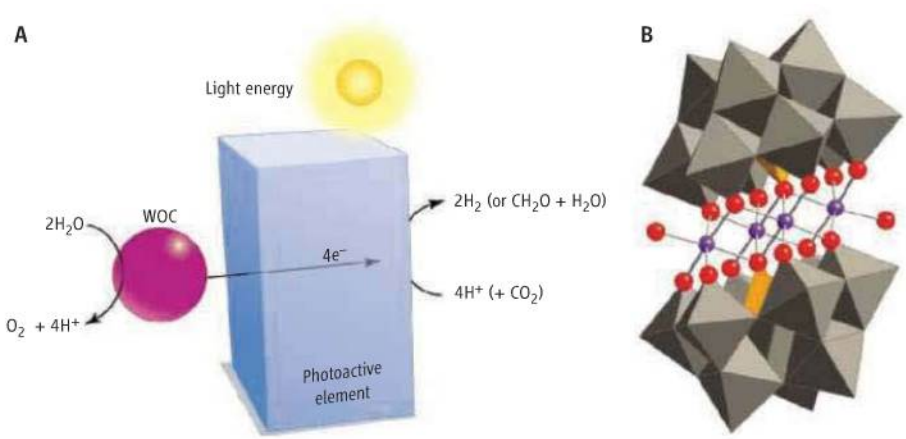

Artificial photosynthesis. (**A**) A water oxidation catalyst (WOC) transfers electrons from water to photoactive assemblies that promote photoinitiated charge separation for reduction of protons to hydrogen or carbon dioxide to organic compounds. In this generic scheme, the photoactive device comprising a photosensitizer and reduction catalyst might be assembled on an electrode, suspensions of small particles, or conducting organic or inorganic membranes capable of directing charge transport. Formaldehyde is shown as one of several possible CO_2 reduction products. (**B**) A schematic drawing of the water oxidation catalyst reported by Yin *et al.* depicts the Co_4O_{16} core with cobalt atoms in purple and oxygen atoms in red. The WO_6 units are depicted as gray octahedra, and phosphate groups are shown as orange tetrahedra.

Department of Chemistry, Washington State University, Pullman, WA 99164–4630, USA. E-mail: hurst@wsu.edu

also not amenable to regenerative self-repair processes. The reactive sites of heterogeneous catalysts are located within chemically robust inorganic lattices, often allowing better retention of activity (*5*, *6*), which may include regeneration by simple dissolution-deposition recycling (*7*). However, these materials are generally less adaptable to device fabrication and mechanistic analyses.

The chemically inert, inorganic polyoxometalate (POM) ligand anions have been used previously to provide a framework for assembly of catalytically active Ru_4O_4 clusters (*8*, *9*). These compounds span the interface between molecular catalysts in solution and solid-phase particulate catalysts, combining the best features of both. Moreover, their relatively high catalytic activity toward water oxidation remains undiminished after many cycles of O_2 formation. However, one serious disadvantage common to many other water oxidation catalysts is the use of ruthenium (or iridium) in the catalytic center. These elements are among the least abundant metals in Earth's crust, more so even than platinum, which calls into question their availability for large-scale application to photoproduction of H_2 or organic fuels.

Seeking alternatives, Yin *et al.* surveyed a group of previously synthesized POM complexes that contain Co, an Earth-abundant metal, for water-oxidizing capabilities (see the figure, panel B). Of the eight compounds investigated, one displayed performance characteristics that were comparable to those of the Ru_4O_4 POM complex ion. This discovery vindicates the strategy implicit in the use of POM ligands to construct superior soluble catalysts. The synthetic versatility of this class of compounds should allow structure-function relations to be explored, which is the key to informed development of more active catalysts. A second highly desirable aspect of these compounds is their capacity for self-assembly, which might be exploited for periodic catalyst rejuvenation similar to that recently demonstrated for cobalt phosphate precipitates (*7*).

Much of the early research on metal ion–catalyzed water oxidation took a biomimetic approach. Attempts were made at duplicating the structural features of the inorganic core of the biological oxygen-evolving complex, now known to be an asymmetrical Mn_4O_4Ca cluster, in simpler multicentered coordination complexes, without much success. Recent discoveries, primarily with Ru complexes, have provided examples of catalysis by mono- (*10*, *11*), di- (*12*, *13*), and tetranuclear complexes (*8*, *9*), some of which have been shown or are predicted to react by very different pathways (*3*, *10*–*14*). A striking example of this variability in structural morphology is found in the POM-ligated catalysts, where the tetraruthenate core adopts an adamatane (cuboidal) arrangement (*8*, *9*), but the four cobalts are aligned in a near-linear array between the two POM ligands (*1*). What is clear from this recent body of work is that there are numerous ways to form O_2 from two water molecules, and that the options for catalyst development available to inorganic chemists are far greater than previously recognized.

References and Notes

1. Q. Yin *et al.*, *Science* **328**, 342 (2010); published online 11 March 2010 (10.1126/science.1185372).
2. L. Duan *et al.*, *Inorg. Chem.* **49**, 209 (2010).
3. J. K. Hurst *et al.*, *Inorg. Chem.* **47**, 1753 (2008).
4. P. K. Ghosh *et al.*, *J. Am. Chem. Soc.* **106**, 4772 (1984).
5. P. G. Hoertz *et al.*, *J. Phys. Chem. B* **111**, 6845 (2007).
6. F. Jiao, H. Frei, *Angew. Chem. Int. Ed.* **48**, 1841 (2009).
7. D. A. Lutterman, Y. Surendranath, D. G. Nocera, *J. Am. Chem. Soc.* **131**, 3838 (2009).
8. Y. V. Geletii *et al.*, *Angew. Chem. Int. Ed.* **47**, 3896 (2008).
9. A. Sartorel *et al.*, *J. Am. Chem. Soc.* **130**, 5006 (2008).
10. H.-W. Tseng, R. Zong, J. T. Muckerman, R. Thummel, *Inorg. Chem.* **47**, 11763 (2008).
11. J. J. Concepcion *et al.*, *Acc. Chem. Res.* **42**, 1954 (2009).
12. S. Romain, F. Bozoglian, X. Sala, A. Llobet, *J. Am. Chem. Soc.* **131**, 2768 (2009).
13. L. Duan, A. Fischer, Y. Xu, L. Sun, *J. Am. Chem. Soc.* **131**, 10397 (2009).
14. J. T. Muckerman *et al.*, *Inorg. Chem.* **47**, 1787 (2008).

15. Research was supported by the Chemical Sciences, Geosciences and Biosciences Division, Office of Basic Energy Sciences, Office of Science, U.S. Department of Energy, under grant DE-FG02-06ER15820.

10.1126/science.1187721

CLIMATE CHANGE

Tracking Earth's Energy

Where has the energy from global warming gone?

Kevin E. Trenberth and John T. Fasullo

By measuring the net radiative incoming and outgoing energy at the top of Earth's atmosphere, it is possible to determine how much energy remains in the Earth system. But where exactly does the energy go? The main energy reservoir is the ocean, which sequesters energy as heat. Because energy is exchanged between the atmosphere and the ocean, this heat can resurface at a later time to affect weather and climate on a global scale. A change in the overall energy balance will thus sooner or later have consequences for the climate. Existing observing systems can measure all the required quantities, but it nevertheless remains a challenge to obtain closure of the energy budget. This inability to properly track energy—due to either inadequate measurement accuracy or inadequate data processing—has implications for understanding and predicting future climate.

National Center for Atmospheric Research, Boulder, CO 80307, USA. E-mail: trenbert@ucar.edu

To understand how energy is taken up and later released by the climate system, consider the natural variability from El Niño Southern Oscillation. The cold sea surface temperatures in the equatorial Pacific present in normal or La Niña conditions create conditions favorable for fewer clouds and more sunshine and a build-up of heat in the ocean as a precursor of El Niño (*1*). The spread of warm waters across the Pacific, together with changing winds, in turn promotes evaporative cooling of the ocean, moistening the atmosphere and fueling tropical storms and convection over and around the anomalously warm waters. The changed atmospheric heating alters the jet streams and storm tracks and controls weather patterns for the duration of the El Niño event (*2*). The loss of heat can in turn lead to La Niña.

A strong La Niña event in 2007–2008 spilled over to the 2008–2009 northern winter, causing cooler than normal weather across North America and elsewhere (*3*). By June 2009, the situation had reversed as the next, comparatively moderate El Niño emerged. Multiple storms barreled into Southern California in January 2010, consistent with expectations from the El Niño.

The human influence on climate, mostly by changing the composition of the atmosphere, must influence energy flows in the climate system (*4*). Increasing concentrations of carbon dioxide (CO_2) (see the figure) and other greenhouse gases have led to a post-2000 imbalance at the top of the atmosphere of 0.9 ± 0.5 W m^{-2} (*5*); it is this imbalance that produces "global warming." It is possible to track how much extra

energy has gone back to space as the planet warms (*6*) and where the rest of the energy has accumulated (*7*) (see the figure). Over the past 50 years, the oceans have absorbed ~90% of the energy added to the climate system; the rest has gone into melting sea and land ice and heating the land surface and atmosphere (*4*). CO_2 concentrations have further increased since 2003, and even more heat should have accumulated at a faster rate since then. Where has this energy gone (see the figure)?

The difference between the incoming and outgoing energy—the planetary energy imbalance—at the top of the atmosphere is too small to be measured directly from satellites. Nevertheless, the satellite measurements are sufficiently stable from one year to the next, so that by measuring incoming solar radiation and outgoing infrared radiation, it is possible to track changes in the net radiation (*8*, *9*). This includes tracking the slight decrease in solar insolation since 2000 with the ebbing 11-year sunspot cycle; this decrease is enough to offset 10 to 15% of the estimated net human-induced warming (*7*).

In 2008, for the tropical Pacific during La Niña conditions, extra energy absorption at the top of the atmosphere was observed as expected (*9*). Since 2004, ~3000 Argo floats have provided regular temperature soundings of the upper 2000 m of the ocean, giving new confidence in the ocean heat content assessment—yet, ocean temperature measurements from 2004 to 2008 suggest a substantial slowing of the increase in global ocean heat content (see the figure, panel A) (*10*). If the extra energy has not gone into the ocean, where has it gone?

Another perspective on where energy from global warming has gone comes from rising sea level. Since 1992, sea level observations from satellite altimeters at millimeter accuracy have revealed an essentially linear global increase of ~3.2 mm per year, with an enhanced rate of rise during the 1997–1998 El Niño and a brief slowdown in the 2007–2008 La Niña. Since 2003, gravity measurements from the Gravity Recovery and Climate Experiment (GRACE) of the change in glacial land ice and water have shown an increase in ocean mass. This eustatic component of sea level rise may have compensated for the decrease in the thermosteric (heat-related expansion) component (*11*, *12*). However, for a given amount of heat, sea level rise can be achieved much more efficiently—by a factor of 40 to 70 typically—by melting land ice rather than expanding the ocean (*7*). So, although some heat has gone into the record-breaking loss of Arctic sea ice, and some has undoubtedly contributed to the unprecedented melting of Greenland (*13*) and Antarctica (*14*), it does not add up to anywhere near enough to account for the measured energy difference at the top of the atmosphere.

Closure of the energy budget over the past 5 years is thus elusive (*7*). State-of-the-art observations are unable to fully account for recent energy variability. Is the warming associated with the latest El Niño a manifestation of the missing energy reappearing?

Proposals for addressing global warming now include geoengineering, whereby tiny particles are injected into the stratosphere to emulate the cooling effects of stratospheric aerosol of a volcanic eruption (*15*). Implicitly, such proposals assume understanding and control of the energy flow, which requires detailed tracking of energy within the climate system. How can we understand whether the strong cold outbreaks of December 2009 are simply a natural weather phenomenon, as they seem to be, or are part of some change in clouds or pollution, if we do not have adequate measurements?

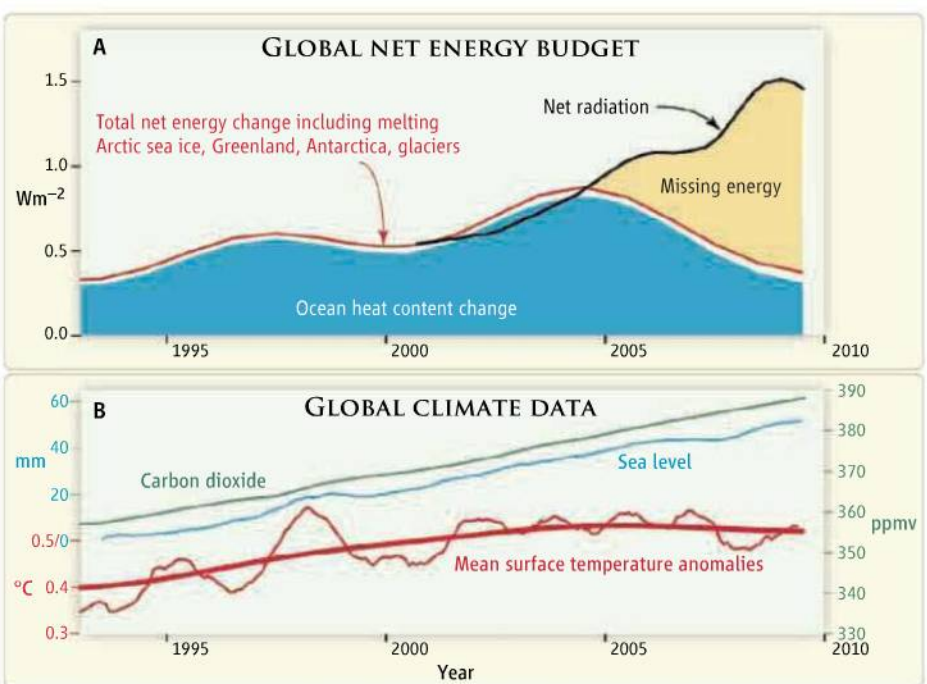

Where does the energy go? (**A**) Estimated rates of change of global energy. The curves are heavily smoothed and somewhat simplified. From 1992 to 2003, the decadal ocean heat content changes (*10*) (blue), along with the contributions from melting glaciers, ice sheets, and sea ice and small contributions from land and atmosphere warming (*7*), suggest a total warming (red) for the planet of 0.6 ± 0.2 W/m² (95% error bars). After 2000, observations from the top of the atmosphere (*9*) (black, referenced to the 2000 values) increasingly diverge from the observed total warming (red). (**B**) The observed steady increases in carbon dioxide and sea level contrast with the variability in global surface air temperature. Shown are the 12-month running means of global mean surface temperature anomalies relative to 1901 to 2000 from NOAA [red (thin) and decadal (thick)] in degrees Celsius (scale lower left), carbon dioxide concentrations (green) in parts per million by volume (ppmv) from NOAA (scale right), and global sea level adjusted for isostatic rebound from AVISO (Archiving, Validation and Interpretation of Satellite Oceanographic Data) (blue, relative to 1993, scale at left in millimeters). Decadal filter from (*4*).

References and Notes

1. K. E. Trenberth, J. M. Caron, D. P. Stepaniak, S. Worley, *J. Geophys. Res.* **107**, (D8), 4065 (2002).
2. K. E. Trenberth *et al.*, *J. Geophys. Res.* **103**, (C7), 14291 (1998).
3. J. Perlwitz, M. Hoerling, J. Eischeid, T. Xu, A. Kumar, *Geophys. Res. Lett.* **36**, L23706 (2009).
4. IPCC, *Climate Change 2007: The Physical Science Basis*, S. Solomon *et al.*, Eds. (Cambridge Univ. Press, New York, 2007).
5. K. E. Trenberth, J. T. Fasullo, J. Kiehl, *Bull. Am. Meteorol. Soc.* **90**, 311 (2009).
6. D. M. Murphy *et al.*, *J. Geophys. Res.* **114**, (D17), D17107 (2009).
7. K. E. Trenberth, *Curr. Opin. Environ. Sustainability* **1**, 19 (2009).
8. N. G. Loeb *et al.*, *J. Clim.* **22**, 748 (2009).
9. T. Wong, P. W. Stackhouse Jr., D. P. Kratz, A. C. Wilber, *Bull. Am. Meteorol. Soc.* **90**, S33 (2009).
10. S. Levitus *et al.*, *Geophys. Res. Lett.* **36**, L07608 (2009).
11. A. Cazenave *et al.*, *Global Planet. Change* **65**, 83 (2009).
12. E. W. Leuliette, L. Miller, *Geophys. Res. Lett.* **36**, L04608 (2009).
13. M. van den Broeke *et al.*, *Science* **326**, 984 (2009).
14. J. L. Chen *et al.*, *Nat. Geosci.* **2**, 859 (2009).
15. S. D. Levitt, S. J. Dubner, *Superfreakonomics: Global Cooling, Patriotic Prostitutes, and Why Suicide Bombers Should Buy Life Insurance* (Harper Collins, New York 2009).

16. NCAR is sponsored by the National Science Foundation. This research is partially sponsored by the NOAA CCDD program under grant NA07OAR4310051 and NASA under grant NNX09AH89G.

10.1126/science.1187272

ENGINEERING

Cooling Energy-Hungry Data Centers

The information technology industry is focusing on approaches to hot-water cooling for the design of energy-efficient data centers.

G. I. Meijer

Soon after the Internet took off in the mid-1990s, enterprise computing infrastructures with warehouses full of servers, known as data centers, became commonplace. The energy consumption challenges posed by such data centers are considerable. The power dissipation of servers has to be managed skillfully. Perhaps surprisingly, the power consumption of the cooling infrastructure that is required to keep the microelectronic components from overheating is on a par with that of the servers themselves.

In 2009, an estimated 330 terawatt-hours of energy—about 2% of the global electricity production—was consumed to operate data centers worldwide (*1*). Apart from the sheer economic impact (U.S.$ 30 billion), there are also considerable ecological consequences. The International Energy Agency estimated that the greenhouse-gas emissions associated with the electricity production was around 200 million metric tons of CO_2 and accounted for 0.7% of the global energy-related CO_2 emissions. This prompted increased scrutiny from regulators (*2*, *3*).

The information-technology industry therefore needs efficacious concepts to reduce the energy consumption of data centers. The key culprits are the server microprocessors, or more precisely, the transistors inside these microprocessors (see the figure, panel A). Currently, transistors with 45-nm lateral features are in volume production, and the pace of miniaturization continues unabated (*4*). It is a formidable challenge to keep the power dissipation of these transistors within acceptable limits. With shrinking dimensions of the transistors, leakage currents consume more power than the actual computational processes. To alleviate this burden, new materials were introduced in the late 2000s. Most notably, the replacement of the SiO_2 gate oxide, which is only a few atomic layers thick, with a physically thicker layer of a hafnium-based oxide enabled an appreciable reduction of the gate tunneling currents while maintaining the electrical performance of the transistor (*5*, *6*). Nevertheless, keeping the gate leakage power per unit area below 1 kW cm^{-2} will remain a particularly difficult issue, especially for scaled-down devices beyond the 2013 horizon.

Consequently, amid the new microprocessor generations, the prospect of restraining the power dissipation at peak performance still looks grim. For high-performance microprocessor circuitry, the power dissipation is projected to stay around 50 W cm^{-2}, a value that is several times greater than that of a stove's hot plate. Hence, if the data-center power-dissipation issue cannot be mitigated at its source, what can be done to reduce the total energy consumption and carbon footprint?

For the newest members of microprocessor families, sophisticated circuit architectures have been introduced, which allow the power associated with computational processes and also the leakage power to be adapted (*7*, *8*). The microprocessor frequency can be adjusted and circuit blocks can be temporarily powered down completely when not in use. These innovations lead to energy savings for a computational load that comes in bursts or that is bound to memory latency or input/output operations.

An alternative approach is to tackle the problem at the cooling infrastructure (*9*). Approximately 50% (industry average) of the electricity consumption currently goes toward powering this cooling infrastructure. It therefore appears ironic that Moore's law (a projection of microprocessor performance) is widely known and often cited, while increasingly critical physical laws of thermodynamics receive little popular attention.

The first law of thermodynamics states that energy is conserved. The electrical energy that is supplied to the computer system is eventually entirely converted into thermal energy. The standard method to remove this heat is by forced circulation of large amounts of chilled air. Massive heat sinks with long and fine-pitched fins protruding from a heat-spreader base are used to enhance the convective heat transfer from the hot modules to the cold air (see the figure, panel B). The collected heat is then expelled to the outside.

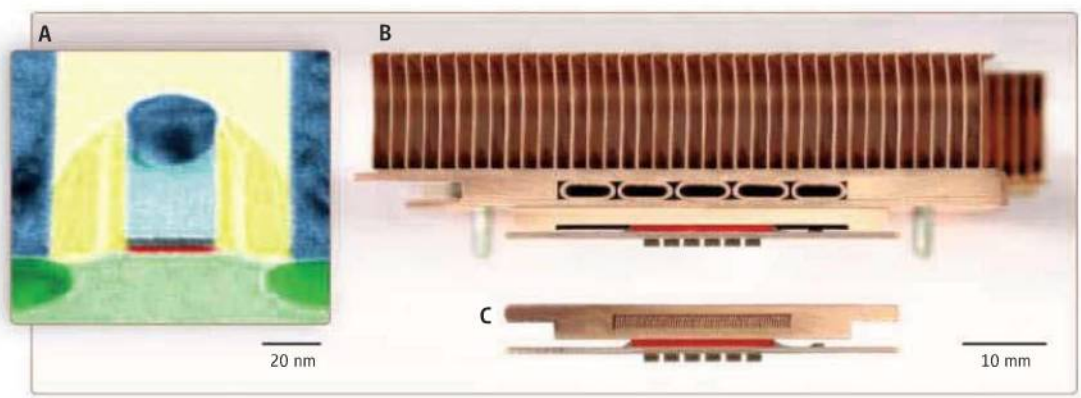

Heat generation and cooling in the data center. (**A**) Transmission electron microcopy image of a transistor. Heat is primarily generated near the gate oxide (marked red). (**B**) Cross-section of microprocessor module with air-cooled heat sink. Area in red indicates location of microprocessor. (**C**) Cross section of microprocessor module with liquid-cooled microchannel heat sink.

A straightforward approach to reducing the energy consumption of the cooling infrastructure is through a careful segregation of the chilled- and the hot-air flows.

The real key to ratcheting down the energy consumption of a computing facility is liquid cooling. The reason is that thermodynamically liquid cooling is much more efficient than air cooling because the heat capacity of liquids is orders of magnitude larger than that of air (for example, for water it is 4 MJ m^{-3} K^{-1} versus 1 kJ m^{-3} K^{-1} for air). Once the heat has been transferred to the liquid, it can be handled very efficiently. Critics of liquid cooling might contend that it comes at the price of increased mechanical complexity. True, but this can be managed as computers were once equipped with liquid cooling when the power density of bipolar-transistor–based computer systems reached its peak during the 1980s. For example, the

IBM Research–Zurich, 8803 Rüschlikon, Switzerland. E-mail: inm@zurich.ibm.com

Cray-2 supercomputer used liquid immersion cooling (*10*).

Recently, chilled-liquid cooling was reintroduced in high-end mainframes and densely packed servers to cope with the high heat fluxes. Yet, liquid cooling can be taken further if we consider a microfluidic heat sink (*11*) (see the figure, panel C). Microchannel heat sinks can be designed such that the thermal resistance between the transistor and the fluid is reduced to the extent that even cooling-water temperatures of 60° to 70°C ensure no overheating of the microprocessors. This hot-water cooling has compelling advantages. First, chillers are no longer required year-round and thus the data-center energy consumption plummets by up to 50%. Second, and perhaps most important, direct utilization of the collected thermal energy becomes feasible, either using synergies with district heating or specific industrial applications. With such an appealing waste-heat recovery system, the green diligence of data centers would be upped substantially.

Reducing the energy consumption of data centers and concomitantly restraining costs, while curtailing carbon emission, is achievable. Despite power dissipation in microprocessors continuing to be a source of severe concern, liquid cooling and deploying waste heat appear to become imperative in the drive for improving the data-center energy efficiency.

References

1. International Data Corporation, Document No. 221346 (2009), www.idc.com.
2. U.S. Environmental Protection Agency, Report to Congress on Server and Data Center Energy Efficiency (2007).
3. European Commission, Code of Conduct on Data Centres Energy Efficiency (2008).
4. International Technology Roadmap for Semiconductors, 2009 Edition, Executive Summary; www.itrs.net/Links/2009ITRS/Home2009.htm.
5. K. Mistry *et al.*, *IEEE IEDM 2007 Tech. Digest*, 10.2 (2007).
6. M. Chudzik *et al.*, *IEEE VLSI 2007 Tech. Digest*, 11A-1 (2007).
7. N. A. Kurd *et al.*, *IEEE ISSCC 2010 Tech. Digest*, 5.1 (2010).
8. M. Ware *et al.*, *IEEE HPCA 2010 Tech. Digest*, 6.4 (2010).
9. L. A. Barroso, U. Hölzle, *The Datacenter as a Computer* (Morgan and Claypool, 2009); www.google.com/corporate/green/datacenters.
10. S. R. Cray Jr., U.S. Patent 4590538 (1986).
11. D. B. Tuckerman, R. F. W. Pease, *Electron Device Lett.* **2**, 126 (1981).

10.1126/science.1182769

MATERIALS SCIENCE

The Future of Metals

Despite advances made in composite materials, metals remain irreplaceable in many important applications.

K. Lu

On 15 December 2009, the world's most fuel-efficient commercial jetliner—the Boeing 787 Dreamliner—completed its first flight. The airliner is mostly made from carbon fiber–reinforced polymeric composites (50% by weight, up from 12% in the Boeing 777) (*1*). Traditional metals are substantially replaced by composites with higher strength/weight ratios; aluminum usage has dropped to 20% (versus 50% in the 777). Ever since the 1950s, when "engineering materials" mainly meant metals (*2*), the share of metals in engineering materials has been diminishing. What are the reasons behind this trend, and which applications are likely to stay in the domain of metals?

The main property limitation of metals as structural materials is their low specific strength (the strength/weight ratio). Most engineering designs call for structural materials that have high strength, fracture toughness (a measure of the energy required for propagating cracks), and stiffness while minimizing weight. Most metals have high strength and stiffness, but because they are dense (steels are several times as dense as ceramics and polymers), their strength/weight and stiffness/weight ratios are low relative to competing materials (see the figure). This is a key reason for replacing metals in aircraft and sporting goods, where weight is a primary concern. Some metals such as aluminum and magnesium are light, but they are too soft for many applications and have low toughness and stiffness. Titanium alloys partly overcome these problems: They are about half as dense as steels, have higher strength, and are very tough. Titanium was first used in airliners in the 1960s in the Boeing 707 and its use has increased to 15% in the Boeing 787 (*1*).

Metals can be strengthened through controlled creation of internal defects and boundaries that obstruct dislocation motion (*3*). But such strategies compromise ductility and toughness, in contrast to the increasing toughness at higher strength seen with polymeric composites (see the figure). Strengthening may also compromise other metal properties, such as conductivity and corrosion resistance. One method for strengthening metals without losing toughness is grain refinement (grain size reduction), but when the grain sizes fall below ~1 μm, strengthening is usually accompanied by a drop in ductility and toughness (*4*). A recent study points the way to overcoming this problem: In a low-alloy steel containing ultrafine elongated ferrite grains strengthened with nanosized carbides, toughness and strength both rose when temperature was lowered from 60° to –60°C (*5*). In contrast, conventional metals become strong but brittle at lower temperatures. The authors attributed the observed toughening to the unique hierarchical anisotropic nanostructures in their steels.

Nanotwinned metals are another example of hierarchical nanostructured metals with extraordinary mechanical properties (*3*). When a high density of twin boundaries (highly symmetrical interfaces between two grains of the same lattice structure) is incorporated into polycrystalline copper grains, with boundary spacing in the nanometer scale, the material becomes stronger than coarse-grained copper by a factor of 10; it is also very ductile. The ultrastrong nanotwinned copper has an electrical conductivity comparable to that of high-conductivity copper (*6*) and a much enhanced resistance against electromigration (*7*). It has great potential for applications in microelectronics.

Corrosion is another headache for metals (*8*). To protect metals from corrosion, they are commonly coated with a layer of corrosion-resistant material. The Hangzhou Bay Bridge in China is an outstanding example of this technique. This 36-km-long bridge—the world's longest to date, with a design life of 100 years—is supported by several thousand pillars made of concrete-filled steel tubes ~80 m in length. The tubes are protected against corrosion in the harsh ocean environment by a coating of novel polymeric composites combined with cathode attachments.

Metal corrosion can also be resisted by forming a continuous protective passivation layer on the metal surface. For example, Yamamoto *et al.* (*9*) have added 2.5% Al to conventional austenitic stainless steels, resulting in the formation of a protective aluminum oxide layer that can resist further oxidation at elevated temperatures. Given their enhanced

Shenyang National Laboratory for Materials Science, Institute of Metal Research, Chinese Academy of Sciences, Shenyang 110016, China. E-mail: lu@imr.ac.cn

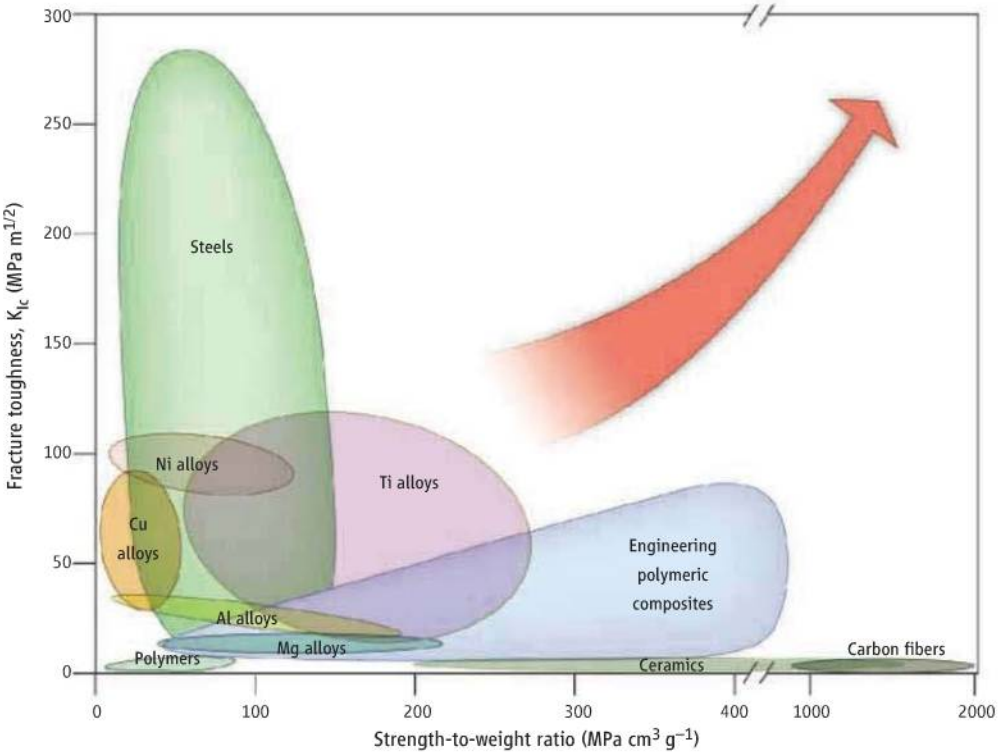

Competing materials. Steels have the highest toughness, whereas carbon fibers have the highest strengths. Titanium alloys and polymer composites are increasingly used in aircraft and sporting goods because of their outstanding combination of properties. Research on advanced materials for structural applications aims toward the upper right corner. [Data from (*2*)]

oxidation resistance, these steels could be used at the high temperatures and aggressive oxidizing conditions of energy conversion systems to replace the currently used expensive nickel-based superalloys (metals specifically developed for high-temperature applications). Another route to enhancing the corrosion resistance of metals is to modify the chemical composition of surface layers. But most such processes require high temperatures that may cause serious deterioration of the metal substrates. The processing temperatures can be lowered substantially if the grains of surface layers are refined into the nanoscale via surface mechanical attrition treatments (*10*).

Metals also get soft at elevated temperatures; they can rarely be used above 1000°C with useful strengths. Superalloys have higher operating temperatures (up to ~1150°C for nickel-based superalloys), enabling their use in high-temperature applications such as jet turbine engines. Superalloys for higher operating temperatures, based on metals with higher melting points such as molybdenum and niobium, are under investigation (*11*).

Despite these limitations, metals are still the major workhorse of our society and will remain so in the future, thanks to unique properties that make them irreplaceable.

First, metals have a much higher fracture toughness than other materials (see the figure); steels are the toughest known materials. Therefore, metals are usually used for key components with the highest requirements for reliability and durability, such as bridge cables, concrete reinforcement in buildings, and vehicle body frames. The Boeing 787 contains a considerable amount of metals (45%), mainly in critical parts with the highest reliability requirements, such as engines, wings, and alighting carriage.

Second, the properties of metals are uniform in all directions, and their strength is the same in tension and compression. Also, the strengths of metals are usually predictable. These features are critically important for predicting fracture in engineering structures. In contrast, it remains very difficult to predict fracture of composites and ceramics; their fracture is often catastrophic (the material fails all at once) and may cause serious economic loss and even loss of life. Hence, many advanced technologies continue to rely on high-performance metals. For instance, only extremely tough metal alloys can survive in the harsh irradiation and temperature conditions in the next generation of nuclear power stations. Body implants must sustain severe corrosive and loading conditions that also call for advanced tough metals.

Third, most metals are more conductive than ceramics and polymers. Copper and aluminum remain the best materials for overhead electricity transmission lines. Conducting lines and thermal spreaders used in information technology are mostly made from copper and its alloys. Metals also have unique magnetic properties that are not easily reproduced in other materials.

Fourth, metals have the best overall mechanical properties at temperatures up to a few hundred degrees. This window covers most of the operation temperatures in chemical engineering processes, power stations, and various engines. Finally, most metals are recyclable, making metals more competitive for quantity applications.

Modern technologies not only strongly rely on these unique properties of metals, but urgently call for even better metals. Increasing the strength of metals without sacrificing other properties is critical for their competitiveness. Multiscale hierarchical structures provide a possible route to optimizing overall properties. Metals may also be mixed with other materials in a controlled way to form composite structures. Assembling metals with other components in this way—for example, in novel reinforcements or hierarchical assemblies—may shift their strength/toughness ratios toward the upper right corner in the figure. Developments in different material families may thus benefit from each other.

References and Notes

1. 787 Dreamliner Program Fact Sheet (Boeing Corp., 2007; see www.boeing.com/commercial/787family/programfacts.html).
2. M. F. Ashby, *Materials Selection in Mechanical Design* (Elsevier, Oxford, ed. 3, 2005).
3. K. Lu, L. Lu, S. Suresh, *Science* **324**, 349 (2009).
4. M. A. Meyers, A. Mishra, D. Benson, *Prog. Mater. Sci.* **51**, 427 (2006).
5. Y. Kimura, T. Inoue, F. Yin, K. Tsuzaki, *Science* **320**, 1057 (2008).
6. L. Lu, Y. Shen, X. Chen, L. Qian, K. Lu, *Science* **304**, 422 (2004).
7. K.-C. Chen, W.-W. Wu, C.-N. Liao, L.-J. Chen, K. N. Tu, *Science* **321**, 1066 (2008).
8. A. King, G. Johnson, D. Engelberg, W. Ludwig, J. Marrow, *Science* **321**, 382 (2008).
9. Y. Yamamoto *et al.*, *Science* **316**, 433 (2007).
10. X. Si, B. N. Lu, Z. B. Wang, *J. Mater. Sci. Technol.* **25**, 433 (2009).
11. J. H. Perepezko, *Science* **326**, 1068 (2009).

12. I thank C. W. Che, R. B. Tan, and R. Yang for their critical comments; Y. Zhang for assistance in figure preparation; and the National Natural Science Foundation of China, the Chinese Academy of Sciences, and the Danish-Chinese Center for Nanometals for financial support.

10.1126/science.1185866

Extending Healthy Life Span—From Yeast to Humans

Luigi Fontana,[1,2]* Linda Partridge,[3]* Valter D. Longo[4]*

When the food intake of organisms such as yeast and rodents is reduced (dietary restriction), they live longer than organisms fed a normal diet. A similar effect is seen when the activity of nutrient-sensing pathways is reduced by mutations or chemical inhibitors. In rodents, both dietary restriction and decreased nutrient-sensing pathway activity can lower the incidence of age-related loss of function and disease, including tumors and neurodegeneration. Dietary restriction also increases life span and protects against diabetes, cancer, and cardiovascular disease in rhesus monkeys, and in humans it causes changes that protect against these age-related pathologies. Tumors and diabetes are also uncommon in humans with mutations in the growth hormone receptor, and natural genetic variants in nutrient-sensing pathways are associated with increased human life span. Dietary restriction and reduced activity of nutrient-sensing pathways may thus slow aging by similar mechanisms, which have been conserved during evolution. We discuss these findings and their potential application to prevention of age-related disease and promotion of healthy aging in humans, and the challenge of possible negative side effects.

Aging is a complex process of accumulation of molecular, cellular, and organ damage, leading to loss of function and increased vulnerability to disease and death. Despite the complexity of aging, recent work has shown that dietary and genetic alterations can substantially increase healthy life span of laboratory model organisms (Fig. 1).

Many of the mutations that extend life span decrease activity of nutrient-signaling pathways, such as the Igf (insulin-like growth factor)/insulin and the TOR (target of rapamycin) pathways, suggesting that they may induce a physiological state similar to that resulting from periods of food shortage. Indeed, dietary restriction, a reduction in food intake without malnutrition, extends life span of diverse organisms, including yeast, flies, worms, fish, rodents, and rhesus monkeys. The level of restriction usually ranges from 10 to 50% below the level in mammals fed ad libitum, but longevity extension can be achieved by complete starvation in yeast and worms. The beneficial effects of dietary restriction in mammals are obtained by reducing glucose consumption, but also by reducing fat or protein intake. Dietary restriction also protects against age-related decline in function and disease in rodents and monkeys (*1*), and in humans, it reduces risk factors for diabetes, cardiovascular disease, and cancer (*2*). Hence, understanding how dietary restriction exerts these effects could reveal targets for drugs and therapies for a broad-spectrum prevention of aging-related loss of function and disease.

Here we consider the role of nutrient-sensing signaling pathways in mediating the beneficial effects of dietary restriction. We focus on processes that are evolutionarily conserved in multiple organisms and discuss the evidence for their potentially protective, and detrimental, effects in humans.

Signaling Pathways and Dietary Restriction

Involvement of pathways in dietary restriction is usually tested by determining if a genetic mutation alters the response. Some methods of dietary restriction allow exploration of a range of food intakes. In worms, flies, and mice, life span rises to a maximum as food intake is lowered, but then declines rapidly through starvation with further reduction of food intake (Fig. 2). The degree of dietary restriction that maximizes life span, and the amplitude of the response, can thus be determined and used to test for genetic effects (*3*).

It is unlikely that a single, linear pathway mediates the effects of dietary restriction in any organism. Matching of metabolism, growth, and fecundity to food intake is crucial for survival and reproduction in nature, and parallel and redundant pathways appear to be involved (Box 1). Different organisms grow and reproduce at different rates and experience different degrees of food shortage in nature. The nutrient content of food and the way it is sensed are also variable. Thus, responses of organisms to dietary restriction may differ in mechanisms, and extent. When developing new or improved model systems to

	Life-span increase		Beneficial health effects	
	Dietary restriction	Mutations/ drugs	Dietary restriction	Mutations/ drugs
Yeast	3-fold	10-fold (with starvation/ DR)	Extended reproductive period	Extended reproductive period, decreased DNA damage/mutations
Worms	2- to 3-fold	10-fold	Resistance to misexpressed toxic proteins	Extended motility Resistance to mis-expressed toxic proteins and germ-line cancer
Flies	2-fold	60–70%	None reported	Resistance to bacterial infection, extended ability to fly
Mice	30–50%	30–50% (~100% in combination with DR)	Protection against cancer, diabetes, atherosclerosis, cardio-myopathy, autoimmune, kidney, and respiratory diseases; reduced neurodegeneration	Reduced tumor incidence; protection against age-dependent cognitive decline, cardio-myopathy, fatty liver and renal lesions. Extended insulin sensitivity
Monkeys	Trend noted	Not tested	Prevention of obesity; protection against diabetes, cancer, and cardiovascular disease	Not tested
Humans	Not determined	Not determined (GHR-deficient subjects reach old age)	Prevention of obesity, diabetes, hypertension Reduced risk factors for cancer and cardiovascular disease	Possible reduction in cancer and diabetes

Fig. 1. Experiments on dietary restriction (DR) and genetic or chemical alteration of nutrient-sensing pathways have been performed on a range of model organisms. The results differ widely, and little is known about the long-term effects in humans.

CREDITS: WIKIMEDIA COMMONS (YEAST), NIH (WORMS), THINKSTOCK (FLIES AND MICE), K. SUTLIFF (MONKEYS), JUPITERIMAGES (HUMANS)

An enhanced version of Fig. 3 and a slide show on aging can be found at www.sciencemag.org/cgi/content/full/328/5976/321.

[1]Division of Geriatrics and Nutritional Science, Washington University School of Medicine, St. Louis, MO 63110, USA. [2]Division of Nutrition and Aging, Istituto Superiore di Sanità, Rome, Italy. [3]Institute of Healthy Aging, and G.E.E., University College London, London WC1E 6BT, UK. [4]Andrus Gerontology Center and Department of Biological Sciences, University of Southern California, Los Angeles, CA 90089, USA.

*E-mail: lfontana@dom.wustl.edu (L.F.); l.partridge@ucl.ac.uk (L.P.); vlongo@usc.edu (V.D.L)

study aging and healthy life span, it will be important to combine studies that mimic the various environments encountered by the organism in the wild with those that simplify the method and facilitate molecular studies.

Studies of Yeast

The single-celled budding yeast is an excellent organism for genetic screens for mechanisms that are candidates for the evolutionarily conserved effects of dietary restriction on life span in multicellular organisms. Both the number of daughter cells generated by a single mother cell (replicative life span) and survival of a population of nondividing cells (chronological life span) have been analyzed.

Nutrient-sensing pathways. Reduced activity of two major nutrient-sensing pathways can extend both types of yeast life span.

The first is centered on an amino acid–sensing pathway, including the target of rapamycin (TOR) and the serine-threonine kinase Sch9. Deletion of SCH9, which has sequence and functional similarity to the ribosomal protein S6 kinase (S6K), causes an increase of up to several-fold in both chronological (Fig. 3) and replicative life span (*4*, *9*), as does deletion or inhibition of *TOR1* (*4*–*6*), probably by inactivating the downstream Sch9 (*4*, *6*, *7*, *9*). Alterations to protein synthesis are strongly implicated in extension of replicative life span by reduced TOR/Sch9 and may play a key role in chronological life span as well (*8*). Extension of chronological life span by reduced activity of the TOR pathway depends on the transcription factor Gis1, which activates many protective systems including Mn-SOD (*6*, *9*). Understanding exactly how reduced activity of this pathway and the activation of the Gis1 transcription factor extend yeast life span will be crucial, because similar effects are seen in worms, flies, and mice.

The second pathway includes three proteins: Ras, adenylate cyclase (AC), and protein kinase A (PKA) (Fig. 3) (*9*, *10*). The activation of two transcription factors (Msn2 and Msn4) that control cellular protection systems is required to mediate the effect of reduced Ras-AC-PKA signaling on chronological life-span extension (*9*) and may also mediate the extension of replicative life span (*11*). Again, analysis of mechanisms in yeast will illuminate the role of this pathway in mice.

Extension of yeast life span by these pathways requires the antioxidant enzyme Mn-SOD (superoxide dismutase), which scavenges the superoxide free radical (*12*). Superoxide level increases during yeast aging and is reduced in long-lived mutants deficient in Ras-AC-PKA or Tor-Sch9 signaling (*9*). However, overexpression of both the antioxidant enzymes SOD1 and SOD2 or catalase in yeast results in a minor extension of mean survival, indicating that many other systems, including DNA-repair genes, are important in longevity modulation (*9*, *13*).

Nondividing yeast cells deplete glucose and produce ethanol and/or acetic acid, which contribute to chronological aging (*13*, *14*). Deletion of *TOR1*or *SCH9* promotes removal of ethanol and acetic acid and accumulation of glycerol in the medium (*6*, *13*). Because acetate and ethanol can be used as nutrients by yeast, their removal may therefore extend chronological life span by mechanisms similar to those of dietary restriction (*6*, *13*, *14*). However, the chronological life span of cells deficient in *TOR-SCH9* or *RAS-AC-PKA* is also extended in media where acetic acid and ethanol are absent (*6*, *13*), indicating that these pathways can increase life span independently of acetic acid (Fig. 3). These findings may point to mechanisms relevant to aging in multicellular eukaryotes, in which analogous effects of the pro-aging pathways on the utilization and storage of carbon sources are observed (Fig. 3).

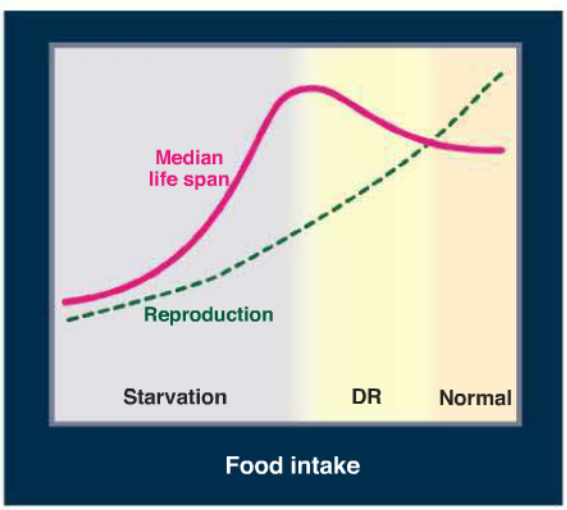

Fig. 2. The median life span and fecundity of higher eukaryotes are negatively affected by a very low food intake. However, life span but not fecundity is optimized by dietary restriction (DR). Unlike what is observed in most higher eukaryotes, starvation extends the yeast chronological life span.

Dietary restriction. In budding yeast, starvation implemented by switching the cells from a medium containing nutrients to one containing water doubles chronological life span (*12*, *15*). More moderate reductions in the concentration of glucose in the growth medium from the standard 2% to 0.5 or 0.05% also extend both replicative and chronological life span, apparently by the regulation of overlapping pathways and mechanisms described below (*4*, *10*, *12*, *16*).

Decreased signaling by the Ras-AC-PKA and Tor-Sch9 pathways is important in the response to glucose restriction (Fig. 3), with increased transcriptional activity of Msn2 and Msn4, and the consequent expression of Pnc1 [a nicotinamide deaminase that regulates the activity of the nicotinamide adenine dinucleotide (NAD)–dependent deacetylase Sir2] (*11*, *17*). Reduced protein synthesis and the breakdown of proteins and intracellular organelles are thought to also contribute to replicative longevity (*17*).

Inhibition of both the Ras-AC-PKA and Tor-Sch9 pathways and the activation of the protective transcription factors described above are also implicated in dietary restriction–dependent extension of chronological life span (Fig. 3) (*12*). It will be important to identify additional mediators of the effects of dietary restriction on life span (Fig. 3).

Studies of the Nematode Worm *Caenorhabditis elegans*

C. elegans was one of the first organisms that allowed the identification of mutations that extend life span. Unlike the unicellular yeast, it allows studies of different cell types and organs, such as the nervous or digestive systems. It is also more closely related to mammals.

Nutrient-sensing pathways. With the onset of multicellularity, nutrient-sensing systems evolved a systemic element that allowed communication at a distance between different parts of the body, while the exact nature of the response could also vary among the cells of different tissues. The worm *C. elegans* is a relatively simple multicellular organism in which to unravel these effects.

Reduced activity of the IIS (insulin/Igf-like signaling) pathway extends life span in *C. elegans* and other multicellular organisms (*18*). This life-span increase requires the Forkhead FoxO transcription factor *daf-16* (Fig. 3), which regulates genes involved in a wide range of defensive activities including cellular stress response, antimicrobial activity, and detoxification of xenobiotics and free radicals. As in yeast, overexpression of the antioxidant SOD-1 causes only a minor extension in life span (*19*). Extension of life span by reducing the activity of the IIS pathway also requires the heat shock factor *hsf-1*, which can itself extend life span and regulates expression of small heat shock proteins (*18*). Reduction of IIS only in specific tissues has revealed that the nervous system and the gut, which includes the white adipose tissue (fat) of the worm, are important. Regulation of insulin ligands by DAF-16 acts systemically to coordinate the rate of aging in the whole worm (*18*).

The TOR pathway interacts intimately with IIS, and inhibition of its activity, including reduction of TOR and S6 kinase, as in yeast, can increase life span in *C. elegans* (Fig. 3) (*18*, *20*, *21*). Autophagy, a process inhibited by TOR that involves digestion of cellular components, is required for the increase in survival (*21*), and altered activity of several other targets of the TOR pathway, such as translation (*22*) and the activity of the HIF-1 (hypoxia-inducible factor 1) transcription factor (*23*, *24*), can independently extend life span.

Dietary restriction. Multiple methods of dietary restriction are used in *C. elegans*, including mutations that reduce pharyngeal pumping, removal of the bacterial food source, dilution of live or dead bacteria in solid or liquid cultures, peptone dilution, and axenic culture (*25*), and these extend life span by both distinct and overlapping

mechanisms (*25*, *26*). Chemosensation may be important in the response to dietary restriction, because diffusible substances from bacteria that are sensed by the worm can reduce life span without any change in food intake (*27*). As in rodents, at least one method of dietary restriction, requiring heat shock factor–1, can protect against age-related proteotoxicity (*28*).

The key IIS effector DAF-16 is required for the response only to some methods of dietary restriction, and for these methods, the adenosine 5′-monophosphate (AMP)–activated protein kinase (AMPK) is also required (Fig. 3) (*26*). Testing of the role of TOR has yielded inconsistent results (*25*). However, targets of the TOR pathway, such as autophagy and HIF-1, clearly contribute to dietary restriction responses (*25*).

Two other transcription factors, Pha-4 and SKN-1, are required for the response to some methods of dietary restriction in *C. elegans* (Fig. 3) (*25*). Pha-4 is the single worm ortholog of the mammalian FOXA family of forkhead transcription factors, which play key roles in metabolic homeostasis. SKN-1 is the worm ortholog of the mammalian Nfe2l1 and Nfe2l2 transcription factors, which induce the phase II detoxification pathway, as does SKN-1 in *C. elegans*. Increased activity of SKN-1 can increase worm life span (*29*).

Although IIS and TOR play a clear role in aging in *C. elegans*, the types of age-related damage ameliorated and the molecular mechanisms by which they are reduced are unknown, as is the extent to which these or other pathways mediate the responses to different forms of dietary restriction.

Studies of the Fruit Fly *Drosophila*

The fly is important for establishing evolutionary conservation of mechanisms; for studying events in different tissues, which are more numerous and differentiated than in *C. elegans*; and for examining sex differences.

Nutrient-sensing pathways. Reduced IIS can extend life span in *Drosophila*, establishing its evolutionarily conserved role (Fig. 3) (*22*). It is not yet known whether, as in *C. elegans*, the fly FOXO is required for extension of life span (Fig. 3).

Changes in gene expression in long-lived IIS mutants of the worm, fly, and mouse have implicated phase 1 and 2 detoxification as evolutionarily conserved targets of IIS (*22*, *30*). Long-lived IIS mutants in all three organisms are resistant to xenobiotics, and up-regulation of transcription factors that regulate xenobiotic metabolism can extend life span in worms and flies (*22*, *29*, *30*).

The *Drosophila* genome contains seven genes encoding *Drosophila* insulin-like peptides (*dilps*), and genetic deletion of three of them made in neuroendocrine cells in the brain extends life span (*31*). Stress signaling and ablation of the germ line reduce expression of one or more *dilps* in the neuroendocrine cells and also extend fly life span (*32*). Identification of the tissues mediating the response to reduced IIS activity, by overexpression of the FOXO transcription factor, which is negatively regulated by IIS, has implicated tissues similar to those in *C. elegans*, namely, the fat body (equivalent of mammalian white adipose tissue and liver) and/or gut.

Down-regulation of TOR pathway activity genetically (*33*) or by rapamycin (*34*) (Fig. 3) extends life span in *Drosophila*, as it does in yeast and *C. elegans*. Extension of life span by rapamycin requires autophagy, reduced S6K activity, and eukaryotic initiation factor 4E binding protein (4E-BP) and is associated with reduced protein turnover (*34*), similar to what is seen in *C. elegans*.

Dietary restriction. Dietary restriction in *Drosophila* is commonly implemented by dilution of the food (*35*, *36*), for which the flies do not compensate by increased food intake (*37*). Per calorie, reduction of amino acid consumption extends life span substantially more than does reduction of sugar intake, with essential amino acids mediating most of the response (*38*). Volatiles from live microorganisms alone can shorten life span, similar to findings in worms, and olfactory mutants can be long-lived (*39*).

As in *C. elegans*, deletion of *Drosophila* FOXO (dFOXO) shortens life span, but the flies continue to respond to dietary restriction (*40*, *41*). However, reduced activity of both IIS and TOR can protect against shortening of life span by increased food intake (*33*, *34*) (Fig. 3). The response to dietary restriction may be mediated by insulin-like peptides, and transcript levels of *dilp5* respond to nutrition (*41*). Thus, reduced IIS plays a role in extension of life span by dietary restriction, but loss of FOXO can be compensated by other pathways such as the TOR pathway (Fig. 3). Reduced IIS and dietary restriction act acutely in *Drosophila* to increase survival (*25*, *40*), and it will be important to determine if this also occurs in mammals, because it would imply that drugs to improve health during aging should be taken over long periods of time. Life span is in general extended more in females than in males, for reasons that are not yet understood.

Studies of Rodents

Invertebrate model organisms have acted as engines of discovery for genes and mechanisms involved in extension of life span, but the mouse is the most practical mammal for establishing if homologous genes and processes can extend healthy life span, and hence lead to human clinical trials.

Nutrient-sensing pathways. As in yeast, worms, and flies, reduced activity of nutrient-sensing pathways can increase mouse life span. Mutations in growth hormone (GH) and IIS genes can substantially increase life span in mice (*42*) (Fig. 3), although precisely how is as yet poorly understood. GH-deficient mice show increased expression of antioxidant enzymes and increased stress resistance in muscle cells and fibroblasts, whereas GH administration decreases antioxidant defenses in the liver, kidney, muscle, and heart (*43*). As observed in yeast, disruption of type 5 adenylyl cyclase (AC5), which is predominantly expressed in the heart and brain, also increases stress resistance and longevity in mice, although GH has not been linked to AC (Fig. 3) (*44*). However, there is little experimental evidence for a conserved role of specific reduction in oxidative stress alone in life-span extension. As in yeast, worms, and flies, inhibition of the mTOR pathway, either with rapamycin (*45*) or deletion of ribosomal S6 protein kinase 1 (S6K1), increases mouse life span, the latter also reducing incidence of age-related pathologies, including bone, immune, and motor dysfunction and insulin resistance (*46*). Nutrient-sensing pathways may extend life span in mammals through transcription factors orthologous to those described in lower eukaryotes (Fig. 3), but data are at present lacking. Systems other than antioxidant enzymes downstream of these transcription factors including heat shock proteins, endoplasmic reticulum (ER) stress and autophagy proteins, apoptosis enzymes, xenobiotic metabolism, and others may have key functions as mediators of life-span extension (*47*).

Remarkably, the up to 50% life-span extension in mice that lack the GH receptor–binding protein (GHR-BP) is associated with lower morbidity and disease-related mortality, with ~47% of long-lived mice dying without obvious lethal pathological lesions and only about 10% of their wild-type

Box 1. Nutrient-sensing pathways and aging.

Nutrient-sensing pathways are fundamental to the aging process. Different nutrients can activate different pathways directly or indirectly. For example, in yeast, glucose activates the Ras-AC-PKA pathway, but in mice nutrients increase the level of IGF-1, which, in turn, activates pro-aging pathways in various mammalian cells (Fig. 3). Dietary restriction partially inactivates one or several nutrient-signaling pathways, thereby causing life-span extension in model organisms. In yeast and worms, this effect on longevity requires one or more transcription factors (proteins that regulate the expression of many genes involved, for example, in cellular protection, metabolic pathways, and processing of damaged proteins). In mice, dietary restriction or the inhibition of nutrient signaling can also reduce various age-related diseases, including cancer. These effects on diseases are believed to be a result of delaying the aging process in the various cells associated with the disease. The reason why these pathways are inactivated or partially inactivated by reduced nutrients is apparently simple: During periods of food scarcity, cells and organisms must be able to enter a standby mode in which cell division and reproduction are halted or minimized to allow energy to be available to maintenance systems. The conserved composition and function of anti-aging pathways in the different organisms indicate that most species have developed anti-aging systems to overcome periods of starvation.

siblings doing so, similar to findings in GH-deficient mice (*42*, *48*). GHR-BP knockout and GH-deficient mice display lower incidence and delayed occurrence of fatal neoplasms, increased insulin sensitivity, and a reduction in age-dependent cognitive impairment (*42*). The reduction in neoplastic diseases may be explained in part by lower somatic mutation frequency in the liver, kidney, and intestine of GH-deficient dwarf mice (*49*).

Some of the effects of dietary restriction can potentially be obtained pharmacologically and in-

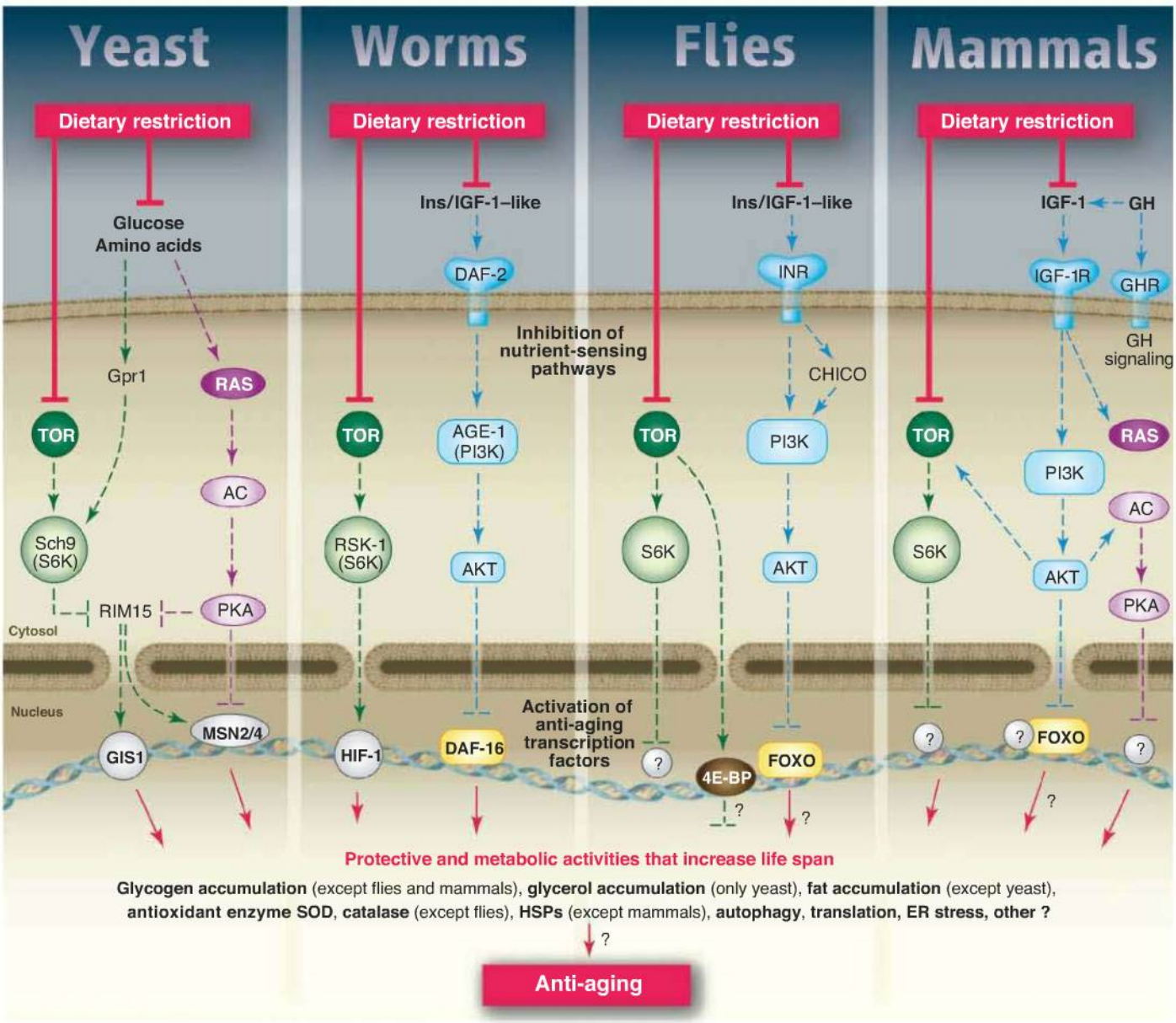

Fig. 3. A model for the conserved nutrient signaling pathways that regulate longevity in various organisms and mammals. Dietary restriction reduces the activity of various signal transduction pathways either directly (yeast) or indirectly through the reduced levels of growth factors such as IGF-1 (worms, flies, mammals). The role of TOR and S6K in promoting aging appears to be conserved in yeast, worms, flies, and mice. By contrast, the AC-PKA pathways and the TOR-S6K pathway promote aging in yeast and mammals, whereas an insulin/IGF-1–like receptor or the upstream growth hormone (mammals) accelerates aging in worms, flies, and mice. Similar transcription factors (GIS1, MSN2/4, DAF-16, FOXO) inactivated by either the AC/PKA, IGF-1/AKT, or TOR/S6K pathways affect cellular protection and/or aging in all the major model organisms. Notably, in the multicellular worms, flies, and mice, these genes may promote aging within the cells in which they are expressed but also in other cells through the regulation of circulating factors. The mechanisms proposed for the longevity extension caused by inhibition of these nutrient signaling pathways include a decrease in the free radical superoxide (mediated in part by SODs) and of its damage to macromolecules, protection of proteins by chaperones (Hsp70), decreased translation, the activation of autophagy, and the switch to hypoxia-associated gene expression patterns (in yeast and mice). In yeast, the effects of DR on life-span extension are also associated with reduced activities of the Tor-Sch9 and Ras-AC-PKA pathways and require the serine-threonine kinase Rim15 and transcription factors Gis1, Msn2, and Msn4. In worms, transcription factors regulated by the TOR-S6K and AGE-1-AKT pathways are implicated in the anti-aging effects of DR and, in flies, reduced activity of both Ins/IGF-1 and TOR can protect against shortening of life span by increased food intake, although in both worms and flies deletion of DAF-2/FOXO shortens life span, but the animal continues to respond to DR. In mice the longevity effects of DR appear to involve reduced activity of the GHR/IGF-1 pathways because DR does not extend further the life span of GHR-deficient mice (*69*). An enhanced version of Fig. 3 is at www.sciencemag.org/cgi/content/full/328/5976/321.

dependently of the inhibition of GH/IGF-1 (insulin-like growth factor 1). For example, treatment of mice on a high-fat diet with resveratrol, a natural compound found in grapes that mimics some of the effects of dietary restriction, results in reduced mortality or protection against morbidity, possibly by activating a set of genes affected by dietary restriction, but resveratrol did not increase survival of mice or flies fed a standard diet (*50*, *51*). Disruption of PKA, downstream of adenylyl cyclase, also causes life-span extension in mice, as it does in yeast (Fig. 3) (*52*), and causes a reduction in age-dependent tumors and insulin resistance (*9*, *52*). It will be important to determine whether superoxide and error-prone polymerases, implicated in the Tor-Sch9- and age-dependent DNA damage/mutations in yeast, are mediators of the GH–IGF-1–dependent genomic instability and cancer in mammals.

Dietary restriction. Dietary restriction increases rodent life span by up to 60%, in part by delaying the occurrence of many chronic diseases (*1*). As in GH–IGF-1 axis mutant mice, ~30% of animals on dietary restriction die without evidence of severe organ pathology, whereas only 6% of controls do so (*53*). Attenuated IIS may mediate some of the anti-aging effects of dietary restriction in mice (Fig. 3). In particular, the reduction of IGF-1 signaling could be responsible for the reduced incidence of spontaneous mutations and tumors in the kidney and small intestine of GH-deficient and dietary-restricted mice (*49*). Part of this protection appears to be mediated by a transcription factor (Nrf2) (*54*), the *C. elegans* and *Drosophila* orthologs of which increase life span when overexpressed.

Dietary restriction in mice greatly increases insulin sensitivity and attenuates β-amyloid deposition in a model for Alzheimer's disease (*55*), in agreement with the effect of reduced IIS signaling in protection against β-amyloid toxicity in mice (*56*) (Fig. 3). Severe dietary restriction or starvation may also be applicable to disease treatment in certain contexts. For example, fasting protects mice against high-dose chemotherapy, in part by reducing serum IGF-1 signaling, but does not protect cancer cells, in which the constitutive activity of pro-aging pathways (oncogenes) blocks the activation of stress resistance in response to nutrient deprivation (*57*).

However, dietary restriction can also impair function such as immunity and wound healing. For example, the healing of skin wounds is reduced in long-term dietary-restricted mice and is greatly accelerated by a short period of ad lib feeding before the wound is inflicted (*58*). Also, dietary-restricted mice are more susceptible to infections by bacteria, virus, and worms, even though dietary restriction can delay the age-dependent decline in certain immune functions (*59*).

Studies of Primates

Findings from model organisms have begun to be tested in monkeys and also in human volunteers, including subjects with mutations analogous to those that extend the healthy life span of laboratory animals.

Nutrient-sensing pathways. Some individuals have naturally occurring deficiencies in the GH–IGF-1 axis (Fig. 4A). In GH receptor–deficient individuals, diabetes or cancer is uncommon, yet these individuals do not appear to have an advantage in reaching very old ages (*60*) (Fig. 4A), possibly because of developmental defects and the increased mortality at younger ages (*61*). In subjects with GH receptor and IGF-1 deficiencies, cancer was absent whereas 9 to 24% of the relatives developed malignancies (*60*), although this report is inconclusive because the mean age of the IGF-1–deficient subjects was much lower than that of controls. Although GH and/or IGF-1 deficiency promotes obesity and hyperlipidemia, whereas treatment with GH has a beneficial effect on both traits, replenishment of GH increases intima media thickness and the number of atherosclerotic plaques. The dyslipidemia and obesity from GH–IGF-1 axis deficiency may therefore not exacerbate vascular aging (*62*).

An overrepresentation of heterozygotes for mutations in the IGF-1 receptor gene was found among Ashkenazi Jewish centenarians as compared to controls (*63*), whereas subjects with a genotype associated with reduced concentration of free IGF-1 in plasma were overrepresented among long-lived people (*64*), indicating that specific polymorphisms that down-regulate the GH and IGF-1 signaling may promote human longevity. Furthermore, genetic variants of FOXO transcription factors, orthologs of the key IIS effector *daf-16* in *C. elegans*, have repeatedly been shown to associate with human life span (*65*).

Further studies of GH/IIS mutants in humans are needed to establish the role of these pathways in cancer and also in diabetes, cardiovascular, and neurodegenerative diseases. If the multiple beneficial effects of reduced signaling observed in mice are confirmed in humans, drugs that block these pathways could be considered for prevention of specific diseases.

Dietary restriction. Recently, a 20-year 30% dietary restriction applied to adult rhesus monkeys was shown to reduce age-related deaths (*66*). The incidence of neoplasia and cardiovascular disease was 50% lower than in the controls (*66*), and 16 of the initial 38 controls but none of the dietary-restricted monkeys developed diabetes or prediabetes. Many metabolic, hormonal, and structural adaptations in dietary-restricted rodents, including a major reduction in body fat mass, higher insulin sensitivity, and reduced inflammation and oxidative damage, were also observed in dietary-restricted monkeys (*1*). In addition, immune senescence, sarcopenia, and brain atrophy of the gray matter were attenuated (*1*, *66*). Possible downsides of dietary restriction, such as reduced resistance to infection or attenuated wound healing, have not been investigated.

In humans, dietary restriction provides major and sustained beneficial effects against obesity, insulin resistance, inflammation, oxidative stress, and left ventricular diastolic dysfunction, in agreement with the metabolic and functional changes observed in dietary-restricted rodents (Fig. 4B) (*2*). Moreover, dietary restriction in humans induces some of the hormonal adaptations observed in dietary-restricted rodents (e.g., increased adiponectin and reduction in triiodothyronine, testosterone, and insulin) and reduced cholesterol, C-reactive protein, blood pressure, and intima-media thickness of the carotid arteries, all risk factors for cardiovascular disease (*2*, *67*).

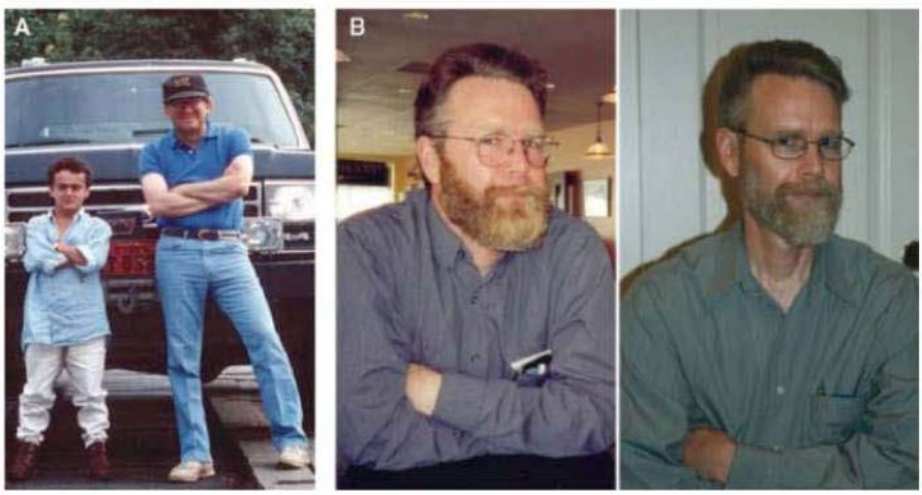

Fig. 4. **(A)** Individual with normal levels of GH receptor (right) and a GH receptor–deficient subject in the mountains of southern Ecuador (left). **(B)** Composite photograph of a dietary restriction practitioner before starting dietary restriction with adequate nutrition [left: weight 180 lb, or 81.6 kg; body mass index (BMI) 26.0 kg/m^2) and after 7 years of dietary restriction (right: weight 134 lb, or 60.8 kg; BMI 19.4 kg/m^2).

However, there are major differences in effects of dietary restriction between rodents and humans. Dietary restriction decreases serum IGF-1 concentration by ~30 to 40% in rodents but does not reduce IGF-1 levels in humans, unless protein intake is also reduced (*68*) (Fig. 4B), raising the possibility that protein restriction alone may provide some benefits, as in *Drosophila* (*38*).

Outlook

Extreme dietary restriction can lead to several detrimental health effects such as amenorrhea, infertility, sarcopenia, osteoporosis, and immune deficiencies. Thus, it will be important to examine these negative side-effects in dietary-restricted subjects that are not malnourished. Indeed, experimental studies are required to evaluate the optimal calorie intake and macro- and micronutrient composition needed for healthy aging in humans, on the basis of age, sex, genotype, and energy expenditure.

Although adjustment of dietary intake and composition may be realistic and beneficial, the severe dietary restriction that induces major health benefits is not a desirable option for most people. Drugs that target nutrient-sensing pathways to obtain the health benefits of dietary restriction are realistic, but the effects of chronic administration require study. For instance, rapamycin, the TOR inhibitor that extends mouse life span (*45*), is an immunosuppressant and may not produce an overall health benefit in humans living in an environment with pathogens. However, genetic deletion of the GH receptor or of the downstream S6 kinase in mice extends life span and induces a broad-spectrum improvement in health (*42*, *46*, *48*). More testing of potential disadvantages is required and many open questions remain (Box 2), but these seem promising drug targets and are hopefully the first of many.

References and Notes

1. R. M. Anderson, D. Shanmuganayagam, R. Weindruch, *Toxicol. Pathol.* **37**, 47 (2009).
2. L. Fontana, S. Klein, *JAMA* **297**, 986 (2007).
3. M. D. Piper, L. Partridge, *PLoS Genet.* **3**, e57 (2007).
4. M. Kaeberlein *et al.*, *Science* **310**, 1193 (2005).
5. R. W. Powers III, M. Kaeberlein, S. D. Caldwell, B. K. Kennedy, S. Fields, *Genes Dev.* **20**, 174 (2006).
6. M. Wei *et al.*, *PLoS Genet.* **5**, e1000467 (2009).
7. Y. Pan, G. S. Shadel, *Aging* **1**, 131 (2009).
8. K. K. Steffen *et al.*, *Cell* **133**, 292 (2008).
9. P. Fabrizio, F. Pozza, S. D. Pletcher, C. M. Gendron, V. D. Longo, *Science* **292**, 288 (2001).
10. S. J. Lin, P. A. Defossez, L. Guarente, *Science* **289**, 2126 (2000).
11. O. Medvedik, D. W. Lamming, K. D. Kim, D. A. Sinclair, *PLoS Biol.* **5**, e261 (2007).
12. M. Wei *et al.*, *PLoS Genet.* **4**, e13 (2008).
13. P. Fabrizio *et al.*, *Cell* **123**, 655 (2005).
14. C. R. Burtner, C. J. Murakami, B. K. Kennedy, M. Kaeberlein, *Cell Cycle* **8**, 1256 (2009).
15. V. D. Longo, L. M. Ellerby, D. E. Bredesen, J. S. Valentine, E. B. Gralla, *J. Cell Biol.* **137**, 1581 (1997).
16. D. L. Smith Jr., J. M. McClure, M. Matecic, J. S. Smith, *Aging Cell* **6**, 649 (2007).
17. M. Kaeberlein, C. R. Burtner, B. K. Kennedy, *PLoS Genet.* **3**, e84 (2007).
18. T. E. Johnson, *Exp. Gerontol.* **43**, 1 (2008).
19. R. Doonan *et al.*, *Genes Dev.* **22**, 3236 (2008).
20. N. Libina, J. R. Berman, C. Kenyon, *Cell* **115**, 489 (2003).
21. M. Hansen *et al.*, *PLoS Genet.* **4**, e24 (2008).
22. M. D. Piper, C. Selman, J. J. McElwee, L. Partridge, *J. Intern. Med.* **263**, 179 (2008).
23. D. Chen, E. L. Thomas, P. Kapahi, S. E. Mango, *PLoS Genet.* **5**, e1000486 (2009).
24. R. Mehta *et al.*, *Science* **324**, 1196 (2009).
25. W. Mair, A. Dillin, *Annu. Rev. Biochem.* **77**, 727 (2008).
26. E. L. Greer, A. Brunet, *Aging Cell* **8**, 113 (2009).
27. E. D. Smith *et al.*, *BMC Dev. Biol.* **8**, 49 (2008).
28. K. A. Steinkraus *et al.*, *Aging Cell* **7**, 394 (2008).
29. J. M. Tullet *et al.*, *Cell* **132**, 1025 (2008).
30. J. J. McElwee *et al.*, *Genome Biol.* **8**, R132 (2007).
31. S. Groenke, D. F. Clarke, S. Broughton, T. D. Andrews, L. Partridge, *PLoS Genet.* **6**, e1000857 (2010).
32. S. J. Broughton *et al.*, *Proc. Natl. Acad. Sci. U.S.A.* **102**, 3105 (2005).
33. P. Kapahi *et al.*, *Curr. Biol.* **14**, 885 (2004).
34. I. Bjedov *et al.*, *Cell Metab.* **11**, 35 (2010).
35. T. Chapman, L. Partridge, *Proc. Biol. Sci.* **263**, 755 (1996).
36. T. M. Bass *et al.*, *J. Gerontol. A Biol. Sci. Med. Sci.* **62**, 1071 (2007).
37. R. Wong, M. D. Piper, E. Blanc, L. Partridge, *Nat. Methods* **5**, 214 (2008).
38. R. C. Grandison, M. D. Piper, L. Partridge, *Nature* **462**, 1061 (2009).
39. S. Libert *et al.*, *Science* **315**, 1133 (2007).
40. M. E. Giannakou, M. Goss, L. Partridge, *Aging Cell* **7**, 187 (2008).
41. K. J. Min, R. Yamamoto, S. Buch, M. Pankratz, M. Tatar, *Aging Cell* **7**, 199 (2008).
42. A. Bartke, *Endocrinology* **146**, 3718 (2005).
43. H. M. Brown-Borg, *Aging Res. Rev.* **6**, 28 (2007).
44. L. Yan *et al.*, *Cell* **130**, 247 (2007).
45. D. E. Harrison *et al.*, *Nature* **460**, 392 (2009).
46. C. Selman *et al.*, *Science* **326**, 140 (2009).
47. D. Amador-Noguez *et al.*, *Aging Cell* **6**, 453 (2007).
48. Y. Ikeno *et al.*, *J. Gerontol. A Biol. Sci. Med. Sci.* **64A**, 522 (2009).
49. A. M. Garcia *et al.*, *Mech. Aging Dev.* **129**, 528 (2008).
50. K. J. Pearson *et al.*, *Cell Metab.* **8**, 157 (2008).
51. T. M. Bass, D. Weinkove, K. Houthoofd, D. Gems, L. Partridge, *Mech. Aging Dev.* **128**, 546 (2007).
52. L. C. Enns *et al.*, *PLoS ONE* **4**, e5963 (2009).
53. I. Shimokawa *et al.*, *J. Gerontol.* **48**, B27 (1993).
54. K. J. Pearson *et al.*, *Proc. Natl. Acad. Sci. U.S.A.* **105**, 2325 (2008).
55. N. V. Patel *et al.*, *Neurobiol. Aging* **26**, 995 (2005).
56. E. Cohen *et al.*, *Cell* **139**, 1157 (2009).
57. L. Raffaghello *et al.*, *Proc. Natl. Acad. Sci. U.S.A.* **105**, 8215 (2008).
58. M. J. Reed *et al.*, *Mech. Ageing Dev.* **89**, 21 (1996).
59. D. M. Kristan, *Age (Dordr.)* **30**, 147 (2008).
60. O. Shevah, Z. Laron, *Growth Horm. IGF Res.* **17**, 54 (2007).
61. M. Gourmelen, L. Perin, M. Binoux, *Acta Paediatr. Scand. Suppl.* **377**, 115 (1991).
62. J. L. Oliveira *et al.*, *J. Clin. Endocrinol. Metab.* **92**, 4664 (2007).
63. Y. Suh *et al.*, *Proc. Natl. Acad. Sci. U.S.A.* **105**, 3438 (2008).
64. M. Bonafè *et al.*, *J. Clin. Endocrinol. Metab.* **88**, 3299 (2003).
65. M. Kuningas *et al.*, *Eur. J. Hum. Genet.* **15**, 294 (2007).
66. R. J. Colman *et al.*, *Science* **325**, 201 (2009).
67. L. Fontana, T. E. Meyer, S. Klein, J. O. Holloszy, *Proc. Natl. Acad. Sci. U.S.A.* **101**, 6659 (2004).
68. L. Fontana, E. P. Weiss, D. T. Villareal, S. Klein, J. O. Holloszy, *Aging Cell* **7**, 681 (2008).
69. M. S. Bonkowski *et al.*, *PLoS ONE* **4**, e4567 (2009).

70. We thank M. Wei for careful reading of the manuscript. This work was supported in part by a grant from the American Federation for Aging Research, Bakewell Foundation, and by NIH grants AG20642, AG025135, and GM075308 (to V.D.L.). Support was also provided by the National Center for Research Resources (grant UL1 RR024992) and the National Institute of Diabetes and Digestive and Kidney Diseases (grant P30DK056341); by grants from Istituto Superiore di Sanità/National Institutes of Health Collaboration Program, Ministero della Salute, the Longer Life Foundation (an RGA/Washington University Partnership), and the Bakewell Foundation; and by a donation from the Scott and Annie Appleby Charitable Trust (to L.F.).

10.1126/science.1172539

Box 2. Some questions for future research.

1. Can aging be delayed and diseases prevented by blocking cellular and molecular damage, or must gene expression be "reprogrammed" to achieve healthy life-span extension?

All four model organisms should help answer this question, but the powerful screening methods in yeast, worms, and flies are more likely to lead to unbiased answers.

2. Which collection of molecular events leads to cellular and organismal aging?

Yeast studies should allow a more in-depth molecular and genetic approach, whereas studies of worms and flies should lead to a better understanding of the relative role of different cell types and tissues in aging. Mouse research should help establish whether these molecular mechanisms are relevant to humans and age-associated diseases.

3. Can protein restriction mimic the effects of dietary restriction and limit cancer growth?

Protein restriction is much less difficult to maintain than dietary restriction and may be more powerful than dietary restriction in reducing the serum IGF-1 concentration in humans. Moreover, protein restriction, by lowering intracellular amino acid levels, reduces mTOR activity and stimulates autophagy, two key processes involved in aging and cancer. Randomized clinical trials of healthy volunteers and patients with cancer are needed to understand the long-term metabolic and clinical effects of protein restriction in humans.

4. Does exercise-induced leanness induce the same metabolic adaptations as dietary restriction and slow aging?

More studies in both rodents and humans are needed to elucidate the metabolic and molecular mechanisms responsible for the different effects of calorie restriction (low-energy flux) and exercise (high-energy flux) on aging and longevity.

5. Can these discoveries be translated into health benefits for humans?

We need to identify candidate drug targets and determine if targeting them with drugs can achieve health benefits in the absence of undesirable side-effects. It will also be essential to determine if long-term drug intervention is required for a full benefit, or if instead the full subsequent benefit can be achieved with drug treatment initiated at later ages.

Caspase-Dependent Conversion of Dicer Ribonuclease into a Death-Promoting Deoxyribonuclease

Akihisa Nakagawa,[1]* Yong Shi,[1]* Eriko Kage-Nakadai,[2] Shohei Mitani,[2] Ding Xue[1]†

Chromosome fragmentation is a hallmark of apoptosis, conserved in diverse organisms. In mammals, caspases activate apoptotic chromosome fragmentation by cleaving and inactivating an apoptotic nuclease inhibitor. We report that inactivation of the *Caenorhabditis elegans dcr-1* gene, which encodes the Dicer ribonuclease important for processing of small RNAs, compromises apoptosis and blocks apoptotic chromosome fragmentation. DCR-1 was cleaved by the CED-3 caspase to generate a C-terminal fragment with deoxyribonuclease activity, which produced 3′ hydroxyl DNA breaks on chromosomes and promoted apoptosis. Thus, caspase-mediated activation of apoptotic DNA degradation is conserved. DCR-1 functions in fragmenting chromosomal DNA during apoptosis, in addition to processing of small RNAs, and undergoes a protease-mediated conversion from a ribonuclease to a deoxyribonuclease.

One of the hallmarks of apoptosis is fragmentation of chromosomal DNA at internucleosomal regions, which generates DNA fragments differing by ~180 base pairs and contributes to the irreversible cell killing process (*1*, *2*). Multiple deoxyribonucleases (DNases) have been implicated in mediating apoptotic DNA fragmentation, including 40-kD DNA fragmentation factor (DFF40), also known as caspase-activated deoxyribonuclease (CAD); endonuclease G (endoG); deoxyribonuclease II (DNase II); and several other nucleases (*3*, *4*). DFF40 is a component of a DNA fragmentation factor complex, which also contains an inhibitory subunit, DFF45 (also known as ICAD, inhibitor of CAD) (*5*–*8*). DFF45 serves both as a chaperone for the proper folding of DFF40 and as a cognate inhibitor that holds DFF40 activity in check in normal cells. During apoptosis, the cleavage of DFF45 by activated caspases, such as caspase-3 and caspase-7, results in the release and activation of DFF40 (*5*–*8*). The activated DFF40 nuclease then associates with chromosomal proteins, such as histone H1, HMG (high-mobility group) proteins, and topoisomerase II, to promote cleavage of internucleosomal DNA, generating 3′ hydroxyl DNA breaks that can be detected by the TUNEL [terminal deoxynucleotidyl transferase (TdT)–mediated deoxyuridine triphosphate (dUTP) nick end labeling] assay (*6*, *9*, *10*). In mice deficient in either DFF40 or DFF45, which is needed for proper folding of DFF40, chromosome fragmentation fails to occur during apoptosis (*11*, *12*).

A mitochondrial nuclease, endoG, mediates residual apoptotic DNA fragmentation observed in DFF45-deficient cells (*13*). EndoG is released from mitochondria during apoptosis and translocates into the nucleus to facilitate chromosome fragmentation (*13*). EndoG is a member of a conserved family of endonucleases, including the *Caenorhabditis elegans* CPS-6 (CED-3 protease suppressor) nuclease (*14*, *15*). In *C. elegans* animals deficient in *cps-6*, TUNEL-stained nuclei accumulate in mutant embryos, and developmental cell death is delayed or even inhibited in sensitized genetic backgrounds, such as animals partially deficient for the CED-3 caspase (*14*), which suggests that CPS-6 is important for apoptotic DNA degradation and the progression of apoptosis. In addition to *cps-6*, seven cell death–related nucleases (named CRN nucleases) have been identified in a candidate-based RNA interference (RNAi) screen in *C. elegans* (*16*). RNAi-mediated depletion of six of these *crn* nuclease genes (*crn-1* to *crn-5* and *cyp-13*) results in similar cell death defects, including accumulation of TUNEL-stained nuclei in RNAi-treated embryos and inhibition of apoptosis in sensitized genetic backgrounds (*16*). Biochemical analysis reveals that some of these CRN nucleases interact with CPS-6 and with one another to promote step-wise DNA degradation, by first turning the 3′ OH DNA nicks into small gaps through their exonuclease activities and then creating double-stranded DNA (dsDNA) breaks via a gap-dependent endonuclease activity (*16*, *17*). Two *C. elegans* DNase II homologs, NUC-1 and CRN-6, function in a later stage to complete degradation of chromosomal DNA (*16*, *18*), as loss of either gene or both also results in accumulation of TUNEL-stained nuclei but does not affect the activation or the kinetics of apoptosis (*14*, *18*). In all instances, loss of any one or a combination of the nine *C. elegans* apoptotic nucleases results in accumulation of TUNEL-stained nuclei, which indicates that these nucleases function in resolving 3′ OH DNA breaks generated during apoptosis and that at least one additional *C. elegans* nuclease—presumably, a functional analog of DFF40—is activated during apoptosis to generate 3′ OH DNA breaks. Because no candidate DFF40 or DFF45 homolog is predicted to be encoded by the *C. elegans* genome (*4*), it remains enigmatic how apoptotic DNA degradation is initiated in *C. elegans*. We report that this role is played by the *C. elegans* Dicer ribonuclease.

Dicer is a highly conserved ribonuclease that plays a central role in processing double-stranded RNA (dsRNA) to generate small RNAs important for various gene-silencing events (*19*–*26*). It is an RNase III enzyme that processes precursor dsRNA into small duplex RNA species of about 21 to 25 nucleotides, with 5′ phosphate and 3′ hydroxyl termini (*22*, *27*–*30*). These small RNAs are then unwound and incorporated into various silencing complexes, such as the RNA-induced silencing complex (RISC), that direct sequence-specific cleavage or translational repression of complementary mRNA (*24*–*26*, *31*–*34*). Multiple proteins have been identified to serve as Dicer cofactors or interactors to mediate various gene silencing events, including proteins in the Argonaute family that contain PAZ (Piwi, Argo, and Zwille) and PIWI domains (*32*–*34*); RDE-1 (RNAi defective, also an Argonaute protein); RDE-4 and its fly homolog R2D2; DRH-1 and DRH-2 (Dicer-related helicases) (*31*, *35*, *36*); ERI-1 (enhanced RNAi); and RRF-3 (RNA-dependent RNA polymerase family) (*26*, *37*, *38*). Dicer enzymes typically contain a DExH-box helicase domain (*39*), a PAZ domain, two tandem RNase III domains (RNase IIIa and IIIb), and a dsRNA binding domain (*40*, *41*). The intramolecular dimerization of the two RNase III domains of Dicer generates the dicing activity (*29*), and the distance between the PAZ and RNase III domains determines the length of small RNA fragments processed (*42*). Dicer is important for multiple cellular processes, including viral defense, chromatin remodeling, genome rearrangement, developmental timing, and stem cell maintenance (*21*, *23*, *43*–*48*). These cellular functions likely are attributed to the generation of small interfering RNAs (siRNAs), microRNAs (miRNAs), and other small RNAs (*34*, *41*). We uncovered a previously uncharacterized role of *C. elegans* Dicer (DCR-1) in activating the apoptotic DNA degradation process that is dependent on generation of a new DNase activity through cleavage by the cell death protease CED-3 and that is independent of Dicer's actions in gene silencing in *C. elegans*.

dcr-1 is required for initiating apoptotic DNA degradation in _C. elegans_. To identify nucleases that function in apoptotic DNA degradation in *C. elegans* and, in particular, nucleases that generate 3′ hydroxyl DNA breaks during apoptosis, we performed RNAi on *cps-6(sm116)* mutant animals, which contain an average of 16 TUNEL-stained cells in early-stage embryos

[1]Department of Molecular, Cellular, and Developmental Biology, University of Colorado, Boulder, CO 80309, USA. [2]Department of Physiology, Tokyo Women's Medical University, School of Medicine, and Core Research for Evolutional Science and Technology (CREST), Japan Science and Technology Agency, Tokyo 162-8666, Japan.

*These authors contributed equally to this work.
†To whom correspondence should be addressed. E-mail: ding.xue@colorado.edu

(Fig. 1, A and B), and looked for RNAi knockdown of nucleases that reduced the number of TUNEL-stained cells in *cps-6(sm116)* embryos (*16*, *17*, *49*). We found that *dcr-1* RNAi reduced the number of TUNEL signals in *cps-6(sm116)* embryos (Fig. 1A). Given that *dcr-1* RNAi also reduces the efficiency of RNA interference, we examined whether two deletion mutations in *dcr-1* (*ok247* and *pk1351*) caused a stronger reduction in TUNEL staining in the *cps-6(sm116)* mutant. Because *dcr-1* loss-of-function (*lf*) mutants are sterile, a balancer, *hT2(qIs48)*, was used to maintain the *dcr-1(lf)* heterozygous strain. *qIs48* is a transgene integrated into the *hT2* chromosome and carries a $P_{myo\text{-}2}gfp$ reporter that directs strong green fluorescent protein (GFP) expression in the pharynx in most developmental stages. *dcr-1(lf)* homozygous embryos derived from the *dcr-1(lf)/hT2* mother can thus be identified as embryos that do not express GFP. We performed TUNEL and anti-GFP double staining to score the number of TUNEL-stained cells in *dcr-1(lf)* embryos (*49*). Although *dcr-1(ok247)* and *dcr-1(pk1351)* homozygous embryos had comparable numbers of TUNEL-stained cells to those seen in *dcr-1(ok247)/hT2* and *dcr-1(pk1351)/hT2* heterozygous embryos or wild-type N2 embryos

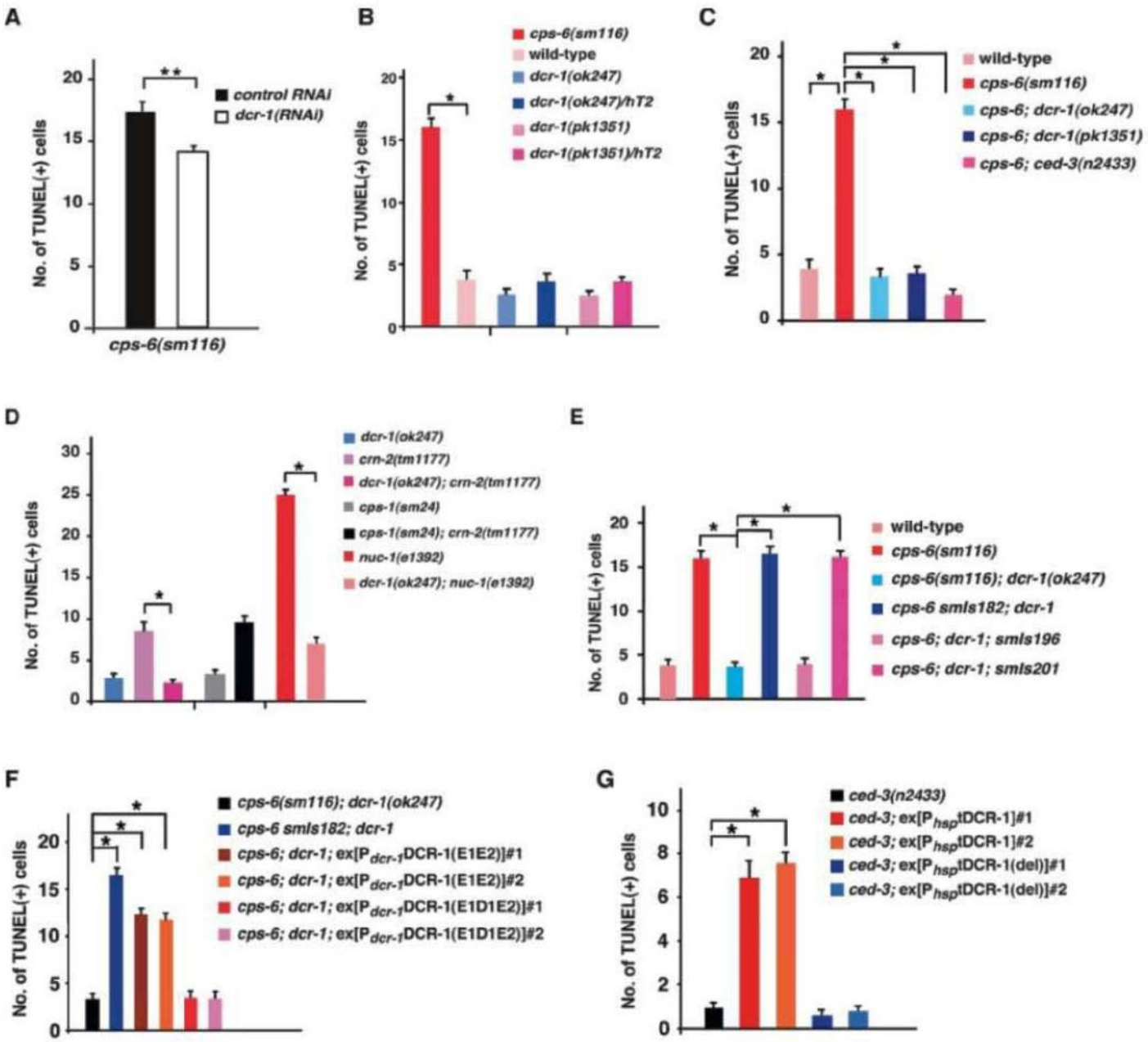

Fig. 1. Role of DCR-1 in creating TUNEL-reactive DNA breaks in apoptotic cells. (**A** to **G**) TUNEL staining was monitored in the indicated strains (*49*). In most cases, GFP-specific immunostaining and TUNEL staining were done to quantify the number of TUNEL-stained cells in *dcr-1(lf)* homozygous embryos (*49*), which were identified as embryos lacking GFP derived from *dcr-1(lf)/hT2(qIs48)* mothers. In animals carrying $P_{sur\text{-}5}sur\text{-}5::gfp$ as a transgenic marker (E and F), *dcr-1(lf)* homozygous transgenic embryos were identified as embryos with nuclear GFP expression in many cells but lacking pharyngeal GFP expression (*qIs48*). RNAi experiments were done as described (*14*). All *cps-6(sm116)* strains also contain *dpy-5(e61)*. *smIs182* is an integrated transgene carrying $P_{dcr\text{-}1}$DCR-1. *smIs196* is an integrated transgene carrying $P_{dcr\text{-}1}$DCR-1(D1742E). *smIs201* is an integrated transgene carrying $P_{dcr\text{-}1}$tDCR-1. Each numbered array represents an independent transgenic line (F and G). The *y* axis represents average number of TUNEL-stained cells scored, and error bars represent SEM. For each strain, 15 comma-stage embryos were scored. The significance of differences between different strains was determined by unpaired *t* test (A) or one-way analysis of variance (ANOVA), followed by Tukey's test (B) to (G). $*P < 0.001$; $**P < 0.05$.

(Fig. 1B), both *dcr-1(ok247)* and *dcr-1(pk1351)* deletion mutations reduced the number of TUNEL signals in *cps-6(sm116)* embryos to that seen in wild-type embryos (Fig. 1C). These findings suggested that *dcr-1* does function in generating TUNEL-reactive DNA breaks that fail to be resolved in *cps-6(sm116)* embryos. Similarly, *dcr-1(ok247)* significantly reduced the number of TUNEL signals in *crn-2(tm1177)* embryos, which are defective in another apoptotic nuclease CRN-2 (Fig. 1D) (*16*). *dcr-1(ok247)* also reduced the number of TUNEL-stained cells in *nuc-1(e1392)* embryos (Fig. 1D). Taken together, these results indicate that DCR-1 functions in creating TUNEL-reactive DNA breaks in apoptotic cells that are later resolved by other apoptotic nucleases, such as CPS-6, CRN-2, and NUC-1, and that *dcr-1* likely acts upstream of *cps-6*, *crn-2*, and *nuc-1* to promote apoptotic DNA degradation.

***dcr-1* promotes apoptosis.** We next investigated whether *dcr-1* affects programmed cell death in *C. elegans*. We examined the appearance of apoptotic cell corpses in developing embryos, which is a sensitive assay for detecting weak cell-death defects (*14*, *16*, *50*). We observed significantly fewer cell corpses in both *dcr-1(ok247)* and *dcr-1(pk1351)* mutants at most embryonic stages than in wild-type embryos (Fig. 2A). Thus, *dcr-1* appears to be a proapoptotic factor. The cell-death defect displayed by the *dcr-1(lf)* mutants is stronger than that observed in the *cps-6(sm116)* mutant or animals deficient in most *crn* genes, in which cell death in developing embryos is delayed rather than reduced (*14*, *16*). Moreover, both *dcr-1(ok247)* and *dcr-1(pk1351)* mutations reduced the number of persistent cell corpses in *ced-1(e1735)* embryos, in which engulfment of cell corpses is blocked (Fig. 2B) (*51*), which confirmed that loss of *dcr-1* reduces the number of embryonic cells undergoing cell death.

To investigate whether a general reduction in embryonic cell death may indirectly affect apoptotic DNA degradation, we performed the TUNEL assay on the *cps-1(sm24)* mutant, a CED-3 protease suppressor mutant that exhibits a cell-death defect similar to that of the *dcr-1(lf)* mutants (Fig. 2A) (*14*). Although *cps-1(sm24)* causes reduced embryonic cell death at most embryonic stages, as did the *dcr-1(lf)* mutations, it did not affect the number of TUNEL-stained cells in the *crn-2(tm1177)* embryos (Fig. 1D). This result suggests that, unlike *cps-1*, *dcr-1* facilitates cell death by promoting apoptotic DNA degradation.

We investigated whether reduction of embryonic cell death caused by *dcr-1(lf)* mutations might result in survival of cells that normally die and thus yield extra "undead" cells in the anterior pharynx of mutant animals (*14*, *49*). Both *dcr-1(ok247)* and *dcr-1(pk1351)* mutants had low numbers of extra cells in the anterior pharynx (table S1). When combined with other weak cell-death mutations, such as the partial loss-of-function mutation *(n2438)* in the gene encoding the CED-3 caspase, *dcr-1(lf)* mutations significantly increased the number of extra cells in the anterior pharynx (table S1). For example, an average of 1.3 extra cells were seen in *ced-3(n2438)* animals, whereas, on average, 3.1 extra cells were present in *dcr-1(lf); ced-3(n2438)* animals (table S1). Although *cps-6(sm116)* or *crn-2(tm1177)* individually also increased the number of extra cells in the *ced-3(n2438)* mutant background, neither *cps-6(sm116)* nor *crn-2(tm1177)* increased the number of extra cells in the *dcr-1(ok247); ced-3(n2438)* mutant (table S1), which indicated that *dcr-1*, *cps-6*, and *crn-2* may act in the same pathway to promote apoptosis and DNA degradation.

Because apoptotic DNA degradation occurs in response to caspase activation (*5*, *7*, *14*), we performed epistasis analysis to examine whether activation of *ced-3* leads to activation of *dcr-1*, using an integrated transgene (*smIs111*) expressing an activated form of CED-3 (acCED-3) under the control of the *egl-1* promoter (*49*, *52*). When *smIs111* was placed in the *ced-1(e1735); egl-1(n3082)* mutant background, in which almost all naturally occurring somatic cell deaths in *C. elegans* are blocked by a loss-of-function mutation *(n3082)* in the cell-death initiator *egl-1*, acCED-3 still induced ectopic cell death and an average of 16.5 and 11 persistent cell corpses in three-fold and four-fold late-stage embryos, respectively (Fig. 2C). The *dcr-1(ok247)* mutation significantly reduced the number of ectopic cell deaths induced by acCED-3 in *ced-1(e1735) smIs111; egl-1(n3082)* embryos, which indicated that *dcr-1* likely acts downstream of *ced-3* to promote apoptosis and DNA degradation.

DCR-1 cofactors in RNA processing do not affect apoptosis. In *C. elegans*, various cofactors interact with DCR-1 to regulate processing of dsRNA and to generate small RNAs, including miRNAs, siRNAs, and siRNAs derived from endogenous triggers (endo-siRNAs) (*21*, *26*, *53*). For example, ALG-1 and ALG-2 (Argonaute-like gene) are required for miRNA production; RDE-1, RDE-4, DRH-1, and DRH-2 are required for siRNA production; and ERI-1 and RRF-3 are required for endo-siRNA production. We thus examined whether these DCR-1 cofactors also functioned in regulating apoptosis and DNA degradation. Loss of DCR-1 cofactors did not affect the number of TUNEL-stained cells in the *cps-6(sm116)* mutant or *cps-6*(RNAi)–treated animals (table S2). Moreover, unlike *dcr-1(lf)* mutants, which have a reduced number of embryonic cell corpses, the numbers of embryonic cell corpses in animals deficient in DCR-1 cofactors were comparable to those seen in wild-type animals (fig. S1). These results indicate that defects in the generation of miRNAs, siRNAs, endo-siRNAs, or other small RNAs do not seem to affect apoptosis or apoptotic DNA degradation and that DCR-1 likely mediates apoptotic DNA degradation through a previously uncharacterized mechanism independent of its roles in RNA processing.

DCR-1 is a substrate of the CED-3 caspase. Given that *dcr-1* acts downstream of *ced-3* to promote apoptosis and DNA degradation, we tested whether DCR-1 itself might be a substrate of the CED-3 protease. We synthesized a glutathione *S*-transferase DCR-1 fusion (GST–DCR-1) and labeled it with [^{35}S]methionine in rabbit re-

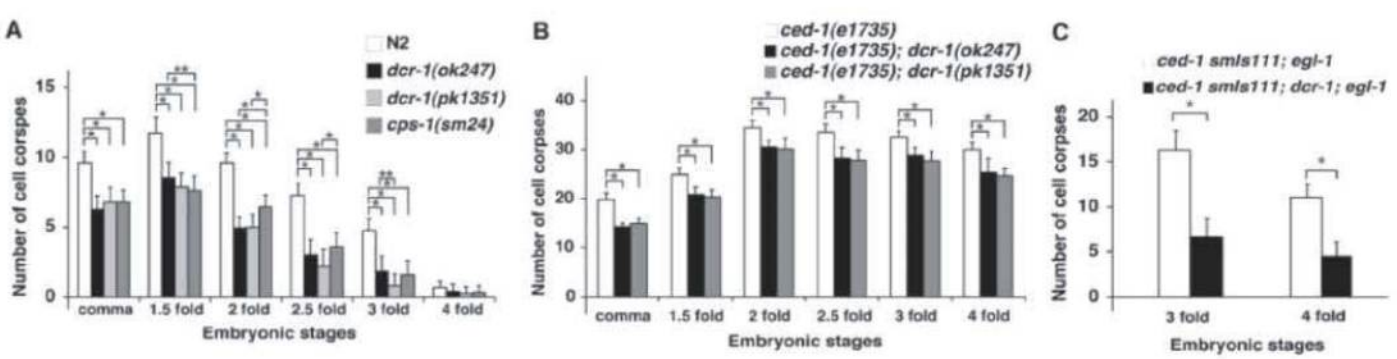

Fig. 2. Function of *dcr-1* downstream of *ced-3* to promote cell death. Embryonic cell corpses were counted in the following animals: **(A)** N2, *dcr-1(ok247)*, *dcr-1(pk1351)*, and *cps-1(sm24)* animals; **(B)** *ced-1(e1735)*, *ced-1(e1735); dcr-1(ok247)*, and *ced-1(e1735); dcr-1(pk1351)* animals; **(C)** *ced-1(e1735) smIs111; egl-1(n3082)* and *ced-1(e1735) smIs111; dcr-1(ok247); egl-1(n3082)* animals. Stages of embryos examined were comma, 1.5-fold, 2-fold, 2.5-fold, 3-fold, and 4-fold. The *y* axis represents average number of cell corpses scored, and error bars represent SD. For each embryonic stage, 15 embryos were counted. The significance of differences between different genetic backgrounds was determined by two-way ANOVA, followed by Bonferroni comparison. $*P < 0.001$; $**P < 0.05$. All other points had *P* values > 0.05.

ticulocyte lysate and incubated it with purified CED-3 protease. [^{35}S]Met-labeled GST–DCR-1 was cleaved by CED-3, which yielded two primary cleavage products of about 193 and 43 kD (Fig. 3A, lanes 1 and 2). A DCR-1 deletion mutant, DCR-1(1045-1845), was also cleaved by CED-3 to yield the same 43-kD cleavage product (fig. S2A), which suggested that CED-3 cleavage occurs at the carboxyl terminus of DCR-1. To determine the CED-3 cleavage site in DCR-1, we expressed and purified a truncated DCR-1 protein with a six-histidine tag, DCR-1(1334-1791)-His$_6$, and incubated the purified protein with the CED-3 protease. The ~37-kD C-terminal DCR-1 cleavage product was subjected to N-terminal sequencing analysis (fig. S2B) (*49*). Residues 1473 to 1477 of DCR-1 (GIETI) (*39*) were found to be the N terminus of this DCR-1 cleavage product, which suggested that DCR-1 was cleaved by CED-3 between Asp^{1472} and Gly^{1473}. When Asp^{1472} of DCR-1 was replaced by Glu through site-directed mutagenesis, the resulting mutant protein GST–DCR-1(D1472E) was not cleaved by CED-3 (Fig. 3A, lanes 3 and 4), which confirmed that Asp^{1472} is the CED-3 cleavage site. Thus, DCR-1 is a substrate of CED-3 in vitro.

Cleavage of DCR-1 by CED-3 destroys the dsRNA dicing activity but activates a DNase activity. Full-length DCR-1 contains a helicase domain at its N terminus; a PAZ domain in the middle; and two RNase III–like domains (indicated as RNase IIIa and RNase IIIb, respectively) and a dsRNA binding domain at the C terminus (Fig. 3A). Cleavage of DCR-1 by CED-3 at Asp^{1472}, which is in the middle of the RNase IIIa domain, presumably would destroy the RNase IIIa domain but leave RNase IIIb unaffected. Consistent with the findings that both RNase III domains of Dicer are required for binding and cleaving dsRNA (*29*, *42*), CED-3 cleavage of GST–DCR-1 abolished the 22- to 23-nucleotide dicing activity of DCR-1 on dsRNA (Fig. 3A, left, lanes 5 to 8). However, the C-terminal cleavage product of DCR-1, which we named tDCR-1, still contains one intact RNase III domain (RNase IIIb) that may retain some endonuclease activity. Given that DCR-1 is also involved in mediating apoptotic DNA degradation, we examined whether DCR-1 or its CED-3 cleavage products might have a deoxyribonuclease activity. GST–DCR-1 and GST–DCR-1(D1472E) synthesized in rabbit reticulocyte lysate were affinity purified using glutathione Sepharose resins and incubated with pUC19 supercoiled plasmid DNA substrate in the presence or absence of the CED-3 protease (*49*). Purified CED-3 protease or GST–DCR-1 alone did not cleave or nick plasmid DNA (Fig. 3B, left, top, lanes 1 to 3). Incubation of CED-3 with GST–DCR-1 resulted in nicking of the plasmid DNA and the mobility shift of the plasmid DNA from the supercoiled form (SC) to the nicked open circle form (Fig. 3B, left, top, lane 4). This plasmid DNA nicking activity required the presence of Mg^{2+} and was not observed when GST–DCR-1(D1472E) was incubated with CED-3 (Fig. 3B,

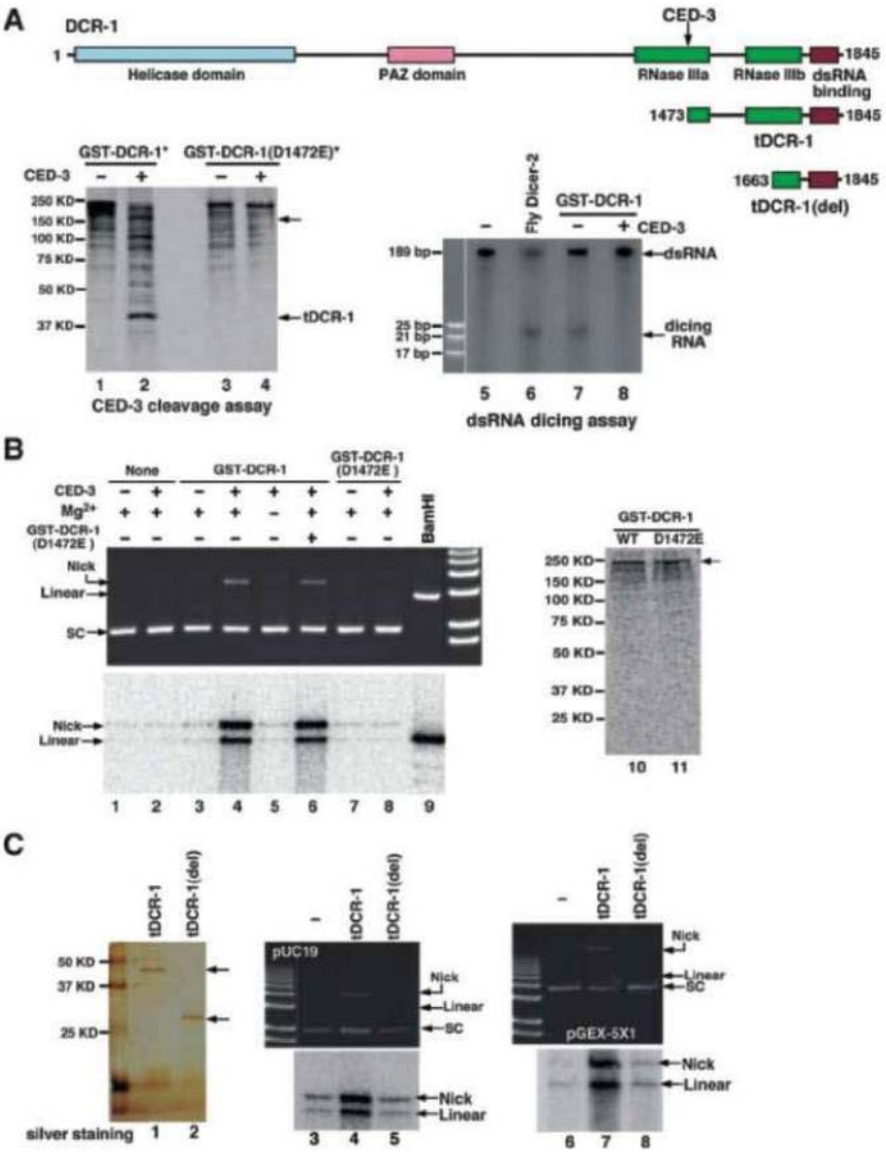

Fig. 3. Activation of a deoxyribonuclease activity after cleavage of DCR-1 by CED-3. (**A**) Cleavage of DCR-1 at Asp^{1472}. (Top) A schematic diagram of DCR-1, tDCR-1, tDCR-1(del), and various DCR-1 domains. The CED-3 cleavage site is indicated. (Bottom) Cleavage of DCR-1 by CED-3 at Asp^{1472} abolished the dsRNA dicing activity of DCR-1. (Lanes 1 to 4) GST–DCR-1 and GST–DCR-1(D1472E) were synthesized in rabbit reticulocyte lysate and labeled with [^{35}S]Met. They were then incubated with or without 5 ng of purified CED-3 for 1 hour and resolved by 12% SDS–polyacrylamide gel electrophoresis (PAGE). (Lanes 5 to 8) GST–DCR-1 was synthesized in rabbit reticulocyte lysate and purified by glutathione Sepharose resins. Purified GST–DCR-1 was first incubated with or without 5 ng of purified CED-3 for 2 hours before addition of [α-^{32}P]UTP–labeled dsRNA probes. Purified fly Dicer-2 protein was included as a positive control. Samples were resolved by 20% native polyacrylamide gel. Autoradiography image is shown. (**B**) Activation of DNase activity after cleavage of DCR-1 by CED-3. (Lanes 10 and 11) GST–DCR-1 and GST–DCR-1(D1472E) were synthesized and purified as in (A) in the presence of both Met and [^{35}S]Met (50:1). pUC19 plasmid DNA (200 ng) was incubated with purified GST–DCR-1 or GST–DCR-1(D1472E) or both (lane 6) in the presence or absence of 5 ng of purified CED-3 for 1 hour at 37°C (*49*). Twice the amount of GST–DCR-1(D1472E) was added in lane 6. One-half of the samples was resolved on 1% agarose gel and then stained with ethidium bromide before an ultraviolet image was taken (top). Two units of TdT, [α-^{32}P]dCTP, and $CoCl_2$ (250 μM) were added to the remaining reactions and incubated for another 2 hours at 37°C. The samples were resolved on 1% agarose gel, then fixed and dried for autoradiography (bottom). In lane 9, only one-fourth of the sample was loaded. A 1-kb Plus DNA ladder was used (Invitrogen). (**C**) DNase activity of tDCR-1. tDCR-1–Flag and tDCR-1(del)–Flag were expressed in *C. elegans*, purified on an anti-Flag affinity column, eluted by Flag peptides (*49*), and resolved on 15% SDS-PAGE, before being subjected to silver staining (lanes 1 and 2). The nuclease activity assay and TdT labeling were done as in (B) with two different plasmids (pUC19 and pGEX-5X1). The TdT labeling method is expected to more efficiently label a linear substrate versus a nicked substrate.

left, top, lanes 5, 7, 8), which indicated that CED-3 cleavage is required to activate this new Mg^{2+}-dependent DNase activity of DCR-1. Incubation of GST–DCR-1(D1472E) with GST–DCR-1 and CED-3 did not prevent the activation of this DNase activity by CED-3 (Fig. 3B, left, top, lane 6). Moreover, when the CED-3 cleavage site in DCR-1 was replaced by a site (ENLYFQG) (*39*) only recognized by the tobacco etch virus (TEV) protease (fig. S3A), the resulting DCR-1 mutant, GST–DCR-1(1472TEV), was not activated by CED-3 to generate a DNase activity (fig. S3B, lanes 1 to 4). By contrast, purified TEV protease cleaved GST–DCR-1(1472TEV) but not GST–DCR-1 to activate a similar DNase activity (fig. S3, A and B, lanes 5 to 10). Together, these results indicate that this CED-3–activated DNase activity is derived from cleavage of DCR-1 at Asp^{1472}

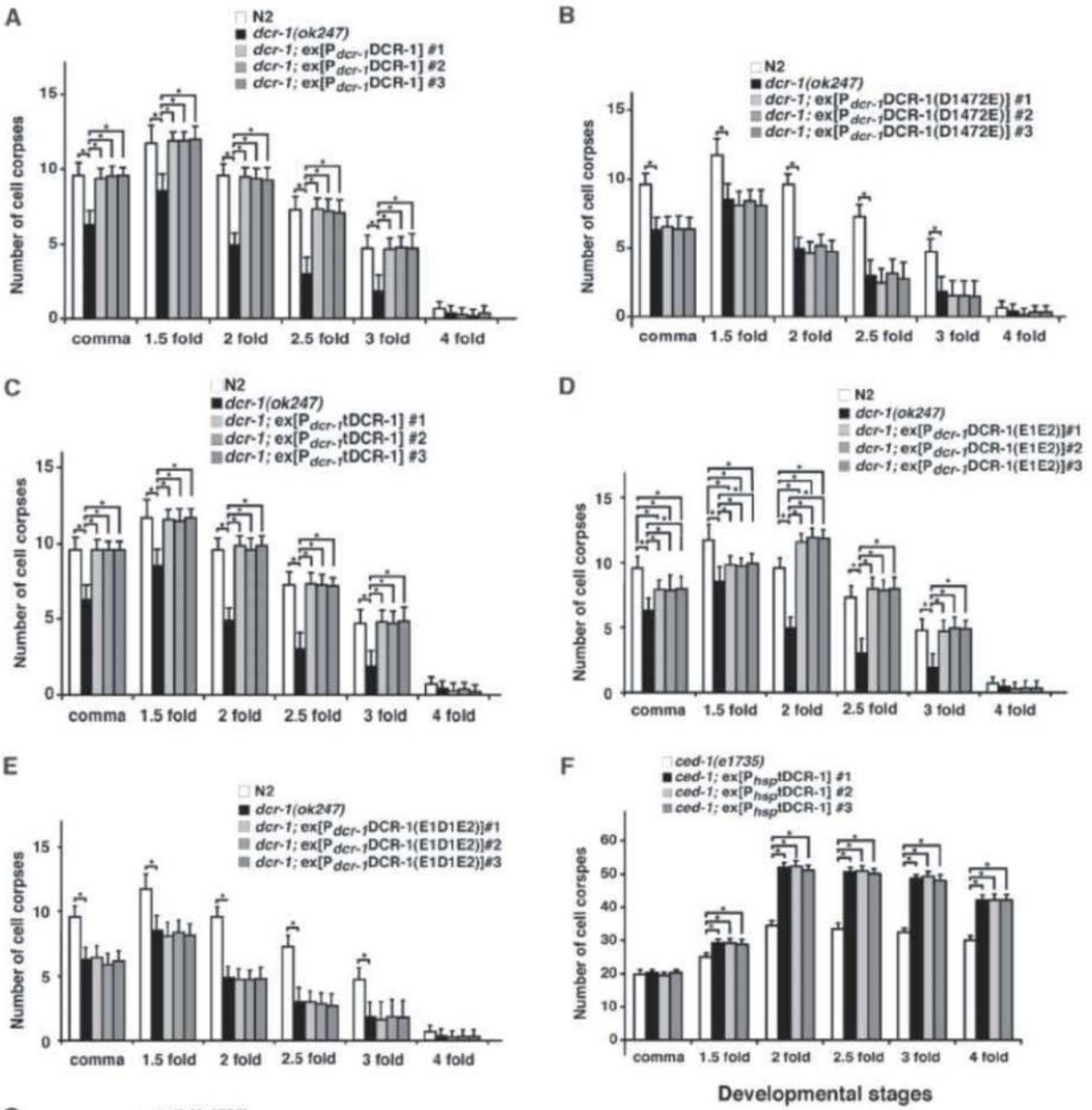

Fig. 4. Requirement of DCR-1 cleavage by CED-3 for its proapoptotic activity. Cell corpses were scored in the following animals: (**A**) N2, *dcr-1(ok247)*, *dcr-1(ok247); ex[$P_{dcr\text{-}1}$DCR-1]* arrays 1 to 3; (**B**) N2, *dcr-1(ok247)*, *dcr-1(ok247); ex[$P_{dcr\text{-}1}$DCR-1(D1472E)]* arrays 1 to 3; (**C**) N2, *dcr-1(ok247)*, *dcr-1(ok247); ex[$P_{dcr\text{-}1}$tDCR-1]* arrays 1 to 3; (**D**) N2, *dcr-1(ok247)*, *dcr-1(ok247); ex[$P_{dcr\text{-}1}$DCR-1(E1E2)]* arrays 1 to 3; (**E**) N2, *dcr-1(ok247)*, *dcr-1(ok247); ex[$P_{dcr\text{-}1}$DCR-1(E1D1E2)]* arrays 1 to 3; (**F**) *ced-1(e1735)*, *ced-1(e1735); ex[P_{hsp}tDCR-1]* arrays 1 to 3; and (**G**) *ced-1(e1735)*, *ced-1(e1735); ex[P_{hsp}tDCR-1(del)]* arrays 1 to 3. Stages of embryos examined were comma, 1.5-fold, 2-fold, 2.5-fold, 3-fold, and 4-fold. The *y* axis represents average number of cell corpses scored, and error bars represent SD. For each developmental stage, 15 embryos were counted. The significance of differences between different genetic backgrounds was determined by two-way ANOVA, followed by Bonferroni comparison. $*P < 0.001$; $**P < 0.05$. All other points had *P* values > 0.05.

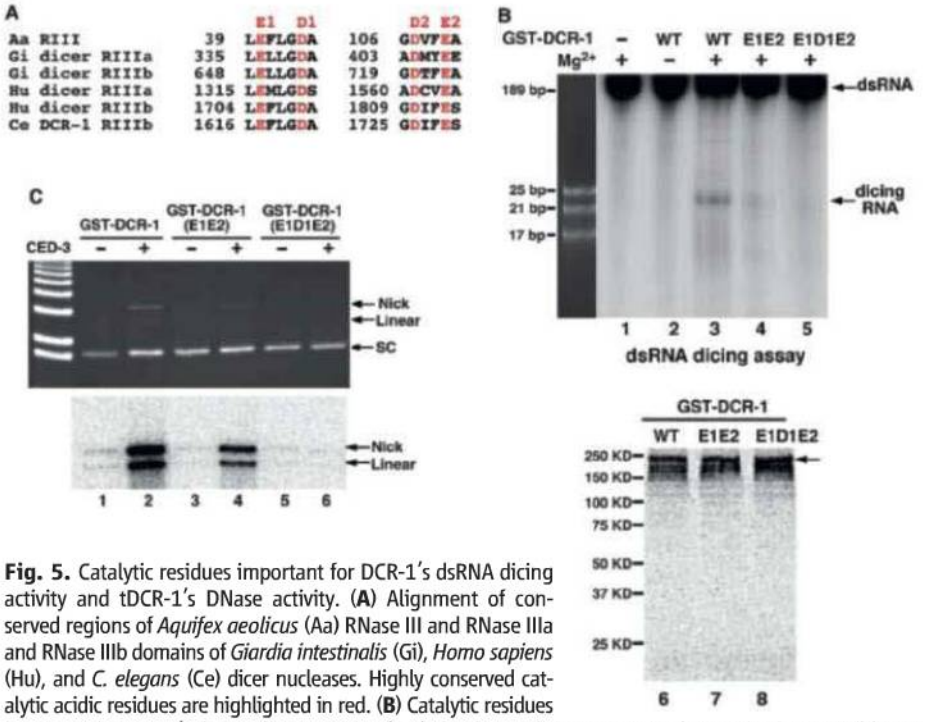

Fig. 5. Catalytic residues important for DCR-1's dsRNA dicing activity and tDCR-1's DNase activity. **(A)** Alignment of conserved regions of *Aquifex aeolicus* (Aa) RNase III and RNase IIIa and RNase IIIb domains of *Giardia intestinalis* (Gi), *Homo sapiens* (Hu), and *C. elegans* (Ce) dicer nucleases. Highly conserved catalytic acidic residues are highlighted in red. **(B)** Catalytic residues important for DCR-1's dsRNA dicing activity. (Top) The dsRNA dicing assay was done as in Fig. 3A. Wild-type (WT) and mutant GST–DCR-1 proteins (E1E2 and E1D1E2), in which the indicated acidic residues were replaced by Ala, were synthesized and purified as in Fig. 3B. (Bottom) Purified GST–DCR-1 proteins. **(C)** Catalytic residues important for tDCR-1's DNase activity. The DNase activity assay on the pUC19 plasmid and TdT labeling were done as in Fig. 3B.

rather than from a protein copurified with DCR-1 and activated by CED-3 cleavage.

Because the RNase III enzyme is known to generate 3′ OH ends (*30*, *40*) and DCR-1 is implicated in generating 3′ OH DNA breaks in *C. elegans* apoptotic cells that are labeled by TUNEL (Fig. 1), we tested whether CED-3–activated DCR-1 produced 3′ OH ends in vitro that could be labeled by [α-^{32}P]deoxycytidine triphosphate (dCTP) catalyzed by TdT. Bam HI, a restriction endonuclease, completely linearized plasmid DNA and generated 3′ OH DNA ends that were strongly labeled by TdT (Fig. 3B, left, bottom, lane 9). GST–DCR-1 but not GST–DCR-1(D1472E), when treated with CED-3, generated both nicked and linearized plasmid DNAs that were labeled by TdT in a Mg^{2+}-dependent manner (Fig. 3B, left, bottom, lanes 3 to 8). This result indicates that cleavage of DCR-1 by CED-3 activates a deoxyribonuclease activity that can nick DNA and create 3′ OH ends.

tDCR-1 has the DNase activity. We further investigated whether tDCR-1, a CED-3 cleavage product that retains a complete RNase IIIb domain and a dsRNA-binding domain, is responsible for the newly generated DNase activity. tDCR-1 tagged with a Flag epitope was expressed in *C. elegans* under the control of heat-shock promoters. A mutant tDCR-1, in which one-half of the RNase IIIb domain is deleted [tDCR-1(del)], was similarly expressed in *C. elegans*. After heat-shock induction, tDCR-1–Flag and tDCR-1(del)–Flag were purified from worm lysate on an anti-Flag affinity column (Fig. 3C, lanes 1and 2) (*49*) and tested for the DNase activity. tDCR-1 nicked supercoiled plasmid DNA and caused a shift of some of the DNA to the nicked open circle form, whereas tDCR-1(del)–Flag failed to do so (Fig. 3C, top, lanes 3 to 5). TdT labeling indicated that tDCR-1 generated both nicked and linearized plasmid DNAs with 3′ OH ends (Fig. 3C, bottom, lane 4), whereas tDCR-1(del) did not nick or linearize plasmid DNA. We observed similar results with two other plasmids with different sizes (Fig. 3C, lanes 6 to 8 and fig. S3C), which indicated that the nicking activity of tDCR-1 may be relatively unspecific as to sequence. Thus, tDCR-1 functions as a DNase to nick DNA and to generate 3′ OH ends.

Cleavage of DCR-1 by CED-3 is important for its proapoptotic activity. We tested whether cleavage of DCR-1 by CED-3 is required for promoting cell death in *C. elegans*. Expression of DCR-1 under the control of the endogenous *dcr-1* promoter ($P_{dcr\text{-}1}$DCR-1) fully rescued the reduced-embryonic-cell-corpse phenotype of *dcr-1(ok247)* animals (Fig. 4A). This construct also rescued the abnormal vulva phenotype (bursting vulva and protruding vulva) of *dcr-1(ok247)* animals (table S3), which is due to a defect in biogenesis of miRNAs (*21*). We were unable to examine rescue of the RNAi defect of *dcr-1(ok247)* animals, because *dcr-1(ok247)* homozygous animals derived from *dcr-1(ok247)*/+ heterozygous mothers show no RNAi defect owing to maternal rescue of *dcr-1* (*21*). $P_{dcr\text{-}1}$DCR-1(D1472E), which drives the expression of the CED-3–resistant DCR-1 mutant, rescued the vulva defects of *dcr-1(ok247)* animals, but failed to rescue the reduced-embryonic-cell-corpse phenotype of *dcr-1(ok247)* animals (table S3 and Fig. 4B). These findings indicate that cleavage of DCR-1 by CED-3 is critical for promoting cell death but is not needed for biogenesis of miRNAs. However, expression of tDCR-1 under the control of the *dcr-1* promoter ($P_{dcr\text{-}1}$tDCR-1) fully rescued the cell-death defect of *dcr-1(ok247)* animals but did not rescue their vulva defects (Fig. 4C and table S3), which confirmed that tDCR-1 is sufficient to mediate DCR-1's proapoptotic function.

We generated three integrated transgenes, *smIs182*, *smIs196*, and *smIs201*, which carry $P_{dcr\text{-}1}$DCR-1, $P_{dcr\text{-}1}$DCR-1(D1742E), and $P_{dcr\text{-}1}$tDCR-1, respectively. These transgenes were crossed into the *cps-6(sm116); dcr-1(ok247)* mutant, and we assessed their ability to rescue the DNA degradation defect of the *dcr-1(ok247)* mutant. Both *smIs182* ($P_{dcr\text{-}1}$DCR-1) and *smIs201* ($P_{dcr\text{-}1}$tDCR-1) restored the number of TUNEL-stained cells in *cps-6(sm116); dcr-1(ok247)* embryos to the level seen in *cps-6(sm116)* embryos alone (Fig. 1E), which suggested that both transgenes rescue the DNA degradation defect of the *dcr-1(ok247)* mutant. In contrast, *cps-6(sm116); dcr-1(ok247)*; *smIs196* embryos had few TUNEL-stained cells (Fig. 1E), which indicated that the $P_{dcr\text{-}1}$DCR-1(D1742E) transgene was unable to rescue the DNA degradation defect of the *dcr-1(ok247)* mutant. These results further indicate that tDCR-1 is sufficient to replace DCR-1 in promoting DNA degradation and apoptosis, whereas the CED-3–resistant DCR-1 mutant is not.

We also induced global overexpression of tDCR-1 under the control of the heat-shock promoters (P_{hsp}tDCR-1) and examined whether tDCR-1 could induce ectopic apoptosis. When expressed in the *ced-1(e1735)* mutant that is defective in engulfment of apoptotic cells and thus allows easy detection of increased apoptosis, tDCR-1 caused an increase of about 45 to 50% in the number of apoptotic cells (Fig. 4F), whereas the DNase-defective tDCR-1(del) mutant had no such activity (Fig. 4G). In the strong *ced-3(n2433)* mutant that is deficient in cell death, tDCR-1 overexpression failed to induce any apoptosis (table S4), possibly because tDCR-1 needs to cooperate with other CED-3–activated cell-death pathways to induce apoptosis. Yet overexpression of tDCR-1 but not tDCR-1(del) still created a significant number of TUNEL-stained cells (Fig.1G), which showed that tDCR-1 can initiate 3′ OH nicks in chromosomal DNA, independently of CED-3. Together, these results indicate that cleavage of DCR-1 by CED-3 during apoptosis is critical for its role in promoting apoptosis and produces a cleavage product, tDCR-1, that initiates apoptotic DNA degradation through its DNase activity.

Conserved acidic residues are important for both DCR-1 cleavage of RNA and tDCR-1 cleavage of DNA. Because DCR-1 is a dsRNA-processing enzyme and the yeast RNA III,

Rnt1p, can cleave the DNA strand of DNA-RNA hybrids in vitro (*54*), tDCR-1 may cleave DNA through the same catalytic mechanism used for dsRNA cleavage. We thus examined whether catalytic residues that are critical for Dicer's ribonuclease activity are also important for tDCR-1's DNase activity (*29*, *42*). Structural analysis of *Giardia* Dicer reveals four highly conserved acidic residues that are involved in binding and positioning of the two catalytic divalent metal cations in each RNase III domain (Fig. 5A; they are named E1, D1, D2, and E2 for simplicity) (*42*). The D1 and E2 residues in both RNase III domains have been shown to be important for the dicing activity of human dicer (*29*). We generated two DCR-1 mutants with altered acidic residues in the RNase IIIb domain, the E1E2 double mutant (E1617A, E1729A) and the E1D1E2 triple mutant (E1617A, D1621A, E1729A). We then assayed their dsRNA dicing activity and CED-3–activated DNase activity. The DCR-1(E1E2) mutant showed significantly reduced dsRNA dicing activity, which was dependent on the presence of Mg^{2+} (Fig. 5B, lanes 1 to 4). The CED-3–activated DNase activity of DCR-1(E1E2) was also impaired (Fig. 5C, lanes 1 to 4). In comparison, no detectable dsRNA dicing activity or CED-3–activated DNase activity was observed with the DCR-1(E1D1E2) triple mutant (Fig. 5B, lane 5, and Fig. 5C, lanes 5 to 6). These results and the observations that the dsRNA dicing activity and the CED-3–activated DNase activity of DCR-1 were both dependent on Mg^{2+} indicate that the catalytic mechanism of DNA cleavage by tDCR-1 is likely similar to that for dsRNA cleavage by DCR-1. They also provide further evidence that the CED-3–activated DNase activity comes from Dicer.

We also tested whether these catalytic residues are important for DCR-1's functions in vivo. Consistent with its reduced RNase and DNase activities in vitro, DCR-1(E1E2) expressed under the control of the *dcr*-1 promoter [$P_{dcr\text{-}1}$DCR-1(E1E2)] partially rescued the vulva defects, the reduced-embryonic-cell-corpse defect, and the DNA degradation defect of *dcr-1(ok247)* animals (table S3, and Figs. 1F and 4D). However, expression of the DCR-1(E1D1E2) mutant [$P_{dcr\text{-}1}$DCR-1(E1D1E2)], which had no detectable RNase or DNase activity in vitro (Fig. 5, B and C), failed to rescue all three defects of *dcr-1(ok247)* animals that we assayed (table S3, Fig. 1F, and Fig. 4E). Thus, the in vitro dsRNA dicing activity and the CED-3–activated DNase activity of two DCR-1 mutants correlate with their abilities to promote small RNA processing and apoptosis in *C. elegans*.

Discussion. The Dicer ribonuclease plays a critical role in processing dsRNA substrates into short dsRNA species, such as siRNAs and miRNAs with diverse regulatory functions (*30*, *40*, *41*). Our findings that *C. elegans* DCR-1 is involved in generating TUNEL-reactive DNA breaks in apoptotic cells that are later resolved by downstream apoptotic nucleases, such as CPS-6 and NUC-1, and that DCR-1 promotes, and even is required for, apoptosis in sensitized genetic backgrounds reveal an unexpected role of DCR-1 in apoptosis and in initiating apoptotic DNA degradation. The observations that inactivation of crucial DCR-1 cofactors in generating siRNAs, miRNAs, endo-siRNAs, and other small RNAs did not affect either apoptotic DNA degradation or apoptosis indicate that DCR-1 likely promotes apoptosis through a distinct mechanism that is not related to dsRNA processing and gene silencing.

Dicer is a member of the RNase III family that recognizes and cleaves dsRNA substrates to various lengths and is not known to contain a deoxyribonuclease activity (*40*, *41*). All RNase III family enzymes contain at least one characteristic RNase III domain and most also have a dsRNA-binding domain (dsRBD). Some, like Dicer, contain two RNase III domains and several additional domains, including the PAZ domain and the DExH helicase domain. Biochemical and structural analyses of the Dicer enzymes indicate that two RNase III domains form an intramolecular dimer, which constitutes a single processing center, with each domain contributing to the hydrolysis of one RNA strand of the duplex substrate through several highly conserved acidic residues that bind and position two catalytic Mg^{2+} cations (*29*, *42*). Interestingly, CED-3 cleaves *C. elegans* DCR-1 in the middle of its first RNase III domain, yielding a C-terminal cleavage product (tDCR-1) with only one complete RNase III domain, and presumably, a disabled dsRNA processing center. Indeed, cleavage of DCR-1 by CED-3 abolishes the dsRNA dicing activity of DCR-1. However, cleavage of DCR-1 by CED-3 appears to also activate a deoxyribonuclease activity that can nick and linearize DNA to generate 3′ OH DNA ends through the same highly conserved catalytic residues and Mg^{2+} cations, and this DNase activity is not observed in full-length DCR-1. The observations that tDCR-1 similarly nicked and linearized DNA in vitro and fully rescued the cell-death defects of the *dcr-1(lf)* mutant when expressed under the control of the *dcr-1* promoter and the findings that expression of DCR-1(D1472E), the CED-3–resistant mutant, fully rescued the developmental defects of the *dcr-1(lf)* mutant but failed to rescue the cell-death defects of the *dcr-1(lf)* mutant indicate that cleavage of the DCR-1 ribonuclease by CED-3 activates a DNase activity that is necessary and sufficient to promote DNA degradation and apoptosis and that the proapoptotic function of DCR-1 is separable from DCR-1's developmental functions. The proteolytic mechanism we discovered, through which a ribonuclease is disabled and converted into a DNase, may have more general implications on regulation of RNases and DNases, RNA and DNA binding proteins, and their associated cellular functions.

In mammals, the apoptotic nuclease DFF40 is kept in check in normal cells by its cognate inhibitor DFF45 (*5*–*8*). During apoptosis, executor caspases, such as caspase-3 and caspase-7, are activated to cleave a plethora of caspase targets, which lead to rapid cell disassembly. One of these targets is DFF45, which is cleaved and inactivated by caspases to unleash DFF40 and to initiate the chromosome fragmentation process. It is intriguing that no DFF40 or DFF45 homologs are found in *C. elegans*, in which other key cell-death components are highly conserved, including apoptotic nucleases endoG and DNase II (*4*). We propose that tDCR-1 is a functional analog of DFF40 and that a conserved, caspase-mediated mechanism activates the apoptotic DNA degradation process in both *C. elegans* and mammals.

References and Notes

1. A. H. Wyllie, *Nature* **284**, 555 (1980).
2. P. Widlak, W. T. Garrard, *J. Cell. Biochem.* **94**, 1078 (2005).
3. K. Samejima, W. C. Earnshaw, *Nat. Rev. Mol. Cell Biol.* **6**, 677 (2005).
4. J. Z. Parrish, D. Xue, *Chromosoma* **115**, 89 (2006).
5. X. Liu, H. Zou, C. Slaughter, X. Wang, *Cell* **89**, 175 (1997).
6. X. Liu *et al.*, *Proc. Natl. Acad. Sci. U.S.A.* **95**, 8461 (1998).
7. M. Enari *et al.*, *Nature* **391**, 43 (1998).
8. H. Sakahira, M. Enari, S. Nagata, *Nature* **391**, 96 (1998).
9. P. Widlak, P. Li, X. Wang, W. T. Garrard, *J. Biol. Chem.* **275**, 8226 (2000).
10. F. Durrieu *et al.*, *Curr. Biol.* **10**, 923 (2000).
11. J. Zhang *et al.*, *Proc. Natl. Acad. Sci. U.S.A.* **95**, 12480 (1998).
12. K. Kawane *et al.*, *Nat. Immunol.* **4**, 138 (2003).
13. L. Y. Li, X. Luo, X. Wang, *Nature* **412**, 95 (2001).
14. J. Parrish *et al.*, *Nature* **412**, 90 (2001).
15. S. Büttner *et al.*, *Mol. Cell* **25**, 233 (2007).
16. J. Z. Parrish, D. Xue, *Mol. Cell* **11**, 987 (2003).
17. J. Z. Parrish, C. Yang, B. Shen, D. Xue, *EMBO J.* **22**, 3451 (2003).
18. Y. C. Wu, G. M. Stanfield, H. R. Horvitz, *Genes Dev.* **14**, 536 (2000).
19. S. M. Hammond, E. Bernstein, D. Beach, G. J. Hannon, *Nature* **404**, 293 (2000).
20. E. Bernstein, A. A. Caudy, S. M. Hammond, G. J. Hannon, *Nature* **409**, 363 (2001).
21. A. Grishok *et al.*, *Cell* **106**, 23 (2001).
22. G. Hutvágner *et al.*, *Science* **293**, 834 (2001).
23. S. W. Knight, B. L. Bass, *Science* **293**, 2269 (2001).
24. J. W. Pham, J. L. Pellino, Y. S. Lee, R. W. Carthew, E. J. Sontheimer, *Cell* **117**, 83 (2004).
25. Y. S. Lee *et al.*, *Cell* **117**, 69 (2004).
26. T. F. Duchaine *et al.*, *Cell* **124**, 343 (2006).
27. S. M. Elbashir, W. Lendeckel, T. Tuschl, *Genes Dev.* **15**, 188 (2001).
28. H. Zhang, F. A. Kolb, V. Brondani, E. Billy, W. Filipowicz, *EMBO J.* **21**, 5875 (2002).
29. H. Zhang, F. A. Kolb, L. Jaskiewicz, E. Westhof, W. Filipowicz, *Cell* **118**, 57 (2004).
30. M. A. Carmell, G. J. Hannon, *Nat. Struct. Mol. Biol.* **11**, 214 (2004).
31. Q. Liu *et al.*, *Science* **301**, 1921 (2003).
32. J. Liu *et al.*, *Science* **305**, 1437 (2004).
33. F. V. Rivas *et al.*, *Nat. Struct. Mol. Biol.* **12**, 340 (2005).
34. R. W. Carthew, E. J. Sontheimer, *Cell* **136**, 642 (2009).
35. H. Tabara, E. Yigit, H. Siomi, C. C. Mello, *Cell* **109**, 861 (2002).
36. H. Tabara *et al.*, *Cell* **99**, 123 (1999).
37. F. Simmer *et al.*, *Curr. Biol.* **12**, 1317 (2002).
38. S. Kennedy, D. Wang, G. Ruvkun, *Nature* **427**, 645 (2004).
39. Single-letter abbreviations for the amino acid residues are as follows: A, Ala; C, Cys; D, Asp; E, Glu; F, Phe; G, Gly; H, His; I, Ile; K, Lys; L, Leu; M, Met; N, Asn; P, Pro; Q,

Gln; R, Arg; S, Ser; T, Thr; V, Val; W, Trp; Y, Tyr; and x, any amino acid
40. I. J. MacRae, J. A. Doudna, *Curr. Opin. Struct. Biol.* **17**, 138 (2007).
41. L. Jaskiewicz, W. Filipowicz, *Curr. Top. Microbiol. Immunol.* **320**, 77 (2008).
42. I. J. MacRae *et al.*, *Science* **311**, 195 (2006).
43. K. Mochizuki, N. A. Fine, T. Fujisawa, M. A. Gorovsky, *Cell* **110**, 689 (2002).
44. T. A. Volpe *et al.*, *Science* **297**, 1833 (2002).
45. E. Bernstein *et al.*, *Nat. Genet.* **35**, 215 (2003).
46. D. Baulcombe, *Nature* **431**, 356 (2004).
47. S. D. Hatfield *et al.*, *Nature* **435**, 974 (2005).
48. K. Förstemann *et al.*, *PLoS Biol.* **3**, e236 (2005).
49. Materials and methods are available as supporting material on *Science* Online.
50. G. M. Stanfield, H. R. Horvitz, *Mol. Cell* **5**, 423 (2000).
51. R. E. Ellis, D. M. Jacobson, H. R. Horvitz, *Genetics* **129**, 79 (1991).
52. D. Kokel, Y. Li, J. Qin, D. Xue, *Nat. Chem. Biol.* **2**, 338 (2006).
53. D. M. Pavelec, J. Lachowiec, T. F. Duchaine, H. E. Smith, S. Kennedy, *Genetics* **183**, 1283 (2009).
54. B. Lamontagne, R. N. Hannoush, M. J. Damha, S. Abou Elela, *J. Mol. Biol.* **338**, 401 (2004).
55. We thank T. Blumenthal, N. Pace, M. Yarus, L. He, X. D. Liu, and S. Marquez for comments; Y. Kohara for *dcr-1* cDNA; Q. H. Liu for purified fly Dicer-2 protein; K. Morita for the *alg-1* RNAi construct; and members of the Xue lab for helpful discussions. This work was supported by a Burroughs Wellcome Fund Award (D.X.), a grant from Ministry of Education, Culture, Sports, Science and Technology (MEXT) of Japan (S.M.), and NIH grants R01 GM59083 and R01 GM79097 (D.X.).

Supporting Online Material

www.sciencemag.org/cgi/content/full/science.1182374/DC1
Materials and Methods
Figs. S1 to S3
Tables S1 to S4
References

23 September 2009; accepted 1 March 2010
Published online 11 March 2010;
10.1126/science.1182374
Include this information when citing this paper.

REPORTS

Detection of a Large-Scale Structure of Intracluster Globular Clusters in the Virgo Cluster

Myung Gyoon Lee,[1]* Hong Soo Park,[1] Ho Seong Hwang[1,2]

Globular clusters are usually found in galaxies, and they are excellent tracers of dark matter. Long ago it was suggested that intracluster globular clusters (IGCs) may exist that are bound to a galaxy cluster rather than to any single galaxy. Here we present a map showing the large-scale distribution of globular clusters over the entire Virgo cluster. It shows that IGCs are found out to 5 million light years from the Virgo center and that they are concentrated in several substructures that are much larger than galaxies. These objects might have been mostly stripped off from low-mass dwarf galaxies.

Almost six decades ago, it was suggested that stars and interstellar medium may exist between galaxies that are in clusters of galaxies (*1*, *2*). To date, there is accumulating evidence for the existence of diffuse optical stellar light, planetary nebulae, resolved red giant stars, and diffuse hot x-ray–emitting gas between galaxies in nearby galaxy clusters (*3*–*7*). Some of these objects are not bound to any single galaxy but are gravitationally controlled by the potential of the galaxy cluster itself. These are called intracluster objects.

It was then suggested that globular clusters should be stripped off from galaxies in a galaxy cluster and that there should be a cluster-wide population of intracluster globular clusters (IGCs) in galaxy clusters (*8*–*10*). However, so far there has been no indication of IGCs in the Coma cluster, and only a small number of IGCs were found in similar studies of other galaxy clusters because of the studies' relatively shallow photometric limits or small area coverage (*11*–*14*). It is not yet known whether this cluster-wide population of IGCs exists in any galaxy cluster or not.

The Virgo cluster is the best target in which to search for a cluster-wide population of IGCs, because it is the nearest massive galaxy cluster. However, because of its largest angular extent (over 10° in the sky) (*15*) and the faintness of its globular clusters, it has been difficult to find and study IGCs over the entire Virgo cluster.

We present the results of a search for globular clusters over the entire Virgo cluster using data from the Sloan Digital Sky Survey (SDSS) (*16*, *17*). The SDSS data are deep enough to study the bright globular clusters in Virgo, and its survey area is wide enough to cover the entire Virgo cluster.

The Virgo cluster is located at a distance of 54 million light years (16.5 mpc); 1° in the sky corresponds to 940,000 light years (288 kpc) at this distance. The globular clusters at the distance of Virgo appear as point sources in the SDSS images; thus, they cannot be distinguished from faint foreground stars in our Galaxy in the images. To overcome this problem and create a map of the globular clusters in Virgo, we used the photometry of the point sources in the SDSS Sixth Data Release (*18*).

We selected bright globular cluster candidates in a circular field with a radius of 9°, including the Virgo cluster, using the criteria for color and magnitude (with reddening corrected): $0.6 < (g-i)_0 < 1.3$ and $19.5 < i_0 < 21.7$ mag (where g and i are

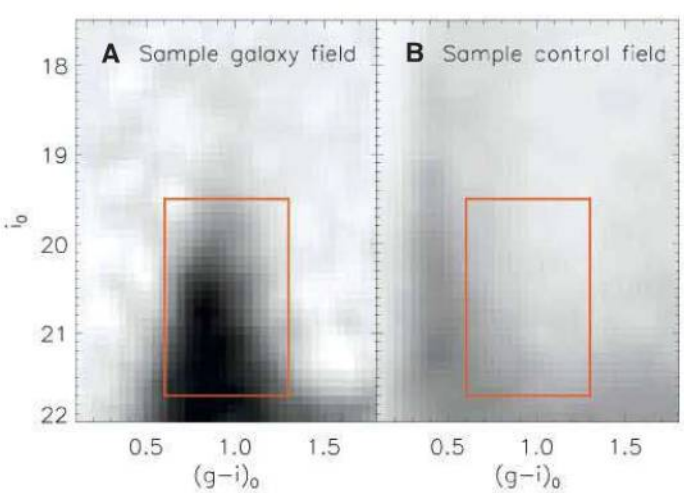

Fig. 1. $i_0 - (g-i)_0$ color-magnitude diagrams for the point sources in Virgo. **(A)** A sample galaxy field composed of 10 circular fields (radius 20 arc min) centered on the brightest galaxies. The contribution of the foreground stars was subtracted. Most of the sources are globular clusters. **(B)** A sample control field located at 6° to 9° from the Virgo center, covering the same area as (A). Most of the sources are foreground stars belonging to our Galaxy. Darker colors represent the higher number density. The box represents the region used for selecting the bright globular cluster candidates in Virgo in this study.

[1]Astronomy Program, Department of Physics and Astronomy, Seoul National University, Seoul 151-742, Korea. [2]CEA Saclay/Service d'Astrophysique, F-91191 Gif-sur-Yvette, France.

*To whom correspondence should be addressed. E-mail: mglee@astro.snu.ac.kr

g-band and i-band magnitudes, respectively, and i_0 is an extinction-corrected i-band magnitude), as marked by the box in Fig. 1. This color range is similar to that used for selecting globular clusters in the galaxy M87 (*19*) and corresponds to a metallicity range of $-2.0 \lesssim$ [Fe/H] $\lesssim +0.4$ (*20*, *21*). The lower magnitude limit, $i_0 < 21.7$ mag, is ~1.5 mag brighter than the peak magnitude in the luminosity function of globular clusters (*19*). By using globular clusters brighter than $i_0 = 21.7$ mag, we covered ~13% of the entire globular cluster population, assuming that their luminosity function is represented by a Gaussian function with peak $i_0 = 23.17$ mag (*19*).

We created a surface number density map for the globular clusters in Virgo after subtracting the contribution of foreground stars [including the Virgo overdensity (*22*)] using the color-magnitude diagram method (details are described in the supporting online material) (Fig. 2A). The surface number density map for the globular clusters reveals the existence of a diffuse large-scale distribution of globular clusters (shown in cyan and green), extending out to about 6° (5 million light years) from the Virgo center, close to the boundary of the Virgo cluster.

It also shows the presence of several strong concentrations of globular clusters. Their locations correspond to the positions of bright elliptical galaxies such as M87, M49, M60, M86/M84, and NGC 4636. However, the sizes of these substructures are much larger than individual galaxies. This population must include not only globular clusters in galaxies but also IGCs.

The large-scale distributions of globular clusters surrounding M87, M49, and M60 are similar in general to that of large-scale x-ray emission seen in the ROSAT (Roentgen Satellite) x-ray map (Fig. 2B). However, one diffuse component of globular clusters in the west of M87 is not seen in the x-ray map, whereas one diffuse x-ray component in the north of M87 is not found in the map of globular clusters.

There are tidal features around some bright galaxies: an elongated structure in the outer part of M87 and bridgelike features between M87 and M86 (also between M87 and M89). These features are similar to the distribution of diffuse stellar light found in the deep optical image of the inner 1.5° × 1.5° region (*6*).

It is known that the color distribution for the globular clusters in giant elliptical galaxies is bimodal, showing that there are two populations: blue and red globular clusters (that is, metal-poor and metal-rich globular clusters, respectively) (*23*, *24*). The large-scale distribution of the blue globular clusters in the Virgo cluster is much more extended than that of the red globular clusters (Fig. 3); a similar trend is seen around bright galaxies (most dramatically around M49 and M87). Therefore, the IGCs are probably dominated by the blue globular clusters.

We derived the radial number density profiles for the globular clusters [σ (number per square arc minute)] as a function of radius from the center of the Virgo cluster (R) (*25*) (Fig. 4). The radial number density profiles of the globular clusters show a change in the slope at $R \approx 40$ arc min, beyond which the slope gets flatter. This break position is consistent with the value for the edge of the stellar halo of M87, $R = 34$ arc min, derived from the kinematic study of planetary nebulae in Virgo (*26*). Therefore, the globular

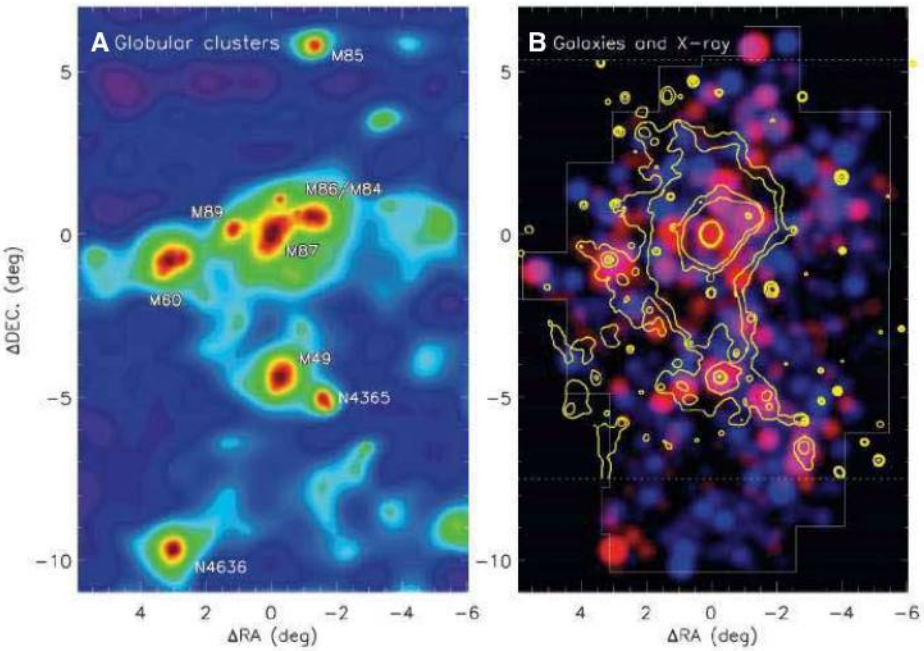

Fig. 2. Surface number density maps for the globular clusters in comparison with the spatial distribution of galaxies and x-ray emission in the Virgo cluster region. ΔDEC and ΔRA are distances from M87 along declination and right ascension, respectively. **(A)** Globular clusters. The levels are 0.012, 0.025, 0.06, and 0.12 per arc min^2, respectively, for cyan, green, yellow, and red boundaries. The positions of several bright elliptical galaxies are labeled. **(B)** Galaxies and x-ray emission. The pseudocolor map represents a luminosity-weighted surface number density map of the early-type (red) and late-type (blue) galaxies that are members of Virgo. The yellow contours represent the contours of x-ray image for the Virgo cluster region in the ROSAT all-sky survey (in the hard energy band 0.4 to 2.4 keV) (*3*). North is up and east is to the left.

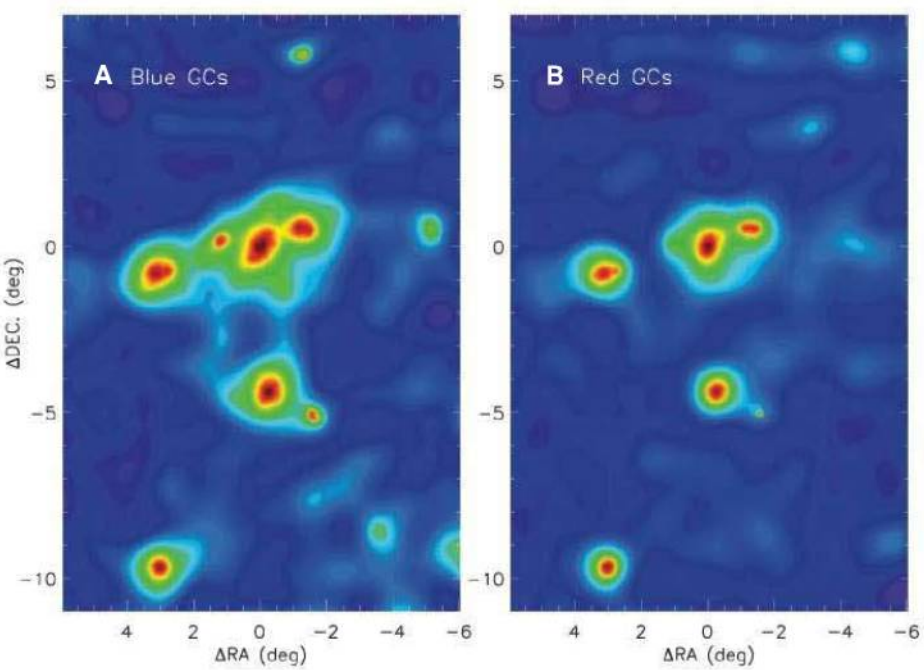

Fig. 3. Surface number density maps of the blue globular clusters (GCs) [$0.6 < (g-i)_0 \leq 0.95$] **(A)** and the red globular clusters [$0.95 < (g-i)_0 < 1.3$] **(B)**. The color for the boundary between the blue and red clusters, $(g-i)_0 = 0.95$, corresponds to the metallicity [Fe/H] ≈ −0.82. The levels are the same as in Fig. 2A.

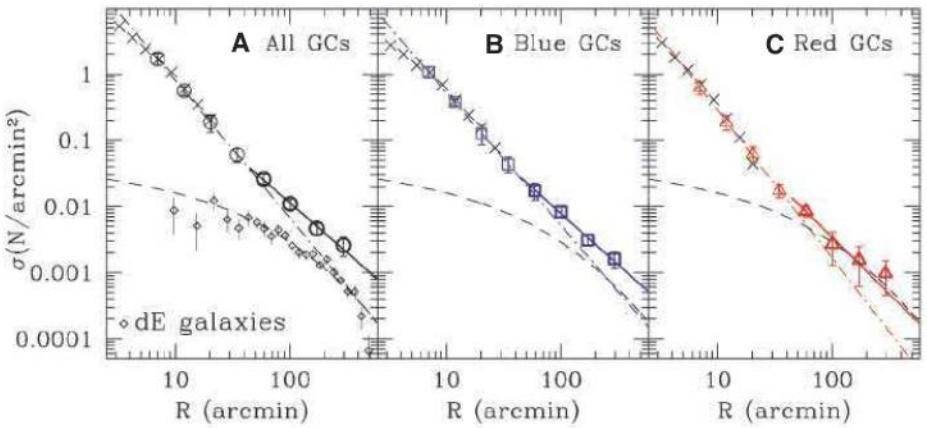

Fig. 4. Radial number density profiles for the globular clusters in Virgo, obtained after masking out a circular region (radius < 5 R_{25}) for each galaxy in the Virgo galaxy catalog except for M87 to remove globular clusters in galaxies. **(A)** All the globular clusters (circles). Dot-dashed lines and solid lines represent the linear fits for the inner region at $R < 40$ arc min and for the outer region at $R > 40$ arc min, respectively. Diamonds represent the radial number density profile for the dwarf elliptical (dE) galaxies that are members of Virgo. Curved dashed lines represent a projected NFW profile (*33*) for the Virgo mass distribution given by McLaughlin (*34*). **(B)** The blue globular clusters (squares) and **(C)** the red globular clusters (triangles). Crosses represent the data including the fainter ($i < 23.0$) globular clusters at $R < 30$ arc min from M87 as given by Harris (*19*), arbitrarily shifted to match the data for $10 < R < 20$ arc min. They are in a good agreement with our data for the inner region.

clusters at $R < 40$ arc min are considered to mostly belong to M87, whereas those at $R > 40$ arc min may be mostly IGCs. Double linear fits for all of the globular clusters yield $\log(\sigma) = -1.49\ (\pm 0.09), \log(R) + 1.05\ (\pm 0.03)$ for the outer region (40 arc min $< R < 6°$) and $\log(\sigma) = -2.07\ (\pm 0.01), \log(R) + 1.99\ (\pm 0.002)$ for the inner region ($R < 40$ arc min). The slope for all the globular clusters at the outer region is similar to that for the dwarf elliptical galaxies and is consistent with the lower limit predicted from numerical simulations: –1.5 to –2.5 (*27*). This result suggests that the IGCs may follow the dark-matter distribution of the Virgo galaxy cluster. If the globular clusters in the core of Virgo undergo a transition from M87-dominated to Virgo-dominated, it is expected that their velocity dispersion profile for $R > 40$ arc min is relatively flat, with a value that is a few hundred kilometers per second higher than that for the inner region (*28*).

The number density of the blue globular clusters is, on average, about twice as large as that of the red globular clusters for the range 40 arc min < $R < 6°$ (Fig. 4, B and C), indicating again that the IGCs may be dominated by the blue globular clusters. For the range 40 arc min $< R < 6°$, we measured $N = 1500 \pm 300$ IGCs with $19.5 < i_0 < 21.7$ mag. This implies that the total number of entire IGCs in that region is $N(\text{total}) \sim 11{,}900$, assuming that the luminosity function for IGCs is similar to that for globular clusters in galaxies.

There are several models to explain the origin of globular clusters in giant elliptical galaxies, but their origin is still controversial (*29*). Our finding that there is a wide distribution of IGCs and that they are mostly blue (metal-poor) indicates that the major origin of these IGCs is low-mass dwarf galaxies (*30*–*32*). This supports the mixture scenario for the origin of globular clusters in giant elliptical galaxies (*29*). According to this scenario, metal-poor globular clusters were formed mostly in low-mass dwarf galaxies, and metal-rich globular clusters were formed later with stars in massive galaxies or in dissipational merging galaxies. Elliptical galaxies grow via dissipational or dissipationless merging of galaxies and via accretion of many dwarf galaxies. The IGCs in Virgo might have been stripped off from low-mass dwarf galaxies and are now being accreted locally to nearby massive galaxies and globally to the center of Virgo.

References and Notes

1. F. Zwicky, *Publ. Astron. Soc. Pac.* **63**, 61 (1951).
2. S. van den Bergh, *Publ. Astron. Soc. Pac.* **68**, 449 (1956).
3. H. Böhringer *et al.*, *Nature* **368**, 828 (1994).
4. P. R. Durrell, R. Ciardullo, J. J. Feldmeier, G. H. Jacoby, S. Sigurdsson, *Astrophys. J.* **570**, 119 (2002).
5. J. J. Feldmeier, R. Ciardullo, G. H. Jacoby, P. R. Durrell, *Astrophys. J.* **615**, 196 (2004).
6. J. C. Mihos, P. Harding, J. Feldmeier, H. Morrison, *Astrophys. J.* **631**, L41 (2005).
7. N. Castro-Rodriguéz *et al.*, *Astron. Astrophys.* **507**, 621 (2009).
8. R. E. White III, *Mon. Not. R. Astron. Soc.* **227**, 185 (1987).
9. J. C. Muzzio, *Publ. Astron. Soc. Pac.* **99**, 245 (1987).
10. M. J. West, P. Côté, C. Jones, W. Forman, R. O. Marzke, *Astrophys. J.* **453**, L77 (1995).
11. A. Jordán, M. J. West, P. Côté, R. O. Marzke, *Astron. J.* **125**, 1642 (2003).
12. A. Marín-Franch, A. Aparicio, *Astrophys. J.* **585**, 714 (2003).
13. N. Tamura *et al.*, *Mon. Not. R. Astron. Soc.* **373**, 601 (2006).
14. B. F. Williams *et al.*, *Astrophys. J.* **654**, 835 (2007).
15. B. Binggeli, A. Sandage, G. A. Tammann, *Astron. J.* **90**, 1681 (1985).
16. D. G. York *et al.*, *Astron. J.* **120**, 1579 (2000).
17. The magnitude limits for point sources in the SDSS catalog are 22.2 mag and 21.3 mag in the *g* and *i* bands, respectively, for 95% completeness.
18. J. K. Adelman-McCarthy *et al.*, *Astrophys. J.* **175** (suppl.), 297 (2008).
19. W. Harris, *Astrophys. J.* **703**, 939 (2009).
20. M. G. Lee *et al.*, *Astrophys. J.* **682**, 135 (2008).
21. We derived a relation between $(g - i)_0$ color and [Fe/H] using the SDSS photometry and [Fe/H] in the literature for the bright globular clusters M49, M60, and M87: $[\text{Fe/H}] = 3.48(g - i)_0 - 4.13$.
22. M. Jurić *et al.*, *Astrophys. J.* **673**, 864 (2008).
23. M. G. Lee, *J. Korean Astron. Soc.* **36**, 189 (2003).
24. E. W. Peng *et al.*, *Astrophys. J.* **639**, 95 (2006).
25. We adopted M87 as the center for deriving the radial profiles (*26*). First we removed globular clusters in galaxies by masking out a circular region with radius 5 R_{25} centered on each galaxy in the Virgo galaxy catalog (all 2095 galaxies except for M87) (*15*) (R_{25} represents a radius of a galaxy where the surface brightness $\mu_B = 25$ mag arc sec^{-2}). We kept M87 to see the radial profile for the central region of Virgo. Then we derived the radial profiles for the remaining globular clusters (IGC candidates and M87 globular clusters).
26. M. Doherty *et al.*, *Astron. Astrophys.* **502**, 771 (2009).
27. K. Bekki, H. Yahagi, *Mon. Not. R. Astron. Soc.* **372**, 1019 (2006).
28. P. Côté *et al.*, *Astrophys. J.* **559**, 828 (2001).
29. M. G. Lee *et al.*, *Astrophys. J.* **709**, 1083 (2010).
30. B. W. Miller, J. M. Lotz, *Astrophys. J.* **670**, 1074 (2007).
31. K. Bekki, H. Yahagi, M. Nagashima, D. A. Forbes, *Mon. Not. R. Astron. Soc.* **387**, 1131 (2008).
32. V. Coenda, H. Muriel, C. Donzelli, *Astrophys. J.* **700**, 1382 (2009).
33. J. F. Navarro, C. S. Frenk, S. D. M. White, *Astrophys. J.* **490**, 493 (1997).
34. D. E. McLaughlin, *Astrophys. J.* **512**, L9 (1999).

35. We thank D. Geisler, M. Im, and N. Hwang for their careful reading of the manuscript and useful comments and the anonymous referees for their comments, which improved the original manuscript significantly. This work was supported by a National Research Foundation of Korea grant funded by the Korean government (grant no. R01-2007-000-20336-0). Funding for the SDSS and SDSS-II has been provided by the Alfred P. Sloan Foundation, the Participating Institutions, NSF, the U.S. Department of Energy, NASA, the Japanese Monbukagakusho, the Max Planck Society, and the Higher Education Funding Council for England. The SDSS Web site is www.sdss.org. The SDSS is managed by the Astrophysical Research Consortium for the Participating Institutions. The Participating Institutions are the American Museum of Natural History, Astrophysical Institute Potsdam, University of Basel, University of Cambridge, Case Western Reserve University, University of Chicago, Drexel University, Fermilab, the Institute for Advanced Study, the Japan Participation Group, Johns Hopkins University, the Joint Institute for Nuclear Astrophysics, the Kavli Institute for Particle Astrophysics and Cosmology, the Korean Scientist Group, the Chinese Academy of Sciences, Los Alamos National Laboratory, the Max Planck Institute for Astronomy, the Max Planck Institute for Astrophysics, New Mexico State University, Ohio State University, University of Pittsburgh, University of Portsmouth, Princeton University, the U.S. Naval Observatory, and the University of Washington.

Supporting Online Material

www.sciencemag.org/cgi/content/full/science.1186496/DC1
Methods
Figs. S1 and S2
References

28 December 2009; accepted 2 March 2010
Published online 11 March 2010;
10.1126/science.1186496
Include this information when citing this paper.

Three-Dimensional Invisibility Cloak at Optical Wavelengths

Tolga Ergin,[1,2]*† Nicolas Stenger,[1,2]* Patrice Brenner,[2] John B. Pendry,[3] Martin Wegener[1,2,4]

We have designed and realized a three-dimensional invisibility-cloaking structure operating at optical wavelengths based on transformation optics. Our blueprint uses a woodpile photonic crystal with a tailored polymer filling fraction to hide a bump in a gold reflector. We fabricated structures and controls by direct laser writing and characterized them by simultaneous high–numerical-aperture, far-field optical microscopy and spectroscopy. A cloaking operation with a large bandwidth of unpolarized light from 1.4 to 2.7 micrometers in wavelength is demonstrated for viewing angles up to 60°.

As today's nanofabrication capabilities continue to improve, we are better able to address the inverse problem of electromagnetism with respect to what nanostructure will perform a requested functionality. In this regard, transformation optics (*1*–*14*) is a unique and intuitive scientific tool that allows for the mathematical mapping of desired distortions of space onto an actual distribution of optical material properties in normal Cartesian space. Tailored inhomogeneous metamaterials enable us to approximate these target distributions. Invisibility-cloaking structures (*1*–*16*) can serve as benchmark examples for the much broader ideas of transformation optics.

[1]Institut für Angewandte Physik, Karlsruhe Institute of Technology (KIT), D-76128 Karlsruhe, Germany. [2]DFG–Center for Functional Nanostructures, KIT, D-76128 Karlsruhe, Germany. [3]Blackett Laboratory, Imperial College London, London SW7 2AZ, UK. [4]Institut für Nanotechnologie, KIT, D-76021 Karlsruhe, Germany.

*These authors contributed equally to this work.
†To whom correspondence should be addressed. E-mail: tolga.ergin@kit.edu

So far, invisibility-cloaking experiments at microwave (*5*, *10*) and optical frequencies (*11*–*14*) have been performed exclusively in two-dimensional (2D) waveguide geometries. In other words, these structures are immediately visible from the third dimension. Cloaking works only in the plane; the viewing angle is effectively zero in one direction. Nevertheless, these structures have supported the validity of the concepts of both transformation optics and metamaterials.

We designed, fabricated, and characterized 3D invisibility-cloaking structures using tailored, dielectric face-centered–cubic (fcc) woodpile photonic crystals. We studied the behavior of these structures from wavelengths near the woodpile rod spacing (where the onset of diffraction of light leads to the Wood or Rayleigh anomaly in transmittance and reflectance) up to wavelengths much larger than this spacing (the effective-medium limit).

In the carpet-cloak geometry (*8*, *10*–*13*), a bump in a metallic mirror is hidden by adding a tailored refractive-index distribution on top. This distribution can be calculated using the rules of transformation optics (*8*, *10*). Though originally designed for two dimensions, it has been shown (by numerical rendering of photorealistic images via ray tracing) that the carpet-cloak concept should also work in a truly 3D setting and also for very large viewing angles (*17*). In our 3D blueprint (Fig. 1A), the bump is translationally invariant along the z direction and follows $y(x) = h\cos^2(\pi x/w)$ for $|x| \le w/2$ and zero otherwise. Here, $h = 1$ μm is the height of the bump, and $w = 13$ μm is its full width. For the quasi-conformal mapping of the cloak, we choose a width of 26 μm in the x direction and 10 μm in the y direction. This cloak is surrounded by a homogeneous woodpile structure, which is characterized in fig. S5 (*18*). Inside the cloak, the local effective refractive index is controlled via the volume filling fraction (f) of the polymer serving as constituent material for a usual woodpile photonic crystal (*19*, *20*). The diamond-symmetry woodpile geometry is chosen because it is expected to lead to nearly isotropic optical properties. The effective refractive index becomes $n = 1.52$ for $f = 1$ (bulk polymer) and $n = 1.00$ for $f = 0$ (air void). For intermediate values of f, we used the Massachusetts Institute of Technology Photonics-Bands package (*21*) to evaluate the effective local refractive index (Fig. 1B) on the basis of usual photonic-band–structure calculations. We found that the calculated 3D isofrequency contours are very nearly spherical in the long-wavelength limit (see inset in Fig. 1B).

Figure 2 shows the target refractive-index distributions obtained from the quasi-conformal mapping (*8*) and corresponding electron micrographs of some of our structures made by standard direct laser writing lithography (*20*, *22*).

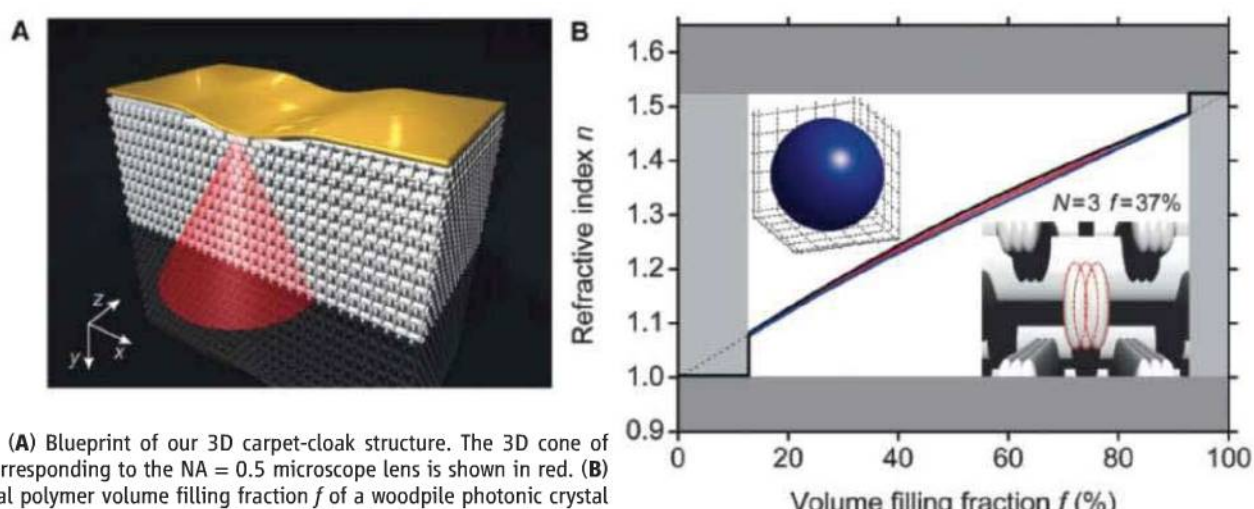

Fig. 1. (**A**) Blueprint of our 3D carpet-cloak structure. The 3D cone of light corresponding to the NA = 0.5 microscope lens is shown in red. (**B**) The local polymer volume filling fraction f of a woodpile photonic crystal composed of rods controls the effective local refractive index n. The black, red, and blue curves correspond to rod aspect ratios (= height/width) of 1, 2, and 3, respectively. The polymer needs to be connected, as do the air voids. These conditions impose lower and upper bounds on f, shown here for a rod aspect ratio of 2. The range of accessible values of n is restricted to be within 1.00 (air) and 1.52 (bulk polymer). The filling fraction is actually controlled by the number of voxels ($N \in \{0,3,4,5,6\}$) that each rod is composed of. The case of $N = 3$ is illustrated by the inset in the lower right corner. For this case and for a vacuum wavelength of 2.4 μm and a rod spacing of 0.8 μm, the upper left inset depicts the nearly spherical isofrequency surface in wave-vector space.

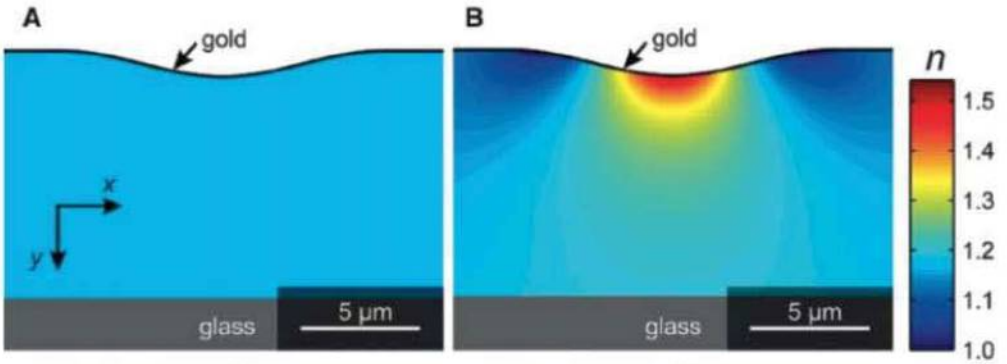

Fig. 2. Target refractive index (n) distributions (top) and oblique-view electron micrographs of fabricated structures after FIB milling (bottom). (**A**) A bump without a cloak. (**B**) A bump with a cloak. Note that the oblique view in the electron micrographs compresses the y direction.

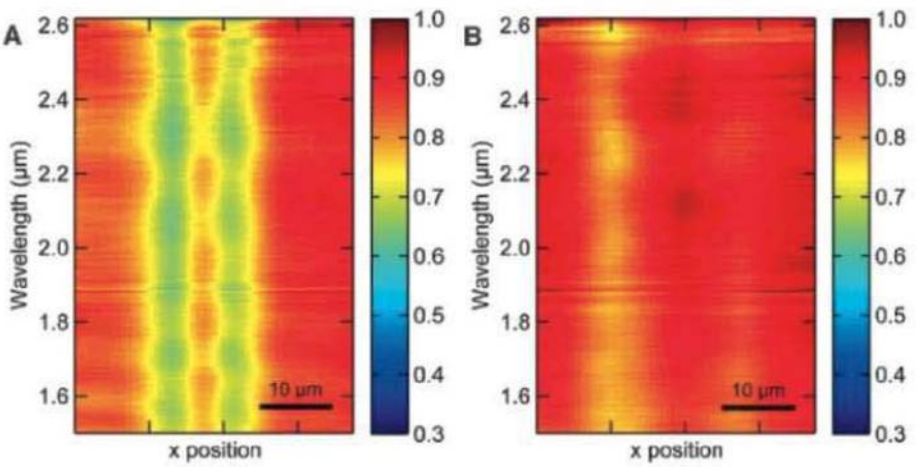

Fig. 3. Optical characterization of the 3D structures (see Fig. 2) with unpolarized light in bright-field mode. The image intensity is shown on a false-color scale. The horizontal axis is a cut through the middle of the structure along the x direction (compare to Fig. 1A); the vertical axis is wavelength. (**A**) A bump without a cloak. The bump is immediately visible. (**B**) Result for a bump with a cloak that approaches the expectation for an ideal cloak (constant intensity).

Fabrication details and sample dimensions are reported in the supporting online material (SOM) (*18*). To reveal their interiors, the structures are cut by means of focused ion beam (FIB) milling. This destructive measure is of utmost importance, as inspection of sample edges can be highly misleading due to the proximity effect.

For what wavelengths do we expect reasonable cloaking? On one hand, it is sometimes argued that the wavelength of light needs to be at least one order of magnitude larger than the period or lattice constant to truly reach the effective-medium limit. This very conservative estimate would lead to operation wavelengths larger than 8 μm for a = 800 nm or a wavelength of 11 μm for the fcc lattice constant of 1.131 μm. On the other hand, the most aggressive and optimistic approach is to argue that the effective-medium method can work up to the Wood anomaly. Once diffraction occurs, the periodic structure can no longer be considered a homogeneous effective material. For normal incidence, diffraction of light becomes possible if the material wavelength is equal to or smaller than the lattice constant. For a = 0.8 μm and a glass-substrate refractive index of n = 1.5, the Wood anomaly is expected to occur at a vacuum wavelength of 1.2 μm. These conservative and aggressive considerations obviously differ by about one order of magnitude in wavelength.

To evaluate the performance of our fabricated samples, we start by discussing the results obtained by bright-field optical microscopy and spectroscopy. The numerical aperture (NA) of the used microscope lens of NA = 0.5 is equivalent to a full opening angle of the cone of light of 60° (Fig. 1A). Therefore, light is propagating not only in the xy plane (which would merely be 2D), but also in oblique directions (3D). Details of the home-built setup are described in the SOM (*18*). Corresponding spatially and spectrally resolved normal-incidence data (normalized) show that the bump is immediately visible by two pronounced spatial minima (Fig. 3A) resulting from light that is reflected by the two slopes of the bump toward the sides and is not collected by the lens. The light reflected from the top of the bump (where the tangent is horizontal) leads to the narrow bright stripe in the middle. The spectral oscillations are Fabry-Perot fringes. Their free spectral range agrees well with the expectation based on the total 10-μm thickness of the woodpile structure. In presence of the cloak and bump (Fig. 3B), the visibility of the bump is strongly suppressed, whereas cloaking is not quite perfect. This recovery works well in the depicted wavelength range of 1.5 to 2.6 μm in Fig. 3 (data over a larger spectral interval are shown in fig. S1). For wavelengths shorter than ~1.2 μm, the image becomes dimmer. Furthermore and most important, in this regime, no recovery due to the presence of the cloak is observed. We interpret this short-wavelength dark region as being due to the Wood anomaly. Indeed, an ideal polymer woodpile can diffract as much as 50% of the incident light for wavelengths smaller than the Wood anomaly (see fig. S5). These levels explain the findings of our present work. For wavelengths shorter than that of the Wood anomaly, the light field can no longer effectively average over the nanostructure. Hence, the structure is not expected to act like a locally homogeneous dielectric, and no cloaking action is expected—consistent with our above observations. For the present conditions, the effective-medium approximation turns out to be much more forgiving than one might be tempted to believe at first sight.

Control samples with only (i) the high-index region or (ii) the two low-index regions are shown in figs. S2 and S3, respectively. For case (ii), the bump appears wider than in Fig. 3A. For case (i), cloaking is worse than for the complete cloak in Fig. 3B. These two observations show that one really needs the complete refractive-index profile

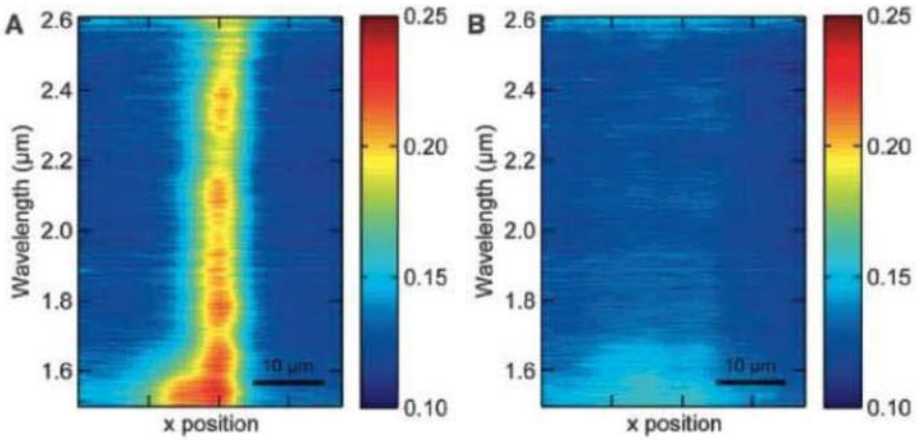

Fig. 4. Optical characterization of the 3D structures with unpolarized light as in Fig. 3, but in dark-field mode. **(A)** The bump is immediately visible by enhanced scattering. **(B)** Scattering is largely reduced with the cloak.

derived from the quasi-conformal mapping in transformation optics to obtain good invisibility-cloaking performance.

Finally, Fig. 4 depicts data taken in dark-field mode from 1.5- to 2.6-μm wavelengths (data over a larger spectral interval are shown in fig. S4). Here, the same sample as in Fig. 3 is tilted such that the optical axis lies within the *xy* plane and includes an angle of 35° with the *y* axis. As usual for the dark-field mode, the collected light results from scattering by the sample. These data are normalized with respect to a normal-incidence reflection spectrum taken on the gold film. The bump without cloak in Fig. 4A is immediately visible. We assign this finding to enhanced scattering from the illuminated side of the bump. The visibility is again drastically reduced for the case of bump with cloak in Fig. 4B.

References and Notes

1. J. B. Pendry, D. Schurig, D. R. Smith, *Science* **312**, 1780 (2006); published online 25 May 2006 (10.1126/science.1125907).
2. U. Leonhardt, *Science* **312**, 1777 (2006); published online 25 May 2006 (10.1126/science.1126493).
3. U. Leonhardt, T. G. Philbin, *New J. Phys.* **8**, 247 (2006).
4. U. Leonhardt, *New J. Phys.* **8**, 118 (2006).
5. D. Schurig *et al.*, *Science* **314**, 977 (2006); published online 19 October 2006 (10.1126/science.1133628).
6. W. Cai, U. K. Chettiar, A. V. Kildishev, V. M. Shalaev, *Nat. Photonics* **1**, 224 (2007).
7. V. M. Shalaev, *Science* **322**, 384 (2008).
8. J. Li, J. B. Pendry, *Phys. Rev. Lett.* **101**, 203901 (2008).
9. U. Leonhardt, T. Tyc, *Science* **323**, 110 (2009); published online 20 November 2008 (10.1126/science.1166332).
10. R. Liu *et al.*, *Science* **323**, 366 (2009).
11. J. Valentine, J. Li, T. Zentgraf, G. Bartal, X. Zhang, *Nat. Mater.* **8**, 568 (2009).
12. L. H. Gabrielli, J. Cardenas, C. B. Poitras, M. Lipson, *Nat. Photonics* **3**, 461 (2009).
13. J. H. Lee *et al.*, *Opt. Express* **17**, 12922 (2009).
14. I. I. Smolyaninov, V. N. Smolyaninova, A. V. Kildishev, V. M. Shalaev, *Phys. Rev. Lett.* **102**, 213901 (2009).
15. G. W. Milton, N. A. P. Nicorovici, *Proc. R. Soc. London Ser. A* **462**, 3027 (2006).
16. A. Alù, N. Engheta, *Phys. Rev. E* **72**, 016623 (2005).
17. J. C. Halimeh, T. Ergin, J. Mueller, N. Stenger, M. Wegener, *Opt. Express* **17**, 19328 (2009).
18. See supporting material available on *Science* Online.
19. K. M. Ho, C. T. Chan, C. M. Soukoulis, R. Biswas, M. Sigalas, *Solid State Commun.* **89**, 413 (1994).
20. M. Deubel *et al.*, *Nat. Mater.* **3**, 444 (2004).
21. S. G. Johnson, J. D. Joannopoulos, *Opt. Express* **8**, 173 (2001).
22. S. Kawata, H.-B. Sun, T. Tanaka, K. Takada, *Nature* **412**, 697 (2001).

23. We thank K. Busch, G. von Freymann, S. Linden, and M. Thiel for discussions and help regarding sample fabrication and photonic band-structure calculations. We acknowledge support from the Deutsche Forschungsgemeinschaft (DFG) and the State of Baden-Württemberg through the DFG–Center for Functional Nanostructures within subprojects A1.4 and A1.5. We also thank the Future and Emerging Technologies (FET) program within the Seventh Framework Programme for Research of the European Commission (FET open grant number 213390) for financial support of the project PHOME. The project METAMAT is supported by the Bundesministerium für Bildung und Forschung. The Ph.D. education of T.E. is embedded in the Karlsruhe School of Optics and Photonics (KSOP); N.S. is supported as a mentor in the KSOP.

Supporting Online Material

www.sciencemag.org/cgi/content/full/science.1186351/DC1
SOM Text
Figs. S1 to S5

23 December 2009; accepted 4 March 2010
Published online 18 March 2010;
10.1126/science.1186351
Include this information when citing this paper.

Dilithioplumbole: A Lead-Bearing Aromatic Cyclopentadienyl Analog

Masaichi Saito,[1]* Masafumi Sakaguchi,[1] Tomoyuki Tajima,[1] Kazuya Ishimura,[2] Shigeru Nagase,[2] Masahiko Hada[3]

Although the concept of aromaticity has long played an important role in carbon chemistry, it has been unclear how applicable the stabilizing framework is to the heaviest elements. Here we report the synthesis of dilithiotetraphenylplumbole by reduction of hexaphenylplumbole. X-ray crystallography revealed a planar structure with no alternation of carbon–carbon bond lengths in the five-membered ring core. Nuclear magnetic resonance spectra and relativistic theoretical calculations show considerable aromatic character in the molecule, thus extending aromaticity to carbon's heaviest congener.

Aromaticity has been a fundamental chemical concept since the discovery of benzene in 1825, and aromatic compounds have long played important roles in all fields of chemistry. The skeletons of most aromatic compounds consist of C atoms, and occasionally N, O, and the third-row elements S and more rarely P. To determine whether the heavier group-14 elements could sustain aromaticity, Si and Ge analogs of carbocyclic aromatic compounds such as benzene, naphthalene (*1*, *2*), cyclopentadienyl anion (*3*–*7*), cyclobutadiene dianion (*8*), and cyclopropenyl cation (*9*–*12*) have recently been synthesized, in which one ring C is replaced by the congener. Most of these have considerable aromatic character, even though some of them have been judged nonaromatic because of their nonplanar structures. Most recently, dilithiostannole (*13*) and 2-stannanaphthalene (*14*) have been synthesized and concluded to be aromatic compounds. Therefore, the concept of aromaticity has been expanded to Sn-containing carbocyclic systems. However, there has been no experimental evidence of whether the concept of aromaticity can be expanded to Pb-containing C rings, even though theoretical calculations predicted that dilithioplumbole would have considerable aromatic character (*15*, *16*). We report here the synthesis of dilithiotetraphenylplumbole, thus expanding the concept of aromaticity to C cycles incorporating the heaviest group-14 element (*17*).

The synthesis of dilithiotetraphenylplumbole **1** was accomplished by the reduction of hexa-

[1]Department of Chemistry, Graduate School of Science and Engineering, Saitama University, Shimo-okubo, Sakura-ku, Saitama-city, Saitama, 338-8570 Japan. [2]Department of Theoretical Molecular and Computational Science, Institute for Molecular Science, Myodaiji, Okazaki, Aichi, 444-8585 Japan. [3]Department of Chemistry, Graduate School of Science and Engineering, Tokyo Metropolitan University, Minami-osawa, Hachiohji, Tokyo, 192-0397 Japan.

*To whom correspondence should be addressed. E-mail: masaichi@chem.saitama-u.ac.jp

phenylplumbole **2** (*18*) with lithium in the presence of a catalytic amount of naphthalene in ether at −78°C; a byproduct, phenyllithium, was also formed (*19*). After treatment of the reaction mixture with dimethoxyethane (DME), the phenyllithium fully decomposed, and dilithioplumbole **1** was isolated in 78% yield (Fig. 1A). The molecular structure of dilithioplumbole **1** was established by x-ray crystallographic analysis (Fig. 1B). One Li atom is coordinated by the plumbole ring in an η^5 fashion, whereas the other Li atom is coordinated by three DME molecules. Because the distance between the Pb and DME-solvated Li atoms is more than 10 Å, the solvated Li atom has no interaction with the plumbole ring. The plumbole ring is planar with a 539.8° sum of the internal angles. The C–C distances within the ring are almost equal [1.410(6), 1.412(6), and 1.431(6) Å], as was observed in the aromatic dilithiostannole, suggesting that dilithioplumbole **1** has considerable aromatic character. In contrast, the C–C bonds of the starting plumbole **2** differ [1.345(6), 1.354(5), and 1.522(5) Å] (*18*). The Pb–C bonds of **1** lengthen to 2.242(4) and 2.265(5) Å, compared with those of **2** [2.202(4) and 2.211(4) Å], resulting in a smaller C–Pb–C angle [75.97(17)°] than in **2** [82.41(14)°].

In the ^{13}C nuclear magnetic resonance (NMR) spectrum of **1**, a signal assignable to the α C was observed at 228 parts per million (ppm), which is a substantial downfield shift as compared with the corresponding resonance in **2** (154 ppm); whereas the β C of **1** resonated at 147 ppm, a slight upfield shift relative to **2** (153 ppm). This trend was also observed in the cases of other aromatic group-14 dilithiometalloles (*13*). In contrast, the resonance of the β C of lithiotriphenylplumbane, which is not aromatic, shifts downfield relative to the tetraphenylplumbane precursor (*20*). This NMR analysis also suggests that dilithioplumbole **1** has considerable aromatic character. Although the upfield resonance in the ^7Li NMR spectrum is diagnostic of the aromatic ring current, the ^7Li NMR signal of **1** was observed at −1.11 ppm, which is in the range of normal organolithium compounds, suggesting that rapid exchange of η^5-coordinated and solvent-coordinated Li cations is occurring in solution. The ^{207}Pb NMR signal of **1** was observed at 1712.8 ppm, remarkably downfield of the signal in the spectrum of **2** (−24.5 ppm) (*18*). The corresponding shifts in the ^{207}Pb NMR spectra of tetraphenylplumbane and lithiotriphenylplumbane are −179 and 1060.1 ppm, respectively (*20*). The downfield ^{207}Pb shift of **1** relative to lithiotriphenylplumbane is probably due to greater anionic character of the lead atom of **1** or some contribution of plumbylene character. A similar contribution of divalent character in the dilithiometalloles has already been proposed (*13*, *21*).

To gain more insight into the structure and electronic states of dilithioplumbole **1**, theoretical calculations were carried out (*22*). Because the x-ray structural analysis of **1** revealed that one of the Li atoms is coordinated by the plumbole ring and the other is separated from the ring, geometric optimization of the dilithioplumbole **3** was carried out at the B3LYP (*23*, *24*) level with the second-order Douglas-Kroll-Hess scalar relativistic term (*25*–*27*) (Fig. 2). The ANO-RCC basis set (*28*) was adopted for Pb. The [6*s*6*p*5*d*1*f*] functions were picked out from the original [11*s*10*p*9*d*8*f*4*g*] functions, and each valence-contracted function was then split into three functions of triple-zeta quality. Furthermore, the functions for 1*s* and 2*p* orbitals were doubly uncontracted to describe the relativistic correction of the inner core region. A polarization *d* function was not added because the exponent was close to that of the uncontracted function described above. The final contraction form was [9*s*9*p*7*d*3*f*]. The 6-311G(2d) basis set (*29*) was used for Li atoms and for C and H atoms of the five-membered ring and those connected to the ring and the Li atoms, whereas the 6-31G basis set (*30*) was used for other C and H atoms. The optimized geometry of **3** was highly consistent with the x-ray structure of **1**. The Pb–C(α), C(α)–C(β), and C(β)–C(β) bond distances were calculated to be (2.292, 2.304), (1,411, 1,429), and 1.452 Å, respectively. The Pb–C(α) bonds of **1** were elongated as compared with those of **2**, even though aromatization usually results in elongation and shortening of the original double and single bonds, respectively. To understand this contradiction, geometric optimization of the model compounds C_4H_6M, C_4H_4M, and $C_4H_4M^{2-}$ (M = Si, Ge, Sn,

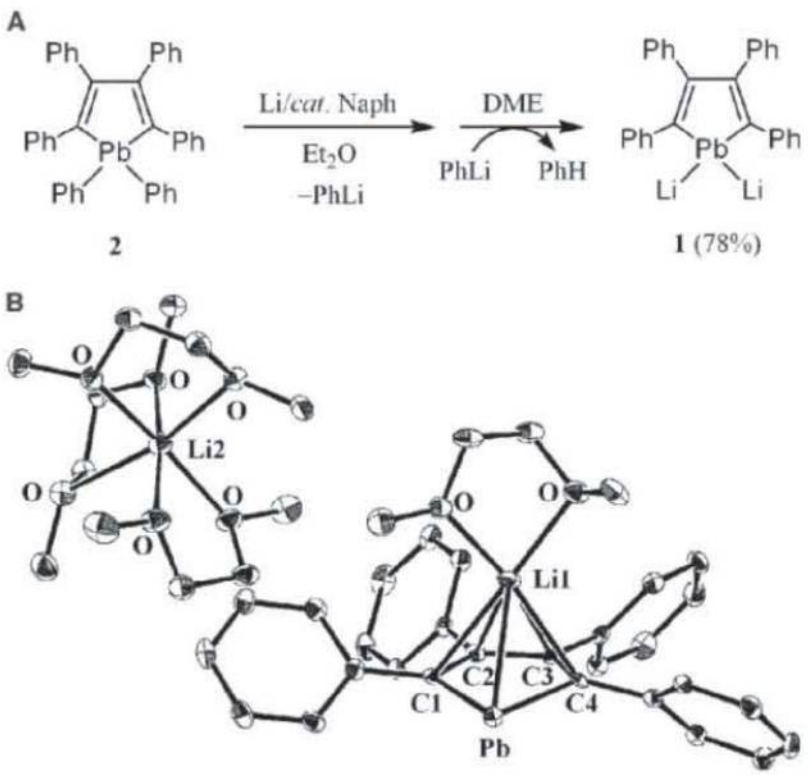

Fig. 1. (**A**) Preparation of dilithiotetraphenylplumbole **1**. (**B**) ORTEP drawing of dilithiotetraphenylplumbole **1** with thermal ellipsoids plots drawn at 40% probability for non-H atoms. All H atoms were omitted for clarity. Selected bond lengths (angstroms) and angles (degrees) are as follows: Pb–C1, 2.242(4); Pb–C4, 2.265(5); C1–C2, 1.410(6); C2–C3, 1.431(6); C3–C4, 1.412(6); and C1–Pb–C4, 75.99(17)

Fig. 2. Comparison of the structures of **1**·4DME and **3**.

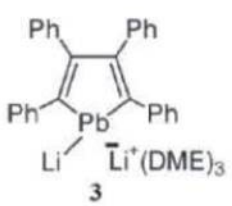

	Crystal structure of **1**·4DME	Calculation of **3**
Pb–C(α)	2.242(4), 2.265(5) Å	2.292, 2.304 Å
C(α)–C(β)	1.410(6), 1.412(6) Å	1.411, 1.429 Å
C(β)–C(β)	1.431(6) Å	1.452 Å

or Pb) was carried out at the B3LYP level using the LanL2DZ basis set (*31*, *32*) (Fig. 3). In the transition from C_4H_6Pb to C_4H_4Pb, which has a divalent Pb atom, the Pb–C(α) bond lengthened from 2.175 to 2.256 Å; whereas in the transition from C_4H_4Pb to $C_4H_4Pb^{2-}$, the corresponding bond shortened to 2.240 Å [2.242(4) and 2.265(5) Å are the two Pb–C(α) bond lengths in **1**]. The elongation of the Pb–C(α) bond from C_4H_6Pb to C_4H_4Pb can reasonably be attributed to an increase in the *p* character of the Pb–C(α) bond caused by a lone pair on the Pb atom having more *s* character than the Pb–H bonds of C_4H_6Pb. In contrast, the shortening of the Pb–C(α) bond from C_4H_4Pb to $C_4H_4Pb^{2-}$ can be attributed to aromatic delocalization of the negative charges. This trend was also observed in all of the heavier group-14 metalloles, even though the Si–C(α) bond of C_4H_6Si is comparable to that of $C_4H_4Si^{2-}$ (Fig. 3).

NMR chemical shifts of dilithioplumbole **1** were also calculated on the basis of the x-ray structure. Relativistic effects were found to be essential for accurate calculations. When they were included, $^{13}C(\alpha)$ and ^{207}Pb chemical shifts of 220.7 and 1655.9 ppm were calculated, which were highly consistent with the experimental values (228.33 and 1712.8 ppm, respectively). Under nonrelativistic conditions, the calculations yielded the considerably less accurate shifts 269.0 and 38110.1 ppm. The Li nucleus above the aromatic plumbole ring was calculated to resonate about 4 ppm higher than the Li nucleus coordinated by three DME molecules. The experimental ^{7}Li NMR chemical shift of −1.11 ppm was therefore suggestive of rapid exchange of the two inequivalent Li cations in solution. The considerably negative NICS(1) (*33*) value of a free plumbole anion was calculated to be −6.28 ppm, suggesting that dilithioplumbole **1** is also aromatic, as the other group-14 dilithiometalloles are.

Dilithioplumbole **1** reacted with bromomesitylene to give lithiomesityltetraphenylplumbole **4** in 25% yield (Fig. 4A) (*19*). The ^{207}Pb NMR signal of **4** was observed at 1095.7 ppm, comparable to that of lithiotriphenylplumbane (1060.1 ppm) (*10*). The structure of lithiomesitylplumbole **4** was established by x-ray diffraction analysis (Fig. 4B) after crystallization with 12-crown-4. The Li atom is coordinated by two molecules of crown ether, and the distance between the Li and the Pb atoms of more than 6 Å suggests no interaction between them. The C–C bonds within the plumbole ring of **4** differ [1.347(8), 1.498(8), and 1.354(8) Å]. The pyramidalization of the Pb center is clearly evident from the angle between the plumbole ring and the Pb–C(mesityl) bond of 103.4°. These geometric features clearly show that lithiomesitylplumbole **4** is nonaromatic, even though the plumbole ring is planar with a sum of internal angles of 539.8°.

The present findings show decisively that 2*p*(C) and 6*p*(Pb) orbitals can overlap sufficiently to create aromatic molecules. We believe that the present dilithioplumbole highlights the future possibility of introducing heavy elements including Pb into a broader range of C frameworks, providing compounds with structures and properties that are applicable to catalytic and materials chemistry.

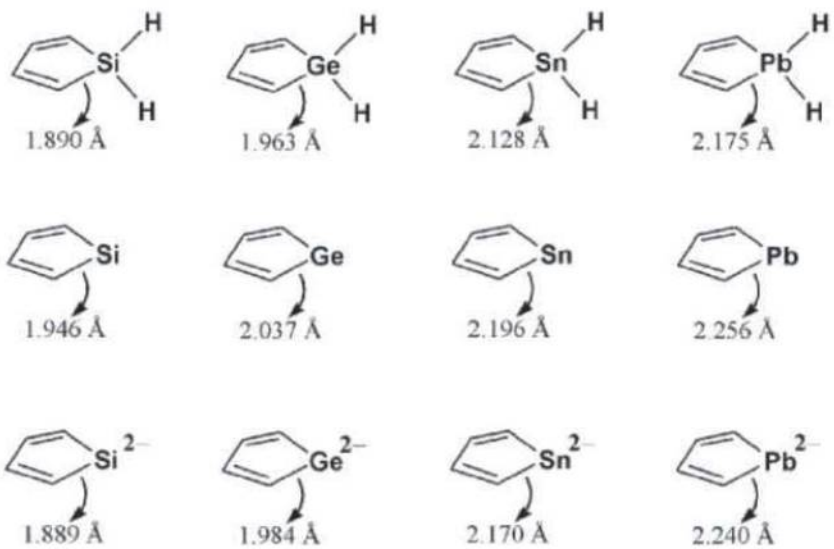

Fig. 3. Comparison of the calculated M–C(α) bond lengths in group-14 metalloles.

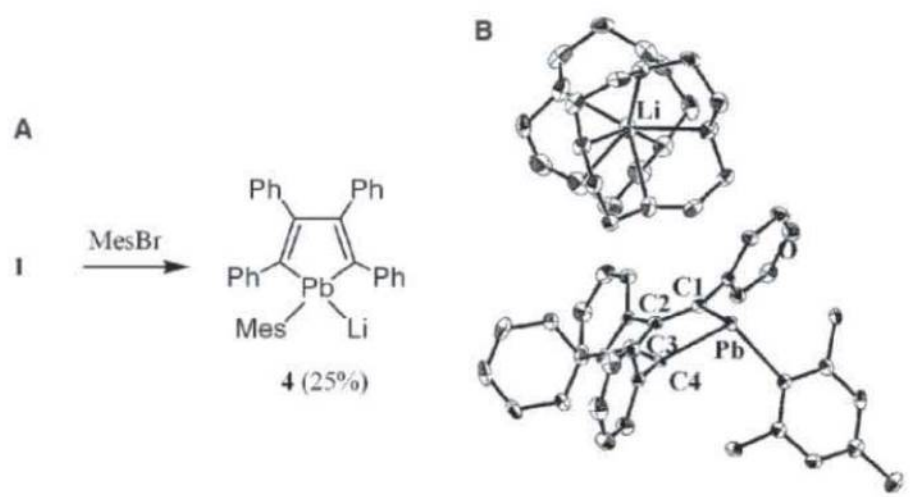

Fig. 4. (**A**) Reaction of **1** with bromomesitylene to afford lithiomesitylplumbole **4**. (**B**) ORTEP drawing of lithiomesitylplumbole **4** with thermal ellipsoids plots drawn at 40% probability for non-H atoms. All H atoms were omitted for clarity. Selected bond lengths (angstroms) and angles (degrees) are as follows: Pb–C1, 2.320(5); Pb–C4, 2.306(5); C1–C2, 1.354(8); C2–C3, 1.498(8); C3–C4, 1.347(8); and C1–Pb–C4, 75.7(2).

References and Notes

1. N. Tokitoh, *Acc. Chem. Res.* **37**, 86 (2004).
2. N. Tokitoh, *Bull. Chem. Soc. Jpn.* **77**, 429 (2004).
3. J. Dubac, C. Guérin, P. Meunier, in *The Chemistry of Organic Silicon Compounds*, Z. Rappoport, Y. Apeloig, Eds. (Wiley, Chichester, UK, 1998), pp. 1961–2036.
4. M. Saito, M. Yoshioka, *Coord. Chem. Rev.* **249**, 765 (2005).
5. V. Y. Lee, A. Sekiguchi, *Angew. Chem. Int. Ed.* **46**, 6596 (2007).
6. Most recently, heavier congeners of the cyclopentadienyl anion incorporating more than two heavy group-14 atoms have been found to be aromatic (*7*, *34*).
7. H. Yasuda, V. Y. Lee, A. Sekiguchi, *J. Am. Chem. Soc.* **131**, 6352 (2009).
8. V. Y. Lee, K. Takanashi, T. Matsuno, M. Ichinohe, A. Sekiguchi, *J. Am. Chem. Soc.* **126**, 4758 (2004).
9. A. Sekiguchi, M. Tsukamoto, M. Ichinohe, *Science* **275**, 60 (1997).
10. M. Ichinohe, M. Igarashi, K. Sanuki, A. Sekiguchi, *J. Am. Chem. Soc.* **127**, 9978 (2005).
11. M. Igarashi, M. Ichinohe, A. Sekiguchi, *J. Am. Chem. Soc.* **129**, 12660 (2007).
12. X. W. Li, W. T. Pennington, G. H. Robinson, *J. Am. Chem. Soc.* **117**, 7578 (1995).
13. M. Saito, R. Haga, M. Yoshioka, K. Ishimura, S. Nagase, *Angew. Chem. Int. Ed.* **44**, 6553 (2005).
14. Y. Mizuhata, T. Sasamori, N. Takeda, N. Tokitoh, *J. Am. Chem. Soc.* **128**, 1050 (2006).
15. B. Goldfuss, P. R. Schleyer, F. Hampel, *Organometallics* **15**, 1755 (1996).
16. B. Goldfuss, P. R. Schleyer, *Organometallics* **16**, 1543 (1997).
17. Although the synthesis of 4-*t*-butylbismabenzene, which contains the heaviest stable element bismuth, was reported, the compound was stable for several hours at 0°C only in solution, and the solid-state structure was not reported (*35*).

18. M. Saito, M. Sakaguchi, T. Tajima, K. Ishimura, S. Nagase, *Phosphorus Sulfur Silicon Relat. Elem.* 10.1080/10426501003773399 (2010).
19. Methods are detailed in supporting material available on *Science* Online.
20. U. Edlund, T. Lejon, P. Pyykkö, T. K. Venkatachalam, E. Buncel, *J. Am. Chem. Soc.* **109**, 5982 (1987).
21. J.-H. Hong, P. Boudjouk, S. Castellino, *Organometallics* **13**, 3387 (1994).
22. All calculations were performed with Gaussian 03 revision D.02 (*36*).
23. A. D. Becke, *J. Chem. Phys.* **98**, 5648 (1993).
24. C. Lee, W. Yang, R. G. Parr, *Phys. Rev. B* **37**, 785 (1988).
25. M. Douglas, N. M. Kroll, *Ann. Phys.* **82**, 89 (1974).
26. B. A. Hess, *Phys. Rev. A* **32**, 756 (1985).
27. B. A. Hess, *Phys. Rev. A* **33**, 3742 (1986).
28. B. O. Roos, R. Lindh, P.-Å. Malmqvist, V. Veryazov, P.-O. Widmark, *J. Phys. Chem. A* **108**, 2851 (2004).
29. R. Krishnan, J. S. Binkley, R. Seeger, J. A. Pople, *J. Chem. Phys.* **72**, 650 (1980).
30. W. J. Hehre, R. Ditchfield, J. A. Pople, *J. Chem. Phys.* **56**, 2257 (1972).
31. W. R. Wadt, P. J. Hay, *J. Chem. Phys.* **82**, 284 (1985).
32. T. H. Dunning Jr., P. J. Hay, *Methods of Electronic Structure Theory*, Vol. 2, H. F. Schaefer III, Ed. (Plenum, New York, 1977).
33. The NICS, which is an abbreviation of nucleus-independent chemical shifts, was first proposed as a probe of aromaticity on the basis of magnetic criteria (*37*) and is now generally used to characterize the aromaticity of compounds (*38*).
34. V. Y. Lee, R. Kato, M. Ichinohe, A. Sekiguchi, *J. Am. Chem. Soc.* **127**, 13142 (2005).
35. A. J. Ashe III, T. R. Diephouse, M. Y. El-Sheikh, *J. Am. Chem. Soc.* **104**, 5693 (1982).
36. M. J. Frisch *et al.*, Gaussian 03 revision D.02 (Gaussian, Wallingford, CT, 2004).
37. P. R. Schleyer, C. Maerker, A. Dransfeld, H. Jiao, N. J. R. E. Hommes, *J. Am. Chem. Soc.* **118**, 6317 (1996).
38. Z. Chen, C. S. Wannere, C. Corminboeuf, R. Puchta, P. v. R. Schleyer, *Chem. Rev.* **105**, 3842 (2005).

39. This work was partially supported by Grants-in-Aid for Scientific Research (no. 20038010 to M.S., no. 18066017 to S.N., and no. 19029037 to M.H.) in Priority Areas "Molecular Theory for Real Systems" and by the Nanotechnology Support Project from the Ministry of Education, Culture, Sports, Science, and Technology of Japan. M.S. acknowledges a research grant from Toray Science Foundation. Deposition nos. CCDC-750458 and 750459 contain the supplementary crystallographic data for compounds **1** and **4**, respectively. These data can be obtained free of charge at www.ccdc.cam.ac.uk/conts/retrieving.html (or from the Cambridge Crystallographic Data Centre, 12 Union Road, Cambridge CB2 1EZ, UK; fax, 44-1223-336-033; e-mail, deposit@ccdc.cam.ac.uk).

Supporting Online Material

www.sciencemag.org/cgi/content/full/328/5976/339/DC1
Methods
Reference

21 October 2009; accepted 11 December 2009
10.1126/science.1183648

A Fast Soluble Carbon-Free Molecular Water Oxidation Catalyst Based on Abundant Metals

Qiushi Yin,[1] Jeffrey Miles Tan,[1] Claire Besson,[1,2] Yurii V. Geletii,[1] Djamaladdin G. Musaev,[1] Aleksey E. Kuznetsov,[1] Zhen Luo,[1] Ken I. Hardcastle,[1] Craig L. Hill[1]*

Traditional homogeneous water oxidation catalysts are plagued by instability under the reaction conditions. We report that the complex $[Co_4(H_2O)_2(PW_9O_{34})_2]^{10-}$, comprising a Co_4O_4 core stabilized by oxidatively resistant polytungstate ligands, is a hydrolytically and oxidatively stable homogeneous water oxidation catalyst that self-assembles in water from salts of earth-abundant elements (Co, W, and P). With $[Ru(bpy)_3]^{3+}$ (bpy is 2,2′-bipyridine) as the oxidant, we observe catalytic turnover frequencies for O_2 production $\geq 5\ s^{-1}$ at pH = 8. The rate's pH sensitivity reflects the pH dependence of the four-electron O_2-H_2O couple. Extensive spectroscopic, electrochemical, and inhibition studies firmly indicate that $[Co_4(H_2O)_2(PW_9O_{34})_2]^{10-}$ is stable under catalytic turnover conditions: Neither hydrated cobalt ions nor cobalt hydroxide/oxide particles form in situ.

Producing renewable clean energy has become one of the most profound challenges of the 21st century (*1*). Most of the world's current energy supplies come from sunlight converted to chemical energy by plant photosynthesis. A central thrust of the current energy research focuses on artificial photosynthesis (*2*, *3*). Despite the intense global efforts to develop viable abiological water splitting systems, breakthroughs are needed in selectivity, speed, and stability of all three operational units: the sensitizer for light absorption and catalysts for water reduction and oxidation. Developing a viable water oxidation catalyst (WOC) has proven particularly challenging (*4*). An effective WOC must be fast; capable of water oxidation at a potential minimally above the thermodynamic value ($H_2O \rightarrow O_2 + 4H^+ + 4e^-$; $1.229 - 0.059 \times$ pH at 25°C); and, critically, stable to air, water, and heat (oxidative, hydrolytic, and thermal stability). There are many research groups working on heterogeneous and homogeneous WOCs. Heterogeneous WOCs generally have the advantages of low cost, ease of interface with electrode systems, and, critically, oxidative stability; but they are harder to study and thus optimize than homogeneous catalysts, and they tend to deactivate by surface poisoning or aggregation (*5*–*9*). Recently, Kanan and Nocera reported a robust heterogeneous WOC based on earth-abundant cobalt and phosphate (*8*), after earlier work by Creutz and Sutin (*10*), and demonstrated self-assembly under turnover conditions, a key to self-repair (*11*). More recently, the groups of Mallouk (*9*) and Frei (*12*) reported high catalytic water oxidation rates by using colloidal $IrO_2 \cdot nH_2O$ particles and Co_3O_4 (spinel) particles, respectively. In contrast, homogeneous WOCs are more amenable to spectroscopic, crystallographic, physicochemical, and computational investigation and thus more readily optimized. In addition, each individual molecule of a homogeneous catalyst is, in principle, capable of doing chemistry (a cost issue when precious metals such as Ru are involved). However, nearly all homogeneous catalysts contain organic ligands that are thermodynamically unstable with respect to oxidative degradation. As a result, all homogenous WOCs with organic ligands reported to date are oxidatively deactivated (*13*–*23*). A

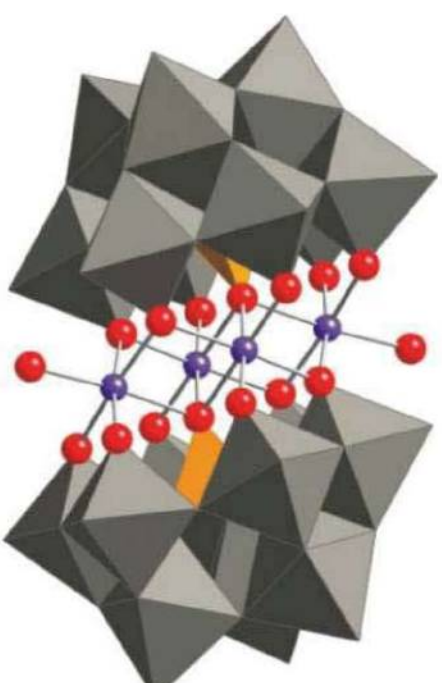

Fig. 1. X-ray structure of $\mathbf{Na_{10}}$-**1** in combined polyhedral ($[PW_9O_{34}]$ ligands) and ball-and-stick (Co_4O_{16} core) notation. Co atoms are purple; O/OH_2(terminal), red; PO_4, orange tetrahedra; and WO_6, gray octahedra. Hydrogen atoms, water molecules, and sodium cations are omitted for clarity.

[1]Department of Chemistry, Emory University, Atlanta, GA 30322, USA. [2]Institut Parisien de Chimie Moléculaire, UMR CNRS 7201, Université Pierre et Marie Curie Univ. Paris 06, Case 42, 4 place Jussieu, 75005 Paris, France.

*To whom correspondence should be addressed. E-mail: chill@emory.edu

general goal is to realize WOCs that have the stability, durability, and accessibility of heterogeneous metal oxide catalysts with the activity, selectivity, and tunability of homogeneous catalysts. To this end, a homogeneous polyoxometalate (POM) WOC with oxidatively resistant polytungstate units multiply ligating a Ru_4O_4 core was recently reported (*24*–*26*). This WOC is as fast as reported homogeneous catalysts containing organic ligands, but Ru is neither abundant nor inexpensive and thus very likely prohibitive for use on a realistic scale. Therefore, discovery of a stable and fast homogenous WOC, without organic ligands, based on earth-abundant elements would be highly useful.

We report here a homogeneous catalyst, B-type $[Co_4(H_2O)_2(\alpha\text{-}PW_9O_{34})_2]^{10-}$ (**1**), that is free of carbon-based ligands (Fig. 1). It is easily prepared from readily available salts and oxides of earth-abundant elements (Co, W, and P). To explore POM-stabilized multi–Co-oxide clusters as WOCs, we used the relatively strong and stable stoichiometric oxidant, tris(2,2′-bipyridyl)triperchlororuthenium(III), (henceforth $[Ru(bpy)_3]^{3+}$; Eq. 1). The oxygen yield was monitored with gas chromatography by withdrawing gas samples from the reaction vessel headspace (*24*, *27*).

$$4[Ru(bpy)_3]^{3+} + 2\ H_2O \xrightarrow{WOC} 4\ [Ru(bpy)_3]^{2+} + 4\ H^+ + O_2 \quad (1)$$

We examined eight cobalt-containing POMs as WOCs (Table 1). Only $[Co_4(H_2O)_2(\alpha\text{-}PW_9O_{34})_2]^{10-}$ (**1**) was active. Cyclic voltammetry of 1 mM **1** shows a large catalytic current with a low overpotential for the water oxidation (Fig. 2A). This characteristic feature is not observed for complexes **2** through **8**. Close examination of the studied complexes reveals that all cobalt-containing POMs have different cobalt-core structures than **1**, with the exception of $[Co_4(H_2O)_2(P_2W_{15}O_{56})_2]^{16-}$ (**2**) (fig. S11). However, **2** was synthesized and crystallized at a much lower pH than **1** and is also known to be unstable under our catalytic conditions (pH = 7.5 to 8.0) (*28*). The total yield of oxygen is always less than 100% based on oxidant because of competing bipyridyl ligand oxidation (*10*). A first-order hyperbolic fit of the O_2 yield to the concentration of **1** is consistent with this description (fig. S1).

The turnover frequency (TOF) for **1** (Eq. 1) at pH = 8 was >5 s^{-1}, which compares well to the 0.9 s^{-1} observed for the [Cp*(Cl)Ir(ppy)] (where Cp* is 1,2,3,4,5-pentamethylcyclopentadiene and ppy is 2-phenylpyridine) WOC recently reported by Brudvig, Crabtree, and coworkers (*22*). The rate of water oxidation catalyzed by **1** is highly sensitive to pH. Increasing pH from the initial value of 7.5 to 8.0 (sodium phosphate buffer, NaPi) decreased the reaction time from 270 s to 90 s (respective final pH values after reaction are 7.3 and 7.5). The reaction was faster still in a solution with a higher buffer capacity at pH = 8.0 (a mixture of 30 mM NaPi and 30 mM sodium borate buffer; final pH > 7.9). With 1.2×10^{-4} mM **1** and 2.4 mM $[Ru(bpy)_3]^{3+}$, we obtained a turnover number (TON, $n_{O2}/n_{catalyst}$) ~ 10^3 in under 3 min. Accordingly, the apparent TON also increases sharply at higher pH because of the faster rate of water oxidation. TON is limited by the concentration of the $[Ru(bpy)_3]^{3+}$, which, in turn, is limited by the formation of an insoluble adduct between **1** and $[Ru(bpy)_3]^{3+/2+}$.

As noted above, the cobalt-containing POM, **1**, is undemanding to synthesize. We prepared it in over 35% yield in a one-pot equilibration synthesis, as first reported by Weakley *et al.*, that entailed simply heating Co^{2+}, phosphate, and tungstate in a 2:1:9 ratio in water at reflux (*29*). This synthesis of **1** defines a mechanism for self-repair, a strategy used in our previous work (*11*) and in the recent work by Kanan and Nocera on their heterogeneous cobalt phosphate catalyst (*8*). Homogeneous catalysts like **1** use discrete molecules in solution for turnover as opposed to only select sites on the surface of most heterogeneous catalysts. This is a likely

Table 1. Catalytic water oxidation by soluble POM systems. Reactions were run in 30 mM NaPi buffer, initial pH = 8.0, 1.5 mM $[Ru(bpy)_3](ClO_4)_3$, and ambient temperature. bpy is 2,2′-bipyridine, and O_2 yield = $\frac{4n_{O_2}}{n_{Ru(bpy)_3}} \cdot 100$.

Complex	Complex concentration (mM)	bpy (mM)	TON	O_2 yield (%)
$[Co_4(H_2O)_2(PW_9O_{34})_2]^{10-}$ (**1**)	0.0032	0.06	75	64
$[Co_4(H_2O)_2(P_2W_{15}O_{56})_2]^{10-}$ (**2**)	0.0064	0.06	0	0
$[Co(H_2O)PW_{11}O_{39}]^{5-}$ (**3**)	0.0064	0.06	0	0
$[Co(H_2O)SiW_{11}O_{39}]^{6-}$ (**4**)	0.0064	0.06	0	0
$[Co_3(H_2O)_3(PW_9O_{34})_2]^{12-}$ (**5**)	0.0064	0.06	0	0
$[Co_3(H_2O)_3SiW_9O_{37}]^{10-}$ (**6**)	0.0064	0.06	0	0
$[WCo_3(H_2O)_2(CoW_9O_{34})_2]^{12-}$ (**7**)	0.0064	0.06	0	0
$[Co_7(H_2O)_2(OH)_2P_2W_{25}O_{94}]^{16-}$ (**8**)	0.0064	0.06	0	0

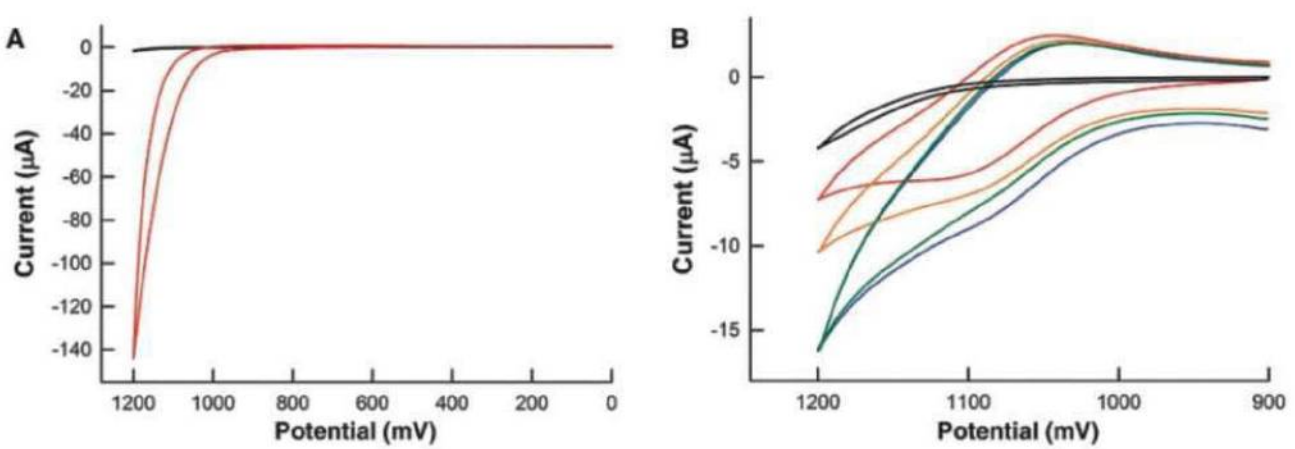

Fig. 2. (**A**) Cyclic voltammogram (CV) of 50 mM sodium phosphate solution at pH = 8 without **1** (black) and with 1 mM **1** (red). (**B**) CV of aqueous 0.857 mM $[Ru(bpy)_3]^{2+}$ alone (red), 3.2 μM **1** alone (black), 0.857 mM $[Ru(bpy)_3]^{2+}$ combined with 3.2 μM **1** (green) or 1.6 μM **1** (yellow), and a postreaction solution in which initially dissolved 0.857 mM $[Ru(bpy)_3]^{3+}$ was reduced through water oxidation catalyzed by 3.2 μM **1** (blue). The series of CVs for 0 μM **1** (red), 1.6 μM **1** (yellow), and 3.2 μM **1** (green) added to 0.857 mM $[Ru(bpy)_3]^{2+}$ shows increasing anodic current and decreasing cathodic current, demonstrating the correlation between increasing catalytic current and the concentration of **1**. Conditions are as follows: 60 mM NaPi, pH = 8, scan rate 25 mV s^{-1}; potentials measured and reported versus an Ag/AgCl reference electrode.

factor in a far higher observed efficiency of catalytic water oxidation per cobalt atom in the case of **1** relative to the heterogeneous cobalt phosphate catalyst.

Aqueous cobalt ions and cobalt hydroxide/oxides that form in situ from the former are both known to be WOCs (*6*, *8*, *10*). Thus, we now describe seven lines of experimental evidence that **1** is a stable molecular WOC under turnover conditions and does not form either aqueous cobalt ions or cobalt hydroxide/oxide. The first two arguments are that no changes are observed in either the ultraviolet and visible absorption (UV-Vis) or the ^{31}P nuclear magnetic resonance (NMR) spectra of a solution of **1** at pH = 8 (the pH in the catalytic experiments) over a 1-month period (figs. S3 and S4C). UV-Vis and ^{31}P NMR spectra also both establish that **1** is stable for at least 1 day within the pH range of 3.5 to 9 (fig. S4).

The third experimental probe of the stability of **1** involved selective catalyst poisoning experiments using 2,2′-bipyridine (bpy) as an inhibitor (fig. S2). Bpy reacts with $Co(aq)^{2+}$ to form $[Co(bpy)_3]^{2+}$ (*30*), inhibiting all water oxidation activity. In contrast, the addition of the same molar excess of bpy to solutions of **1** has a relatively minor effect on the apparent water oxidation activity (Table 2). The observed slight decrease in activity can be attributed to bpy competitively coordinating to the cobalt core of **1** or the irreversible oxidative degradation of bpy, which is proportional to the bpy concentration. Similarly, aging **1** under reaction conditions for 3 days had no effect on its catalytic water oxidation activity (Table 2), whereas aging $Co(NO_3)_2$ under the same conditions for 3 days substantially decreased its catalytic activity. This observation tracks with well-known cobalt hydroxide/oxide formation above neutral pH (*31*), decreasing the effective surface area and catalytic activity. In addition, at pH = 6.2, no water oxidation was observed for reactions catalyzed by **1**, whereas $Co(NO_3)_2$ was still capable of catalyzing a small extent of water oxidation (Table 2). These results are consistent with **1** being the catalytically active species and its polydentate polytungstate ligands preventing formation of cobalt hydroxide/oxide particles.

For our fourth probe of the stability of **1**, we characterized the postreaction solution containing **1** by using ^{31}P NMR despite the low solubility of **1** in the presence of excess $[Ru(bpy)_3]^{2+}$. When [**1**] = 0.015 mM, as few as 40 equivalents of $[Ru(bpy)_3]^{3+/2+}$ (corresponding to a TON of eight to nine) made the postreaction solution supersaturated, as indicated by the formation of a light yellow precipitate that forms in minutes to hours. To prevent precipitation, we removed $[Ru(bpy)_3]^{2+}$ from the postreaction solution by adding $NaBPh_4$ and removing solid $[Ru(bpy)_3][BPh_4]_2$ by filtration. In the ^{31}P NMR spectrum of this solution, **1** [1850 parts per million, full width at half maximum ($\Delta\nu_{1/2}$) = 600 Hz] was the only species detected besides the free phosphate originating from the buffer solution, indicating that **1** remains intact under catalytic water oxidation conditions (fig. S5).

The fifth and sixth experimental probes of the stability of **1** involved IR characterization and reuse of the WOC after an initial catalytic run, which we carried out under conditions scaled up by a factor of 19 relative to run 1 in Table 2. After the reaction was complete, we saturated the solution with $[Ru(bpy)_3]^{2+}$, which acts as a counterion for complex **1**, resulting in its precipitation. The infrared spectrum of the precipitate showed the characteristic peaks of **1**, a B-type sandwich polytungstate, $[Co_4(H_2O)_2(PW_9O_{34})_2]^{10-}$, at 1037, 939, 882, and 767 cm^{-1} (fig. S6), indicating that the POM framework remains intact after catalysis. For simplicity, we assumed a 1:1 ratio of the $[Ru(bpy)_3]^{2+}$ and **1** in the precipitate and assigned the molecular formula of the precipitate to be **$Na_8Ru(bpy)_3$-1**. Applying the corresponding molecular weight, we used ~0.0032 mM **$Na_8Ru(bpy)_3$-1** as catalyst in the reaction of $[Ru(bpy)_3]^{3+}$ with water in pH = 8 NaPi buffer in the presence of bpy. This reaction gave an O_2 yield of 49.3% and a TON of 58 per **1**, exactly reproducing the activity of pure crystalline **Na_{10}-1** (run 2, Table 2).

The seventh argument for the stability of **1** during catalysis is voltammetric behavior demonstrating that catalytic activity of the active species is retained after turnover. Specifically, we document an electrochemical-chemical mechanism involving **1**: in absence of **1**, a conventional voltammogram was observed for the $[Ru(bpy)_3]^{3+}/[Ru(bpy)_3]^{2+}$ couple; however, upon addition of **1**, an increased anodic current peak and a decreased cathodic current peak were observed for this couple (Fig. 2B). This indicates the rapid reduction of $[Ru(bpy)_3]^{3+}$ by **1** followed by reduction of the oxidized **1** by water. The observed catalytic current increased with catalyst concentration (*24*). In addition, Fig. 2B compares the current for a freshly prepared solution of $[Ru(bpy)_3]^{2+}$ and **1** (green line) with that for a solution that has already undergone catalytic chemical reduction of an equivalent amount of $[Ru(bpy)_3]^{3+}$ by **1** (blue line). These two catalytic currents match, implying that there is no evident catalyst deactivation and that the concentration of **1** remains constant after catalysis. In contrast, the same cyclic voltammetric experiment using $Co(NO_3)_2$ in place of **1** showed a marked decrease in the catalytic water oxidation current for the solution after chemical water oxidation when compared with that of an analogous solution containing unreacted $[Ru(bpy)_3]^{2+}$ and $Co(NO_3)_2$ (fig. S7). Once again, this finding is consistent with aqueous cobalt hydrolyzing and condensing to hydroxide/oxide particles under oxidative conditions, decreasing the effective catalyst concentration.

Computational studies of the electronic structure of **1** provide additional support for the oxidative stability of the polytungstate ligands. The four highest occupied molecular orbitals (HOMOs) of a high-spin ground state **1** are mostly cobalt core orbitals, and there is almost no involvement of tungstate orbitals (fig. S8). These findings indicate that the polytungstate ligands are unlikely to participate in the water oxidation reaction and should be effectively inert under catalytic conditions.

Our reporting of this catalyst establishes d-electron–transition metal oxide clusters stabilized by robust polydentate POM ligands as a compelling class of self-assembling inorganic complexes capable of catalyzing fast water oxidation in a homogeneous medium. This prompts the examination of other POM-stabilized multi–

Table 2. The effect of bpy on the catalytic water oxidation activity of **1** and $Co(aq)^{2+}$. Dashed entry indicates not applicable.

Run	Complex	Complex concentration (mM)	bpy (mM)	Buffer	TON	O_2 yield (%)
1	**1**	0.0032	0	pH = 8 NaPi	78.1	66.7
2	**1**	0.0032	0.3012	pH = 8 NaPi	56	48
3	$Co(NO_3)_2$	0.013*	0.3012	pH = 8 NaPi	0	0
4	$Co(NO_3)_2$	0.060†	0.3012	pH = 8 NaPi	0.2	<4
5	$Co(NO_3)_2$	0.013	0	pH = 8 NaPi	23.4	80
6	No catalyst	–	0	pH = 8 NaPi	0	0
7	**1**	0.0032	0	pH = 6.2 NaPi/phthalic acid‡	0	0
8	$Co(NO_3)_2$	0.013	0	pH = 6.2 NaPi/phthalic acid	10	35
9	**1**	0.0032	0.135	pH = 8 NaPi	70.3	60
10	**1** (aged)§	0.0032	0.135	pH = 8 NaPi	71.2	60.8
11	$Co(NO_3)_2$ (aged)§	0.013	0	pH = 8 NaPi	9.8	33.6
12	CoO‖	0.0032	0	pH = 8 NaPi	0	0

*Same theoretical cobalt concentration as 0.0032 mM **1**. †Same solid mass as 0.0032 mM **1**. ‡A mixed buffer of 30 mM NaPi and 30 mM phthalic acid at pH = 6.2 was used. §A 1 mM stock solution in 30 mM pH = 8 NaPi was left for 72 hours before use. ‖Not soluble, suspension obtained after 10 min of sonication.

transition-metal oxide cluster molecules involving both other metals (e.g., Fe and Mn) and new POM ligands as candidate WOCs. Moreover, the identification of a molecular Co-based WOC may allow further investigation of its mechanism of action, providing a basis for the understanding of Co-based water oxidation catalysis in general. In addition, **1** may serve as a template for future optimizations of all-inorganic WOCs as well as their incorporation into water splitting systems. No photosensitizers were used in this report. Although $[Ru(bpy)_3]^{3+}$ was used as a stoichiometric oxidant in this study in order to demonstrate the water oxidation activity of **1**, it is ultimately desirable to use solar power to accomplish water oxidation. The apparently straightforward use of $[Ru(bpy)_3]^{2+}$ as a photosensitizer, however, might not be optimal given the oxidative instability of this complex.

References and Notes

1. J. Chow, R. J. Kopp, P. R. Portney, *Science* **302**, 1528 (2003).
2. N. S. Lewis, D. G. Nocera, *Proc. Natl. Acad. Sci. U.S.A.* **103**, 15729 (2006).
3. V. Balzani, A. Credi, M. Venturi, *ChemSusChem* **1**, 26 (2008).
4. R. Eisenberg, H. B. Gray, *Inorg. Chem.* **47**, 1697 (2008).
5. V. Y. Shafirovich, N. K. Khannanov, V. V. Strelets, *Nouv. J. Chim.* **4**, 81 (1980).
6. A. Harriman, I. J. Pickering, J. M. Thomas, P. A. Christensen, *J. Chem. Soc., Faraday Trans. I* **84**, 2795 (1988).
7. G. L. Elizarova, G. M. Zhidomirov, V. N. Parmon, *Catal. Today* **58**, 71 (2000).
8. M. W. Kanan, D. G. Nocera, *Science* **321**, 1072 (2008); published online 31 July 2008 (10.1126/science.1162018).
9. W. J. Youngblood *et al.*, *J. Am. Chem. Soc.* **131**, 926 (2009).
10. P. K. Ghosh, B. S. Brunschwig, M. Chou, C. Creutz, N. Sutin, *J. Am. Chem. Soc.* **106**, 4772 (1984).
11. I. A. Weinstock *et al.*, *Nature* **414**, 191 (2001).
12. F. Jiao, H. Frei, *Angew. Chem. Int. Ed.* **48**, 1841 (2009).
13. S. W. Gersten, G. J. Samuels, T. J. Meyer, *J. Am. Chem. Soc.* **104**, 4029 (1982).
14. T. Wada, K. Tsuge, K. Tanaka, *Angew. Chem. Int. Ed.* **39**, 1479 (2000).
15. J. Limburg *et al.*, *J. Am. Chem. Soc.* **123**, 423 (2001).
16. J. K. Hurst, *Coord. Chem. Rev.* **249**, 313 (2005).
17. R. Zong, R. P. Thummel, *J. Am. Chem. Soc.* **127**, 12802 (2005).
18. J. T. Muckerman, D. E. Polyansky, T. Wada, K. Tanaka, E. Fujita, *Inorg. Chem.* **47**, 1787 (2008).
19. R. Brimblecombe, G. F. Swiegers, G. C. Dismukes, L. Spiccia, *Angew. Chem. Int. Ed.* **47**, 7335 (2008).
20. S. Romain, F. Bozoglian, X. Sala, A. Llobet, *J. Am. Chem. Soc.* **131**, 2768 (2009).
21. S. W. Kohl *et al.*, *Science* **324**, 74 (2009).
22. J. F. Hull *et al.*, *J. Am. Chem. Soc.* **131**, 8730 (2009).
23. H. Kunkely, A. Vogler, *Angew. Chem. Int. Ed.* **48**, 1685 (2009).
24. Y. V. Geletii *et al.*, *Angew. Chem. Int. Ed.* **47**, 3896 (2008).
25. A. Sartorel *et al.*, *J. Am. Chem. Soc.* **130**, 5006 (2008).
26. Y. V. Geletii *et al.*, *J. Am. Chem. Soc.* **131**, 7522 (2009).
27. Materials and methods are available as supporting material on *Science* Online.
28. L. Ruhlmann, L. Nadjo, J. Canny, R. Contant, R. Thouvenot, *Eur. J. Inorg. Chem.* **2002**, 975 (2002).
29. T. J. R. Weakley, H. T. Evans Jr., J. S. Showell, G. F. Tourné, C. M. Tourné, *J. Chem. Soc. Chem. Commun.* **4**, 139 (1973).
30. F. H. Burstall, R. S. Nyholm, *J. Chem. Soc.* **1952**, 3570 (1952).
31. J. Baes, F. Charles, R. E. Mesmer, *The Hydrolysis of Cations* (Wiley, New York, 1976).

32. We thank the U.S. Department of Energy through grant DE-FG02-03ER-15461 for support of this work. C.B. thanks the French Ministère de l'Éducation Nationale, de la Recherche, et de la Technologie for a research fellowship. Additional details on the crystal structure investigations may be obtained from the Fachinformationszent Wrum Karlsruhe, 76344 Eggenstein-Leopoldshafen, Germany, on quoting registry number CSD-421465.

Supporting Online Material

www.sciencemag.org/cgi/content/full/science.1185372/DC1
Materials and Methods
Figs. S1 to S11
References

1 December 2009; accepted 25 February 2010
Published online 11 March 2010;
10.1126/science.1185372
Include this information when citing this paper.

Oxoboryl Complexes: Boron–Oxygen Triple Bonds Stabilized in the Coordination Sphere of Platinum

Holger Braunschweig,* Krzysztof Radacki, Achim Schneider

Monomeric oxoboranes have hitherto been detected only as short-lived species in gas-phase or low-temperature matrix experiments. Here, we report formation of the oxoboryl complex *trans*-[$(Cy_3P)_2BrPt(B{\equiv}O)$] (Cy being cyclohexyl) by means of reversible liberation of trimethylsilylbromide from the boron–bromine oxidative addition product of dibromo (trimethylsiloxy)borane and $[Pt(PCy_3)_2]$ in room-temperature toluene solution. The platinum complex is inert toward oligomerization, even under photolytic conditions and at elevated temperatures. The bromide was substituted by thiophenolate, and spectral parameters of both products as well as results of computational and x-ray diffraction studies are in agreement with the formulation of a triple bond between boron and oxygen. The boron–oxygen distance of 120.5(7) picometers shows a bond shortening of 7.2% as compared with a double bond, which is similar to the shortening observed in carbon–carbon analogs.

The element boron is popularly known for its unique propensity to participate in multicenter bonds to compensate its intrinsic electron-deficiency. Thus, various structural motifs have been described that exhibit boron with coordination numbers higher than its actual valency (*1*). However, not least because of the importance of boranes in organic syntheses (*2*) the chemistry of boron-containing compounds featuring exclusively classical, electron-precise bonds has been established during the last century, and therefore examples with tricoordinate boron likewise are plentiful. Though species with dicoordinate boron are considerably more unusual, different strategies to prepare and stabilize those compounds have been applied successfully (*3*–*8*).

Since boroxine ($H_3B_3O_3$) could be identified as the product of highly energetic reactions of different ternary systems (*9*), numerous attempts have been undertaken to synthesize its monomeric counterparts, namely oxoboranes (XBOs). However, those species could be detected only in either gas-phase (*10*–*13*) or low-temperature matrix isolation studies (*14*–*19*). Further evidence for the existence of those compounds was obtained through different trapping experiments (*20*–*22*) or nuclear magnetic resonance (NMR) spectroscopic observation of the corresponding Lewis base adduct (*22*). Microwave (*11*) and infrared (IR) data (*14*–*19*) suggest a very strong linkage of boron and oxygen; because of the similarity of the photoelectron spectrum of H_3CBO with the isoelectronic H_3CCN molecule (*12*, *13*), the B–O linkage was described by a triple bond. Nevertheless, probably because of the polar nature of this bond, the highly reactive monomers readily undergo cyclooligomerization even at temperatures of approximately 50 K (*19*, *23*) and an x-ray structural elucidation could not be performed.

Commonly, kinetic lability of low-valent species can be compensated by use of bulky substituents that inhibit bimolecular attack, as was successfully demonstrated by the preparation of a stable disilyne (*24*). In contrast, XBOs contain-

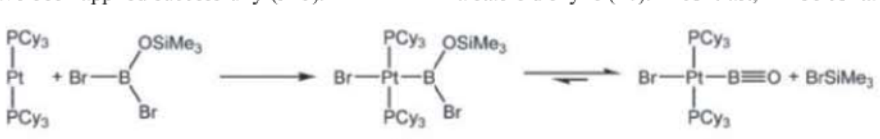

Scheme 1. Preparation of *trans*-[$(Cy_3P)_2BrPt(BO)$] (**2**).

Institut für Anorganische Chemie, Julius-Maximilians-Universität Würzburg, Am Hubland, 97074 Würzburg, Germany.

*To whom correspondence should be addressed. E-mail: h.braunschweig@mail.uni-wuerzburg.de

ing sterically demanding substituents were shown to undergo intramolecular stabilization reactions instead (*21*, *25*). Only drastic modifications in not just steric parameters but rather fundamental electronics led to a stable and isolable derivative of an XBO (*26*). Hence, combination of a Lewis acid coordinated to oxygen and a backbone structure additionally stabilizing the boron center reduced the bond order, and the boron–oxygen linkage was characterized as a double bond.

Recently, synthesis of the previously elusive iminoboryl complexes [L_nM–B≡N–R] under remarkably mild reaction conditions, and their inertness toward cyclooligomerization, demonstrated the stabilizing effect that late-transition-metal fragments can exert on low-coordinate boron centers (*27*–*29*). Furthermore, theoretical calculations predicted the anionic BO^- ligand to be an electronically complementary isolobal alternative to the CO ligand, exhibiting extraordinarily strong σ-donating abilities and correspondingly poor π-acceptor properties (*30*). Thus, generation of the B≡O triple bond in the coordination sphere of a transition metal appeared to be a promising approach. The starting material suitable for this purpose, $Br_2BOSiMe_3$, has been noted to be unstable (*31*); however, when prepared in dilute toluene solution it can be handled and stored for several months without any signs of decomposition.

Analysis by means of multinuclear NMR spectroscopy of the reaction mixture prepared by mixing toluene solutions of $Br_2BOSiMe_3$ and [$Pt(PCy_3)_2$] (Cy being cyclohexyl) at room temperature reveals immediate consumption of the starting materials and initial formation of one product (*32*). Phosphorus (^{31}P) NMR data [21.2 parts per million (ppm), $^1J_{Pt\text{-}P}$ = 2777 Hz] are indicative of a platinum(II) boryl complex featuring a tricoordinate boron center (*33*–*36*) and thus were assigned to the boryl complex *trans*-[$(Cy_3P)_2BrPt\{B(Br)OSiMe_3\}$] (**1**) obtained by B–Br oxidative addition of the borane to platinum (Scheme 1). In the further course of the reaction, liberation of $BrSiMe_3$ can be observed with proton NMR spectroscopy, and the signals assigned to **1** gradually decrease. Likewise, ^{31}P NMR spectroscopy indicates predominant formation of another new phosphorus-containing product (32.5 ppm, $^1J_{Pt\text{-}P}$ = 2294 Hz), which could be isolated and fully characterized as *trans*-[$(Cy_3P)_2BrPt(BO)$] (**2**). Because of the large peak width at half height, the ^{11}B NMR resonance of the product (17 ppm) can be detected only in solutions with a concentration of more than approximately 0.3 M and appears upfield of the starting borane $Br_2BOSiMe_3$ (21 ppm) and boryl species **1** (32 ppm) resonances. At room temperature, the reaction reaches a stationary point, with the two reaction products **1** and **2** in a ratio of approximately 1:4. However, repeated removal of all volatile components in high vacuum at ambient temperature and redissolution of the residue affords complete conversion of **1** to **2**. These findings suggest that the liberation of bromosilane is a reversible process. To validate this result, pure **2** was reacted portion-wise with $BrSiMe_3$, and successive formation of increasing amounts of **1** can be observed spectroscopically. In fact, the presence of a large excess of bromosilane enables the NMR spectroscopic characterization of **1**.

Recrystallization of **2** from varying solvents (such as hexane, toluene, tetrahydrofuran, and mixtures thereof) gave several single crystals suitable for x-ray diffraction studies, which exhibited different crystallographic space groups and in some cases contained co-crystallized solvent molecules. However, structural parameters of the crystallographic data are not fully reliable because of massive disorder of the two anionic ligands in all cases. Nevertheless, the obtained molecular structures leave no doubt of the constitutional composition of compound **2**: an oxoboryl ligand coordinated terminally via boron to the metal center (Fig. 1, left). More specific information on the linkage between boron and oxygen could be obtained by means of IR spectroscopy. Complex **2** shows two absorption bands (1853 and 1797 cm^{-1}), which because of intensities and relative position can be assigned to the BO stretching vibrations of the two boron isotopologues. The values are in good agreement with the vibrational spectra of oxoboryl species observed in matrix studies (*14*–*19*), suggesting that complex **2** should exhibit a similar bonding situation. In marked contrast to the matrix-isolated compounds, however, is the unusual thermal stability of the oxoboryl moiety in **2**. A solution of **2** in benzene-D_6 did not show any evidence of oligomerization or decomposition after 24 hours of heating to 100°C or irradiation with a Hg/Xe arc lamp, respectively.

To understand this remarkable stability of **2** and investigate the nature of the linkage between boron and oxygen in more detail, density functional theory (DFT) studies at the B3LYP level of theory were performed on the slightly simplified complex *trans*-[$(Me_3P)_2BrPt(BO)$] (**2′**). The calculations reproduced the IR data well (the calculated values were 1886 and 1828 cm^{-1}), and the natural resonance theory (NRT) bond index of 2.83 in combination with the short calculated interatomic distance between boron and oxygen (122.6 pm) are in full agreement with the formulation of a triple bond. Detailed analyses of the molecular orbitals (MOs) inter alia revealed bond-

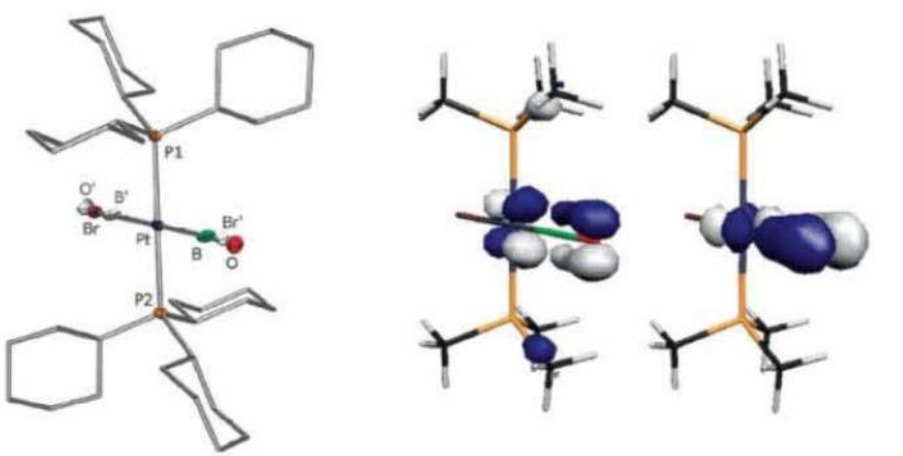

Fig. 1. X-ray molecular structure of *trans*-[$(Cy_3P)_2BrPt(BO)$] (**2**) (left) and π-MOs of the model complex *trans*-[$(Me_3P)_2BrPt(BO)$] (**2′**) (right). The bond lengths and angles of **2** are not fully reliable because of the disorder indicated by the white ellipsoids. Thermal ellipsoids are represented at the 50% probability level. Hydrogen atoms and ellipsoids of the carbon atoms of **2** are omitted for clarity.

Scheme 2. Preparation of *trans*-[$(Cy_3P)_2(PhS)Pt(BO)$] (**3**).

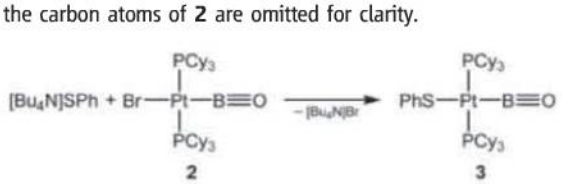

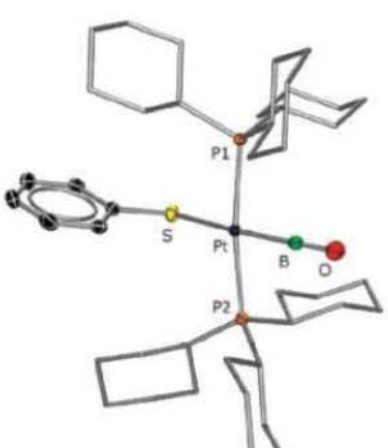

Fig. 2. Molecular structure of *trans*-[$(Cy_3P)_2(PhS)Pt(BO)$] (**3**) • 2 CH_2Cl_2. Thermal ellipsoids are represented at the 50% probability level. Hydrogen atoms, solvent molecules and ellipsoids of the cyclohexyl carbon atoms are omitted for clarity. Selected Bond lengths (pm) and angles (°): B–O 121.0(3), Pt–B 198.3(3), Pt–S 241.06(6); Pt–B–O 177.3(2), B–Pt–P1 87.75(8), B–Pt–P2 86.80(8), B–Pt–S 171.3(2), Pt–S–C 111.33(8). Estimated standard deviations are given in parentheses.

ing interactions that can be described essentially as two π-bonds (Fig. 1, right). Those MOs are localized slightly more on oxygen than on boron, reflecting the polar nature of this interaction. Additionally, they show substantial stabilizing contributions of the symmetry-equivalent d-orbitals of platinum.

Further evidence for the remarkable stability of the oxoboryl moiety in the coordination sphere of platinum was the clean reaction of **2** with $[Bu_4N]SPh$ (Ph being phenyl), as was evinced by means of NMR spectroscopy. The product features spectroscopic parameters very similar to those of the starting complex, and in particular IR data (1849 and 1793 cm^{-1}) indicate only minor influence of the *trans* ligand substitution on the oxoboryl moiety. As evidenced with x-ray analyses, the thiolate anion does not affect the boron center but instead reacts through substitution of the bromide ligand, yielding *trans*-$[(Cy_3P)_2(PhS)Pt(BO)]$ (**3**) (Scheme 2), which could be isolated in 62% yield.

The solid structure of **3** (Fig. 2) exhibits an almost square-planar geometry at platinum (sum of bond angles of 359.1°); however, the phosphine ligands are bent slightly toward the oxoboryl moiety [$<_{B–Pt–P}$ = 87.75(8) and 86.80(8)°, respectively, the numbers in parentheses being the estimated SD]. The latter is coordinated to platinum terminally via the boron atom [$<_{Pt–B–O}$ = 177.3(2)°], reflecting its sp-hybridization. The Pt–B distance [198.3(3) pm] is slightly longer than in the corresponding iminoboryl complex *trans*-$[(Cy_3P)_2(Br)Pt(BNSiMe_3)]$ [196.0(3) pm] (*27*, *28*) but in the typical range of classical boryl complexes of platinum with trivalent boron atoms *trans* to a bromide [196.3(6)–209.(3) pm] (*35*). The B–O bond length of 121.0(3) pm in **3** is slightly smaller than the value obtained for **2′** from DFT calculations and statistically indistinguishable from the distance calculated from microwave data of gaseous HBO [120.04(3) pm] (*11*). However, it is considerably smaller than the B–O double bond in the coordinated XBO [130.4(2) pm] (*26*). The observed bond shortening of 7.2% is only slightly smaller than the corresponding difference between alkynes and alkenes (9.9%) (*37*), providing further evidence of the presence of a triple bond between boron and oxygen.

Our approach of generating unusual ligand systems in the coordination sphere of transition metals has enabled us to access the previously elusive boron monoxide moiety. In marked contrast to main group–substituted XBOs, which are high-energy intermediates, compound **2** exhibits a remarkable thermal and light stability. Despite the stabilizing effect that the platinum fragment exerts on the oxoboryl moiety, we realized interesting reaction chemistry on both the BO ligand itself and on the metal center. Hence, the bromide ligand undergoes clean metathesis with the thiophenolate anion, leaving the BO ligand intact, whereas trimethyl(bromo)silane adds reversibly to the BO ligand. We anticipate a diverse range of further reactivity along both lines.

References and Notes

1. W. N. Lipscomb, *Science* **196**, 1047 (1977).
2. H. C. Brown, *Science* **210**, 485 (1980).
3. P. Paetzold, *Adv. Inorg. Chem.* **31**, 123 (1987).
4. A. Berndt, *Angew. Chem.* **105**, 1034 (1993).
5. A. Berndt, *Angew. Chem. Int. Ed. Engl.* **32**, 985 (1993).
6. W. E. Piers, S. C. Bourke, K. D. Conroy, *Angew. Chem.* **117**, 5142 (2005).
7. W. E. Piers, S. C. Bourke, K. D. Conroy, *Angew. Chem. Int. Ed.* **44**, 5016 (2005).
8. H. Braunschweig, C. Kollann, F. Seeler, *Struct. Bonding* **130**, 1 (2008).
9. L. Barton, F. A. Grimm, R. F. Porter, *Inorg. Chem.* **5**, 2076 (1966).
10. D. L. Hildenbrand, L. P. Theard, A. M. Saul, *J. Chem. Phys.* **39**, 1973 (1963).
11. Y. Kawashima, Y. Endo, K. Kawaguchi, E. Hirota, *Chem. Phys. Lett.* **135**, 441 (1987).
12. H. Bock *et al.*, *Angew. Chem.* **101**, 77 (1989).
13. H. Bock *et al.*, *Angew. Chem. Int. Ed. Engl.* **28**, 88 (1989).
14. E. R. Lory, R. F. Porter, *J. Am. Chem. Soc.* **93**, 6301 (1971).
15. A. Snelson, *High Temp. Sci.* **4**, 318 (1972).
16. A. Snelson, *High Temp. Sci.* **4**, 141 (1972).
17. L. Andrews, T. R. Burkholder, *J. Phys. Chem.* **95**, 8554 (1991).
18. D. V. Lanzisera, L. Andrews, *J. Phys. Chem. A* **101**, 1482 (1997).
19. H. F. Bettinger, *Organometallics* **26**, 6263 (2007).
20. B. Pachaly, R. West, *J. Am. Chem. Soc.* **107**, 2987 (1985).
21. P. Paetzold, S. Neyses, L. Geret, *Z. Anorg. Allg. Chem.* **621**, 732 (1995).
22. M. Ito, N. Tokitoh, R. Okazaki, *Tetrahedron Lett.* **38**, 4451 (1997).
23. P. Paetzold, P. Bohm, A. Richter, E. Scholl, *Z. Naturforsch. B* **31B**, 754 (1976).
24. A. Sekiguchi, R. Kinjo, M. Ichinohe, *Science* **305**, 1755 (2004).
25. M. Groteklaes, P. Paetzold, *Chem. Ber.* **121**, 809 (1988).
26. D. Vidovic, J. A. Moore, J. N. Jones, A. H. Cowley, *J. Am. Chem. Soc.* **127**, 4566 (2005).
27. H. Braunschweig, K. Radacki, D. Rais, K. Uttinger, *Angew. Chem.* **118**, 169 (2006).
28. H. Braunschweig, K. Radacki, D. Rais, K. Uttinger, *Angew. Chem. Int. Ed.* **45**, 162 (2006).
29. H. Braunschweig *et al.*, *J. Am. Chem. Soc.* **130**, 7974 (2008).
30. A. W. Ehlers, E. J. Baerends, F. M. Bickelhaupt, U. Radius, *Chem. Eur. J.* **4**, 210 (1998).
31. E. Wiberg, U. Kruerke, *Z. Naturforsch. B* **8b**, 610 (1953).
32. Materials and methods are available as supporting material on *Science* Online.
33. G. J. Irvine *et al.*, *Chem. Rev.* **98**, 2685 (1998).
34. W. Clegg *et al.*, *J. Organomet. Chem.* **550**, 183 (1998).
35. H. Braunschweig *et al.*, *Chem. Eur. J.* **13**, 7171 (2007).
36. D. L. Kays, S. Aldridge, *Struct. Bonding* **130**, 29 (2008).
37. R. C. Weast, Ed., *Handbook of Chemistry and Physics* (CRC Press, Boca Raton, FL, ed. 60, 1979).

38. This work was supported by the Deutsche Forschungsgemeinschaft. A.S. is grateful for a doctoral fellowship of the Fonds der Chemischen Industrie. Crystallographic data for compounds **2** and **3** can be obtained free of charge from the Cambridge Crystallographic Data Centre via www.ccdc.cam.ac.uk/data_request/cif, under reference nos. CCDC 758828 and 758829, respectively.

Supporting Online Material

www.sciencemag.org/cgi/content/full/328/5976/345/DC1
Materials and Methods
SOM Text
Fig. S1
References

16 December 2009; accepted 3 March 2010
10.1126/science.1186028

A Younger Age for ALH84001 and Its Geochemical Link to Shergottite Sources in Mars

T. J. Lapen,[1]* M. Righter,[1] A. D. Brandon,[1,2] V. Debaille,[3] B. L. Beard,[4,5] J. T. Shafer,[1,7] A. H. Peslier[6,8]

Martian meteorite ALH84001 (ALH) is the oldest known igneous rock from Mars and has been used to constrain its early history. Lutetium-hafnium (Lu-Hf) isotope data for ALH indicate an igneous age of 4.091 ± 0.030 billion years, nearly coeval with an interval of heavy bombardment and cessation of the martian core dynamo and magnetic field. The calculated Lu/Hf and Sm/Nd (samarium/neodymium) ratios of the ALH parental magma source indicate that it must have undergone extensive igneous processing associated with the crystallization of a deep magma ocean. This same mantle source region also produced the shergottite magmas (dated 150 to 570 million years ago), possibly indicating uniform igneous processes in Mars for nearly 4 billion years.

The orthopyroxene cumulate ALH84001 is unique in having an igneous crystallization age more than 2 billion years older than any other martian meteorite (*1*–*11*), providing critical timing constraints on the formation of Mars. Its igneous crystallization age has been difficult to determine because of its complex postcrystallization history of aqueous alteration and shock metamorphism (*12*, *13*). Although crystallization ages obtained on ALH range from 3.9 to 4.56 billion years ago (Ga) (*1*–*10*), the weighted average of Rb-Sr and Sm-Nd isotope data (*2*) yield a generally accepted age of 4.51 ± 0.11 Ga (all errors are ±2σ) (*11*). This age has important implications for the formation history of martian crust and mantle, crater chronology, and the onset of the Mars magnetic field. An age of 4.51 ± 0.11 Ga requires that a stable crust existed very early in Mars' history, not long after the onset of solar system formation at 4.568 Ga (*14*). If ALH represents crustal material formed at 4.51 Ga, then this crust must

have survived a period of intense bombardment between 4.25 and 4.10 Ga (*15*, *16*), similar to the late heavy bombardment or terminal lunar cataclysm on the Moon, without suffering the intense brecciation observed in prebombardment lunar rocks. A further implication of this age is the potential presence of a magnetic field and core convection in Mars 27 to 48 million years after core formation (*17*, *18*). In order to better refine the timing of these events and to evaluate potential magmatic source affinities, we applied ^{176}Lu-^{176}Hf and ^{146,147}Sm-^{142,143}Nd chronometry to ALH.

ALH is an igneous cumulate rock that has been affected by shock-induced metamorphism and precipitation of secondary phases including carbonate and magnetite (*13*, *19*). ALH is composed of mosaic-grained orthopyroxene (~97 vol %) crystals, 4 to 5 mm in diameter, that enclose euhedral to subhedral chromite (~2 vol %) locally preserved as clasts within recrystallized granular bands. Interstitial to the mosaic-grained orthopyroxene are chromite, maskelynite, phosphate (apatite and merrillite), augite, olivine, and SiO_2 (which total ~1 vol %). The 3.6 g of ALH used in this study (sample allocations ALH84001, 365 and ALH84001, 403) have an exceptionally well-preserved igneous texture with no optical evidence of secondary phases and minimal (5 to 10 vol %) granular banding. One portion was separated into oxide (~100% chromite, sample S1) and nearly pure orthopyroxene-rich (sample S2) fractions. Two other fractions—representing the bulk rock (sample S3) and a bulk fraction after chromite removal (sample S4)—are from the disaggregated and processed material of this portion. A second portion was leached with 2.5 M HCl, resulting in a leachate-residue pair (samples L1 and R1) that was analyzed for ^{147}Sm-^{143}Nd. A third portion was crushed into a powder for high-precision ^{142}Nd/^{144}Nd analysis. Sample preparation, chemical separation, and analytical procedures are described in (*20*).

A ^{176}Lu-^{176}Hf isochron age of 4.091 ± 0.030 Ga for ALH is defined by samples S1 to S4 (Fig. 1). This age is consistent with ^{207}Pb-^{206}Pb ages of 4.074 ± 0.099 Ga (*4*) and 4.135 ± 0.012 Ga (*5*) and a U-Pb age of 4.117 ± 0.003 Ga (*5*). The Lu-Hf age is substantially younger than the respective Sm-Nd and Rb-Sr ages of 4.50 ± 0.13 Ga and 4.55 ± 0.30 Ga (*2*, *11*). The measured Lu-Hf, Pb-Pb, and U-Pb ages are similar to but slightly older than the respective Rb-Sr and Pb-Pb ages of secondary carbonate phases, 3.90 ± 0.04 Ga and 4.04 ± 0.10 Ga (*9*), as well as the U-Pb age of whitlockite and apatite, 4.018 ± 0.081 Ga (*10*). The ^{39}Ar-^{40}Ar ages of 3.92 ± 0.10 Ga and 4.1 ± 0.2 Ga (*6*, *8*) are similar to the Lu-Hf age, but shock disturbances, trapped atmospheric components, and ^{39}Ar recoil make comparisons between these isotope systems difficult. The ^{147}Sm-^{143}Nd data of samples S2 to S4 indicate an "age" of 4.405 ± 0.026 Ga, ~315 million years older than the Lu-Hf age and consistent with the previous Rb-Sr and Sm-Nd age determinations (*2*, *11*). The ^{147}Sm-^{143}Nd age of 4.889 ± 0.020 Ga defined by samples L1 and R1 is older than the age of the solar system and has an initial ^{143}Nd/^{144}Nd less than the solar system initial value (fig. S1). The counterclockwise rotation of these older isochrons requires either open-system behavior of Sm and Nd or decoupling of Sm-Nd isotope systematics during subsolidus alterations.

In ALH, 58% and 78% by weight of Sm and Nd, respectively, reside in the phosphate phases whitlockite and apatite (Table 1). The Sm-Nd apparent isochron defined by samples S2 to S4 is controlled by distribution of light rare earth element (LREE)–rich phosphates, as shown by the strong correlation (R^2 = 0.99998) between measured ^{143}Nd/^{144}Nd and Nd concentrations for each fraction (fig. S2). Because phosphates are reactive in low-pH and weathering environments, there was great potential for redistribution of Sm, Nd, and Sr in ALH resulting in spurious age and initial isotope ratios for both the Sm-Nd and Rb-Sr isotope systems. The relatively high scatter of ^{232}Th-^{208}Pb data (*5*) and a younger average U-Pb age of 4.018 ± 0.081 Ga (*10*) of apatite and whitlockite are consistent with disturbance of phosphate phases after igneous crystallization. For counterclockwise rotation of a Sm-Nd isochron, the low-Sm/Nd phase, phosphate in this case, must lose Nd relative to Sm, and the high-Sm/Nd phase orthopyroxene must have its Sm/Nd ratio decreased or unchanged. The precise mechanism of this alteration is unknown, but disturbance of the Sm-Nd system in ALH is demonstrated by the ages being too old for the leachate-residue pair coupled with a ^{143}Nd/^{144}Nd less than the solar system initial value. In contrast, orthopyroxene and chromite are the dominant Lu and Hf reservoirs (Table 1), which implies that phosphate disturbance will not affect the Lu-Hf system. Although 3% Lu resides in phosphate, its mobility would have little impact on the slope of the isochron. Because of its resistance to disturbance resulting from phosphate alteration and mutual agreement between U-Pb and Pb-Pb ages, we conclude that the Lu-Hf isochron defines the true igneous crystallization age.

The Lu-Hf age of 4.091 ± 0.030 Ga precludes it from being a remnant of primordial crust formed during solidification of an early martian magma ocean (MO). Instead, the magma that crystallized to produce ALH was derived from mantle reservoirs that have evolved isotopically since about 4.54 to 4.46 Ga (*21*). The initial ^{176}Hf/^{177}Hf of ALH cast in $\varepsilon^{176}Hf_{CHUR}$ notation (*22*) is –4.64 ± 1.04 (Table 2). This indicates that the ^{176}Hf/^{177}Hf of its parental magma source is less than CHUR (Fig. 2A). The calculated source ^{176}Lu/^{177}Hf—assuming a two-stage mantle evolution model (*23*), a source formation age of 4.513 Ga, a chondritic bulk Mars, and a Mars formation age of 4.567 Ga (*20*)—is 0.0183 ± 0.0036. This is similar to but substantially lower than the average source ^{176}Lu/^{177}Hf of 0.02795 ±

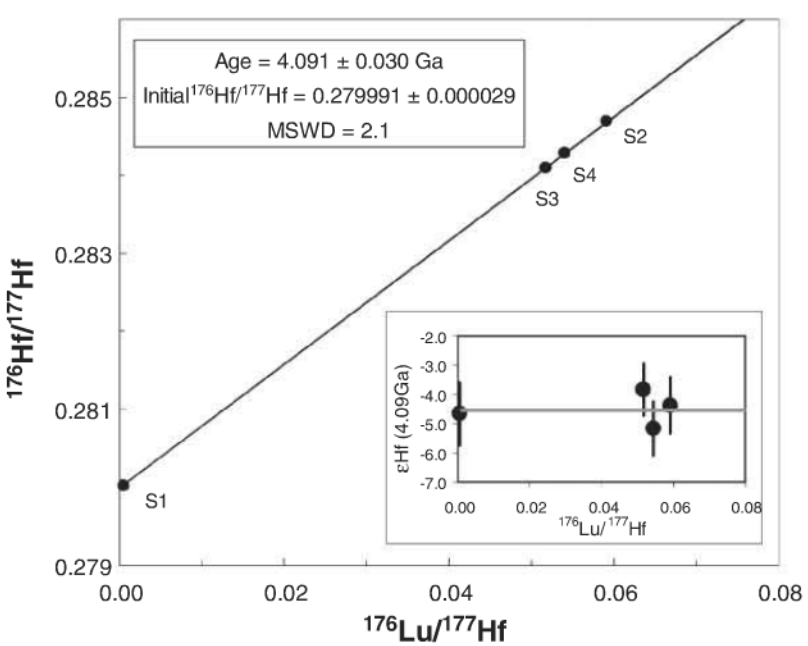

Fig. 1. Lu-Hf isochron for ALH. Inset shows Hf isotope data relative to CHUR at 4.091 Ga. Data are listed in Table 2; errors are 2σ. The isochron was calculated using IsoPlot (*34*) and a ^{176}Lu decay constant of 1.865^{-11} year^{-1} (*35*).

[1]Department of Earth and Atmospheric Sciences, University of Houston, Houston, TX 77204, USA. [2]NASA Johnson Space Center, Mail Code KR, Houston, TX 77058, USA. [3]Département des Sciences de la Terre et de l'Environnement, Université Libre de Bruxelles, 1050 Brussels, Belgium. [4]Department of Geosciences, University of Wisconsin, Madison, WI 53706, USA. [5]NASA Astrobiology Institute, University of Wisconsin, Madison, WI 53706, USA. [6]Jacobs Technology, Engineering and Science Contract Group, Houston, TX 77058, USA. [7]Lunar and Planetary Institute, Houston, TX 77058, USA. [8]ARES, NASA Johnson Space Center, Houston, TX 77058, USA.

*To whom correspondence should be addressed. E-mail: tjlapen@uh.edu

0.00010 (weighted mean) calculated for the distinct martian meteorite group of enriched shergottites (*24*) (Fig. 2A). The calculated source $^{147}Sm/^{144}Nd$ using the bulk-rock sample S3 is 0.172, slightly lower than the average source $^{147}Sm/^{144}Nd$ of 0.185 for the enriched shergottites (*21*). Also, the measured $^{142}Nd/^{144}Nd$ of ALH [$\varepsilon^{142}Nd = -0.23 \pm 0.05$ relative to the terrestrial standard (*20*)] is slightly lower than (but within error of) the enriched shergottite average of –0.19 ± 0.05. Combined, ALH and the enriched shergottites have distinctly lower $\varepsilon^{142}Nd$ than all other martian meteorites that have $\varepsilon^{142}Nd$ values of –0.23 ± 0.03 to +0.65 ± 0.05 (*21*). The ALH carbonate $^{87}Sr/^{86}Sr$ is identical to its measured bulk rock at 3.90 ± 0.04 Ga, indicating that the carbonate Sr was primarily, if not wholly, derived from ALH (*9*). Given this, the calculated source $^{87}Rb/^{86}Sr$ is 0.41 to 0.35, similar to the average source of enriched shergottites of ~0.36 (*23*). Finally, similarities between ALH and enriched shergottite primary magmas are also indicated by the incompatible trace element abundances of coexisting melts with the cumulate phases in ALH (*25*). Combined, these observations indicate that ALH is derived from a source that is more incompatible trace element–enriched than shergottites. When source Sm/Nd and Lu/Hf ratios of shergottites and ALH are plotted together, they define a mixing array between hypothetical incompatible trace element–depleted and –enriched end members (Fig. 2B).

In principle, the enriched source characteristics constrained by ALH and less so by the enriched shergottites could potentially be derived from variable amounts of crustal assimilation during magma differentiation (*26*, *27*). However, from the coupled relationships between Os and Nd isotopes, shergottites cannot be related by simple mixing of depleted mantle and crust (*28*). Furthermore, crustal assimilation is not consistent with major element compositions of shergottites and their trace element and isotope systematics (*23*). From mixing calculations, the ratio of enriched component to depleted component in the martian mantle that yields the measured source $^{147}Sm/^{144}Nd$ and $^{176}Lu/^{177}Hf$ of ALH is about 0.6:0.4. Because ALH falls on the well-defined binary mixing array for Sm-Nd and Lu-Hf source compositions, it would also be highly unlikely that assimilation of mineralogically diverse crustal rocks would yield such a tight array for rocks representing parental magmas formed billions of years apart. Thus, the source for ALH was most likely in the martian mantle. This source has trace element and lithophile isotope characteristics similar but not identical to lunar KREEP (potassium–rare earth element–phosphorus) basalt sources and was likely produced by similar mechanisms (Fig. 2, A and B) (*23*, *29*).

The enriched and depleted end-member compositions in Mars likely formed from the progressive crystallization of its MO, where the residual trapped liquid components are enriched in incompatible trace elements relative to the cumulate fractions at any given point during the crystallization process (*23*, *29*–*31*) creating a hybridized mantle source with the degree of enrichment controlled by the relative proportion of trapped liquid relative to cumulate minerals. The $^{147}Sm/^{144}Nd$ and $^{176}Lu/^{177}Hf$ ratios of enriched residual liquid and depleted cumulate end-member components not only vary with degree of MO crystallization, but also with depth of equilibration and initial MO depth (Fig. 2C) (*30*). Because the modeled enriched end-member contribution to ALH parental magma is high (~60%), the composition of the enriched end

Table 1. Lu, Hf, Sm, and Nd concentrations and their calculated absolute amounts in each listed phase. See (*20*) for data reduction and analytical procedures. Modal proportions from (*19*); plagioclase and phosphate data from (*36*); orthopyroxene and chromite data from this study (*20*).

	Orthopyroxene	Chromite	Plagioclase (maskelynite)	Phosphate
Modal proportions	97%	2%	<1%	0.15%
	Element concentrations			
Lu (ppb)	48.6	0.74		900
Hf (ppb)	116.8	219.2		
Sm (ppb)	49.1		34	43,580
Nd (ppb)	73.3		378.5	179,500
	Percentage hosted in each phase			
Lu	97%	0.03%		3%
Hf	96%	4%		
Sm	42%		0.30%	58%
Nd	21%		1%	78%

Table 2. Lu-Hf and Sm-Nd isotope data measured in this study. See (*20*) for data reduction and analytical procedures.

	ALH84001, 403						ALH84001, 365
	Oxide	Pure pyroxene	Bulk rock	Dirty pyroxene	Bulk rock residue	Bulk rock leachate	Bulk rock
Sample	S1	S2	S3	S4	R1	L1	B1
Sample weight (g)	0.0127	0.0892	0.1005	0.0966	0.5052		1.01142
Lu (ppm)*	0.0007	0.0486	0.0511	0.0490			
Hf (ppm)*	0.2192	0.1168	0.1402	0.1280			
$^{176}Lu/^{177}Hf$*	0.0005	0.0592	0.0518	0.0545			
$^{176}Hf/^{177}Hf$ (±2 SE)*	0.280029 ± 0.000030	0.284686 ± 0.000016	0.284116 ± 0.000011	0.284290 ± 0.000010			
$\varepsilon^{176}Hf_{(today)}$ (±2 SD)	−97.12 ± 1.06	67.58 ± 0.56	47.42 ± 0.38	53.59 ± 0.37			
$\varepsilon^{176}Hf_{(4.09\ Ga)}$ (±2 SD)	−4.66 ± 1.06	−3.84 ± 0.97	−4.37 ± 0.89	−5.15 ± 0.92			
$d\varepsilon^{176}Hf/d$Ga	0.32	39.08	34.21	35.97			
Sm (ppm)*		0.0562	0.1587	0.0925	0.0344	(12.57 ng)	
Nd (ppm)*		0.1003	0.5165	0.2476	0.0540	(47.71 ng)	
$^{147}Sm/^{144}Nd$*		0.3387	0.1857	0.2258	0.3850	0.1594	
$^{143}Nd/^{144}Nd$ (±2 SE)*		0.516738 ± 0.000014	0.512266 ± 0.000004	0.513453 ± 0.000005	0.518544 ± 0.000008	0.511214 ± 0.000005	0.513226 ± 0.000002
$\varepsilon^{143}Nd_{(today)}$ (±2 SD)		80.00 ± 0.28	−7.24 ± 0.08	15.92 ± 0.09	115.23 ± 0.15	−27.76 ± 0.09	
$\varepsilon^{143}Nd_{(4.09\ Ga)}$ (±2 SD)		4.79 ± 0.38	−1.60 ± 0.21	0.37 ± 0.25	15.61 ± 0.43	−8.29 ± 0.18	
$\varepsilon^{142}Nd$ (±2 SE)							−0.23 ± 0.05

*Concentrations and isotope ratios are corrected for the following blank values: 18 pg Lu; 80 pg Hf with $^{176}Hf/^{177}Hf = 0.2822$; 20 pg Sm; and 50 pg Nd with $^{143}Nd/^{144}Nd = 0.5116$.

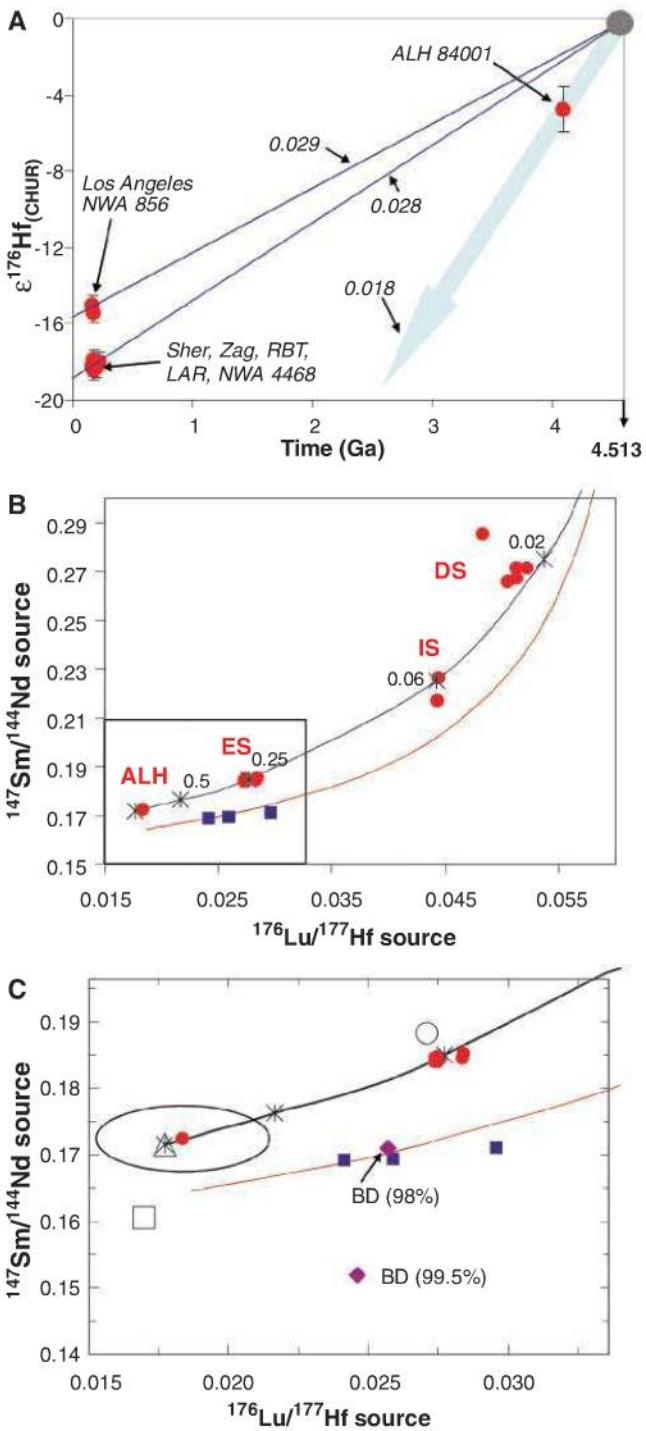

Fig. 2. (**A**) Hf isotope evolution diagram relative to CHUR (*33*) of sources for enriched shergottites RBT 04262 (RBT), NWA 4468, Shergotty (Sher), Zagami (Zag), LAR 06319 (LAR), Los Angeles, and NWA 856 (*24*, *30*, *37*–*40*) as well as ALH. There are different recent interpretations of the ages of the shergottites. We have calculated all of the source $^{176}Lu/^{177}Hf$ and $^{147}Sm/^{144}Nd$ ratios of shergottites assuming that their igneous crystallization ages are given by their internal isochron ages (0.15 to 0.57 Ga) (*11*, *23*, *24*, *29*, *38*–*40*), not their older Pb-Pb ages (~4.1 Ga) (*4*, *38*, *39*); see (*20*) for further discussion. The isotopic evolution of the sources for the plotted samples is based on a two-stage model (*23*, *29*) where the sources formed from a chondritic reservoir at 4.513 Ga. The $^{176}Lu/^{177}Hf$ source values are indicated by the numbers referencing the isotopic evolution lines. (**B**) Mixing diagram for shergottites and ALH $^{147}Sm/^{144}Nd$ and $^{176}Lu/^{177}Hf$ source compositions. Red dots, shergottites; DS, depleted shergottites DaG 476, QUE 94201, SaU 094, DaG 476, and SaU 008; IS, intermediate shergottites EETA 79001 and ALH 77005; ES, enriched shergottites RBT 04262, LAR 06319, Shergotty, Zagami, NWA 4468, NWA 856, and Los Angeles; ALH, ALH 84001. The black binary mixing line is based on source compositions of residual trapped liquid (RTL) and cumulates in the upper mantle assemblage (UM1) of (*30*) produced in MO 2000 to 1350 km deep. The red mixing line was calculated with source end-member compositions used in (*23*). Blue squares are calculated sources for KREEP-rich lunar basalts. Isotope data used for the source calculations of shergottites come from (*21*, *23*, *24*, *29*, *30*, *37*–*40*). Labeled mixing proportions (black symbols) are based on the fractions of RTL. (**C**) Enlargement of boxed area of (B). Solid symbols are defined as in (B) and represent calculated source compositions; open symbols represent the $^{147}Sm/^{144}Nd$ and $^{176}Lu/^{177}Hf$ compositions of liquid in equilibrium with cumulates during MO crystallization (*30*). For MO 2000 to 1350 km deep, the open square represents RTL in the shallow upper mantle after 98% MO crystallization, the open triangle represents RTL in the upper mantle [UM1 of (*30*)] after 90 to 94% crystallization, and the open circle is RTL in the upper mantle [UM2 of (*30*)] after ~66% crystallization. Enriched end-member compositions (*31*) are labeled BD; percent values represent degree of MO crystallization. Ellipse reflects 2σ error of calculated source compositions for ALH.

member is nearly identical to its calculated source composition. The enriched component likely represents deep (200 to 750 km) residual trapped liquid (RTL) equilibrated with cumulates after ~93% MO crystallization (*30*) (Fig. 2C). This component is unlike that derived from shallow, very late-stage liquids remaining after >98% MO crystallization that explains lunar KREEP (*31*) (Fig. 2C). Additionally, cumulates in equilibrium with this RTL are a good match for the composition of the depleted mantle end-member composition as evidenced by shergottite source modeling (*30*) and our finding that mixtures of these two components can generate the observed sources of shergottites and ALH that range in age from 0.165 to 4.091 Ga (Fig. 2B). Therefore, it is likely that similar magmatic source regions in Mars that produced the long-lived Tharsus and Elysium volcanic regions have been producing magmas for at least the past 4 billion years.

The igneous crystallization of ALH occurred at 4.091 ± 0.030 Ga, during a period of intense bombardment and slightly prior to cessation of the Mars global magnetic field (*15*, *16*, *32*). As such, the magnetic properties of the igneous phases in ALH (*17*) do not record early planetary magnetic fields, as implied for a crystallization age of ~4.5 Ga, and must instead reflect conditions after accretion and ~400 million years of cooling in Mars. The Lu-Hf age requires a much shorter time interval between igneous formation and aqueous alteration at 4.04 ± 0.10 to 3.90 ± 0.04 Ga, necessitating a revision of the timing of pre-alteration textures (*13*). The younger age predicts that the primordial martian crust was likely largely destroyed from intense bombardment at 4.25 to 4.1 Ga (*15*).

References and Notes

1. E. Jagoutz, A. Sorowka, J. D. Vogel, H. Wanke, *Meteoritics* **29**, 478 (1994).
2. L. E. Nyquist, B. M. Bansal, H. Wiesmann, C.-Y. Shih, *Lunar Planet. Sci. Conf.* **26**, 1065 (1995).
3. M. Wadhwa, G. Lugmair, *Meteorit. Planet. Sci.* **31**, A145 (1996).
4. A. Bouvier, J. Blichert-Toft, F. Albarède, *Earth Planet. Sci. Lett.* **280**, 285 (2009).
5. E. Jagoutz *et al.*, *Lunar Planet. Sci. Conf.* **40**, 1662 (2009).
6. G. Turner, S. F. Knott, R. D. Ash, J. D. Gilmour, *Geochim. Cosmochim. Acta* **61**, 3835 (1997).
7. S. Ilg *et al.*, *Meteorit. Planet. Sci.* **32**, A65 (1997).
8. D. D. Bogard, D. H. Garrison, *Meteorit. Planet. Sci.* **34**, 451 (1999).
9. L. E. Borg *et al.*, *Science* **286**, 90 (1999).
10. K. Terada, T. Monde, Y. Sano, *Meteorit. Planet. Sci.* **38**, 1697 (2003).
11. L. E. Nyquist *et al.*, *Space Sci. Rev.* **96**, 105 (2001).
12. K. L. Thomas-Keprta, S. J. Clemett, D. S. McKay, E. K. Gibson, S. J. Wentworth, *Geochim. Cosmochim. Acta* **73**, 6631 (2009).
13. A. H. Treiman, *Meteorit. Planet. Sci.* **33**, 753 (1998).
14. A. Bouvier, J. Blichert-Toft, F. Moynier, J. Vervoort, F. Albarede, *Geochim. Cosmochim. Acta* **71**, 1583 (2007).
15. H. V. Frey, *Geophys. Res. Lett.* **35**, L13203 (2008).
16. R. J. Lillis, H. V. Frey, M. Manga, *Geophys. Res. Lett.* **35**, L14203 (2008).
17. B. P. Weiss *et al.*, *Earth Planet. Sci. Lett.* **201**, 449 (2002).
18. T. Kleine *et al.*, *Geochim. Cosmochim. Acta* **73**, 5150 (2009).
19. C. Meyer, Mars meteorite compendium, NASA-ARES JSC #27672 Revision C (2008).

20. See supporting material on *Science* Online.
21. V. Debaille, A. D. Brandon, Q. Z. Yin, B. Jacobsen, *Nature* **450**, 525 (2007).
22. $\varepsilon^{176}Hf_{CHUR} = ({}^{176}Hf/{}^{177}Hf_{CHUR}/{}^{176}Hf/{}^{177}Hf_{CHUR} - 1) \times 10{,}000$; CHUR refers to chondritic uniform reservoir model values for the Lu-Hf, as well as Sm-Nd, isotope systems. Hf and Nd CHUR reference values are from (*33*) and references therein.
23. L. E. Borg *et al.*, *Geochim. Cosmochim. Acta* **67**, 3519 (2003).
24. T. J. Lapen *et al.*, *Lunar Planet. Sci. Conf.* **40**, 2376 (2009).
25. J. A. Barrat, C. Bollinger, *Meteorit. Planet. Sci.* **44** (suppl.), abstr. 5106 (2009) (www.lpi.usra.edu/meetings/metsoc2009/pdf/5106.pdf).
26. J. H. Jones, *Lunar Planet. Sci. Conf.* **19**, 465 (1989).
27. D. Rumble, A. J. Irving, *Lunar Planet. Sci. Conf.* **40**, 2293 (2009).
28. A. D. Brandon *et al.*, *Geochim. Cosmochim. Acta* **64**, 4083 (2000).
29. L. E. Borg *et al.*, *Geochim. Cosmochim. Acta* **61**, 4915 (1997).
30. V. Debaille, Q.-Z. Yin, A. D. Brandon, B. Jacobsen, *Earth Planet. Sci. Lett.* **269**, 186 (2008).
31. L. E. Borg, D. S. Draper, *Meteorit. Planet. Sci.* **38**, 1713 (2003).
32. J. H. Roberts, R. J. Lillis, M. Manga, *J. Geophys. Res.* **114**, (E4), E04009 (2009).
33. A. Bouvier, J. Vervoort, P. Patchett, *Earth Planet. Sci. Lett.* **273**, 48 (2008).
34. K. R. Ludwig, *Berkeley Geochronology Center Spec. Pub. 1a*, 59 (2003).
35. E. E. Scherer, C. Münker, K. Mezger, *Science* **293**, 683 (2001).
36. M. Wadhwa, G. Crozaz, *Meteorit. Planet. Sci.* **33**, 1713 (1998).
37. J. Blichert-Toft *et al.*, *Earth Planet. Sci. Lett.* **173**, 25 (1999).
38. A. Bouvier, J. Blichert-Toft, J. D. Vervoort, F. Albarède, *Earth Planet. Sci. Lett.* **240**, 221 (2005).
39. A. Bouvier, J. Blichert-Toft, J. D. Vervoort, P. Gillet, F. Albarède, *Earth Planet. Sci. Lett.* **266**, 105 (2008).
40. C.-Y. Shih, L. E. Nyquist, Y. Reese, *Lunar Planet. Sci. Conf.* **40**, 1360 (2009).

41. Supported by NASA Cosmochemistry grants (T.J.L. and A.D.B.), a NASA Astrobiology grant (B.L.B.), the University of Houston Institute for Space Systems Operations (T.J.L.), and the Belgian Fund for Scientific Research (V.D.). We thank three anonymous reviewers for improving the clarity of the manuscript.

Supporting Online Material

www.sciencemag.org/cgi/content/full/328/5976/347/DC1
Materials and Methods
Figs. S1 to S5
References

1 December 2009; accepted 3 March 2010
10.1126/science.1185395

Evolution of an Expanded Sex-Determining Locus in *Volvox*

Patrick Ferris,[1]* Bradley J. S. C. Olson,[1]* Peter L. De Hoff,[1] Stephen Douglass,[2] David Casero,[2] Simon Prochnik,[3] Sa Geng,[1] Rhitu Rai,[1,4] Jane Grimwood,[5] Jeremy Schmutz,[5] Ichiro Nishii,[6] Takashi Hamaji,[7] Hisayoshi Nozaki,[7] Matteo Pellegrini,[2] James G. Umen[1]†

Although dimorphic sexes have evolved repeatedly in multicellular eukaryotes, their origins are unknown. The mating locus (*MT*) of the sexually dimorphic multicellular green alga *Volvox carteri* specifies the production of eggs and sperm and has undergone a remarkable expansion and divergence relative to *MT* from *Chlamydomonas reinhardtii*, which is a closely related unicellular species that has equal-sized gametes. Transcriptome analysis revealed a rewired gametic expression program for *Volvox MT* genes relative to *Chlamydomonas* and identified multiple gender-specific and sex-regulated transcripts. The retinoblastoma tumor suppressor homolog *MAT3* is a *Volvox MT* gene that displays sexually regulated alternative splicing and evidence of gender-specific selection, both of which are indicative of cooption into the sexual cycle. Thus, sex-determining loci affect the evolution of both sex-related and non–sex-related genes.

Sexually dimorphic gametes have evolved in every major group of eukaryotes, and are thought to be selected when parents can differentially allocate resources to progeny (*1*). However, the origins of oogamy (large eggs and small sperm) and the contribution of sex-determining loci to such evolution are largely unknown (*2*, *3*) [see the glossary of terms (*4*) for further explanation of terminology].

The Volvocine algae are a group of chlorophytes comprising unicellular species, such as *Chlamydomonas reinhardtii* (hereafter *Chlamydomonas*), and a range of multicellular species of varying complexity, such as *Volvox carteri* (hereafter *Volvox*). *Volvox* has a vegetative reproductive form containing 16 large germ cells (gonidia) and ~2000 terminally differentiated somatic cells (fig. S1) (*4*, *5*).

Chlamydomonas and other Volvocine algae also undergo a sexual cycle in which a large, haploid mating locus (*MT*) controls sexual differentiation, mating compatibility, and zygote development (*6*). *MT* in *Chlamydomonas* is a 200- to 300-kb multigenic chromosomal region (Fig. 1A) within which gene order is rearranged between the two sexes (*MT*+ and *MT*–) and meiotic recombination is suppressed, thus leading to its inheritance as a single Mendelian trait. Within each *MT* allele are gender-limited genes (allele present in only one of the two sexes), which are required for the sexual cycle, as well as shared genes (alleles present in both sexes), most of which have no known function in sex or mating (*7*). The rearrangements that suppress recombination serve to maintain linkage of gender-limited genes, but they also reduce genetic exchange between shared genes, leading to their meiotic isolation. Thus, *Chlamydomonas MT* bears similarity to sex chromosomes and to expanded mating-type regions of some fungi and bryophytes (*8*–*10*).

Although *Chlamydomonas* is isogamous (producing equal-sized gametes), *Volvox* and several other Volvocine genera have evolved oogamy that is under the control of female and male *MT* loci (fig. S1) (*11*). Moreover, the *Volvox* sexual cycle is characterized by a suite of other traits not found in *Chlamydomonas*, such as a diffusible sex-inducer protein rather than nitrogen deprivation (–N) as a trigger for gametogenesis (table S1). A detailed characterization of *MT* in *Volvox* would be expected to shed light on the transition from isogamy to oogamy and on other properties of the sexual cycle that evolved in this multicellular species (table S1).

The *MT*+ allele of *Chlamydomonas* was previously sequenced and resides on chromosome 6 (Fig. 1A and fig. S2) (*12*). To enable a comparison of mating loci evolution between two related species with markedly different sexual cycles, we sequenced *Chlamydomonas MT*– and both alleles of *Volvox MT* (Fig. 1 and table S2) (*4*). *Volvox MT* was previously assigned to linkage group I (LG I) (*5*), but the locus had not been further characterized. We mapped *Volvox MT* to the genome sequence and assembled most of LG I (table S3) (*4*). Extensive synteny with *Chlamydomonas* chromosome 6 indicates that *MT* has remained on the same chromosome in both lineages for ~200 million years since their estimated divergence, despite numerous intrachromosomal rearrangements between the two (fig. S2) (*13*).

Although the haploid *Volvox* genome is ~17% larger than that of *Chlamydomonas* (138 Mb versus 118 Mb) and the two have very similar predicted proteomes (*12*, *14*), *Volvox MT* is ~500% larger than *Chlamydomonas MT* and contains over 70 protein-coding genes in each allele (Fig. 1B and tables S4 and S5). Compared with autosomes, *Volvox MT* is unusually repeat-rich (greater than three times the genomic average), has lower gene density, and has genes with more intronic sequence (table S6), all of which are properties that suggest an unusual evolutionary history and distinguish it from *Chlamydomonas MT*.

Only two gender-limited genes from *Chlamydomonas MT*–, *MID* and *MTD1*, have recognizable homologs in *Volvox* that are both in male *MT*

[1]The Salk Institute for Biological Studies, La Jolla, CA 92037, USA. [2]Institute for Genomics and Proteomics and Department of Molecular, Cell and Developmental Biology, University of California, Los Angeles, CA 90095, USA. [3]U.S. Department of Energy (DOE) Joint Genome Institute (JGI), Walnut Creek, CA 95498, USA. [4]Laboratory of Plant Microbe Interaction, National Research Center on Plant Biotechnology, Pusa Campus, Indian Agricultural Research Institute, New Delhi 110012, India. [5]Genome Sequencing Center, Hudson Alpha Institute for Biotechnology, Huntsville, AL 35806, USA. [6]Department of Biological Science, Nara Women's University, Nara 630-8506, Japan. [7]Department of Biological Sciences, University of Tokyo, Tokyo 113-0033, Japan.

*These authors contributed equally to this work.
†To whom correspondence should be addressed. E-mail: umen@salk.edu

30. D. Bachtrog, *Curr. Opin. Genet. Dev.* **16**, 578 (2006).

31. We thank D. Kirk for DNA from *Volvox* mapping populations. We thank V. Lundblad and S. Merchant for advice on the manuscript. This work was supported by the Coypu Foundation and from grants NIH R01 GM078376 to J.G.U.; NIH F32 GM086037 to B.O.; Japan Society for the Promotion of Science grant S05750/L06701 to P.F.; Grant-in-Aid for Scientific Research (20247032) from the Ministry of Education, Culture, Sports, Science and Technology, Japan to H.N.; NIH grant T32-HG002536 to S.D.; and DE-FC02-02ER63421 and AFOSR to M.P. DOE-JGI provided sequencing and analyses for algal mating loci under the Community Sequencing Program (776835) supported by the Office of Science of DOE under contract DE-AC02-05CH11231. Sequencing of the *V. carteri* genome was performed under the auspices of DOE's Office of Science, Biological and Environmental Research Program and by the University of California, Lawrence Berkeley National Laboratory under contract DE-AC02-05CH11231, Lawrence Livermore National Laboratory under contract DE-AC52-07NA27344, and Los Alamos National Laboratory under contract DE-AC02-06NA25396. Sequences generated in this study have been deposited in GenBank under accession numbers GU814014, GU814015, GU784915, GU784916, and GU735444-GU735478. Materials used in this study will be made available upon request with the completion of a Materials Transfer Agreement from Salk Institute.

Supporting Online Material

www.sciencemag.org/cgi/content/full/328/5976/351/DC1
Materials and Methods
SOM Text
Figs. S1 to S17
Tables S1 to S15
References

22 December 2009; accepted 12 March 2010
10.1126/science.1186222

Resolving Mechanisms of Competitive Fertilization Success in *Drosophila melanogaster*

Mollie K. Manier, John M. Belote, Kirstin S. Berben, David Novikov, Will T. Stuart, Scott Pitnick*

Our understanding of postcopulatory sexual selection has been constrained by an inability to discriminate competing sperm of different males, coupled with challenges of directly observing live sperm inside the female reproductive tract. Real-time and spatiotemporal analyses of sperm movement, storage, and use within female *Drosophila melanogaster* inseminated by two transgenic males with, respectively, green and red sperm heads allowed us to unambiguously discriminate among hypothesized mechanisms underlying sperm precedence, including physical displacement and incapacitation of "resident" sperm by second males, female ejection of sperm, and biased use of competing sperm for fertilization. We find that competitive male fertilization success derives from a multivariate process involving ejaculate-female and ejaculate-ejaculate interactions, as well as complex sperm behavior in vivo.

Remating with different males by females generates sexual conflict over paternity (*1*) and sets the stage for postcopulatory sexual selection (*2*–*4*), which can drive diversification of both male and female biochemistry, physiology, morphology, and behavior (*4*, *5*). Most investigations of postcopulatory sexual selection have focused on the pattern of sperm precedence, such as the proportion of progeny sired by the second of two males subsequent to female remating (P_2). However, without knowledge of underlying mechanisms, these patterns reveal little about the intensity of selection or sex-specific adaptation (*4*–*6*). Consequently, even with *Drosophila melanogaster*, there is contention over the mechanisms giving rise to the roughly 80% last-male sperm precedence observed (*7*–*12*). Our understanding of these and other phenomena has been constrained by the technical challenge of directly observing sperm dynamics within the female reproductive tract and our limited ability to discriminate between sperm of different males (*7*, *13*, *14*).

We have overcome these challenges by transforming *D. melanogaster* to express a protamine labeled with green fluorescent protein (GFP) or red fluorescent protein (RFP) in sperm heads, which can be easily observed and unambiguously differentiated within the female reproductive tract (figs. S1 and S2 and movies S1 to S3). These lines enable direct visualization of sperm competition in vivo, in real time, and over extensive periods of time, allowing us to discriminate among alternative hypothesized mechanisms of sperm precedence. Multiple indices of male fitness relevant to sperm and/or ejaculate function were assayed, with transgenic males compared with each other and with a wild-type LH_m strain (into which the GFP and RFP constructs were backcrossed for six generations). Although some significant differences were found, with transformed lines performing less well, equivalent to, or better than the wild type in different fitness assays, all three strains fell within the typical range of values reported in the literature for all assays (figs. S3 to S7), which suggested there was no dysfunction of transformant sperm. Moreover, results of the sperm precedence experiments reported below are unbiased, because GFP and RFP males (i) were competed using a reciprocal mating order design and (ii) did not differ in female remating interval, P_1, or P_2 in those experiments (*15*).

We quantified (i) spatiotemporal patterns of sperm storage and use by the female after remating, (ii) the extent and timing of sperm ejection by females, and (iii) the influence of remating on resident sperm motility. Unless otherwise specified, in all experiments, 3-day-old, virgin LH_m females were randomly assigned to all treatment groups, initially mated to a GFP or an RFP male, and, beginning 3 days later (the typical remating latency for *D. melanogaster*), provided a daily, 6-hour opportunity to remate to a male of the alternative genotype (reciprocal male mating order balanced). All copulations were observed, and copulation durations recorded (*15*).

Department of Biology, Syracuse University, Syracuse, NY 13244–1270, USA.

*To whom correspondence should be addressed. E-mail: sspitnic@syr.edu

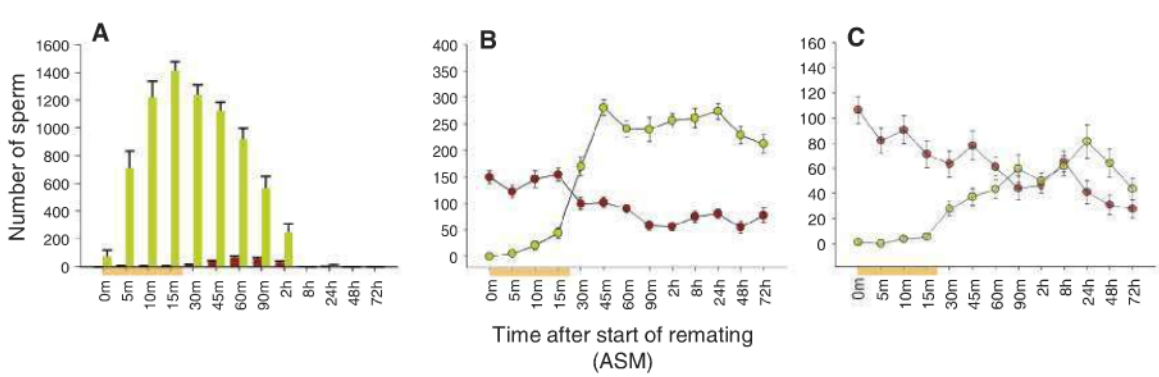

Fig. 1. Numbers of first-male (red) and second-male (yellow) sperm in the **(A)** bursa, **(B)** seminal receptacle, and **(C)** spermathecae for 13 time points ASM, averaged over two experimental replicates and both reciprocal mating orders. Error bars represent SEM.

To quantify temporal dynamics of sperm fate, females in two experimental replicates were flash-frozen at randomly assigned times after the start of the second mating (ASM): 0 min (immediately after second male mounting), 5 min, 10 min, 15 min, 30 min, 45 min, 60 min, 2 hours, 8 hours, and 24 hours, with three additional time points in the second replicate: 90 min, 48 hours, and 72 hours. For the last three time treatments of the second replicate (24 hours, 48 hours, 72 hours), all progeny were reared, and the proportion sired by the second male (P_2) was determined by assaying all sons for green or red sperm. Frozen females were dissected, and red and green sperm were counted in the bursa (the site of insemination), paired spermathecae (including spermathecal ducts), and the seminal receptacle (SR), distinguishing between the proximal and distal halves. For illustrative purposes, results from both replicates and male mating orders are combined in Fig. 1 [individual replicates and male mating orders shown in figs. S8 to S10; see (*15*) for tests of differences], with sample sizes per time treatment ranging from 30 to 50 females (total $N = 543$) (table S1).

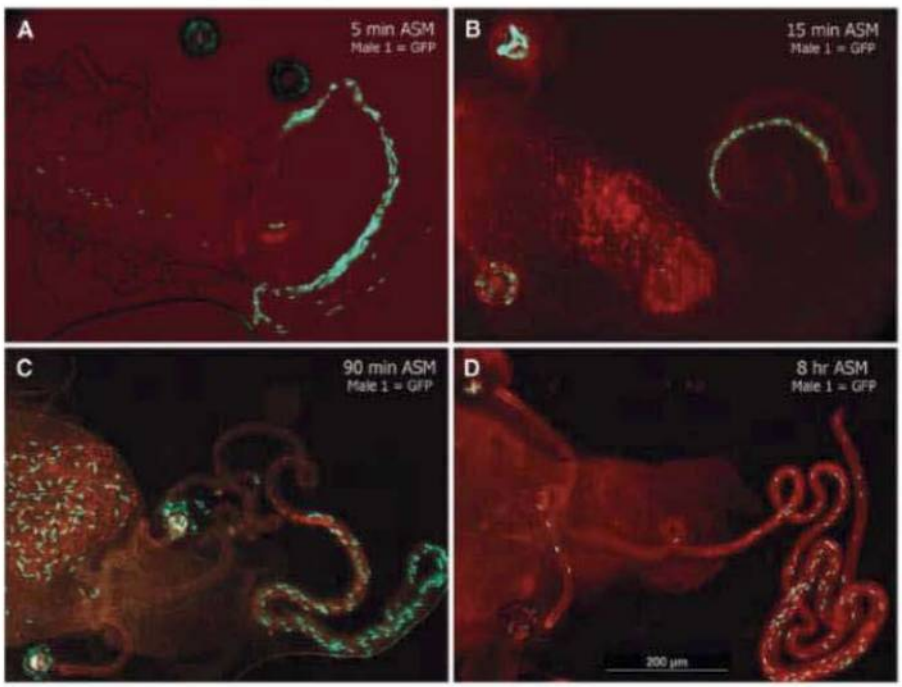

Fig. 2. Representative female reproductive tracts at (**A**) 5 min, (**B**) 15 min, (**C**) 90 min, and (**D**) 8 hours ASM, showing relative abundances and locations of first-male (GFP) and second-male (RFP) sperm.

Fig. 3. Ejected sperm mass containing both first-male (GFP) and second-male (RFP) sperm under (**A**) differential interference contrast and (**B**) fluorescence.

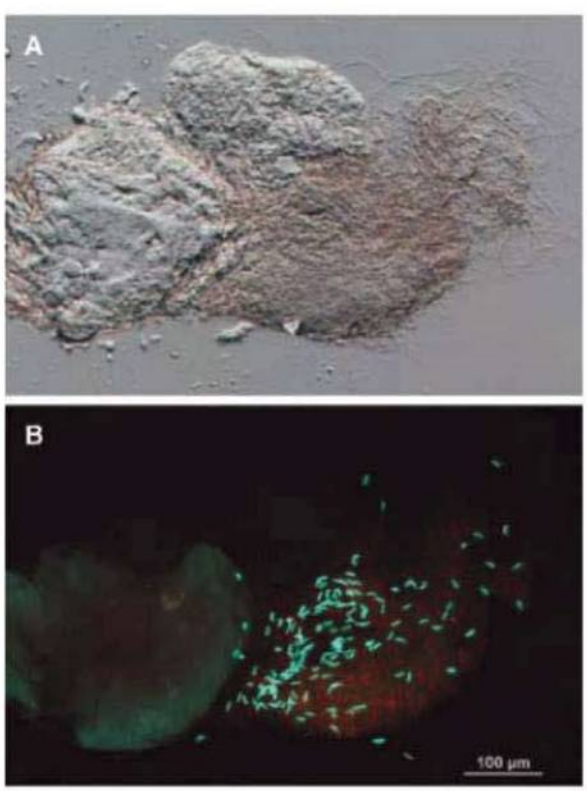

We revealed two different mechanisms by which resident sperm are displaced from the sperm-storage organs after remating and which contribute to last-male sperm precedence. First, there was an early release of some resident sperm from storage into the bursa, a process that does not involve second-male sperm. Second, resident sperm appear to have been physically displaced over time from both the SR and the spermathecae by incoming second-male sperm. Wild-type females store ~400 sperm at maximum in their SR and 130 sperm in the paired spermathecae (Fig. 1). Upon remating (i.e., time 0 ASM), resident sperm were depleted from this maximum capacity, because sperm were used for fertilization over the preceding days to 149 (± 12) sperm in the SR and 108 (± 11) sperm in the spermathecae. Resident sperm were rarely observed in the bursa (Fig. 1) or in the spermathecal ducts at time 0. Insemination of second-male sperm began as early as 5 min ASM (25 out of 46 cases or 54% of the time), and in 19% of cases where second-male sperm had not yet been transferred (5 out of 26), some resident sperm (17 ± 5) were observed in the bursa 5 to 10 min ASM (Figs. 1 and 2). We also saw first-male sperm in the bursa in 14% of observations where second-male sperm had been transferred but had not yet entered storage (5 out of 37). This release of resident sperm was presumptively female mediated and triggered by male accessory gland proteins (Acps) and/or mechanical stimulation of copulation.

First-male sperm continued to be displaced as second-male sperm entered storage, soon after insemination (the SR earlier than the spermathecae) (Fig. 1) (*16*). Sperm transfer peaked at 15 min ASM (1412 ± 66 sperm, or ~2.7 times the female's storage capacity), after which second-male sperm steeply declined in the bursa, while resident sperm steadily increased. Although sperm storage leveled off around 45 min ASM, the first- and second-male sperm proportions continued to change, with displacement peaking 60 to 90 min ASM (Fig. 1), when 26% of resident stored sperm had been relocated into the bursa. Although this process is likely to displace some of the second male's own sperm (*17*), it will also increase the proportion of second-male sperm in storage (as observed) because of their overrepresentation in the bursa. This outcome also depends on active motility within the storage organs (movies S1 to S3) and adequate mixing of first- and second-male sperm, consistent with our observations (fig. S11 and movies S4 and S5). Competing sperm were highly stratified during and immediately after

(Fig. 1 and figs. S3 and S4). *MID* is a conserved RWP-RK family transcription factor whose expression in other Volvocine algae is induced by –N (*15*–*17*), as is also the case for *MTD1* (*18*, *19*). Both *MTD1* and *MID* are expressed constitutively in *Volvox* (fig. S5), indicating that their transcription is uncoupled from sexual differentiation. This result suggests that additional *MT* genes might play a role in gametogenesis.

We used differential deep transcriptome sequencing (tables S7 and S8) (*4*) to identify *MT* genes in *Volvox*, a method that helped to mitigate problems associated with automated gene prediction in atypical genomic regions such as *MT*. We identified transcripts for five new female-limited and eight new male-limited genes that do not have detectable homologs in *Chlamydomonas* and found that most of these gender-limited genes are sex-regulated (expression was induced or repressed during sexual differentiation) (Fig. 1C and table S9) (*4*). *HMG1* encodes a female-limited HMG domain protein (figs. S6 and S7 and table S10) that belongs to a family of DNA-binding proteins whose members regulate mammalian and fungal sex determination (*20*, *21*). However, HMG proteins had not been previously implicated in the sexual cycles of green algae or plants. A second previously unknown female-limited gene, *FSI1*, is strongly induced during gametogenesis and encodes a small predicted transmembrane protein with no identifiable homologs (Fig. 1C and fig. S7).

Besides identification of new gender-limited genes, our transcriptome data provided empirical support for 51 of 52 single-copy shared genes in *Volvox MT* that previously had limited expressed sequence tag (EST) support for the female allele (33 of 52) and no EST support for the male allele. Moreover, some of these shared genes showed patterns of expression that suggest co-option into the *Volvox* sexual cycle. These patterns include gender-biased expression (male:female expression ratio ≠ 1) and sex-regulated expression (Fig. 1C and fig. S7) (*4*). This set of genes encodes putative signaling, extracellular matrix, and chromatin-associated proteins with known or potential roles in gametogenesis and fertilization and are candidates for further investigation (fig. S7).

In diploid species, heterogametic sex chromosomes evolve rapidly (*22*) and lose genes that are not related to sex (*23*). Because of suppressed recombination, genes within large haploid mating loci are predicted to accumulate mutations more rapidly than would genes in autosomal regions, but they are continuously exposed to selection (*24*). Suppressed recombination also appears to have played a role in diversification of mating locus–linked genes in haploid fungi and bryophytes (*8*–*10*). Our data allowed us to compare the evolutionary history of *Volvox MT* genes from this oogamous species to each other and to genes from *MT* of its isogamous relative *Chlamydomonas*.

Divergence was measured from synonymous (d_S) and nonsynonymous (d_N) substitutions (Fig.

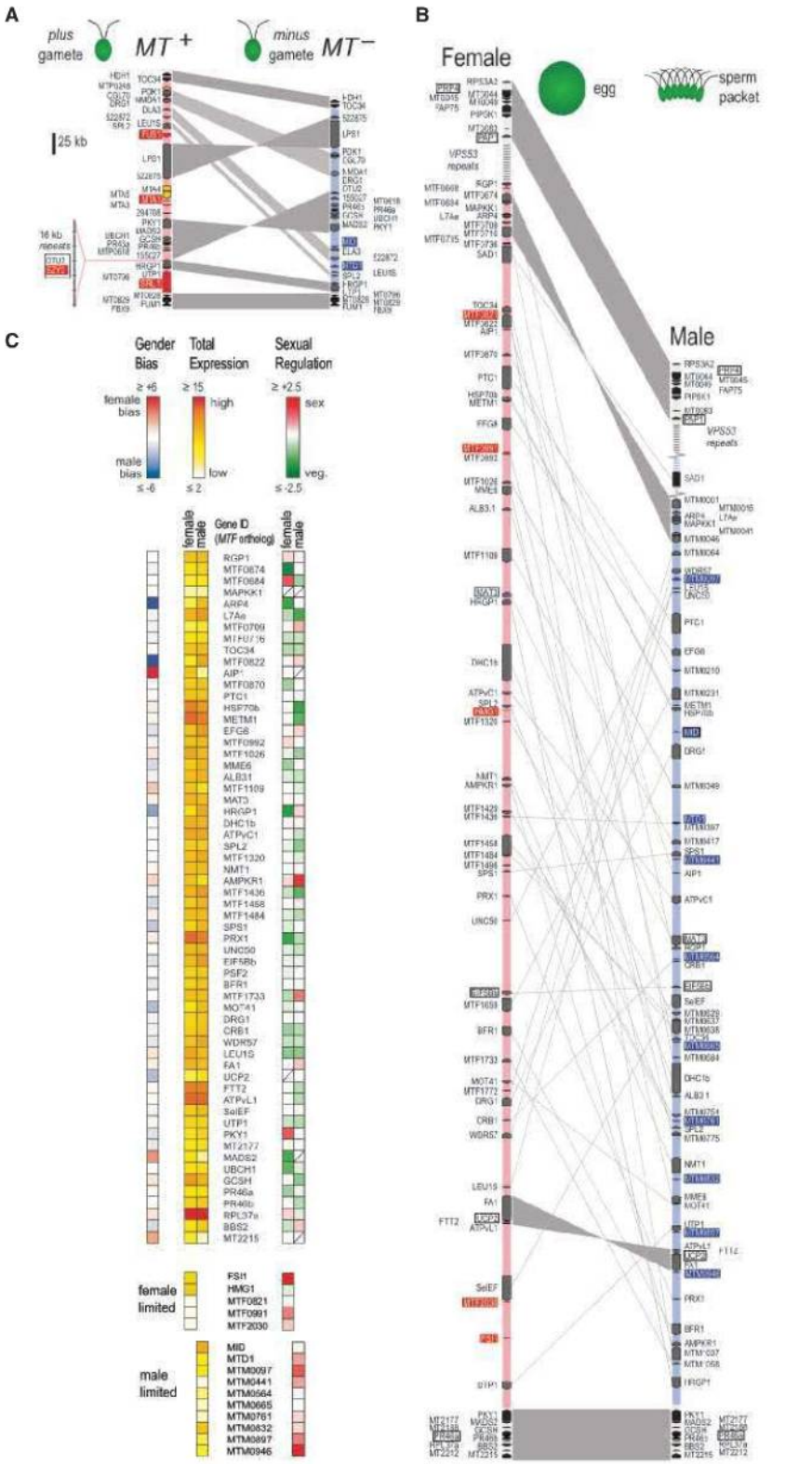

Fig. 1. Expansion of *Volvox MT* and sex-regulated gene expression. (**A**) Schematic of *Chlamydomonas* mating locus with rearranged domains in light blue or pink. *MT*+-limited genes are shaded red if unique or orange if they have an autosomal copy. *MT*−-limited genes are shaded blue. Flanking and shared genes are shaded black and gray, respectively. Synteny is indicated by gray shading. (**B**) Schematic of *Volvox MT* scaled as in (A). Boxed genes were used for mapping. The broken segment represents a transposon repeat region containing copies of *VPS53*. (**C**) Expression heat maps of *Volvox MT* genes. (Left) Female/male expression ratio. (Middle) Total expression. (Right) Sexual induction (Sex) or repression (Veg). Diagonal hatch indicates insufficient data.

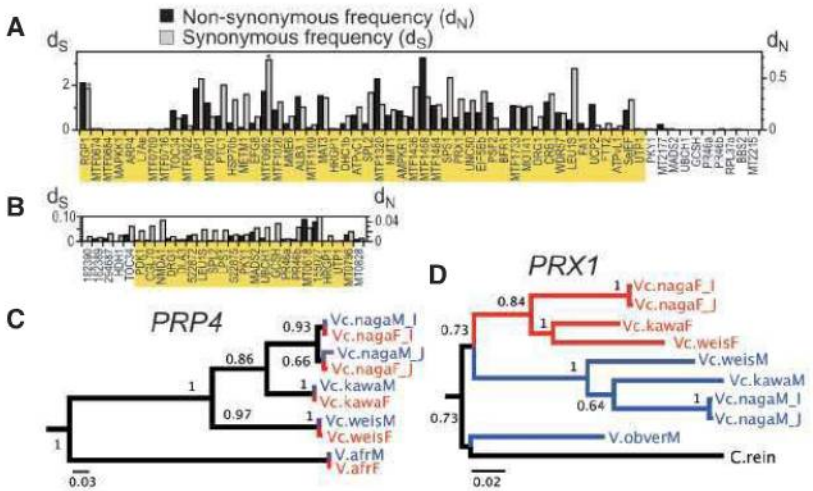

Fig. 2. Divergence of *MT* genes. (**A** and **B**) d_N and d_S for shared *Volvox* (A) or *Chlamydomonas* (B) genes within *MT* (orange shading) or flanking *MT*. Asterisks indicate saturated d_S values. (**C** and **D**) Maximum likelihood phylogenies for *PRP4* (C) and *MT* gene *PRX1* (D). Red and blue respectively indicate female and male strains and clades.

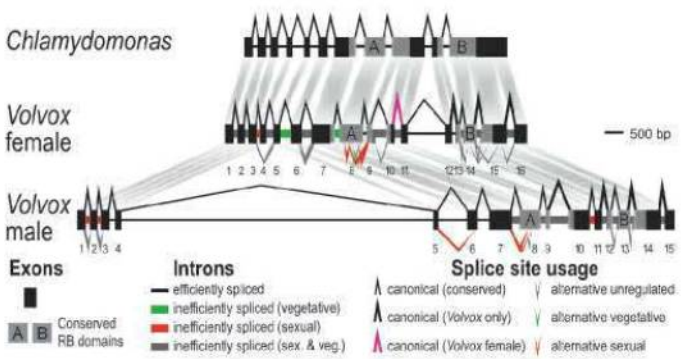

Fig. 3. Gender-specific divergence and splicing of *MAT3*. Shown is a schematic of *MAT3* from *Chlamydomonas* (top), *Volvox* female (middle), and *Volvox* male (bottom). *Volvox* exons are numbered.

2, A and B) and from total nucleotide distances for shared genes (tables S11 and S12) (*4*). Unexpectedly, divergence for *Volvox MT* allelic pairs is up to two orders of magnitude larger than for allelic pairs in *Chlamydomonas MT*, suggesting that *Volvox MT* alleles may have been subject to more intense and/or more prolonged recombinational suppression than *Chlamydomonas MT* alleles have been. In contrast, two internal syntenic blocks within *Volvox MT* are relatively similar (Figs. 1B and 2A), suggesting that they were acquired more recently in an ongoing stratification process as first described for the human X chromosome (*25*). *Volvox MT* genes also showed reduced codon usage bias relative to autosomal genes (fig. S8), which is most likely due to suppressed recombination (*26*).

We sequenced three *MT* genes and a flanking gene, *PRP4*, from a set of related *Volvox* species in order to determine the extent of *MT* gene isolation (*4*). Phylogenies revealed the expected pattern for *PRP4*, which grouped by species and geographical location (Fig. 2C). In contrast, the *MT* genes grouped by gender (Fig. 2D and fig. S9). These data demonstrate that the shared genes in *Volvox MT* have essentially become gender-specific and have remained genetically isolated during speciation. Thus, the *MT* locus in *Volvox* has become a repository of genetic diversity that is linked to the sexual cycle.

In *Chlamydomonas*, the retinoblastoma (RB) tumor suppressor pathway controls cell division in response to cell size (*27*), and the RB homolog encoded by *MAT3* is adjacent to *MT* (*28*). *Volvox MAT3*, on the other hand, is within *MT* (Fig. 1B), and we investigated its evolution and expression as a candidate regulator of sexually dimorphic cell divisions (fig. S1). The *Volvox* male and female MAT3 proteins are exceptionally diverged from each other (figs. S9 to S11). Moreover, male and female *Volvox MAT3* have different structures: The female allele contains an intron that is absent from males, whereas the male allele contains an unusually large fourth intron as compared with that of females (Fig. 3). Although *MAT3* shows signs of having undergone purifying selection (d_N/d_S = 0.23) (table S11), several short sequences in the male and female proteins are asymmetric in their conservation pattern, suggesting that the two alleles are under different selective constraints (figs. S10 and S11). We also found dozens of alternatively processed *MAT3* mRNAs from both *Volvox* sexes, representing most types of alternative splicing (Fig. 3 and fig. S12) (*29*). In addition, sex-regulated pre-mRNA splicing of *MAT3* was found for both genders and might be controlled by the *MT*-encoded splicing factor *SPL2*, whose expression level is sex-regulated in males (Fig. 1C and fig. S13). The predominant *MAT3* isoform in sexual males retains the first two introns, leading to inclusion of an early termination codon (Fig. 3 and fig. S12). *mat3* mutants in *Chlamydomonas* produce tiny gametes (*28*), and down-regulation of *MAT3* in *Volvox* males through alternative splicing may be linked to the production of small-celled sperm.

The accelerated divergence of sex chromosomes is usually associated with gene loss and degeneration (*23*), although adaptive evolution of sex chromosomes is an emerging theme (*30*). Our data suggest that expansion, loss of recombination, and rapid divergence can be mutually reinforcing properties of sex-determining regions that facilitate cooption into the sexual cycle and provide previously undiscovered sources of developmental innovation (fig. S14).

References and Notes

1. G. A. Parker, R. R. Baker, V. G. Smith, *J. Theor. Biol.* **36**, 529 (1972).
2. B. Charlesworth, *J. Theor. Biol.* **73**, 347 (1978).
3. T. M. Williams, S. B. Carroll, *Nat. Rev. Genet.* **10**, 797 (2009).
4. Materials and methods are available as supporting material on *Science* Online.
5. D. L. Kirk, *Volvox: Molecular-Genetic Origins of Multicellularity and Cellular Differentiation*, J. B. L. Bard, P. W. Barlow, P. B. Green, D. L. Kirk, Eds. (Cambridge Univ. Press, Cambridge, 1998).
6. U. Goodenough, H. Lin, J.-H. Lee, *Semin. Cell Dev. Biol.* **18**, 350 (2007).
7. P. J. Ferris, E. V. Armbrust, U. W. Goodenough, *Genetics* **160**, 181 (2002).
8. J. A. Fraser *et al.*, *PLoS Biol.* **2**, e384 (2004).
9. A. Menkis, D. J. Jacobson, T. Gustafsson, H. Johannesson, G. McVean, *PLoS Genet.* **4**, e1000030 (2008).
10. K. T. Yamato *et al.*, *Proc. Natl. Acad. Sci. U.S.A.* **104**, 6472 (2007).
11. H. Nozaki, *J. Plant Res.* **109**, 353 (1996).
12. S. S. Merchant *et al.*, *Science* **318**, 245 (2007).
13. M. D. Herron, J. D. Hackett, F. O. Aylward, R. E. Michod, *Proc. Natl. Acad. Sci. U.S.A.* **106**, 3254 (2009).
14. Available at http://genomeportal.jgi-psf.org/Volca1/Volca1.home.html
15. P. J. Ferris, U. W. Goodenough, *Genetics* **146**, 859 (1997).
16. T. Hamaji *et al.*, *Genetics* **178**, 283 (2008).
17. H. Nozaki, T. Mori, O. Misumi, S. Matsunaga, T. Kuroiwa, *Curr. Biol.* **16**, R1018 (2006).
18. T. Hamaji, P. J. Ferris, I. Nishii, H. Nozaki, *J. Phycol.* **45**, 1310 (2009).
19. H. Lin, U. W. Goodenough, *Genetics* **176**, 913 (2007).
20. A. Idnurm, F. J. Walton, A. Floyd, J. Heitman, *Nature* **451**, 193 (2008).
21. P. D. Waters, M. C. Wallis, J. A. Marshall Graves, *Semin. Cell Dev. Biol.* **18**, 389 (2007).
22. J. F. Hughes *et al.*, *Nature* **463**, 536 (2010).
23. B. Charlesworth, D. Charlesworth, *Philos. Trans. R. Soc. Lond. B Biol. Sci.* **355**, 1563 (2000).
24. J. Bull, *Am. Nat.* **112**, 245 (1978).
25. B. T. Lahn, D. C. Page, *Science* **286**, 964 (1999).
26. R. M. Kliman, J. Hey, *Mol. Biol. Evol.* **10**, 1239 (1993).
27. S.-C. Fang, C. de los Reyes, J. G. Umen, *PLoS Genet.* **2**, e167 (2006).
28. J. G. Umen, U. W. Goodenough, *Genes Dev.* **15**, 1652 (2001).
29. A. J. Matlin, F. Clark, C. W. Smith, *Nat. Rev. Mol. Cell Biol.* **6**, 386 (2005).

copulation, with resident sperm concentrated in the distal half of the SR (Fig. 2, B and C), but dynamic mobility of sperm in storage increased mixing over time (Fig. 2D and fig. S11).

The question of why males ejaculate many more sperm than can be stored has long puzzled researchers, given that the (1.8 mm) sperm of *D. melanogaster* are many times longer than any distance they travel within the female and that storage appears to be a rapid and efficient process (*18*). We postulate that excess sperm and, perhaps, their mobility (movie S6) are adaptations to sperm competition in this species, specifically to physical displacement of resident sperm. Indeed, the size of the second male's ejaculate was significantly correlated with the amount of resident sperm displaced from storage, and the strength of this relation increased substantially between 45 and 60 min ASM (fig. S12) [45 min ASM: $n = 45$, $F_{1, 43} = 6.85$, coefficient of determination (R^2) = 0.137, $P = 0.012$; 60 min ASM: $n = 34$, $F_{1, 32} = 30.95$, $R^2 = 0.49$, $P < 0.0001$]. These results also suggest that ejaculate size is evolving via sexual selection mediated by sperm competition.

Sperm storage and displacement dynamics cease when the female ejects excess second-male and displaced first-male sperm from her reproductive tract. To establish that females are ejecting sperm, as previously inferred (*13*), we doubly mated wild-type females to GFP and RFP males and, within 30 min after copulation, transferred females in groups of up to five (mean = 4.7) into 20 cubes constructed of glass coverslips. Cubes were deconstructed 3 hours later, and the coverslips were examined under fluorescence. We found several ejected sperm masses per cube, highly stereotypical in form (Fig. 3), consisting of mixed (but predominantly second-male) sperm in association with the gelatinous mating plug. To better quantify ejection, wild-type females were isolated in glass three-well spot plates beneath coverslips immediately after mating to GFP males, and we checked for ejection every 10 min for up to 5 hours using a stereomicroscope. Ejected masses were immediately transferred to saline on slides and examined under epifluorescence to confirm the presence of GFP sperm, and females were dissected to examine the bursa for sperm. We found that 84% of females ($n = 61$) ejected sperm within five hours of mating (181 ± 11 min, mean ± SEM), and none of these females had any sperm in their bursa, nor had they laid any eggs. Additionally, on examination, first eggs laid in media vials in the time-series experiment (above) were never associated with large amounts of sperm, which suggests that active sperm ejection by females is typical, if not universal.

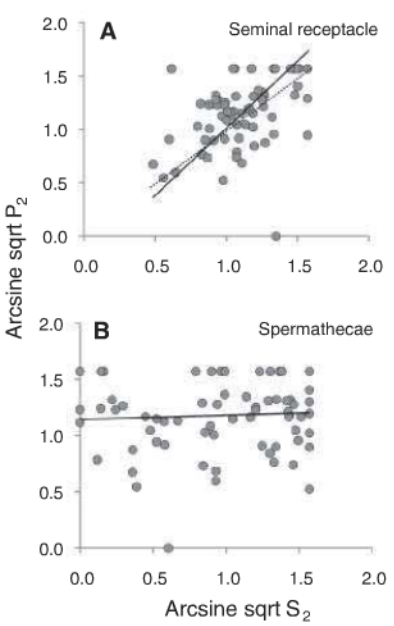

Fig. 4. Relation between P_2 and S_2 (both variables arcsine square root transformed) in the (**A**) seminal receptacle and (**B**) spermathecae. Seminal receptacle: $y = 1.203x - 0.191$ (reduced major axis regression); spermathecae: $y = 0.0383x + 1.144$ (simple linear regression).

After ejection, remaining stored sperm make up the "fertilization set" (*19*) or the population of sperm directly engaging in sperm-sperm competition. To delineate which storage organs house the fertilization set, we compared simple linear regressions of P_2 on the proportion of second-male sperm in storage (S_2) (Fig. 4) (*15*). S_2 was found to be a highly significant predictor of P_2 for the SR ($F_{1, 73} = 25.55$, $P < 0.0001$, $R^2 = 0.259$) but not the spermathecae ($F_{1, 70} = 0.26$, $P = 0.614$, $R^2 = 0.004$), reinforcing previous indirect evidence (*20*) that sperm in the SR constitutes the more immediate fertilization set. Proportional representation in the proximal versus distal regions of the SR may further contribute to differential fertilization success and has been shown to be influenced by sperm length (*21*, *22*). However, sperm length here did not systematically vary between first and second males, and sperm proportions did not differ regionally in the SR in the hours immediately after mating (fig. S11).

We finally tested if each male's sperm in the SR post ejection was equally competitive, akin to a "fair raffle" (*19*), with sperm used for fertilization in direct proportion to their prevalence. Two results suggest that they were: (i) in vivo sperm motility did not change upon remating and (ii) sperm were used in direct proportion to their abundance. First, we examined if female remating induces a change in motility of GFP resident sperm in the SR, by quantifying their velocity and percent motility (i) 5 min ASM to an RFP male, (ii) 60 min ASM to an RFP male, (iii) 60 min after the first mating, and (iv) 3 days after the first mating (*15*). Percent motility and sperm velocity showed no significant changes, which suggested that in the SR, neither several days of storage nor female remating had any detrimental effect on sperm survival or motility (fig. S13 and movies S5 and S6). Second, if sperm competition was disproportionately and systematically biased toward one male over another ("loaded raffle"), the slope of the regression of P_2 on S_2 would be either significantly less than 1 (favoring the first male) or greater than 1 (favoring the second male). However, the slope of the reduced major axis regression was not significantly different from 1 [slope = 1.203, $t(68) = 0.81$, $P = 0.422$] (Fig. 4A), which supported the fair-raffle hypothesis.

Our observations of in vivo motility and fine-scale spatiotemporal patterns of sperm fate corroborate some previously conjectured mechanisms underlying competitive fertilization success, including sperm displacement (*10*, *12*, *23*) and sperm ejection by females (*13*), but fail to support other proposed mechanisms, such as sperm incapacitation (*9*–*11*). We cannot exclude the possibility that Acp-mediated incapacitation contributes to the early release of some resident sperm from storage. However, we would then expect to see dead or dying sperm in storage and in the bursa, yet neither sperm velocity nor sperm motility in storage changed upon remating. Our results complement other investigations of sperm mortality of competing ejaculates in vivo (*13*) and in vitro (*24*), which suggested that incapacitation makes little to no contribution to sperm precedence in *D. melanogaster*. The present investigation reveals that postcopulatory sexual selection in *D. melanogaster* includes the early release of resident sperm from storage, the heterogeneous distribution of competing sperm proportions in different storage organs, fair-raffle sperm use in the SR, and the surprising level of sperm mobility within female sperm-storage organs (movies S1 to S5). Most important, a complex and dynamic array of processes underlying patterns of sperm precedence (e.g., P_2) can now be dissected in targeted, detailed genetic analyses to reveal specific behavioral, physiological, and biochemical mechanisms relevant to postcopulatory sexual selection.

References and Notes

1. G. A. Parker, in *Sexual Selection and Reproductive Competition in Insects*, M. S. Blum, N. A. Blum, Eds. (Academic Press, New York, 1979), pp. 123–166.
2. G. A. Parker, *Biol. Rev. Camb. Philos. Soc.* **45**, 525 (1970).
3. W. G. Eberhard, *Female Control: Sexual Selection by Cryptic Female Choice* (Princeton Univ. Press, Princeton, NJ, 1996).
4. T. R. Birkhead, A. P. Møller, *Sperm Competition and Sexual Selection* (Academic Press, London, 1998).
5. T. R. Birkhead, D. J. Hosken, S. Pitnick, *Sperm Biology: An Evolutionary Perspective* (Academic Press, London, 2009).
6. A. Bjork, S. Pitnick, *Nature* **441**, 742 (2006).
7. A. Bjork, W. T. Starmer, D. M. Higginson, C. J. Rhodes, S. Pitnick, *Proc. Biol. Sci.* **274**, 1779 (2007).
8. T. Pizzari, G. A. Parker, in *Sperm Biology: An Evolutionary Perspective*, T. R. Birkhead, D. J. Hosken, S. Pitnick, Eds. (Academic Press, London, 2009), pp. 207–245.
9. A. Civetta, *Curr. Biol.* **9**, 841 (1999).
10. C. S. C. Price, K. A. Dyer, J. A. Coyne, *Nature* **400**, 449 (1999).
11. L. G. Harshman, T. Prout, *Evolution* **48**, 758 (1994).
12. A. S. Gilchrist, L. Partridge, *J. Insect Physiol.* **41**, 1087 (1995).
13. R. R. Snook, D. J. Hosken, *Nature* **428**, 939 (2004).

14. A. D. Stewart, A. M. Hannes, W. R. Rice, *Evolution* **61**, 636 (2007).
15. Materials, methods, supplementary analyses, and discussion are available as supporting material on *Science* Online.
16. E. M. Adams, M. F. Wolfner, *J. Insect Physiol.* **53**, 319 (2007).
17. G. A. Parker, L. W. Simmons, *Proc. Biol. Sci.* **246**, 107 (1991).
18. K. Ravi Ram, M. F. Wolfner, *Integr. Comp. Biol.* **47**, 427 (2007).
19. G. A. Parker, in *Sperm Competition and the Evolution of Animal Mating Systems*, R. L. Smith, Ed. (Academic Press, Orlando, FL, 1984), pp. 1–60.
20. S. Pitnick, T. A. Markow, G. S. Spicer, *Evolution* **53**, 1804 (1999).
21. J. M. Pattarini, W. T. Starmer, A. Bjork, S. Pitnick, *Evolution* **60**, 2064 (2006).
22. G. T. Miller, S. Pitnick, *Science* **298**, 1230 (2002).
23. G. Lefevre Jr., U. B. Jonsson, *Genetics* **47**, 1719 (1962).
24. L. Holman, *Funct. Ecol.* **23**, 180 (2009).
25. Supported by the NSF (grants DEB-9806649 and DEB-0814732). We thank S. McClear for assistance with the protamine constructs and M. Wong for technical assistance.

Supporting Online Material
www.sciencemag.org/cgi/content/full/science.1187096/DC1
Materials and Methods
SOM Text
Figs. S1 to S13
Table S1
References
Movies S1 to S6

14 January 2010; accepted 3 March 2010
Published online 18 March 2010;
10.1126/science.1187096
Include this information when citing this paper.

Structural Basis of Preexisting Immunity to the 2009 H1N1 Pandemic Influenza Virus

Rui Xu,[1]* Damian C. Ekiert,[1]* Jens C. Krause,[2] Rong Hai,[3] James E. Crowe Jr.,[2] Ian A. Wilson[1,4]†

The 2009 H1N1 swine flu is the first influenza pandemic in decades. The crystal structure of the hemagglutinin from the A/California/04/2009 H1N1 virus shows that its antigenic structure, particularly within the Sa antigenic site, is extremely similar to those of human H1N1 viruses circulating early in the 20th century. The cocrystal structure of the 1918 hemagglutinin with 2D1, an antibody from a survivor of the 1918 Spanish flu that neutralizes both 1918 and 2009 H1N1 viruses, reveals an epitope that is conserved in both pandemic viruses. Thus, antigenic similarity between the 2009 and 1918-like viruses provides an explanation for the age-related immunity to the current influenza pandemic.

Influenza pandemics in humans tend to occur decades apart and infect a large percentage of the human population with substantial mortality. In the 20th century, three pandemics were caused by the emergence of different influenza A subtypes that were antigenically divergent from human viruses circulating at the time: 1918 H1N1 ("Spanish flu"), 1957 H2N2 ("Asian flu"), and 1968 H3N2 ("Hong Kong flu") (*1*). Since April 2009, the outbreak of a novel influenza A H1N1 virus (2009 H1N1) in Mexico has spread globally and developed into the first human influenza pandemic in 40 years. The 2009 H1N1 virus has now infected the human population worldwide and contributed to at least 16,000 deaths as of 26 February 2010 (*2*).

The influenza virus envelope protein, hemagglutinin (HA), is the principal surface antigen (*3*) and the most critical component of flu vaccines (*4*). At the beginning of a flu pandemic, preexisting immunity to the HA of the newly emerging virus is generally low, guaranteeing a large pool of susceptible hosts for rapid spread and infection of 10 to 40% of the population worldwide. After a new HA becomes fixed in circulating human viruses, it undergoes gradual changes in its antigenic structure in a process called antigenic drift, so as to escape recognition by the human immune system. Such drift leads to loss of immunity and is associated with the frequent flu epidemics that occur during interpandemic periods.

The 2009 pandemic virus HA originated from the swine lineage of H1 HAs and closely resembles that of current circulating H1 viruses in swine (Fig. 1A) (*5*–*7*), whereas seasonal human H1 HAs diverged from the swine lineage early in the 20th century (*8*). Descendants of the human 1918 H1N1 virus continued to circulate

[1]Department of Molecular Biology, Scripps Research Institute, 10550 North Torrey Pines Road, La Jolla, CA 92037, USA. [2]Departments of Pediatrics and Microbiology and Immunology, Vanderbilt University Medical Center, Nashville, TN 37232, USA. [3]Department of Microbiology, Mount Sinai School of Medicine, New York, NY 10029, USA. [4]Skaggs Institute for Chemical Biology, Scripps Research Institute, 10550 North Torrey Pines Road, La Jolla, CA 92037, USA.

*These authors contributed equally to this work.
†To whom correspondence should be addressed. E-mail: wilson@scripps.edu

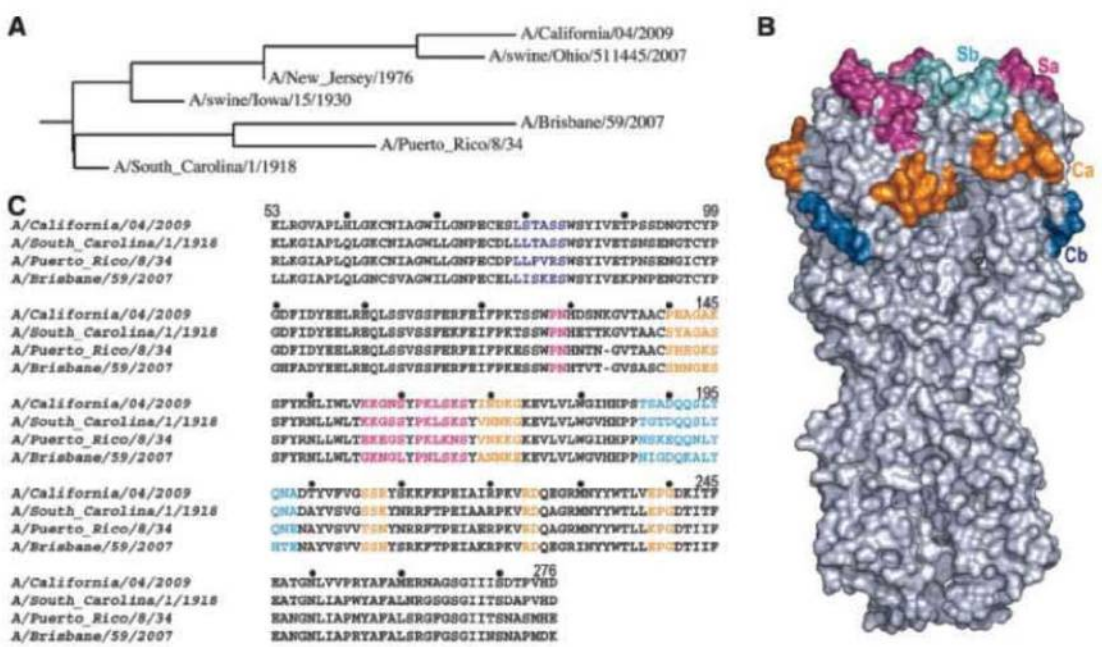

Fig. 1. Crystal structure, phylogeny, and antigenic variation in influenza A 2009 H1N1 HA. (**A**) Phylogenetic tree of selected H1 HAs in swine and human. (**B**) Antigenic structure of CA04 HA from the 2009 H1N1 pandemic virus. A trimer complex is shown in surface representation with the antigenic sites highlighted: Sa site in magenta, Sb site, cyan; Ca site, orange; and Cb site, blue. Sa and Sb sites are located near the receptor-binding site. The Ca site straddles the subunit interface in the trimer. (**C**) Sequence alignment of membrane-distal domains from representative H1 HAs (*38*). Antigenic epitopes are color-coded as in (B).

until the 1957 pandemic, when they were replaced by H2N2 viruses. H1N1 reappeared in humans in the late 1970s, and H1N1 viruses remain a component of seasonal influenza today. In the meantime, H1 viruses continued to circulate in the swine population, remaining antigenically stable and causing only sporadic human infections, including the 1976 outbreak in Fort Dix, New Jersey (*9*, *10*).

To understand the structural basis for the high antigenicity of this emerging pandemic virus, we determined the crystal structure of the HA from the H1N1 A/California/04/2009 (CA04) virus (*11*). Our structural analysis reveals that the 2009 H1 HA shares conserved antigenic epitopes with human and swine H1 viruses from the early 20th century. This observation is supported by the crystal structure of the 1918 H1 HA in complex with a neutralizing antibody that cross-reacts with both pandemic viruses. These structures shed light on the basis of preexisting immunity against these novel H1N1 pandemic viruses in people born early in the 20th century.

The entire ectodomain structure of CA04 HA was determined by molecular replacement at 2.6 Å resolution (table S1). Its overall structure is similar to other H1 HA structures from avian (*12*), swine (*13*), and human viruses (*13*, *14*). The HA homotrimer comprises a long, extended stem region and a membrane-distal, globular cap that includes the receptor-binding domain and the vestigial esterase domain. Whereas the stem region houses the membrane fusion machinery, the membrane-distal domain mediates cell attachment through receptor binding and displays most of the epitopes for antibody recognition.

The antigenic sites of H1 HA are distributed roughly over four conformational epitopes (Fig. 1, B and C) (*15*–*17*); the Sa and Sb sites are proximal to the receptor-binding pocket, the Ca site (Ca1 and Ca2) is at the subunit interface, and the Cb site is within the vestigial esterase domain (Figs. 1B and 2A). The majority of the epitopes contain highly variable, protruding loops that can be accessed readily by approaching antibodies. Although the protein sequences are diverse, the CA04 epitopes maintain highly similar backbone conformations to those in other H1 structures (*18*, *19*), with the only exception being the Cb site, in which a flexible loop adopts variable conformations. This structural conservation facilitates comparisons of antigenic structures at the sequence level.

The 2009 pandemic virus displays distinct antigenic properties from the circulating seasonal H1 viruses (*6*, *20*). The previous influenza pandemics of last century all were initiated by antigenic shift: the introduction of a new HA subtype into humans. The 2009 swine flu marks the first time that a distant variant of a current circulating HA subtype has triggered a new pandemic (*21*). Vaccines for current seasonal flu do not elicit any cross-reactivity in humans against the 2009 pandemic virus, highlighting their considerable antigenic divergence (*22*, *23*). Furthermore, the 2009 pandemic exhibits an unusual pattern of age-related morbidity and mortality reminiscent of the 1918 Spanish flu, because it disproportionately affects children and young adults (ages 4 to 25) (*24*). The frequency of severe disease decreases with age, with the lowest occurrence in the population 65 years and older (*25*–*30*). The low frequency of severe disease associated with 2009 infection in the elderly, the common victims of seasonal flu, suggests some preexisting immunity to the 2009 pandemic viruses (*22*).

The CA04 HA structure reveals the molecular basis for its antigenic properties. Compared with seasonal H1 HAs, substantial amino acid differences are found in all four antigenic regions (Fig. 2, B to D). However, among other human viruses, the HA from the 1918 influenza pandemic (A/South Carolina/1/1918, SC1918) is a remarkably close relative of CA04, with only 20% amino acid difference in the antigenic sites. Moreover, these differences are restricted mainly to the Ca region, with high conservation of the Sa, Sb, and Cb epitopes. The largely conserved antigenic surface between SC1918 and CA04 suggests a potential for substantial antibody cross-reactivity between these two pandemic strains. Indeed, serological tests suggest that individuals who likely experienced the 1918 Spanish flu carry the highest titers of neutralizing antibodies against the novel 2009 H1N1

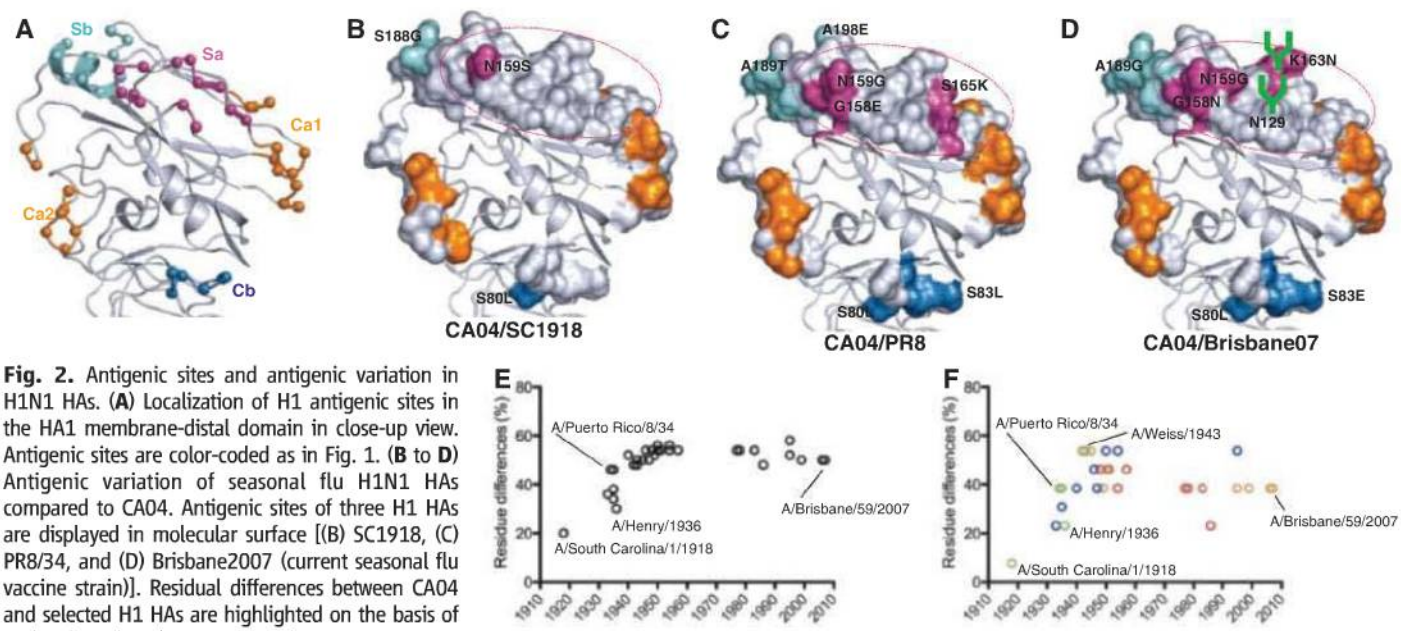

Fig. 2. Antigenic sites and antigenic variation in H1N1 HAs. (**A**) Localization of H1 antigenic sites in the HA1 membrane-distal domain in close-up view. Antigenic sites are color-coded as in Fig. 1. (**B** to **D**) Antigenic variation of seasonal flu H1N1 HAs compared to CA04. Antigenic sites of three H1 HAs are displayed in molecular surface [(B) SC1918, (C) PR8/34, and (D) Brisbane2007 (current seasonal flu vaccine strain)]. Residual differences between CA04 and selected H1 HAs are highlighted on the basis of antigenic regions (Sa, magenta; Sb, cyan; Ca, orange; Cb, blue). The SC1918 HA antigenic surface is highly conserved in CA04. In later years (1930–2007), the H1N1 HA antigenic surface has become more variable through mutations and, importantly, acquired additional N-glycosylation sites (shown as a cartoon with branched sticks in green) that mask the surface from recognition by neutralizing antibodies. The Sa region (highlighted in pink ovals) is the epitope for cross-reactive antibodies against 1918 and 2009 pandemic viruses. (**E**) Increased variation over these time periods is shown in the plot of residual differences between CA04 and selected human H1 HAs in the antigenic sites over time. Sequences of H1 HA in the early half of the 20th century were selected from the National Center for Biotechnology Information (NCBI) Influenza Virus Resource (www.ncbi.nlm.nih.gov/genomes/FLU/FLU.html). After 1977, only the nine H1N1 vaccine strains are shown. The sequences and antigenic site variation of the HAs analyzed in (E) and (F) are listed in table S2. (**F**) Similar plot for the Sa site color-coded by the number of potential N-glycosylation sites in the Sa antigenic region (green, zero glycans; blue, one glycan; orange, two glycans; and red, three glycans).

viruses among all age groups (*20*, *22*). In contrast, the antigenic sites of all known human H1 HAs from the 1930s to the present are highly divergent from CA04. HAs from A/Puerto Rico/8/1934 (PR8/34) and A/Brisbane/59/2007 (Brisbane07) differ from CA04 by 46% and 50%, respectively, in the residues corresponding to the antigenic sites. A comparison of all available H1 HA sequences with CA04 reveals a steady increase in divergence during the 1930s to about 50% residue difference in the HA antigenic sites in the 1940s, which has remained stable at that level since then (Fig. 2E and table S2). Thus, exposure to early H1N1 viruses that present conserved patches of antigenic surface would explain production of CA04 cross-reactive antibodies, whereas increased drift in later strains would make generation of such antibodies in the population increasingly rare.

Variation in glycosylation is also used by influenza and other viruses to interfere with surveillance by the host immune system. Acquisition of a glycosylation site masks the protein surface from antibody recognition because the glycans themselves are host-derived and hence considered as "self" by the immune system (*31*). Whereas SC1918 HA lacks any N-glycosylation sites within or near Sa, human H1 HAs have gradually acquired up to three such sites in the relatively conserved Sa region from 1930 to 2007 (Fig. 2, D and F, and table S2) (*32*), paralleling the evolution of protein sequence differences. What is most important is that CA04 (Fig. 2B), like SC1918, does not have any glycosylation in or around the Sa site; hence, the epitope is exposed for antibody recognition.

In light of the relative conservation of the Sa site in human H1 viruses, Sa-specific antibodies are potentially the major underlying basis of age-related immunity to the 2009 H1N1 virus. Recently, antibody 2D1, isolated from an elderly survivor of the 1918 pandemic (*33*), showed high affinity for the pandemic 2009 H1 HA (CA04) (Fig. 3C) and cross-neutralized the 2009 H1N1 viruses in vivo (*34*). To understand the basis of 2D1 cross-reactivity against these two pandemic viruses, we determined the crystal structure of the 2D1 Fab in complex with the 1918 HA (table S1).

The 2D1 Fab recognizes an epitope at the apex of the receptor-binding domain (Fig. 3A). The footprint of the Fab on the HA largely coincides with the previously defined Sa region but extends its boundaries (*15*, *16*) (Fig. 3B). Binding of 2D1 to SC1918 HA buries a total surface area of 1506 Å^2 (743 Å^2 on HA and 763 Å^2 on the Fab) with typical, heavy chain–dominant binding [~63% on the variable region of the immunoglobulin heavy chain (V_H) and 37% on the variable region of the immunoglobulin light chain (V_L)]. The epitope is conformational and consists primarily of HA1 residues 125C to 129 and 157 to 169 (Fig. 3B and table S3). Heavy chain complementarity-determining region 1 (HCDR1) adopts an unusual, open loop conformation when compared with other Fab structures that have identical HCDR1 sequences (fig. S2). As a result, HCDR1 makes few contacts with HA and is likely very flexible in solution (*35*). Instead, HCDRs 2 and 3 dominate the interaction, along with light chain CDRs (LCDRs) 1 and 3. The heavy and light chains recognize separate, nearly discontinuous surfaces on HA, with a small cavity being formed at the junction between V_H, V_L, and the HA. Of the 18 HA residues contacting Fab 2D1, 11 lie within the previously defined Sa site, accounting for three of three salt bridges, 7 of 13 hydrogen bonds, and 92 of 123 van der Waals contacts. Indeed, the Sa site comprises the centerpiece of the antibody binding surface for 2D1, with the remaining contact residues lining its borders along the periphery of the Fab-HA interface (Fig. 3B).

The antibody binding site for 2D1 is well conserved in SC1918 and CA04, but not in seasonal HAs (table S3). A conservative variation at position 169 in HA1 (Val in SC1918 and Ile in CA04) and a Ser^{159} to Asn^{159} (S159N) substitution are the only differences within the 2D1 footprint between these two pandemic viruses and do not appear to adversely affect 2D1 binding (Fig. 3B and table S3). Val^{169} lies on the edge of the 2D1 epitope and makes a single van der Waals contact with HCDR1. Ser^{159} also lies along the periphery and makes minor contacts with the highly flexible HCDR1 and a single contact with HCDR3. The 1934 PR8 isolate carries three amino acid variations from SC1918 in that region, all of which lie within the Sa site, including Lys^{166} → Asn^{166} (K166N), which would abolish the salt bridge with Asp^{93} in the 2D1 light chain. Mutations of Lys^{166} significantly decrease binding affinity for antibody 2D1 (table S3). Furthermore, escape mutants for 2D1 were also selected at position 166 in 2009 H1N1, as well as in SC1918 human and 1930 swine viruses (*33*, *34*). Brisbane07 shows an even more diverse antigenic surface. Seven amino acid differences from SC1918 (three of which map to Sa), along with two potential N-glycosylation sites in the center of the epitope, reveal why 2D1 does not cross-react with the current seasonal viruses.

This increased divergence in the antigenic surface of human H1N1 viruses, especially the

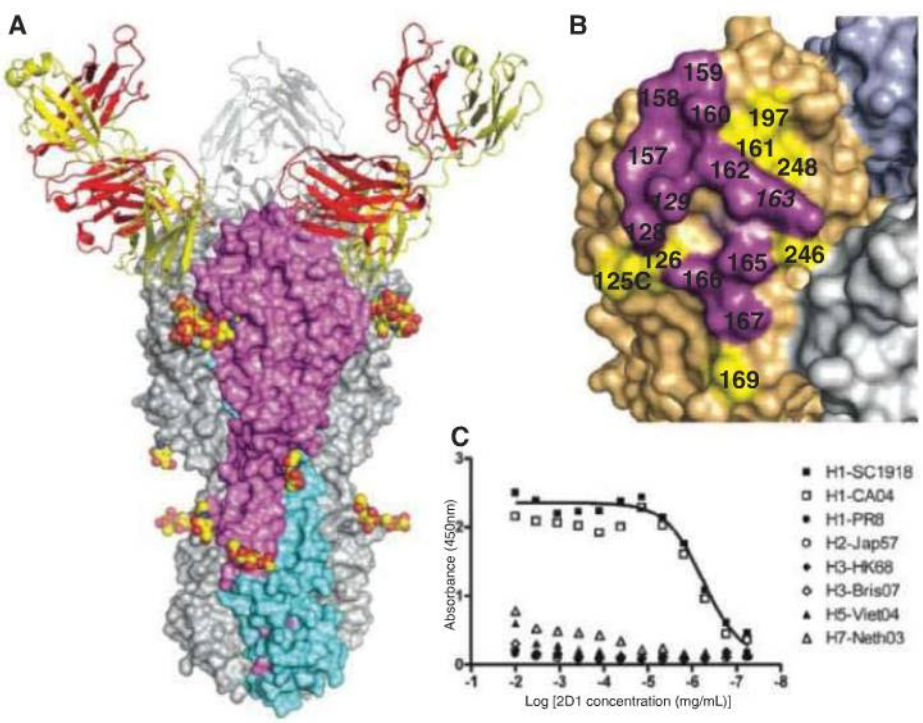

Fig. 3. Crystal structure of cross-neutralizing antibody 2D1 in complex with SC1918. (**A**) Antibody 2D1, with the light and heavy chains of the Fab in yellow and red, respectively, recognizes the Sa site of SC1918 HA, where HA1 is shown in magenta and HA2 in cyan in one subunit of the HA trimer (gray surface) with N-linked carbohydrates in yellow (carbon) and red (oxygen) balls. (**B**) Footprint of antibody 2D1 on the SC1918 HA shows the central role of the Sa site residues for 2D1 binding. The interacting surface contributed by residues from the Sa site is colored in magenta, whereas residues that contribute to the epitope, but are outside of the "canonical" Sa site, are colored in yellow. Sa site residues (e.g., 164) not in contact with 2D1 are shown in pink. SC1918 and CA04 do not have N-glycosylation sites in the Sa region, whereas the vaccine strain Brisbane07, like many other seasonal H1 HAs, have acquired potential glycosylation sites at positions 129 and 163 (italics on surface). (**C**) Antibody 2D1 exhibits strong binding to both 1918 HA and CA04 HA but not to PR8 and HAs of other influenza subtypes, as tested in enzyme-linked immunosorbent assay.

Sa site, directly correlates with decreasing antibody cross-reactivity to CA04 among serum donors when grouped by age (*22*, *23*). Thus, the highest titers of cross-reactive antibodies to CA04 are elicited in the population born before the 1930s and '40s, whereas individuals born after ~1940 generally have lower titers and lack cross-protection from previous exposure to influenza viruses, except for U.S. adults immunized with the swine A/NJ/76 vaccine (*22*). Current vaccine guidelines place those 65 and above into the less-at-risk group with lower priority for vaccination (*25*), consistent with the extent of the antigenic variation observed in the H1 HA structures since 1918. Cross-reactive antibodies elicited by infection with H1N1 viruses in the first few decades of the 20th century, along with preexisting cell-mediated immunity (*36*, *37*), contribute to the overall milder symptoms and lower-than-expected mortality rate in the elderly.

References and Notes

1. P. Palese, *Nat. Med.* **10** (suppl.), S82 (2004).
2. World Health Organization, www.who.int.
3. J. J. Skehel, D. C. Wiley, *Annu. Rev. Biochem.* **69**, 531 (2000).
4. Most neutralizing antibodies that result from viral infection or vaccination specifically target the HA. The current seasonal flu vaccine formulation includes representative strains from the circulating H1N1, H3N2, and influenza B viruses.
5. G. J. Smith *et al.*, *Nature* **459**, 1122 (2009).
6. R. J. Garten *et al.*, *Science* **325**, 197 (2009); published online 22 May 2009 (10.1126/science.1176225).
7. Three H1 genes from the human lineage are included. They respresent human H1 HAs from the 1918 influenza pandemic (A/South Carolina/1/18) and later seasonal strains (A/Puerto Rico/8/34 and A/Brisbane/59/2007). A/Brisbane/59/2007 is the current seasonal vaccine strain. In the swine lineage, classical swine HAs (A/swine/Iowa/15/1930 and A/swine/Ohio/511445/2007) are listed along with swine-origin human viruses (A/New Jersey/1976 and A/California/04/2009).
8. G. J. Smith *et al.*, *Proc. Natl. Acad. Sci. U.S.A.* **106**, 11709 (2009).
9. S. M. Zimmer, D. S. Burke, *N. Engl. J. Med.* **361**, 279 (2009).
10. J. C. Gaydos, F. H. Top Jr., R. A. Hodder, P. K. Russell, *Emerg. Infect. Dis.* **12**, 23 (2006).
11. Materials and methods are avaliable as supporting material on *Science* Online.
12. T. Lin *et al.*, *Virology* **392**, 73 (2009).
13. S. J. Gamblin *et al.*, *Science* **303**, 1838 (2004); published online 5 February 2004 (10.1126/science.1093155).
14. J. Stevens *et al.*, *Science* **303**, 1866 (2004); published online 5 February 2004 (10.1126/science.1093373).
15. A. J. Caton, G. G. Brownlee, J. W. Yewdell, W. Gerhard, *Cell* **31**, 417 (1982).
16. G. G. Brownlee, E. Fodor, *Philos. Trans. R. Soc. London Ser. B* **356**, 1871 (2001).
17. Residue numbering based on H3 HA, as in I. A. Wilson *et al.*, *Nature* **289**, 366 (1981).
18. The RMSD between the membrane-distal domain of CA04 to other H1 HA structures [as Protein Data Bank identification codes (PDB IDs)] are as follows: 1RD8 (A/South Carolina/1/18, 0.58 Å); 1RUZ (A/South Carolina/1/18, 0.76 Å); 1RU7 (A/Puerto Rico/8/34, 0.63 Å); 1RUY (A/swine/Iowa/15/1930, 0.62 Å); 3HTO (A/wild duck/Jiangxi/12416/2005, 0.60 Å).
19. In the crystal structures of H1 HA, the three peptide segments composing the Sa site are all anchored at both ends by aromatic residues whose side chains are buried inside the HA1 receptor binding domain. These residues are absolutely conserved in all H1 HAs, and the numbers of residues between these hydrophobic anchors remain the same, thus maintaining the structural integrity of the Sa site. Across different subtypes, however, these aromatic residues are less well conserved, and slight variations in the length of the component peptide segments may occur.
20. Y. Itoh *et al.*, *Nature* **460**, 1021 (2009).
21. A similar situation may presumably have happened before the 1900s, for which we have insufficient data.
22. K. Hancock *et al.*, *N. Engl. J. Med.* **361**, 1945 (2009).
23. Centers for Disease Control and Prevention (CDC), *MMWR Morb. Mortal. Wkly. Rep.* **58**, 521 (2009).
24. J. K. Taubenberger, D. M. Morens, *Emerg. Infect. Dis.* **12**, 15 (2006).
25. Centers for Disease Control and Prevention, www.cdc.gov/h1n1flu/.
26. S. Jain *et al.* [2009 Pandemic Influenza A (H1N1) Virus Hospitalizations Investigation Team], *N. Engl. J. Med.* **361**, 1935 (2009).
27. S. A. Webb *et al.* (ANZIC Influenza Investigators), *N. Engl. J. Med.* **361**, 1925 (2009).
28. G. Chowell *et al.*, *N. Engl. J. Med.* **361**, 674 (2009).
29. B. Cao *et al.* [National Influenza A Pandemic (H1N1) 2009 Clinical Investigation Group of China], *N. Engl. J. Med.* **361**, 2507 (2009).
30. D. N. Fisman *et al.*, *N. Engl. J. Med.* **361**, 2000 (2009).
31. I. T. Schulze, *J. Infect. Dis.* **176** (suppl. 1), S24 (1997).
32. Because of limited surveillance during this time period, it is difficult to estimate exactly when most H1 viruses acquired glycosylation sites in the vicinity of Sa. Between 1933 and 1943, some isolates have predicted glycans in the region and others do not, suggesting that variants with and without Sa glycans cocirculated during this time. The last isolate without any predicted glycans in the Sa site was A/Weiss/1943 (Fig. 2F and table S2).
33. X. Yu *et al.*, *Nature* **455**, 532 (2008).
34. J. C. Krause *et al.*, *J. Virol.* **84**, 3127 (2010).
35. Indeed, the electron density is weak in this region and is probably only present at all because of a weak crystal contact to an adjacent HA molecule.
36. Z. Xing, C. J. Cardona, *Emerg. Infect. Dis.* **15**, 1847 (2009).
37. J. A. Greenbaum *et al.*, *Proc. Natl. Acad. Sci. U.S.A.* **106**, 20365 (2009).
38. Single-letter abbreviations for the amino acid residues are as follows: A, Ala; C, Cys; D, Asp; E, Glu; F, Phe; G, Gly; H, His; I, Ile; K, Lys; L, Leu; M, Met; N, Asn; P, Pro; Q, Gln; R, Arg; S, Ser; T, Thr; V, Val; W, Trp; and Y, Tyr.

39. The work was supported in part by NIH grants AI058113 (I.A.W., J.E.C., and P. Palese) and AI057157 (J.E.C.), predoctoral fellowships from the Achievement Rewards for College Scientists Foundation and the NIH Molecular Evolution Training Program GM080209 (D.C.E.), and the Skaggs Institute for Chemical Biology. X-ray diffraction data sets were collected at the Stanford Synchrotron Radiation Lightsource beamline 9-2 and at the Advanced Photon Source beamline 23ID-B (GM/CA-CAT). The GM/CA CAT 23-ID-B beamline has been funded in whole or in part with federal funds from National Cancer Institute (Y1-CO-1020) and National Institute of General Medical Sciences (Y1-GM-1104). Use of the Advanced Photon Source (APS) was supported by the U.S. Department of Energy, Basic Energy Sciences, Office of Science, under contract no. DE-AC02-06CH11357. We thank P. Palese (Mount Sinai School of Medicine) for providing the CA04 clone and helpful comments, X. Dai and M. A. Elsliger (Scripps Research Institute) and C. J. Huffman (Vanderbilt University) for expert technical assistance, H. Tien and D. Marciano of the Robotics Core at the Joint Center for Structural Genomics for automated crystal screening, and M. Becker and the staff of the APS GM/CA CAT 23-ID-B for beamline support. This is publication 20395 from the Scripps Research Institute. Coordinates and structure factors are deposited in the PDB [3LZG for CA04 HA (two trimers) and 3LZF for 1918 HA/2D1 complex]. Vanderbilt University has applied for a provisional patent covering the diagnostic and therapeutic use of antibodies described in this paper. J.E.C. Jr. is a founder of the vaccine company Corbeau Biotech LLC and has consulted for MedImmune, Novartis, Sanofi, and Immunobiosciences. J.C.K. is funded by a Pediatric Infectious Diseases Society Fellowship funded by MedImmune and AstraZeneca.

Supporting Online Material

www.sciencemag.org/cgi/content/full/science.1186430/DC1
Materials and Methods
Figs. S1 and S2
Tables S1 to S4
References

24 December 2009; accepted 9 March 2010
Published online 25 March 2010;
10.1126/science.1186430
Include this information when citing this paper.

Divided Representation of Concurrent Goals in the Human Frontal Lobes

Sylvain Charron[1,2] and Etienne Koechlin[1,3,4]*

The anterior prefrontal cortex (APC) confers on humans the ability to simultaneously pursue several goals. How does the brain's motivational system, including the medial frontal cortex (MFC), drive the pursuit of concurrent goals? Using brain imaging, we observed that the left and right MFC, which jointly drive single-task performance according to expected rewards, divide under dual-task conditions: While the left MFC encodes the rewards driving one task, the right MFC concurrently encodes those driving the other task. The same dichotomy was observed in the lateral frontal cortex, whereas the APC combined the rewards driving both tasks. The two frontal lobes thus divide for representing simultaneously two concurrent goals coordinated by the APC. The human frontal function seems limited to driving the pursuit of two concurrent goals simultaneously.

The anteriormost part of the frontal lobes, the so-called frontopolar cortex, subserves the human ability to engage in multitasking behaviors and to pursue multiple goals concurrently (*1*–*4*). More specifically, the frontopolar cortex subserves cognitive branching, i.e., the temporary maintenance of a task in a pending state during the performance of an alternative task (*1*, *4*, *5*). This frontopolar function operates in relation to expected rewards (*5*, *6*). However, it remains unknown how the brain's motivational system, especially the medial frontal cortex

(MFC) that monitors motivationally salient events and drives ongoing behavior according to expected rewards (*6*–*11*), drives the pursuit of concurrent goals and related performance. On the basis of a neurocomputational model (*4*), we conjectured that MFC resources divide to concomitantly maintain separate representations of rewards expected from two concurrent tasks, whereas frontopolar activations implementing cognitive branching result from the integration of both expected rewards.

We tested this conjecture using functional magnetic resonance imaging and standard tasks (*1*, *12*). We recorded brain activity in 32 healthy right-handed participants while they were performing a backward letter-matching task on a series of visually presented letters. Contextual cues appeared at random times and instructed participants to start a secondary backward letter-matching task by either abandoning the primary task (switching condition) or delaying its execution (branching condition) (Fig. 1). When contextual cues disappeared, participants abandoned the secondary task and either started the primary task over again (switching condition) or reverted back to the primary task awaiting execution (branching condition). In the switching condition, the execution of primary and secondary task corresponded to successive single-task performances. In the branching condition, by contrast, secondary task performance corresponded to dual-task performance, because secondary tasks were executed, while primary tasks were awaiting subsequent execution. In both conditions, furthermore, letters were accompanied by incentive cues indicating the reward associated with the ongoing task, which could be either small or large and was earned only when the task was performed with no errors. Thus, the protocol formed a 2 × 2 × 2 factorial design crossing condition (switching versus branching), primary task reward (small versus large), and secondary task reward (small versus large) as within-subject factors.

Behavioral results confirmed that in both conditions, primary and secondary rewards drive primary and secondary task performance, respectively: Reaction times (RTs) and error rates (ERs) for primary tasks decreased when primary rewards increased (both F's > 9.85, P < 0.004), notably in the return trials immediately following secondary task performance (RTs: F = 3.80, P = 0.06; ERs: F = 7.07, P = 0.012; Fig. 2, E and F). All these effects were independent of conditions and secondary rewards (all two- and three-way interactions: F's < 2.23, P > 0.15). Similarly, RTs for secondary tasks decreased when secondary rewards increased (F = 10.11, P = 0.003; interaction with condition: F = 1.17, P = 0.29). ERs for secondary tasks exhibited a similar but not significant trend (Fig. 2, A and B). These effects were also independent of conditions and primary rewards (all two- and three-way interactions: F's < 2.86, P > 0.1), except the effects of secondary rewards on RTs, which attenuated when primary rewards became larger (interaction primary × secondary rewards on RTs: F = 13.0, P = 0.001). This attenuation effect was virtually identical in both conditions (three-way interaction for RTs: F = 0.1), thereby reflecting the devaluation of secondary rewards when large primary rewards were already expected.

In the branching condition, MFC motivational resources presumably divide during secondary task performance between the two tasks. Consequently, the performance of secondary tasks should be affected by the allocation of motivational resources to primary tasks awaiting execution. Consistently, secondary task performance was altered in the branching compared to switching condition (RTs and ERs: both F's > 16.37, P < 0.001), and this branching-related alteration increased with primary rewards (interaction condition × primary rewards for RTs: F = 3.72, P = 0.063; for ERs: F = 7.97, P = 0.008; Fig. 2, C and D).

Consistent with previous results (*10*, *13*, *14*), brain activations in single-task trials (secondary task performance in the switching condition) show that the MFC bilaterally drives single-task performance according to rewards (*12*). In single-task trials, the main effect of secondary rewards involved bilaterally the dorsal anterior cingulate cortex (dACC) and pre-supplementary motor area. Consistently, the same effect also involved bilaterally the ventral striatum, insula,

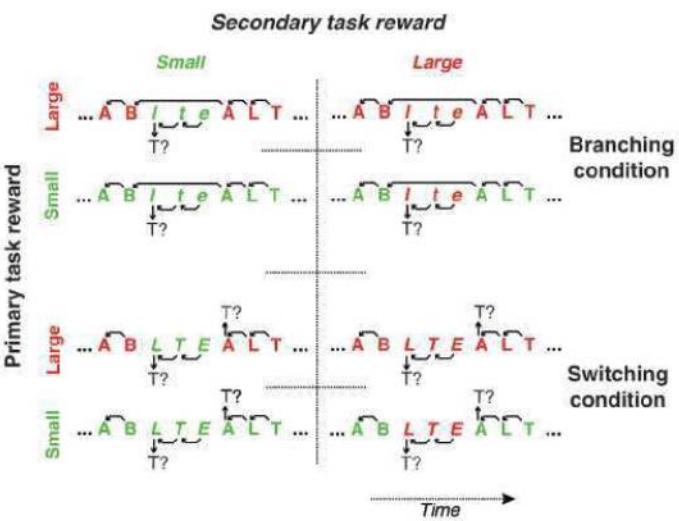

Fig. 1. Behavioral protocol. Blocks of successively presented stimuli (letters from the word "tablet") formed the factorial design. Subjects began each block with the primary task (trials shown here with regular capital letters) and performed the secondary task when instructed by contextual cues (represented here by italicized letters). Colors of letters indicated the reward at stake in each task. Each block ended by a visual feedback (not shown) indicating the actual monetary reward obtained from this block. Subjects started each task by determining whether the first letter was a "t", then proceeded by determining whether two successively presented letters were also in immediate succession in the word "tablet" (upper and lower arrows show successive letter matching for the primary and secondary task, respectively). All task parameters (letter identity, stimulus-onset asynchrony, trial number, response side, block order) were pseudo-randomized and orthogonalized with experimental factors (*12*).

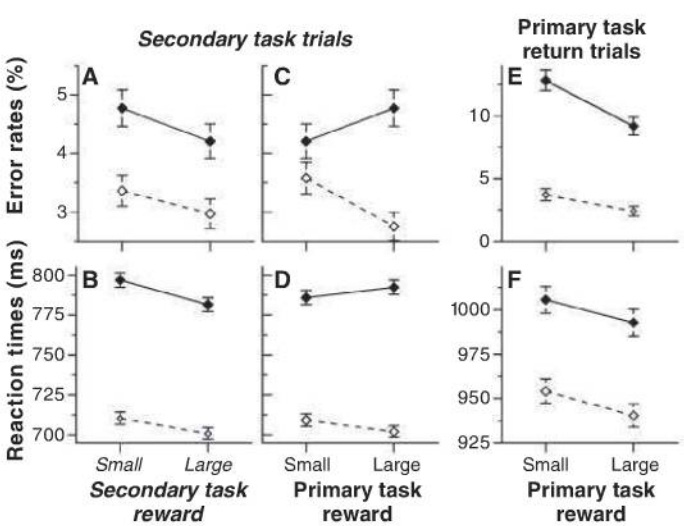

Fig. 2. Behavioral performances. Mean ERs and RTs for correct trials (±SE across subjects) in the switching (dashed lines) and branching (solid lines) conditions. Secondary task performances are shown according to secondary (**A** and **B**) and primary (**C** and **D**) rewards. (**E** and **F**) Primary task performances in return trials according to primary rewards.

[1]Institut National de la Santé et de la Recherche Médicale, Paris F-75654 Cedex 13, France. [2]Ecole Polytechnique, Palaiseau F-91128, France. [3]Ecole Normale Supérieure, Paris F-75230 Cedex 05, France. [4]CENIR, Université Pierre et Marie Curie, Paris F-75651 Cedex 13, France.

*To whom correspondence should be addressed. E-mail: etienne.koechlin@upmc.fr

and lateral prefrontal cortex. As expected, all these activations were unaffected by primary rewards (main and interaction effect: all F's < 1.16, P's > 0.29) (fig. S1).

Compared to single-task trials, dual-task trials (secondary task performance in the branching condition) engaged bilaterally the frontopolar regions previously shown to subserve cognitive branching (*1*, *3*) (*12*) (Fig. 3 and fig. S2, A and B, orange regions) and in agreement with the top-down, rostrocaudal cascade of prefrontal control processes (*15*): lateral prefrontal, dorsal premotor, and inferior parietal cortex (fig. S2).

Consistent with the conjecture, dual-task trials also engaged the MFC regions reported above (fig. S1). Furthermore, in dual-task trials, these regions maintained separate representations of primary and secondary rewards (*12*). The main effect of secondary rewards involved only the right dACC, whereas the main effect of primary rewards involved the left dACC only (Fig. 3, E and F): Right activations increasing with secondary rewards were unaffected by primary rewards, whereas left activations increasing with primary rewards were unaffected by secondary rewards (main and interaction effects: F's < 1). Statistical independent analyses confirmed the lateral segregation of such reward effects (Fig. 4). Furthermore, the primary reward effect in dual-task trials could not simply result from rewards at stake in the preceding or subsequent performance of primary tasks, because in single-task trials primary rewards had no effects. The left dACC therefore encoded the primary rewards driving the actual maintenance of primary tasks in a pending state, while the right dACC was encoding the secondary rewards driving the concomitant performance of secondary tasks.

By contrast, the aforementioned frontopolar regions showed no independent effects of primary and secondary rewards in dual-task trials (both F's < 2, P > 0.17). Instead, dual-task activations in these regions increased only when primary and secondary rewards jointly increased (Fig. 3, A and B). This finding matches the computational model prediction that the involvement of frontopolar resources in carrying out cognitive branching varies as a strongly nonlinear combination of rewarding values of concurrent tasks (*4*), which reflects the incentives of pursuing the two goals concurrently.

The other reward-related activations on dual-task trials (*12*) were found in the ventral tegmental area (secondary reward effect only, fig. S4) and aforementioned dorsal premotor regions, which showed the same segregation as the dACC: Right premotor activations increased with secondary rewards, whereas left premotor activations increased with primary rewards only (all other main and interaction effects: P's > 0.26) (Fig. 3, C and D, and fig. S3). In single-task trials, these premotor regions exhibited a secondary reward effect only (F = 8.7, P < 0.006; all other effects: P > 0.1). Knowing that dorsal premotor regions encode stimulus-response associations in relation with expected rewards (*15*–*17*), we concluded that in dual-task trials, left and right premotor regions divide and separately represent letter-response associations related to the pending and ongoing task, respectively.

Additional analyses [see supplementary results in supporting online material (SOM) text] confirmed the dichotomy observed in dual-task trials between the left and right frontal lobe within the dACC and premotor cortex. The dissociation cannot be ascribed to differences between concurrent tasks. Response sides were balanced across tasks, conditions, and rewards. Both tasks involved identical reward schemes and letter-response sets (Fig. 1) and should preferentially involve the left frontal lobe (*18*). The two frontal lobes therefore divide for disentangling and driving independently the two concurrent tasks. Accordingly, the right lobe drove the secondary task in dual-task trials presumably because in the preceding trials, the primary task started to engage predominantly the left lobe, and/or the right frontal lobe is biased toward controlling externally oriented mental activity (*19*).

If disentangling and driving two concurrent tasks involves the two frontal lobes, then the frontal function should be unable to accurately drive more than two concurrent tasks at one time. We tested this prediction on 16 additional healthy participants using a self-paced behavioral protocol including the simple branching condition described above and a double branching condition, which required participants to also delay the secondary task performance in order to first execute a tertiary task (triple-task performance) (fig. S5).

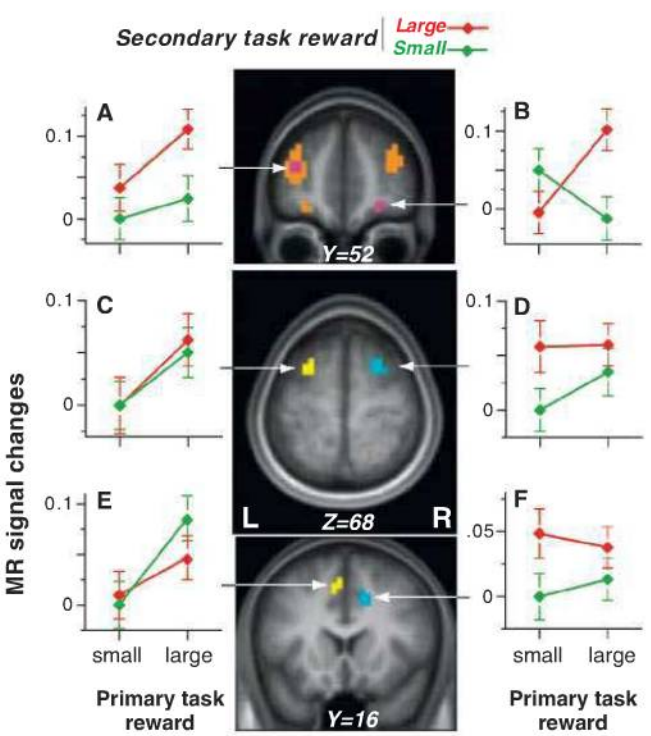

Fig. 3. Reward-related activations in dual-task trials. Activations superimposed on anatomical slices averaged across subjects (neurological convention, voxel-wise threshold: T > 2.95, P < 0.005; corrected clusterwise threshold: P < 0.05) and indexed by MNI coordinates (*X*/*Y*/*Z* in Montreal Neurological Institute atlas). MNI coordinates of maximal T scores are provided below. Cyan, activations in dual-task trials increasing significantly with secondary rewards: right ACC: 12/16/40; right premotor cortex: 20/8/68. Yellow, activations in dual-task trials increasing significantly with primary rewards: left ACC: −8/16/52; left premotor cortex: −28/8/68. Orange, frontopolar activations in dual-task compared to single-task trials: left and right BA10: −36/52/16 and 36/48/28. Violet, activations increasing significantly with joint increases of primary and secondary rewards: left and right BA10: −32/52/20 and 28/60/−8. (**A** to **F**) Factorial analyses of dual-task activations [averaged over each cluster (±SE across subjects) crossing primary and secondary reward factors.

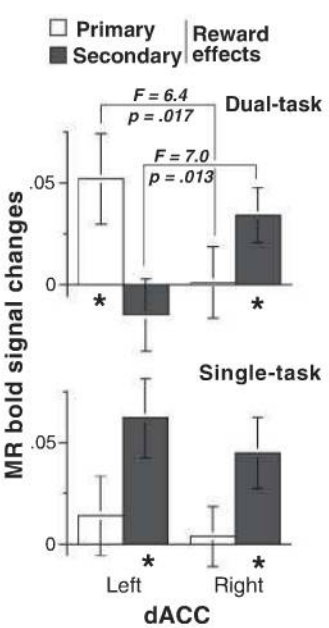

Fig. 4. Reward effects on left and right dACC activations. Analyses of variances statistically independent of cluster identifications crossing primary rewards, secondary rewards, and hemispheres as within-subjects factors (±SE across subjects) in single- and dual-task trials. (*) Significant post-hoc effects at P < 0.05 (see supplementary results in SOM text).

The hypothesis predicts that in the double condition, participants should be impaired only in returning to pending tasks. Furthermore, return ERs should be close to the theoretical level (=25%) (*12*) predicted by the ability to drive only a single pending task during tertiary task performance.

As predicted, RTs and ERs recorded in the different tasks were similar between the two branching conditions ($F < 1$), except return ERs ($F = 20$, $P < 0.001$; fig. S6): Return ERs in the double condition (primary task: 21.3%; secondary task: 20.0%) were three times as large as those in the simple condition (7%) and similar to the predicted level (=25%, both F's < 1.25, $P > 0.23$). This poor accuracy confined to return trials can be ascribed neither to time pressure, global cognitive factors (attention, motivation, etc.), speed-accuracy trade-off, nor increased working-memory load (see Supplementary Discussion in SOM text). Instead, the results support the hypothesis that the frontal function is unable to accurately drive more than two concurrent tasks at one time.

Our results show that the dACC represents concurrently immediate and future behavioral goals, i.e., the rewards driving ongoing behavior and those pertaining to subsequent behavior, whereas frontopolar regions implementing branching processes are increasingly recruited according to the incentives of pursuing the two goals concurrently, i.e., the joint increases of both expected rewards. This finding is consistent with reciprocal projections connecting the dACC and frontopolar cortex (*20*, *21*) and with previously proposed neurocomputational mechanisms of frontopolar function (*4*). Because the dACC monitors rewarding values of action sets according to outcomes (*6*, *9*, *11*, *22*), our results indicate that the interplay between the dACC and frontopolar cortex has a central role in forward and backward inferences underlying human reasoning (*4*, *23*), i.e., in evaluating alternative or future courses of action according to outcomes of ongoing action or conversely, evaluating such outcomes according to future goals and arbitrating between concurrent plans.

Moreover, the two frontal lobes, which jointly drive the pursuit of a single goal, divide for driving concurrently the pursuit of two independent goals. This finding suggests that the human frontal function is limited to accurately driving the pursuit of two concurrent goals at one time. Consistent with the previously suggested inability of frontopolar function to recursively compute cognitive branching (*4*), this capacity limit places a severe constraint bearing upon human higher cognition and may clarify several limitations in human decision-making and reasoning abilities (*4*). However, no functional dichotomies were observed in the lateral prefrontal and frontopolar cortex despite their involvement in dual-task performance, indicating that these regions in both hemispheres jointly control the serial execution of tasks rather than processing them independently. The lateral prefrontal and frontopolar cortex thus appear to maintain the integrity of volition, at least in healthy human brains.

References and Notes

1. E. Koechlin, G. Basso, P. Pietrini, S. Panzer, J. Grafman, *Nature* **399**, 148 (1999).
2. P. W. Burgess, *Psychol. Res.* **63**, 279 (2000).
3. K. Sakai, J. B. Rowe, R. E. Passingham, *Nat. Neurosci.* **5**, 479 (2002).
4. E. Koechlin, A. Hyafil, *Science* **318**, 594 (2007).
5. E. D. Boorman, T. E. Behrens, M. W. Woolrich, M. F. Rushworth, *Neuron* **62**, 733 (2009).
6. N. D. Daw, J. P. O'Doherty, P. Dayan, B. Seymour, R. J. Dolan, *Nature* **441**, 876 (2006).
7. K. Shima, J. Tanji, *Science* **282**, 1335 (1998).
8. K. Matsumoto, W. Suzuki, K. Tanaka, *Science* **301**, 229 (2003).
9. S. W. Kennerley, M. E. Walton, T. E. Behrens, M. J. Buckley, M. F. Rushworth, *Nat. Neurosci.* **9**, 940 (2006).
10. F. Kouneiher, S. Charron, E. Koechlin, *Nat. Neurosci.* **12**, 939 (2009).
11. B. Y. Hayden, J. M. Pearson, M. L. Platt, *Science* **324**, 948 (2009).
12. Materials and methods are available as supporting online materials on *Science* Online.
13. B. Knutson, J. Taylor, M. Kaufman, R. Peterson, G. Glover, *J. Neurosci.* **25**, 4806 (2005).
14. B. Knutson, A. Westdorp, E. Kaiser, D. Hommer, *Neuroimage* **12**, 20 (2000).
15. E. Koechlin, C. Summerfield, *Trends Cogn. Sci.* **11**, 229 (2007).
16. M. R. Roesch, C. R. Olson, *Science* **304**, 307 (2004).
17. N. Ramnani, R. C. Miall, *Cereb. Cortex* **13**, 318 (2003).
18. K. E. Stephan *et al.*, *Science* **301**, 384 (2003).
19. M. Corbetta, G. L. Shulman, *Nat. Rev. Neurosci.* **3**, 201 (2002).
20. D. N. Pandya, E. H. Yeterian, in *Neurobiology of Decision-Making*, A. R. Damasio, H. Damasio, Y. Christen, Eds. (Springer-Verlag, Berlin and Heidelberg, Germany, 1996), pp. 13–46.
21. M. Petrides, D. N. Pandya, *J. Neurosci.* **27**, 11573 (2007).
22. M. Matsumoto, K. Matsumoto, H. Abe, K. Tanaka, *Nat. Neurosci.* **10**, 647 (2007).
23. P. R. Montague, B. King-Casas, J. D. Cohen, *Annu. Rev. Neurosci.* **29**, 417 (2006).

24. Supported by the Bettencourt-Schueller Foundation and a EURYI award to E.K. We thank L. Sabarly for his help in conducting the behavioral experiment.

Supporting Online Material

www.sciencemag.org/cgi/content/full/328/5976/360/DC1
Materials and Methods
SOM Text
Figs. S1 to S6

20 October 2009; accepted 5 March 2010
10.1126/science.1183614

Cbln1 Is a Ligand for an Orphan Glutamate Receptor δ2, a Bidirectional Synapse Organizer

Keiko Matsuda,[1] Eriko Miura,[1] Taisuke Miyazaki,[2] Wataru Kakegawa,[1] Kyoichi Emi,[1] Sakae Narumi,[1] Yugo Fukazawa,[3] Aya Ito-Ishida,[1,4] Tetsuro Kondo,[1,5] Ryuichi Shigemoto,[3] Masahiko Watanabe,[2] Michisuke Yuzaki[1]*

Cbln1, secreted from cerebellar granule cells, and the orphan glutamate receptor δ2 (GluD2), expressed by Purkinje cells, are essential for synapse integrity between these neurons in adult mice. Nevertheless, no endogenous binding partners for these molecules have been identified. We found that Cbln1 binds directly to the N-terminal domain of GluD2. GluD2 expression by postsynaptic cells, combined with exogenously applied Cbln1, was necessary and sufficient to induce new synapses in vitro and in the adult cerebellum in vivo. Further, beads coated with recombinant Cbln1 directly induced presynaptic differentiation and indirectly caused clustering of postsynaptic molecules via GluD2. These results indicate that the Cbln1-GluD2 complex is a unique synapse organizer that acts bidirectionally on both pre- and postsynaptic components.

Glutamate and its receptors mediate fast excitatory neurotransmission in the mammalian brain. Although the glutamate receptor δ2 (GluD2) belongs to the ionotropic glutamate receptor (iGluR) family, it is referred to as an orphan receptor because it has no known endogenous ligands. Nevertheless, GluD2 is essential for the normal development of cerebellar circuits; the numbers of parallel fiber (PF)–Purkinje cell synapses are specifically and dramatically reduced in the *GluD2*-null cerebellum (*1*). In addition, GluD2 rapidly induces synapse formation (*2*) and is essential for synapse maintenance in the adult cerebellum (*3*). Cbln1, a member of the C1q tumor necrosis factor superfamily (*4*), is expressed and secreted from cerebellar granule cells. The behavioral, physiological, and anatomical phenotypes of *cbln1*-null mice precisely mimic those of *GluD2*-null mice (*5*), which suggests that Cbln1 and GluD2 may be engaged in a common signaling pathway that is required for the formation and maintenance of

[1]Department of Physiology, School of Medicine, Keio University, Tokyo 160-8582, Japan. [2]Department of Anatomy, Hokkaido University Graduate School of Medicine, Sapporo 060-8638, Japan. [3]Division of Cerebral Structures, National Institutes for Physiological Sciences, Okazaki 444-8787, Japan. [4]Department of Cellular Neurobiology, Graduate School of Medicine, University of Tokyo, Tokyo 113-0033, Japan. [5]Molecular Neurophysiology, Neuroscience Research Institute, National Institute of Advanced Industrial Science and Technology, Tsukuba 305-8566, Japan.

*To whom correspondence should be addressed. E-mail: myuzaki@a5.keio.jp

PF synapses (*6*, *7*). Nevertheless, a binding partner for Cbln1 has remained elusive. Therefore, we examined the hypothesis that GluD2 serves as a receptor for Cbln1 and that this receptor complex may regulate cerebellar synapse formation and maintenance.

First, we tested if hemagglutinin (HA)–tagged recombinant Cbln1 could bind to GluD2 using cell-based assays (*8*). Immunohistochemical (Fig. 1A) and immunoblot (Fig. 1B) analyses revealed that HA-Cbln1 could bind to human embryonic kidney (HEK) 293 cells expressing GluD2. In contrast, HA-Cbln1 did not bind to cells expressing the GluK2 kainate receptor, a different member of the iGluR family. To examine the GluD2 region responsible for this binding, we interchanged the extracellular domains of GluD2 and GluK2 (Fig. 1A). HA-Cbln1 could

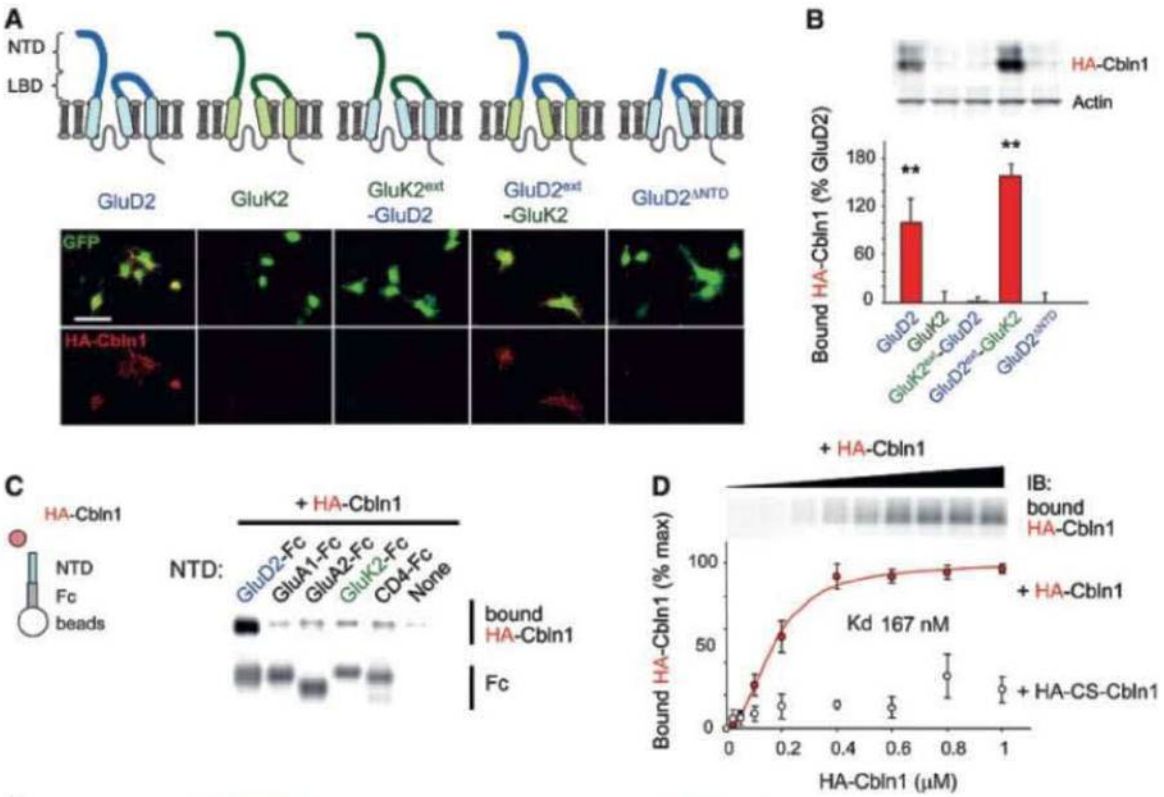

Fig. 1. Cbln1 binds to the NTD of GluD2. (**A** and **B**) Cbln1 binding assay. Binding to HA-Cbln1 (red) on HEK293 cells (GFP, green) expressing GluD2, GluK2, or chimeric constructs was visualized by immunostaining (A) and quantified using immunoblot analysis (B). The mean amount of HA-Cbln1 bound to cells expressing GluD2 was defined as 100%. Three independent experiments. $^{**}P = 3.56 \times 10^{-5}$. Scale bar, 50 μm. (**C**) Direct interaction between HA-Cbln1 and the NTD of GluD2. The NTD of iGluRs or the extracellular domain of CD4 was fused to Fc and coupled to protein G beads. Bound HA-Cbln1 was quantified using an immunoblot analysis. (**D**) Dose-dependent interaction between HA-Cbln1 and the NTD of GluD2 immobilized on beads. Each point represents the mean amount of bound HA-Cbln1 (filled circles) or HA-CS-Cbln1 (open circles) for three independent experiments, quantified using an immunoblot analysis. The line indicates a logistic equation. (**E**) Confocal images of Purkinje cells immunostained for calbindin (calb; green) and HA (red). Purkinje cell dendrites marked by the white boxes are enlarged below. Scale bars, 50 μm and 20 μm. (Right) HA-Cbln1 immunoreactivity along the dendrites is quantified. At least 27 cells for each group were analyzed in three independent experiments. $^{**}P = 2.37 \times 10^{-16}$. (**F**) Wild-type (wt) and *GluD2*-null cerebella immunostained for Cbln1 (red) and calbindin (green). (Bottom) Enlarged images of the molecular layer. Arrows indicate Cbln1 immunoreactivity on the dendritic spines. Scale bars, 20 μm and 1 μm. (**G**) Postembedding immunogold EM images of endogenous Cbln1. Cbln1 and vesicular glutamate transporter 1 (a marker for parallel fiber) were immunolabeled with 10-nm (arrows) and 15-nm gold particles, respectively. Arrowheads indicate the edges of the PSD on Purkinje cell spines (sp). Scale bar, 100 nm.

bind to HEK293 cells expressing GluD2^{ext}-GluK2, in which the extracellular domain of GluD2 replaced that of GluK2, whereas no binding was observed for HEK293 cells expressing GluK2^{ext}-GluD2, in which the extracellular domain of GluK2 replaced that of GluD2 (Fig. 1, A and B). To further narrow down the binding site for Cbln1 within the extracellular domain, which comprised an N-terminal domain (NTD) and a ligand-binding domain (LBD), we introduced various mutations in these domains. Most mutants did not reach the cell surface (fig. S1), except for GluD2$^{\Delta NTD}$, in which the NTD was deleted (*2*). Nevertheless, no binding was observed for HA-Cbln1 in cells expressing GluD2$^{\Delta NTD}$ (Fig. 1, A and B).

To confirm whether the NTD of GluD2 (GluD2^{NTD}) was a binding site for Cbln1, we purified GluD2^{NTD} by fusing it to an immunoglobulin Fc fragment. The NTDs of GluK2, the AMPA receptors GluA1 and GluA2, and the extracellular domain of the CD4 lymphocyte surface protein were used as controls. Immunoblot analysis showed that HA-Cbln1 bound specifically to GluD2^{NTD}-Fc (Fig. 1C). The amount of bound HA-Cbln1 increased with high doses of HA-Cbln1 (apparent binding dissociation constant of ~167 nM) (Fig. 1D).

We assumed that if GluD2 is a receptor for Cbln1, the binding of exogenously applied Cbln1, as well as endogenous Cbln1, should be reduced for *GluD2*-null Purkinje cells. First, we incubated cerebellar cultures [14 to 16 days in vitro (DIV)]

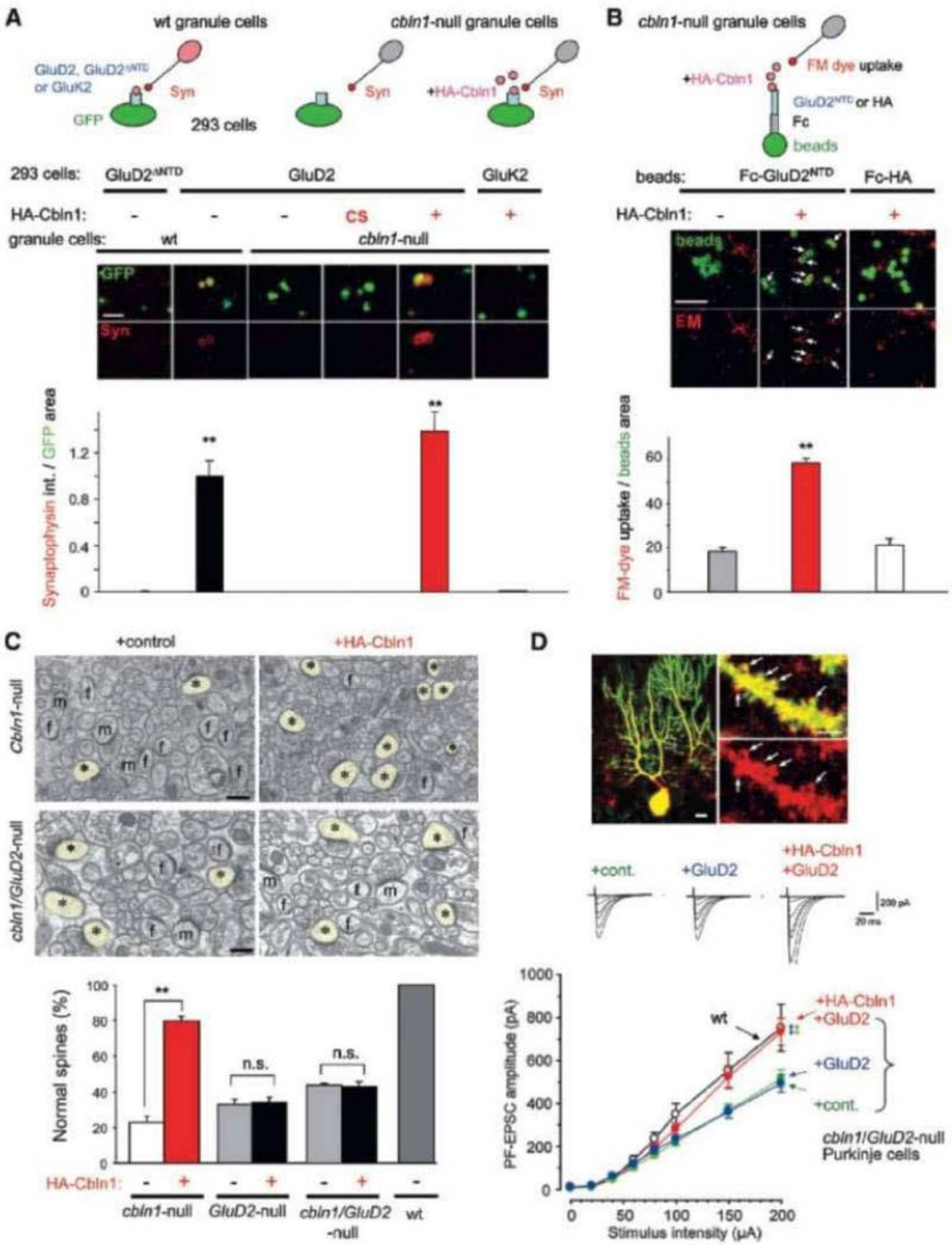

Fig. 2. Cbln1 and the NTD of GluD2 cooperatively induce synaptogenesis in vitro and in vivo. (**A**) HEK293 cells expressing GluD2, GluD2$^{\Delta NTD}$, or GluK2 and GFP were cocultured with wild-type (wt) or *cbln1*-null cerebellar granule cells with or without HA-Cbln1 or HA-CS-Cbln1. HEK293 cells were immunostained for GFP (green) and synaptophysin (Syn; red) and the mean intensities of synaptophysin immunoreactivity in the GFP-positive area are quantified. Scale bar, 50 μm. At least 24 fields were analyzed in three independent experiments. $^{**}P = 9.22 \times 10^{-22}$. (**B**) GluD2^{NTD} and Cbln1 induced functional synapses of granule cells. GluD2^{NTD}-Fc or HA-Fc was conjugated with protein G beads (green) and added to *cbln1*-null cerebellar granule cells with or without HA-Cbln1. Functional presynaptic terminals were labeled with FM4-64 (red), and the mean intensities in the bead areas are quantified. Arrows indicate FM4-64 fluorescence around the beads. Scale bar, 20 μm. At least 150 beads were analyzed for each group in two independent experiments. $^{**}P = 9.52 \times 10^{-49}$. (**C**) EM analysis on the effect of HA-Cbln1. Two days after we injected HA-Cbln1, the percentage of normal synapses (asterisks) was counted in *cbln1*-null, *GluD2*-null, and *cbln1/GluD2*-null mice. Free spines and mismatched synapses are indicated by f and m, respectively. Scale bars, 500 nm. $^{**}P = 5.14 \times 10^{-4}$. (**D**) Functional restoration of PF synapses. PF-evoked EPSC traces (middle traces) were recorded in *cbln1/GluD2*-null Purkinje cells transduced with Sin-GFP or Sin-GluD2-GFP after the subdural injection of HA-Cbln1 in acutely prepared cerebellar slices. GluD2 (red) is expressed in GFP (green)–positive Purkinje cell spines (arrows). Scale bars, 20 μm and 2 μm. The averaged input-output relationship of PF-EPSCs for each condition ($n = 30$ each) is summarized in the lower graph. $^{**}P = 0.0032$ (+HA-Cbln1+GluD2 versus +cont.), $^{**}P = 0.001$ (+HA-Cbln1+GluD2 versus +GluD2) at 200 μA.

with HA-Cbln1 and performed immunohistochemical analysis with antibodies against HA and calbindin (a marker for Purkinje cells). A mutant Cbln1 (HA-CS-Cbln1), in which hexamer formation was disrupted by replacing two cysteines with serines (*9*), was used as a negative control (*10*). Strong punctate immunoreactivity for HA-Cbln1, but not for HA-CS-Cbln1, was observed along the dendrites of wild-type Purkinje cells. In contrast, HA-Cbln1 did not bind to *GluD2*-null Purkinje cells (Fig. 1E). Next, we used antigen-exposing methods, i.e., pepsin pretreatment for light microscopy and postembedding immunogold for electron microscopy, to visualize endogenous Cbln1 in the cerebellum (*11*) using specific antibody (fig. S2). Immunohistochemical analysis of cerebellar slices detected punctate Cbln1 immunoreactivity in the molecular layer of the wild-type, but not the *GluD2*-null, cerebellum (Fig. 1F). Similarly, postembedding immunogold electron microscopic (EM) analysis found that Cbln1 immunoreactivity, which was highly abundant at PF–Purkinje cell synaptic clefts in the wild-type cerebellum [7.8 ± 0.7 particles/μm of postsynaptic density (PSD), n = 100 spines; versus 0.01 ± 0.01 particles/μm of nonsynaptic membranes], was essentially absent in the *GluD2*-null cerebellum (0.2 ± 0.1 particles/μm of PSD, n = 70 spines) (Fig. 1G). In contrast, immunoblot analysis indicated that the Cbln1 protein levels for wild-type and *GluD2*-null cerebella were similar (fig. S3) (*7*), which suggested that endogenous Cbln1 may have been washed away from the *GluD2*-null cerebellum during the immunostaining procedures.

To identify a role for Cbln1-GluD2 interactions in synapse formation, we performed a neuron–HEK293 cell coculture assay. GluD2 expressed in HEK293 cells has been shown to induce synapse formation with cocultured wild-type granule cells in vitro (Fig. 2A) (*2*, *12*, *13*). However, HEK293 cells expressing GluD2 did not accumulate in the synaptic terminals (immunopositive for synaptophysin) of *cbln1*-null granule cells (Fig. 2A). Similarly, HEK293 cells expressing GluD2$^{\Delta NTD}$ did not accumulate in the synaptic terminals of wild-type granule cells (Fig. 2A). In contrast, when HEK293 cells expressing GluD2, but not those expressing GluK2, were incubated with HA-Cbln1, they were able to form synapses even with *cbln1*-null granule cells (Fig. 2A). Although applying HA-Cbln1 induced PF synapse formation in dissociated *cbln1*-null Purkinje cells in culture, it failed to do so in *GluD2*-null or *cbln1*- and *GluD2*-double null (*cbln1*/*GluD2*-null) Purkinje cells (fig. S4). Finally, wild-type Purkinje cells incubated with GluD2^{NTD}-Fc showed a significant reduction in synaptophysin immunoreactivity on their dendrites compared with those treated with HA-Fc (fig. S5), which suggested that GluD2^{NTD}-Fc inhibited synaptogenesis, probably by disrupting endogenous Cbln1-GluD2 interactions.

To determine whether synapses that formed by the Cbln1-GluD2 interactions were functional, we assessed the uptake of the fluorescent styryl dye FM4-64 into presynaptic vesicles (*14*). We incubated *cbln1*-null granule cells with protein G beads coupled to GluD2^{NTD}-Fc or HA-Fc along with HA-Cbln1. Significant FM4-64 fluorescence was detected on the beads coupled to GluD2^{NTD}-Fc only when HA-Cbln1 was coapplied (Fig. 2B).

To determine whether the Cbln1-GluD2 complex was also capable of inducing functional synapses in vivo, we injected HA-Cbln1 into the subarachnoid supracerebellar space above the cerebellar vermis in adult *cbln1*-null (*10*), *GluD2*-null, or *cbln1*/*GluD2*-null mice. *Cbln1*/*GluD2*-null mice displayed ataxia (fig. S6) and a reduced number of PF-Purkinje cell synapses (Fig. 2C) (*5*). Although a single injection of HA-Cbln1 (1 μg/g body weight) restored the ultrastructures of PF–Purkinje cell synapses in adult *cbln1*-null mice (*10*), it was ineffective in the *GluD2*-null or *cbln1*/*GluD2*-null cerebellum (Fig. 2C). We also assessed the recovery of functional PF–Purkinje cell synapses by recording PF-evoked excitatory postsynaptic currents (PF-EPSCs) using the whole-cell recordings in cerebellar slices. We injected Sindbis virus carrying a gene encoding GluD2 with green fluorescent

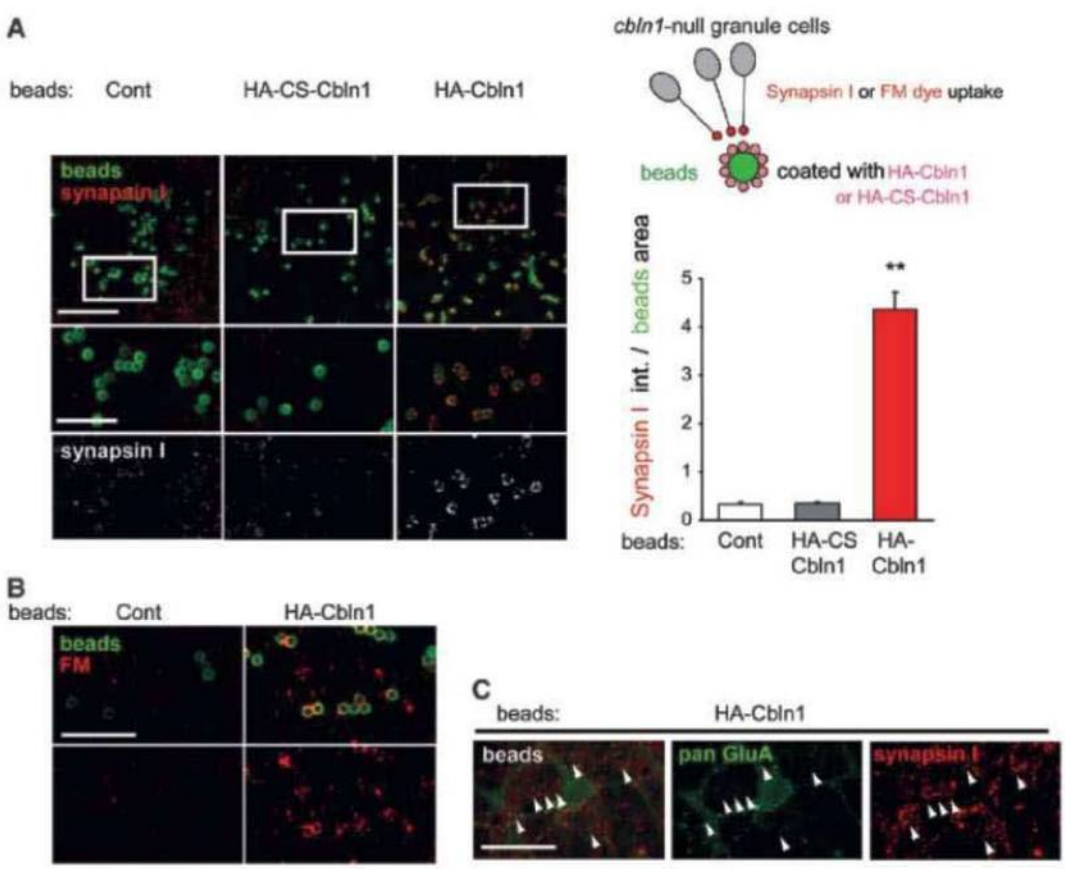

Fig. 3. Cbln1 is a direct presynaptic organizer. (**A** to **C**) HA-Cbln1 or HA-CS-Cbln1 was conjugated with beads and added to *cbln1*-null granule cells at 8 DIV as illustrated in the schematic diagram. (A) HA-Cbln1 immobilized on beads was sufficient for the accumulation of presynaptic terminals. (Left) Confocal images of granule cells (13 DIV) immunostained for synapsin I (red) and beads (green). Regions marked by the white boxes are enlarged below. Scale bars, 50 μm and 20 μm. The averaged intensity of synapsin I in the bead area is quantified on the right. At least 30 fields were analyzed in three independent experiments. $^{**}P = 1.05 \times 10^{-11}$. (B) HA-Cbln1 immobilized on beads was sufficient for the accumulation of functional presynaptic terminals. At 13 DIV, functional presynaptic terminals were labeled with FM4-64 (red). Scale bar, 20 μm. (C) Synaptic terminals were directly induced by HA-Cbln1–coated beads. Synapsin I–immunopositive terminals (red) were induced around HA-Cbln1–coated beads (arrowheads), which were located at extrasynaptic sites lacking endogenous AMPA receptors (pan GluA, green). Scale bar, 20 μm.

protein (GFP) (Sin-GluD2-GFP) into the subarachnoidal space of *cbln1*/*GluD2*-null mice (aged 26 to 33 days) with or without HA-Cbln1 (Fig. 2D). Although the expression of GluD2 restored the reduced PF-EPSCs in adult *GluD2*-null mice (*2*), it was ineffective for *cbln1*/*GluD2*-null Purkinje cells (Fig. 2D). When HA-Cbln1 was injected together with Sin-GluD2-GFP, *cbln1*/*GluD2*-null Purkinje cells displayed PF-EPSCs comparable to those in wild-type Purkinje cells, and these were significantly larger than those transduced with Sin-GluD2-GFP or Sin-GFP [$n = 30$ each; analysis of variance (ANOVA) followed by Bonferroni test, $P < 0.001$] (Fig. 2D).

To further define the roles of each component of the Cbln1-GluD2 complex for organizing synapses, we used a bead-induced synaptic differentiation assay. First, to examine if Cbln1 alone could induce presynaptic terminals, we incubated *cbln1*-null granule cells with beads coated with HA-CS-Cbln1 or HA-Cbln1 (Fig. 3A). Immunocytochemical analysis using an antibody against synapsin I (a marker for presynaptic terminals) revealed that presynaptic terminals accumulated only on beads coated with HA-Cbln1, even in the absence of GluD2 (Fig. 3A). In addition, significant FM4-64 fluorescence was detected on the beads coated with HA-Cbln1 (Fig. 3B). Further, synapsin I–immunopositive terminals accumulated around HA-Cbln1–coated beads at extrasynaptic sites that lacked endogenous AMPA receptor clusters (Fig. 3C).

To determine whether the Cbln1-GluD2 complex could also convey signals to postsynaptic sites, we incubated *cbln1*-null Purkinje cells with beads coated with HA-Cbln1. Immunocytochemical analysis showed that GluD2 clustered in Purkinje cells around beads coated with HA-Cbln1, but not those coated with HA-CS-Cbln1 (not shown) or beads alone (Fig. 4A). GluD2 clustering was also induced around HA-Cbln1–coated beads at extrasynaptic sites that

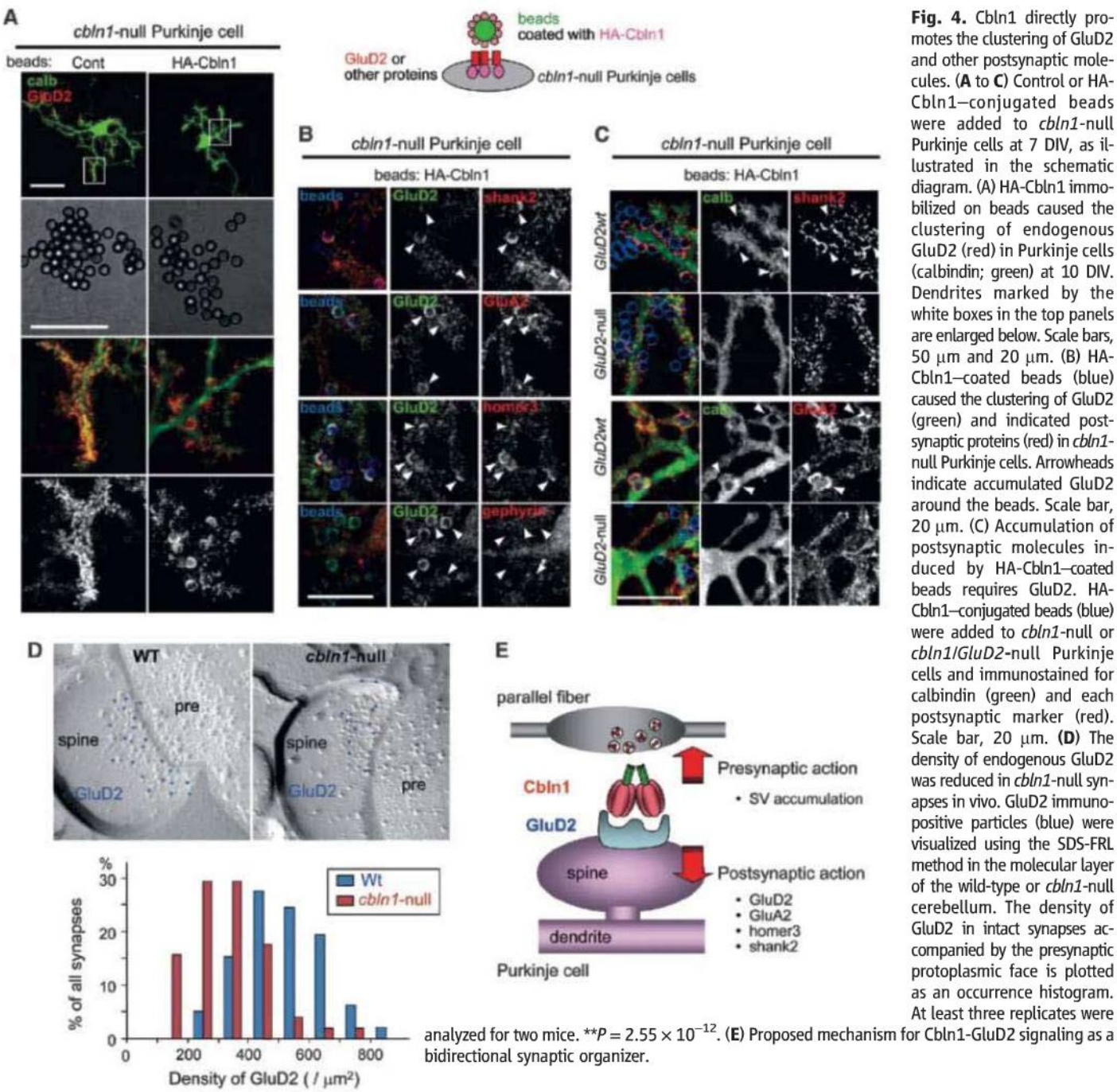

Fig. 4. Cbln1 directly promotes the clustering of GluD2 and other postsynaptic molecules. (**A** to **C**) Control or HA-Cbln1–conjugated beads were added to *cbln1*-null Purkinje cells at 7 DIV, as illustrated in the schematic diagram. (A) HA-Cbln1 immobilized on beads caused the clustering of endogenous GluD2 (red) in Purkinje cells (calbindin; green) at 10 DIV. Dendrites marked by the white boxes in the top panels are enlarged below. Scale bars, 50 μm and 20 μm. (B) HA-Cbln1–coated beads (blue) caused the clustering of GluD2 (green) and indicated postsynaptic proteins (red) in *cbln1*-null Purkinje cells. Arrowheads indicate accumulated GluD2 around the beads. Scale bar, 20 μm. (C) Accumulation of postsynaptic molecules induced by HA-Cbln1–coated beads requires GluD2. HA-Cbln1–conjugated beads (blue) were added to *cbln1*-null or *cbln1*/*GluD2*-null Purkinje cells and immunostained for calbindin (green) and each postsynaptic marker (red). Scale bar, 20 μm. (**D**) The density of endogenous GluD2 was reduced in *cbln1*-null synapses in vivo. GluD2 immunopositive particles (blue) were visualized using the SDS-FRL method in the molecular layer of the wild-type or *cbln1*-null cerebellum. The density of GluD2 in intact synapses accompanied by the presynaptic protoplasmic face is plotted as an occurrence histogram. At least three replicates were analyzed for two mice. $^{**}P = 2.55 \times 10^{-12}$. (**E**) Proposed mechanism for Cbln1-GluD2 signaling as a bidirectional synaptic organizer.

lacked endogenous synapsin I–immunopositive presynaptic terminals (fig. S7). Further, HA-Cbln1–coated beads induced clustering of GluD2 and GluD2^{ext}-GluK2, but not GluD2$^{\Delta NTD}$, GluK2, or GluK2^{ext}-GluD2, in HEK293 cells (fig. S8).

The C terminus of GluD2 interacts directly with several intracellular molecules, such as shank-2 (*15*) and PSD-93/95 (*16*); many of these serve as scaffolds for other postsynaptic molecules, including homer-3, transmembrane AMPA receptor regulatory protein (TARP), and AMPA glutamate receptors (GluAs). Thus, we examined if the clustering of GluD2 induced by the Cbln1-coated beads might accumulate with other postsynaptic molecules in Purkinje cells. With GluD2, shank-2, homer-3, and GluA2 clustered in Purkinje cells around the beads coated with HA-Cbln1 (Fig. 4B). In contrast, HA-Cbln1–coated beads did not accumulate gephyrin [an anchoring protein for the γ-aminobutyric acid (GABA) receptor] (Fig. 4B) or excitatory amino acid transporter 4 (EAAT4, a neuronal glutamate transporter) (fig. S9) in Purkinje cells. HA-Cbln1–coated beads did not induce clustering of shank-2 or GluA2 in *cbln1/GluD2*-null Purkinje cells (Fig. 4C). Shank-2 and PSD-95 accumulated around HA-Cbln1–coated beads only when the responsible C-terminal domains of GluD2 were intact (fig. S10).

To further identify a role for Cbln1 as a postsynaptic organizer in vivo, we examined if the distribution of GluD2 was affected in *cbln1*-null Purkinje cells using the SDS-digested freeze-fracture replica labeling (SDS-FRL) method, which has a nearly one-to-one detection sensitivity for each iGluR on the surface of the postsynaptic membrane specialization (*17*). To exclude a possible effect of the presence of non-innervated spines in the *cbln1*-null cerebellum (Fig. 2C), we counted the number of immunoparticles detected by GluD2-specific antibody (fig. S11) in intact synapses, which were accompanied by the presynaptic protoplasmic face. The number of GluD2 immunoparticles located on postsynaptic membranes was significantly reduced in *cbln1*-null Purkinje cells (Fig. 4D, $P < 0.001$), which indicated that Cbln1 serves as a postsynaptic organizer in vivo and contributes to the clustering of postsynaptic GluD2.

We have demonstrated that Cbln1 is a ligand for the orphan receptor GluD2. Among known synapse-organizing molecules, such as neuroligin-neurexin (*18*), SynCAM-SynCAM (*19*), EphrinB-EphB (*20*), fibroblast growth factor (FGF) 22–FGF receptor 2b (*21*), Narp-GluAs (*22*), and netrin-G ligand-3 and leukocyte common antigen-related (NGL-3–LAR) (*23*), Cbln1-GluD2 signaling is unique in that without each component, synapse formation was severely abrogated in the cerebellum in vivo as well as in heterologous cells in vitro. Its bidirectional mode of action is also unique; at synaptic junctions, presynaptically derived Cbln1 accumulates and directly induces presynaptic differentiation, possibly by interacting with unidentified proteins on the presynaptic membrane (Fig. 4E). Because beads coated with HA-Cbln1 induced accumulation of functional presynaptic terminals (Fig. 3), GluD2 may simply serve as a scaffold to accumulate and stabilize Cbln1 at synaptic junctions. Conversely, Cbln1 probably serves as a postsynaptic organizer by clustering GluD2, which may regulate synaptic plasticity via its interacting intracellular proteins (*24*).

Cbln1 is also expressed in various brain regions where GluD2 is not expressed, such as the olfactory bulb, the entorhinal cortex, and certain thalamic nuclei (*25*), which indicates that Cbln1 may bind to other receptors in these regions. An alternative candidate receptor is GluD1, which is highly expressed in these brain regions, especially during development (*26*). Indeed, HA-Cbln1 could bind to HEK293 cells that expressed GluD1 (fig. S12A) or beads coated with GluD1^{NTD}-Fc (fig. S12B). Furthermore, other Cbln family proteins (Cbln2 and Cbln4) are expressed in various brain regions (*25*). Therefore, further studies are warranted to elucidate the synaptic roles of Cbln and GluD family proteins in normal and pathological conditions in the CNS.

References and Notes

1. N. Kashiwabuchi *et al.*, *Cell* **81**, 245 (1995).
2. W. Kakegawa *et al.*, *J. Neurosci.* **29**, 5738 (2009).
3. T. Takeuchi *et al.*, *J. Neurosci.* **25**, 2146 (2005).
4. M. Yuzaki, *Cell. Mol. Life Sci.* **65**, 1698 (2008).
5. H. Hirai *et al.*, *Nat. Neurosci.* **8**, 1534 (2005).
6. M. Yuzaki, *Neuroscience* **162**, 633 (2009).
7. P. Wei, Y. Rong, L. Li, D. Bao, J. I. Morgan, *Mol. Cell. Neurosci.* **41**, 258 (2009).
8. Materials and methods are available as supporting material on *Science* Online.
9. D. Bao, Z. Pang, J. I. Morgan, *J. Neurochem.* **95**, 618 (2005).
10. A. Ito-Ishida *et al.*, *J. Neurosci.* **28**, 5920 (2008).
11. E. Miura, K. Matsuda, J. I. Morgan, M. Yuzaki, M. Watanabe, *Eur. J. Neurosci.* **29**, 693 (2009).
12. T. Uemura, M. Mishina, *Biochem. Biophys. Res. Commun.* **377**, 1315 (2008).
13. T. Kuroyanagi, M. Yokoyama, T. Hirano, *Proc. Natl. Acad. Sci. U.S.A.* **106**, 4912 (2009).
14. T. Iijima, K. Emi, M. Yuzaki, *J. Neurosci.* **29**, 5425 (2009).
15. T. Uemura, H. Mori, M. Mishina, *Mol. Cell. Neurosci.* **26**, 330 (2004).
16. K. W. Roche *et al.*, *J. Neurosci.* **19**, 3926 (1999).
17. M. Masugi-Tokita *et al.*, *J. Neurosci.* **27**, 2135 (2007).
18. B. Chih, H. Engelman, P. Scheiffele, *Science* **307**, 1324 (2005).
19. T. Biederer *et al.*, *Science* **297**, 1525 (2002).
20. M. S. Kayser, A. C. McClelland, E. G. Hughes, M. B. Dalva, *J. Neurosci.* **26**, 12152 (2006).
21. H. Umemori, M. W. Linhoff, D. M. Ornitz, J. R. Sanes, *Cell* **118**, 257 (2004).
22. R. O'Brien *et al.*, *J. Neurosci.* **22**, 4487 (2002).
23. J. Woo *et al.*, *Nat. Neurosci.* **12**, 428 (2009).
24. W. Kakegawa *et al.*, *J. Neurosci.* **28**, 1460 (2008).
25. E. Miura, T. Iijima, M. Yuzaki, M. Watanabe, *Eur. J. Neurosci.* **24**, 750 (2006).
26. H. Lomeli *et al.*, *FEBS Lett.* **315**, 318 (1993).

27. We thank J. Motohashi for excellent technical support. This work was supported by a grant-in-aid from Japanese Government Ministry of Education, Culture, Sports, Science and Technology (MEXT) (M.Y.), the Takeda Science Foundation (M.Y.), the Naito Memorial Grant for Female Researchers (K.M.), and the Core Research for Evolutional Science and Technology from the Japanese Science and Technology Agency (M.Y.).

Supporting Online Material

www.sciencemag.org/cgi/content/full/328/5976/363/DC1
Materials and Methods
Figs. S1 to S12
References

25 November 2009; accepted 5 March 2010
10.1126/science.1185152

Rapid Diversification of Cell Signaling Phenotypes by Modular Domain Recombination

Sergio G. Peisajovich,[1]* Joan E. Garbarino,[1,2] Ping Wei,[1,3] Wendell A. Lim[1,2]†

Cell signaling proteins are often modular, containing distinct catalytic and regulatory domains. Recombination of such biological modules has been proposed to be a major source of evolutionary innovation. We systematically analyzed the phenotypic diversity of a signaling response that results from domain recombination by using 11 proteins in the yeast mating pathway to construct a library of 66 chimeric domain recombinants. Domain recombination resulted in greater diversity in pathway response dynamics than did duplication of genes, of single domains, or of two unlinked domains. Domain recombination also led to changes in mating phenotype, including recombinants with increased mating efficiency over the wild type. Thus, novel linkages between preexisting domains may have a major role in the evolution of protein networks and novel phenotypic behaviors.

Domains are the basic functional and structural modules in proteins (*1*). In signaling networks, domains generally encode one of two major functions: (i) regulation or localization and (ii) catalysis. Catalytic domains directly transmit signaling information (e.g., through phosphorylation), whereas regulatory domains mediate interactions that either target or regulate this catalytic activity. The vast number of domain combinations found in the proteome suggests that domain shuffling could be a major source of evolutionary innovation in signaling behaviors (*2*–*4*). Three principal lines of evidence support this view. First, specific

changes in protein functions have been associated with domain recombination (*5*). Second, mutations leading to the fusion of protein-coding genes may lead to the improper activation of signaling networks that result in oncogenic transformations (*6*, *7*). Third, fusions of diverse regulatory and catalytic domains can yield synthetic proteins with non-natural input/output relationships, both in vitro (*8*) and in vivo (*9*–*11*).

To investigate whether recombination of signaling protein domains provides a route for evolutionary innovation, analogous to the swapping of cis-regulatory elements and coding sequences in transcriptional circuits (*12*–*14*), we have systematically determined the effects of domain recombination on the behavior of a well-understood signaling network, the yeast mating pathway (Fig. 1A), and compared it to the effects brought about by gene or domain duplication. We used the domains of 11 proteins belonging to the mating pathway to construct a library of 66 recombinant proteins (Fig. 1B). Specifically, all native proteins composed of at least two domains were split in a manner that separated regulatory and catalytic domains. The split points were chosen to ensure that domains were left intact and therefore are located within interdomain connecting regions. We then created a library of chimeric proteins that includes all possible recombinations of N-terminal and C-terminal blocks to systematically map the resulting phenotypic effects (Fig. 1C and fig. S1). Each protein was transformed into a yeast strain that retained the endogenous copies of the 11 mating pathway genes, such that an additional protein (with altered domain combination) was added to the existing network. To distinguish the effects of domain recombination from those of gene or domain duplication, we created three additional sets of strains (Fig. 1D): In the first one, each of the 11 genes analyzed was duplicated; in the second one, each of the N- or C-terminal blocks was duplicated; and in the third one, each possible pair of N- and C-terminal blocks were duplicated and coexpressed (all 66 combinations lacking domain recombination). To prevent any bias that might be related to differential transcriptional control, we expressed all constructs at low abundance using a 250 base pair segment of the constitutive *cyc1* promoter.

As a metric for how each additional protein altered signaling behavior, we measured the dynamics of mating pathway activation by flow cytometry. A green fluorescent protein (GFP) reporter was controlled by a mating-responsive promoter from the *fus1* gene (*15*) in an a-type, Δ*far1* strain [to prevent cell cycle arrest and the formation of mating projections that could affect flow cytometry measurements (*16*)]. We measured the intensity of GFP fluorescence before and after activation of the mating pathway with α-factor and used those values to calculate the baseline and slope of activation (Fig. 2A). The normalized baseline and slope values for each variant in our libraries (relative to wild type) were plotted on a "morphospace" diagram. Gene and domain duplications had little effect on the dynamics of pathway activation (Fig. 2, B and C). Only three domain duplication variants showed changes, slightly inhibiting pathway activation (variants with lower slopes in Fig. 2C), perhaps by acting as dominant negative fragments. In contrast, recombination of domains resulted in

[1]Department of Cellular and Molecular Pharmacology, University of California, San Francisco, 600 16th Street, San Francisco, CA 94158, USA. [2]Howard Hughes Medical Institute, University of California, San Francisco, CA, USA. [3]Center for Theoretical Biology, Peking University, Beijing 100871, China.

*Present address: Illumina, Inc., San Diego, CA 92121, USA. †To whom correspondence should be addressed. E-mail: lim@cmp.ucsf.edu

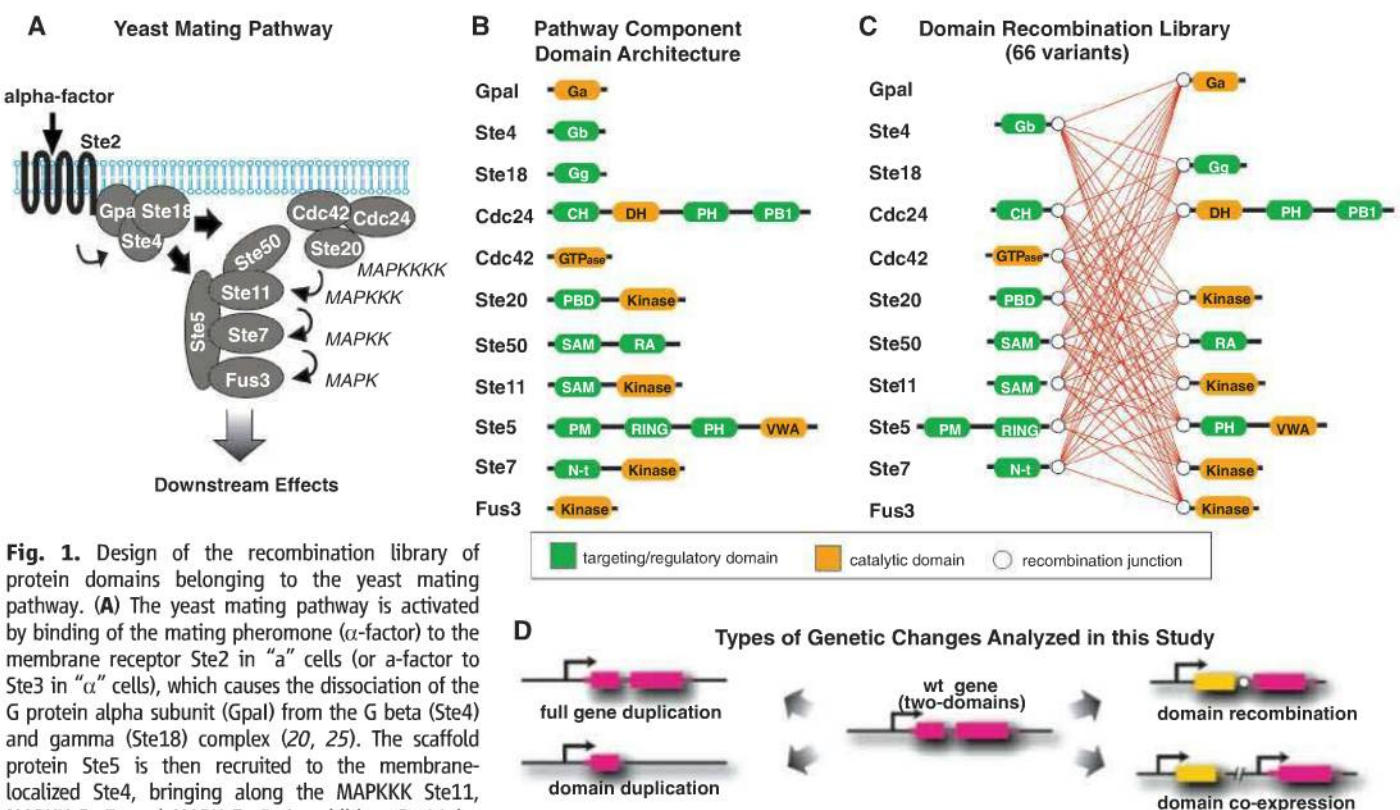

Fig. 1. Design of the recombination library of protein domains belonging to the yeast mating pathway. **(A)** The yeast mating pathway is activated by binding of the mating pheromone (α-factor) to the membrane receptor Ste2 in "a" cells (or a-factor to Ste3 in "α" cells), which causes the dissociation of the G protein alpha subunit (Gpa1) from the G beta (Ste4) and gamma (Ste18) complex (*20*, *25*). The scaffold protein Ste5 is then recruited to the membrane-localized Ste4, bringing along the MAPKKK Ste11, MAPKK Ste7, and MAPK Fus3. In addition, Ste11 interacts with the bridging protein Ste50, which by binding to the small guanosine triphosphatase (GTPase) Cdc42, positions Ste11 near its upstream activator, the PAK kinase Ste20 (*26*). Activated Ste11 phosphorylates Ste7, which in turn phosphorylates Fus3. The activated MAPK translocates to the nucleus, where it phosphorylates a number of transcription factors, leading to changes in gene transcription, cell cycle progression, and cell morphology and culminating in the fusion between "a" and "α" cells. **(B)** Domain architecture of the yeast mating signaling pathway components. Regulatory domains are shown in green; catalytic domains are shown in orange. Fully annotated domain maps are given in fig. S8. **(C)** Domain recombination library. Recombination junctions are depicted as white circles; all possible recombinations are shown as red connecting lines. **(D)** Possible evolutionary events analyzed in this work. Gene duplication, domain duplication, domain recombination, and coexpression of two duplicated domains.

a wide range of altered dynamic behaviors, with variants that either prevented pathway activation or led to stronger activation of the mating pathway (Fig. 2D). These altered signaling behaviors appear to depend on domain recombination, because coexpression of all analogous pairs of unlinked N- and C-terminal domain blocks had limited effects on pathway activation (Fig. 2E). At least for the genes and signaling pathway analyzed here, gene or domain duplication alone may contribute little to the immediate diversification of signaling phenotypes; changes in pathway behaviors probably require sequence divergence of the duplicates [e.g., by neofunctionalization or by differential transcriptional regulation of subfunctionalized duplicates (*17*, *18*); see fig. S2]. In contrast, shuffling of domains provides a more direct path to functional divergence (*19*), resulting in readily available alterations in signaling behaviors.

Beyond changes in gene expression, activation of the mating pathway leads to a coordinated response that arrests cell cycle, alters cell morphology, and ultimately results in the fusion of mating partners (*20*). To determine whether changes in reporter gene expression dynamics caused by domain recombination were mirrored by changes in overall pathway outcome, we measured the efficiency with which "a" strains, expressing domain recombination variants, mated with wild-type "α" cells. We focused on the 10 recombination variants with dynamic behaviors most different from wild type and from the corresponding coexpressed N- and C-domain pair (figs. S3 and S4) and measured the percentage of "a" cells that successfully mated when coincubated with "α" cells (*21*). Yeast strains expressing domain recombination variants with slopes of pathway activation greater than that of wild type mated more efficiently than did wild-type yeast (Fig. 3A and table S1). The same was true for one variant with high baseline of pathway activation but slightly lower slope (Ste4[N]-Ste5[C]). In contrast, yeast strains expressing variants with activation slopes lower than that of wild type mated more poorly. The observed changes in mating efficiency also appeared to depend on domain recombination, because there were marked differences between the mating efficiencies of corresponding recombination and coexpression variants (Fig. 3B). Thus, domain recombination can alter complex pathway outputs, such as the biochemical and morphological changes needed for mating. At least under laboratory conditions, recombination of protein domains can lead to strains that mate more efficiently than wild type, although further work is needed to determine whether the changes in mating efficiency we observed could confer a selective advantage.

Activation of the mating pathway response alters the regulation of the cell cycle (*16*). In addition, the mating pathway shares several proteins with other signaling pathways, such as the high osmolarity pathway. Thus, domain

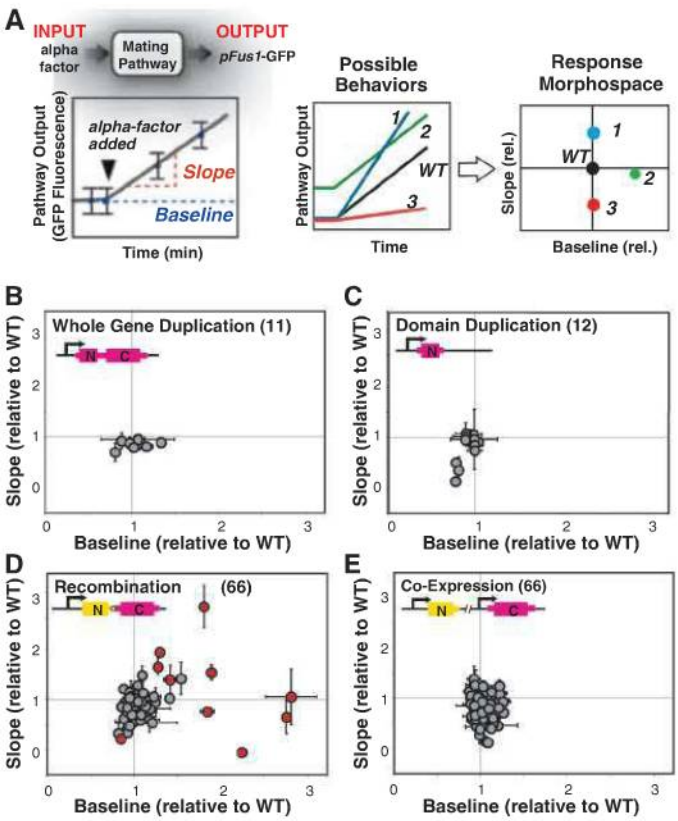

Fig. 2. Recombination of protein domains results in diversification in signaling behaviors. (**A**) Mating pathway activation was measured by flow cytometry, using a GFP reporter under the control of a promoter (from the Fus1 gene) that responds to pathway activation, in an a-type ΔFar1 strain. Time course measurements of GFP fluorescence were done to calculate the baseline and slope of pathway activation under conditions of linear pathway response. Baseline and slopes were then normalized relative to wild-type values, and the resulting values were plotted in pathway morphospace. (**B**) Gene duplications had minor effects on mating pathway response dynamics, with most values clustered around wild type. (**C**) Domain duplications also had minor effects on mating pathway response dynamics; duplication of Ste50[N] (Ste50's SAM domain), Ste5[N] (which includes Ste5's RING domain), and Ste11[N] (Ste11's SAM domain) are exceptions with low slopes and may act as dominant negative. (**D**) Domain recombination led to a diverse set of novel signaling behaviors. Recombination variants with dynamic behaviors most different from wild type and from the corresponding coexpressed N- and C-domain pair (fig. S3) are shown in red. (**E**) These behaviors could not be recapitulated by coexpression of the unlinked corresponding pairs of domains. Fluorescent values were measured in at least two independent experiments, each time in triplicate. Error bars: mean values ± SD.

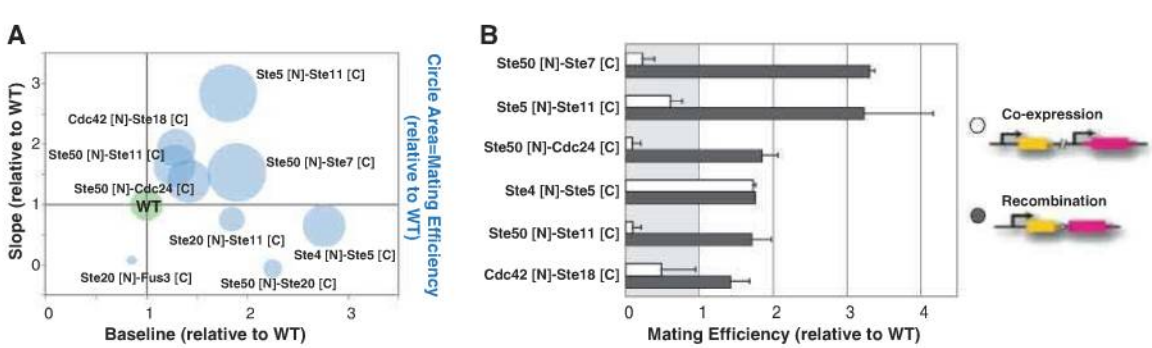

Fig. 3. Domain recombination can lead to strains that mate more efficiently than wild type. (**A**) Mating efficiencies were measured for recombination variants with slope and baseline values that were substantially different from wild type (>1 SD) and also different from the slope and baseline values of the corresponding coexpressed N and C pair (figs. S3 and S4). Mating efficiencies of wild type and recombination variants are depicted as circles, with areas representing relative mating efficiencies. (**B**) Comparison of domain recombination to coexpression of the corresponding domain pairs (wild-type values are set to 1). Ste50 SAM domain interacts with the Ste11 (MAPKKK) N-terminal SAM domain, facilitating the interaction of Ste11 with Ste20, its upstream activator. Thus, it is possible that, as an isolated domain, Ste50[N] (as well as Ste11[N]) act as dominant negatives, competing for the interaction between the wild-type proteins.

recombination variants that alter the mating pathway response could also have pleiotropic effects on other cellular processes. To investigate this possibility, we measured growth rate, as well as the response to high osmolarity stimulus, for the recombination variants that most substantially affected mating response. We found that variants with growth rate deficiencies of only 2 to 3% compared to wild type (fig. S5A) mate up to ~3 times better than wild type. This suggests that, in some cases and under laboratory conditions, the cost in asexual growth likely imposed by recombination-induced network remodeling could be compensated in part by the benefit in mating efficiency it confers (fig. S5B). In addition, we observed that the response to high osmolarity is only marginally affected (fig. S5C). We cannot rule out the possibility that some of the variants analyzed might have detrimental effects on other signaling pathways or cellular processes.

Signaling responses are often characterized by their dynamics of temporal activation, as well as by the specific dose-response profile: Whereas some pathways follow a graded dose response, others have switch-like activation profiles (*22*). To explore whether domain recombination could also alter the dose-response profile, we measured pathway response at different concentrations of pheromone for two of the domain recombination variants that most markedly affected the mating pathway temporal response. We found that cells expressing the domain recombination variants Ste50[N]-Ste7[C] and Ste5[N]-Ste11[C] have dose-response profiles similar to that of wild-type cells, with only a small shift toward lower concentrations of pheromone for cells expressing Ste5[N]-Ste11[N] (fig. S6A). In addition, we observed a wider cell-to-cell variation in pathway response for the domain recombination variant Ste5[N]-Ste11[C] (fig. S6B). These results suggest that domain recombination might slightly alter the sensitivity of the mating pathway to pheromone levels.

We investigated the mechanisms by which recombination variants might alter the dynamics of the response. We first measured protein abundance for some duplication or recombination variants and found that there is no clear correlation between changes in mating response and protein abundance (fig. S7). Mating pathway signaling requires interactions between three major functional complexes: the membrane-bound G protein complex, the mitogen-activated protein kinase (MAPK) complex, and the membrane-bound polarity complex (Fig. 1). Recruitment of the MAPK complex to the membrane, by its interaction with the G protein complex, positions the MAPKKK, Ste11, close to its p21-activated protein kinase (PAK) kinase activator, Ste20 (also referred to as the MAPKKKK), a member of the polarity complex (*20*, *23*).

Close examination of the 10 recombination variants that most markedly changed signaling behavior revealed that 7 of the 10 created novel links between the different signaling complexes, whereas only three created linkages within an individual functional complex (Fig. 4A). Thus, new behaviors may arise when key components change in their localization or complex formation. To explore this hypothesis, we examined three recombinant variants in greater detail. The Ste20[N]-Ste11[C] fusion [which tethers the Cdc42 binding domain of Ste20 to the kinase domain of Ste11 (fig. S8)] resulted in higher baseline output (Fig. 4B). This fusion protein may result in the recruitment of Ste11 kinase domain to the polarity complex, even in the absence of α-factor stimulation, where it can be constitutively activated by Ste20 [the MAPKKKK (fig. S9A)]. This relocalization to sites of polarity was confirmed by microscopy experiments with the GFP-labeled fusion protein (Fig. 4C). The Ste5[N]-Ste11[C] fusion [which tethers the Ste4 binding domain of Ste5 to the kinase domain of Ste11 (fig. S8)] resulted in a large increase in the slope of output (Fig. 4D). This fusion may result in an additional population of Ste11 kinase domain that, because it is covalently fused to Ste5[N], is more efficiently recruited to the membrane upon α-factor stimulation, which may increase signaling (fig. S9B). Microscopy studies confirmed that this fusion protein is inducibly localized to membrane sites of polarization (Fig. 4E). The Ste50[N]-Ste20[C] fusion [which tethers Ste11 binding sterile alpha motif (SAM) domain of Ste50 to the kinase domain of Ste20 (Fig. S8)] resulted in high constitutive activation (Fig. 4F). This fusion protein may bring the Ste20 kinase domain to the MAPK complex, where it will constitutively activate Ste11 and trigger the MAPK cascade, without the need for membrane recruitment of the MAPK complex (fig. S9C). Microscopy studies confirmed that this fusion localizes to the cytoplasm both with and without α-factor stimulation (Fig. 4G). Overall, these more detailed observations are consistent with a model in which shuffling of a catalytic domain with different regulatory domains results in novel regulation or localization of the catalytic domain, leading to distinct changes in signaling behavior and cellular phenotype.

The high frequency with which the limited diversity encoded in our recombination library led to novel signaling behaviors suggests that domain recombination might have an important role in the generation of phenotypic novelty from simple genotypic changes and could likely complement the role of cis-regulatory elements

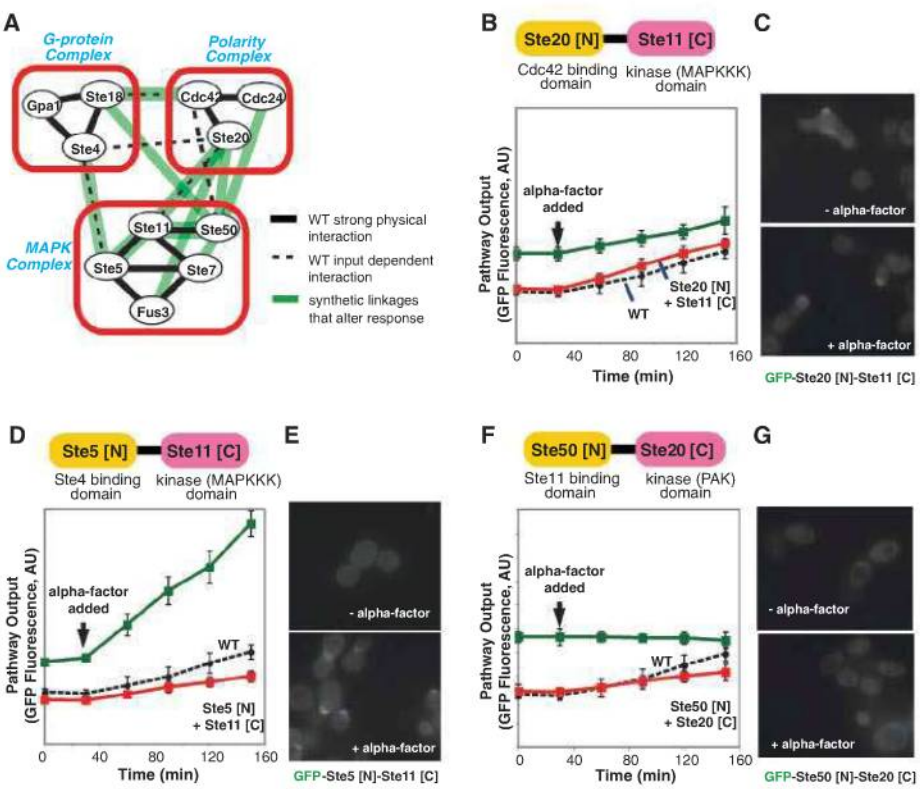

Fig. 4. Mechanisms of recombination-derived changes in signaling behavior. (**A**) Activation of the mating pathway requires interactions between three multiprotein complexes: the membrane-bound G protein complex, the membrane-bound polarity complex, and the MAPK complex. Seven novel connections between the three multiprotein complexes and three novel connections within an individual complex formed by the recombination variants were analyzed. (**B**, **D**, and **F**) Flow cytometry time course of pFus1-GFP for strains expressing Ste20[N]-Ste11[C], Ste5[N]-Ste11[C], and Ste50[N]-Ste20[C], respectively. (**C**, **E**, and **G**) Fluorescence microscopy of strains expressing GFP-labeled Ste20[N]-Ste11[C], Ste5[N]-Ste11[C], and Ste50[N]-Ste20[C], respectively.

in the evolution of global cellular regulatory networks composed of both transcriptional and signaling elements (*24*). Further work will be needed to compare in quantitative terms the contributions of gene duplication and recombination to the evolutionary process.

The strategy used here of targeted domain recombination between proteins that belong to a specific signaling network could facilitate the engineering of other protein networks of interest, a fundamental goal of synthetic biology. Genes known to belong to a target pathway could be deconstructed into domains and used to build small libraries of domain recombinations that are subsequently screened for the desired function.

References and Notes

1. C. Chothia, J. Gough, C. Vogel, S. A. Teichmann, *Science* **300**, 1701 (2003).
2. C. Vogel, M. Bashton, N. D. Kerrison, C. Chothia, S. A. Teichmann, *Curr. Opin. Struct. Biol.* **14**, 208 (2004).
3. T. Pawson, P. Nash, *Science* **300**, 445 (2003).
4. C. A. Voigt, C. Martinez, Z. G. Wang, S. L. Mayo, F. H. Arnold, *Nat. Struct. Biol.* **9**, 553 (2002).
5. M. Bashton, C. Chothia, *Structure* **15**, 85 (2007).
6. T. Pawson, N. Warner, *Oncogene* **26**, 1268 (2007).
7. C. A. Maher *et al.*, *Nature* **458**, 97 (2009).
8. J. E. Dueber, B. J. Yeh, K. Chak, W. A. Lim, *Science* **301**, 1904 (2003).
9. K. Harris *et al.*, *Curr. Biol.* **11**, 1815 (2001).
10. P. L. Howard, M. C. Chia, S. Del Rizzo, F. F. Liu, T. Pawson, *Proc. Natl. Acad. Sci. U.S.A.* **100**, 11267 (2003).
11. B. J. Yeh, R. J. Rutigliano, A. Deb, D. Bar-Sagi, W. A. Lim, *Nature* **447**, 596 (2007).
12. M. C. King, A. C. Wilson, *Science* **188**, 107 (1975).
13. S. B. Carroll, *PLoS Biol.* **3**, e245 (2005).
14. B. Prud'homme, N. Gompel, S. B. Carroll, *Proc. Natl. Acad. Sci. U.S.A.* **104** (suppl. 1), 8605 (2007).
15. C. J. Bashor, N. C. Helman, S. Yan, W. A. Lim, *Science* **319**, 1539 (2008).
16. M. Peter, A. Gartner, J. Horecka, G. Ammerer, I. Herskowitz, *Cell* **73**, 747 (1993).
17. M. Lynch, A. Force, *Genetics* **154**, 459 (2000).
18. F. A. Kondrashov, I. B. Rogozin, Y. I. Wolf, E. V. Koonin, *Genome Biol.* **3**, RESEARCH0008 (2002).
19. R. L. Rogers, T. Bedford, D. L. Hartl, *Genetics* **181**, 313 (2009).
20. H. G. Dohlman, J. W. Thorner, *Annu. Rev. Biochem.* **70**, 703 (2001).
21. G. F. Sprague Jr., *Methods Enzymol.* **194**, 77 (1991).
22. S. Takahashi, P. M. Pryciak, *Curr. Biol.* **18**, 1184 (2008).
23. P. M. Pryciak, F. A. Huntress, *Genes Dev.* **12**, 2684 (1998).
24. J. Gerhart, M. Kirschner, *Proc. Natl. Acad. Sci. U.S.A.* **104** (suppl. 1), 8582 (2007).
25. L. Marsh, A. M. Neiman, I. Herskowitz, *Annu. Rev. Cell Biol.* **7**, 699 (1991).
26. L. Bardwell, *Peptides* **26**, 339 (2005).

27. We thank A. Chau for help with Matlab, N. Helman and J. Walter for help with fluorescence microscopy, and members of the Lim laboratory for critical reading of this manuscript and assistance. This work was supported by grants from the Howard Hughes Medical Institute, the Packard Foundation, the NIH, and the NIH Nanomedicine Development Centers (W.A.L.). S.G.P. was supported by a Long-Term Postdoctoral Fellowship from the Human Frontier Science Program. P.W. was supported by the Li Foundation. S.G.P. and W.A.L. conceived the project. S.G.P. and J.G. performed the experiments. P.W. assisted with initial experiments. S.G.P., J.G., and W.A.L. analyzed the results. S.G.P. and W.A.L. wrote the manuscript. The authors declare no competing financial interests.

Supporting Online Material

www.sciencemag.org/cgi/content/full/328/5976/368/DC1
Materials and Methods
Figs. S1 to S9
Table S1
References

23 September 2009; accepted 9 March 2010
10.1126/science.1182376

Protein Kinase C-θ Mediates Negative Feedback on Regulatory T Cell Function

Alexandra Zanin-Zhorov,[1] Yi Ding,[1] Sudha Kumari,[1] Mukundan Attur,[2] Keli L. Hippen,[3] Maryanne Brown,[4] Bruce R. Blazar,[3] Steven B. Abramson,[2] Juan J. Lafaille,[1] Michael L. Dustin[1]*

T cell receptor (TCR)–dependent regulatory T cell (T_{reg}) activity controls effector T cell (T_{eff}) function and is inhibited by the inflammatory cytokine tumor necrosis factor–α (TNF-α). Protein kinase C-θ (PKC-θ) recruitment to the immunological synapse is required for full T_{eff} activation. In contrast, PKC-θ was sequestered away from the T_{reg} immunological synapse. Furthermore, PKC-θ blockade enhanced T_{reg} function, demonstrating PKC-θ inhibits T_{reg}-mediated suppression. Inhibition of PKC-θ protected T_{reg} from inactivation by TNF-α, restored activity of defective T_{reg} from rheumatoid arthritis patients, and enhanced protection of mice from inflammatory colitis. T_{reg} freed of PKC-θ–mediated inhibition can function in the presence of inflammatory cytokines and thus have therapeutic potential in control of inflammatory diseases.

$CD4^+$ $CD25^+$ regulatory T cells (T_{reg}) suppress the function of $CD4^+$ and $CD8^+$ effector T cells (T_{eff}) through a T cell receptor (TCR) engagement and cell contact–dependent mechanism (*1*–*3*). Inflammatory signals delivered by cytokines like tumor necrosis factor–α (TNF-α) decrease T_{reg} activity (*4*, *5*), perhaps as a mechanism to reduce interference by T_{reg} cells in immune responses to pathogens. In rheumatoid arthritis, T_{reg} cells circulate in normal numbers, but they have decreased activity ex vivo (*5*, *6*). Besides the negative signals initiated by TNF-α, T_{reg} also receive inhibitory signals via the TCR. Akt activation by the TCR can reduce T_{reg} function and thus appears to be tightly regulated (*7*). This suggests TCR signaling in T_{reg} can negatively feed back to inhibit T_{reg}-mediated suppression. Moreover, TCR signaling leads to formation of the immunological synapse within seconds of T cell activation. Thus, the differences in TCR signaling in T_{reg} may emerge at the level of the immunological synapse (IS), a structured interface between T cells and antigen-presenting cells (APCs) where TCR signalosomes are assembled (*8*). Whereas T_{reg} can form stable contacts with APCs with functional consequences both in vitro and in vivo (*9*–*11*), signaling events in the T_{reg} IS have not been investigated.

To study signaling in the human T_{reg} IS, we developed a model system on supported planar bilayers containing the mobile fluorescently labeled intercellular adhesion molecule–1 (ICAM-1) and antigen surrogate anti-CD3 (the signaling subunit of the TCR) antibodies and $CD4^+$ $CD25^+$ T_{eff} or $CD4^+$ $CD25^+$ T_{reg} freshly isolated from peripheral blood (fig. S1, A to C). T_{eff} and T_{reg} both formed IS, defined by a symmetric pattern consisting of a central cluster of anti-CD3 surrounded by a ring of ICAM-1 (*12*, *13*) (Fig. 1A). T_{reg} ISs were more stable than T_{eff} ISs (fig. S2, A and B), which displayed symmetry breaking within 20 min as previously described (*14*). Ex vivo expanded, human umbilical cord blood T_{reg} (*15*) displayed similar behavior to adult peripheral blood T_{reg} (fig. S2, C to E). We measured recruitment of TCR proximal signaling molecules to IS by staining with phospho-Src kinase activation loop and Zap70 kinase interdomain A tyrosine 319 antibodies and imaging with total internal reflection fluorescence microscopy (TIRFM) (*16*). Signals were quantified on the basis of unbiased measurement of IS proximal fluorescence intensity. T_{eff} IS displayed significantly higher amounts of phospho-Src than T_{reg} (fig. S3A); however, we observed a similar intensity of phosphorylation of the downstream kinase Zap70 (fig. S3B). We next explored the protein kinase C-θ (PKC-θ) pathway, which is downstream of Src family kinases (*17*) and mediates IS breaking (*14*), because Zap70 phosphorylation appeared normal in T_{reg}.

[1]Molecular Pathogenesis Program, Helen and Martin Kimmel Center for Biology and Medicine, Skirball Institute of Biomolecular Medicine, Department of Pathology, New York University School of Medicine, New York, NY 10016, USA. [2]Division of Rheumatology, New York University School of Medicine and New York University Hospital for Joint Diseases, New York, NY 10003, USA. [3]University of Minnesota Cancer Center and Department of Pediatrics, Division of Bone, Blood and Marrow Transplantation, Minneapolis, MN 55455, USA. [4]Boehringer Ingelheim, Ridgefield, CT 06877, USA.

*To whom correspondence should be addressed. E-mail: michael.dustin@med.nyu.edu

PKC-θ recruitment to the IS leads to recruitment of Carma-1, a MAGUK (membrane-associated guanylate kinase) protein, which enables the assembly of a Carma-1-Bcl10-Malt1 complex necessary for transcription factor NF-κB activation and subsequent T_{eff} activation (*18*). We quantified PKC-θ and Carma-1 recruitment in ISs on planar bilayers by TIRFM. T_{eff} ISs recruited PKC-θ in a broad pattern overlapping with early TCR signaling, as previously reported (*14*) (Fig. 1B). T_{reg} displayed sixfold lower PKC-θ recruitment to IS than that of T_{eff}, and this recruitment was focused in a limited area defined by a small number of bright puncta (Fig. 1B). The same difference in the ability to recruit PKC-θ was found with ex vivo expanded, human umbilical cord blood T_{reg} and expanded $CD4^+$ $CD25^-$ T_{eff} cells (fig. S4). CD28 co-stimulation plays an important role in PKC-θ recruitment to IS (*13*, *17*). Thus, we compared the ability of T_{reg} and T_{eff} to recruit PKC-θ in the presence of a CD28 ligand, CD80, in the bilayer. The co-stimulatory signal increased the amounts of PKC-θ recruited to ISs in both T_{reg} and T_{eff} (fig. S5). Even in the presence of CD80 in the bilayer, the T_{reg} still have significantly less PKC-θ recruited to the IS than T_{eff} ($P < 0.001$). Interestingly, total PKC-θ expression was even higher in T_{reg} compared with T_{eff} (fig. S6). Moreover, the confocal imaging revealed that PKC-θ was sequestered away from the T_{reg} IS, whereas PKC-θ in T_{eff} accessed the IS and formed cytoplasmic puncta (Fig. 1C and fig. S7). T_{reg} IS also displayed significantly less Carma-1 recruitment than T_{eff} IS (Fig. 1D). Thus, recruitment of PKC-θ and its downstream target to the IS are reduced in T_{reg}.

We further dissected the TCR and LFA-1 integrin-dependent components of PKC-θ recruitment by using bilayers containing either anti-CD3 or ICAM-1, respectively. TCR engagement in T_{eff} was necessary and sufficient for increased PKC-θ recruitment on the basis of a twofold increase in PKC-θ fluorescence intensity on anti-CD3–only bilayers compared with fluorescence on ICAM-1–alone bilayers (Fig. 1, E and F). TCR engagement alone in T_{reg} recruited 11-fold less PKC-θ than in T_{eff}, whereas LFA-1 engagement alone recruited 3.5-fold more PKC-θ than in T_{eff} (Fig. 1, E and F). Thus, TCR triggering in T_{reg} actually down-regulates PKC-θ recruitment to the IS by 7.7-fold compared with basal recruitment by LFA-1 engagement alone (Fig. 1F).

We hypothesized that PKC-θ activation may be part of a negative feedback loop controlling T_{reg} function because TCR signals are essential for T_{reg} function but suppress PKC-θ recruitment. We investigated whether inhibition of PKC-θ with compound 20 (C20) (*19*) may affect the suppressive function of human $CD4^+$ $CD25^+$ T_{reg} cells. T_{eff} function was measured as cytokine secretion and cell proliferation. C20 treatment of only the T_{reg} cells significantly up-regulated their suppressive ability, even in the presence of CD28-mediated costimulation, but did not induce suppressive activity in treated T_{eff} (Fig. 2, A

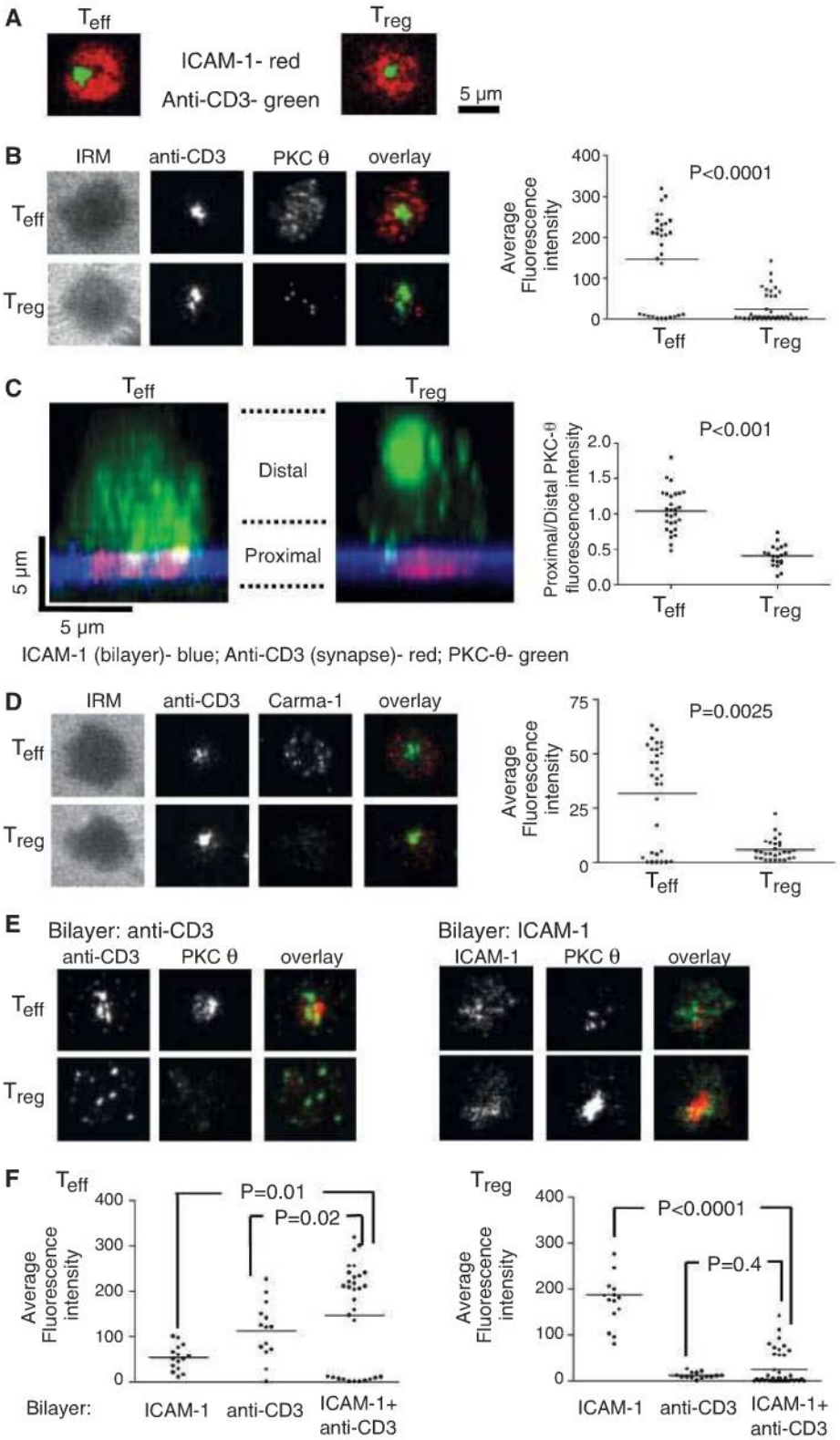

Fig. 1. Human T_{reg} form altered ISs. Human T_{eff} and T_{reg} were introduced into bilayers containing anti-CD3 (5 μg/ml) and ICAM-1 at 250 molecules/mm^2 (**A** to **D**); fixed at 6 min; and permeabilized, stained, and imaged by TIRFM [(A), (B), (D), and (E)] or by confocal microscopy (C). (A) Localization of ICAM-1 (red) and anti-CD3 (green) in the IS. (B and D) Staining and average fluorescence intensity of PKC-θ (B) and Carma-1 (D). (C) Distribution of endogenous PKC-θ in cells. Histogram shows average of (bottom planes "proximal"/upper planes "distal") ratio of anti-PKCθ intensity per cell. The images show representative images. (**E** and **F**) PKC-θ staining (E) and average fluorescence intensity (F) in T_{eff} or T_{reg} on bilayers containing only anti-CD3 (left) or ICAM-1 (right). Data are representative of three [(A) to (D)] or five [(E) and (F)] different experiments. *P* values were calculated by Mann-Whitney test.

and B, and fig. S8A). Consistent with imaging data showing that co-stimulation up-regulates the recruitment of PKC-θ to ISs in T_{reg} (fig. S5), untreated T_{reg} demonstrated reduced ability to suppress T_{eff} function in the presence of CD28 antibodies [40% and 25%, respectively (fig. S8A)], and this difference was abrogated by treatment with C20. Inhibition of PKC-θ seemed to increase T_{reg} suppressive function in general, without preference for specific helper T cell type (fig. S8B). C20 also significantly increased T_{reg} function in an APC-dependent assay (fig. S8C).

It has been reported that the $CD4^+$ $CD25^{high}$ T_{reg} cells are the most potent suppressors in vitro (*20*); we therefore sorted $CD4^+$ T cells according to their CD25 expression (fig. S1D), pretreated the sorted T_{reg} with C20, and cocultured the $CD4^+$ $CD25^{int}$ or $CD4^+$ $CD25^{high}$ T cells with target $CD4^+$ $CD25^-$ T cells. Although the $CD4^+$ $CD25^{high}$ T cells manifested a greater suppressive activity, pretreatment with C20 significantly enhanced their suppression of interferon-γ (IFN-γ) secretion (fig. S8D). Lastly, the effect of C20 on T_{reg} function was time-dependent; we observed the peak of suppressive function after 30 min of treatment (fig. S8E).

TCR-induced DNA binding of NF-κB p65 and p50 subunits, which indicates NF-κB activation, and the ability to proliferate were greatly reduced by C20 in both T_{reg} and T_{eff} (Fig. 2C and fig. S9). To test whether activation of NF-κB was a critical PKC-θ target in control of T_{reg} activity, we inhibited NF-κB activation by using two different types of inhibitors, and both significantly increased T_{reg} activity (Fig. 2D). Moreover, treatment of T_{reg} with analogs of C20 with different median inhibitory concentration (IC_{50}) values demonstrated that, of the analogs tested, only PKC-θ inhibitors with $IC_{50} \leq 1$ nM significantly up-regulated T_{reg} suppressive function (fig. S10). Lastly, neutralizing antibodies against transforming growth factor–β (TGF-β) receptor II completely blocked the suppressive function of T_{reg} induced by inhibition of PKC-θ either in APC-free or in presence of APC in the coculture (Fig. 2E and fig. S8C), suggesting the possible involvement of TGF-β presented by T_{reg} as a suppressive mechanism. To confirm the conclusion that inhibition of PKC-θ up-regulates the suppressive activity of human T_{reg}, we specifically silenced PKC-θ gene expression by using RNA interference (*21*). The specific PKC-θ small interfering RNA (siRNA) reduced PKC-θ expression by 80% (Fig. 2F). Moreover, silencing of PKC-θ significantly increased T_{reg}-mediated suppression of IFN-γ secretion by T_{eff} (Fig. 2F). PKC-θ silencing in T_{eff} resulted in the expected down-regulation of IFN-γ secretion and cell proliferation (fig. S11). We concluded that PKC-θ activity induced by TCR signaling mediates a negative feedback loop that reduces the activity of human $CD4^+$ $CD25^{high}$ T_{reg} to suppress cytokine secretion and proliferation of T_{eff} in vitro.

Rheumatoid arthritis (RA) is a chronic autoimmune disorder that results in the destruction of joint architecture (*22*). Recent studies in RA patients demonstrated that the function of $CD4^+$ $CD25^{high}$ T_{reg} is impaired (*5*, *6*). We used T_{reg} purified from peripheral blood of 25 RA patients

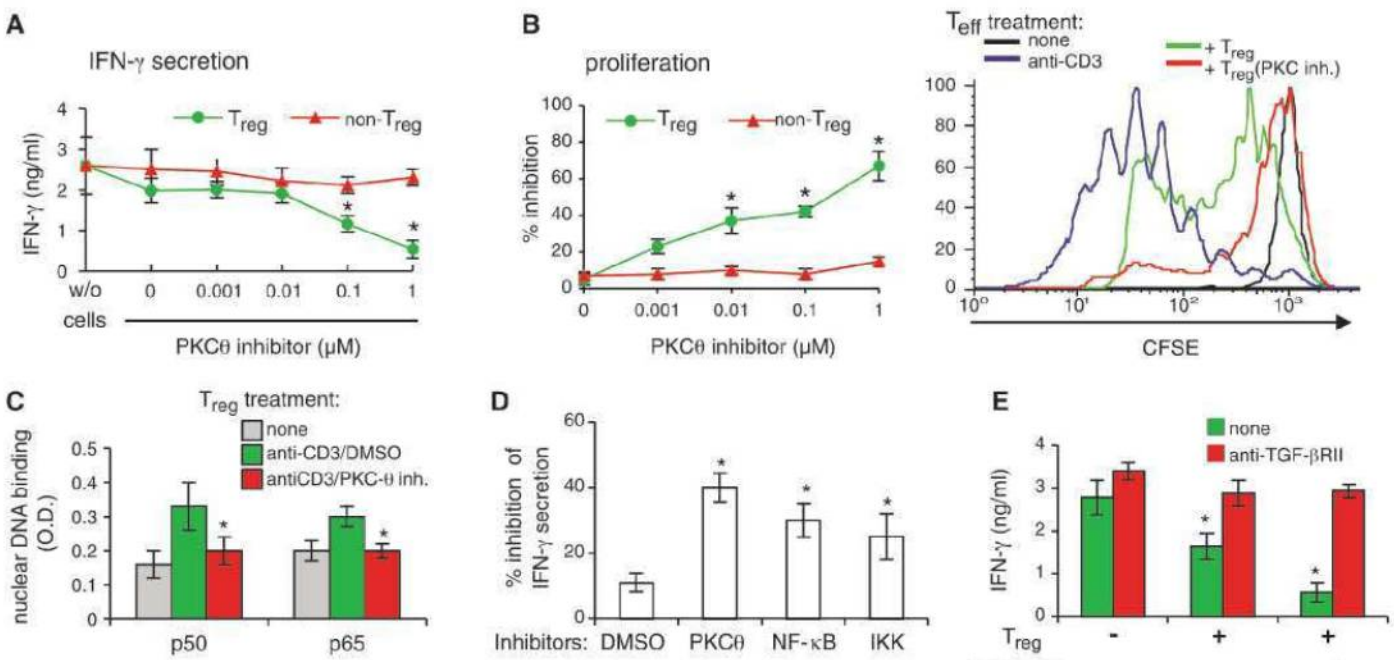

Fig. 2. PKC-θ inhibition up-regulates the suppressive function of T_{reg} in vitro. Average of four different experiments are shown for all graphs. *P* values were calculated by *t* test. (**A** and **B**) T_{reg} and T_{eff} were treated with PKC-θ inhibitor C20 at 0.001 to 1 μM for 30 min and washed three times. Treated cells were then mixed with $CD4^+$ $CD25^-$ T (T_{eff}) cells at a 1:9 ratio and plated on immobilized monoclonal antibody (mAb) against CD3 (anti-CD3). Error bars indicate standard deviation. (**A**) The supernatants were analyzed for IFN-γ after 24 hours by enzyme-linked immunosorbent assay (ELISA). (B) Cell proliferation was determined after 96 hours by Alamar Blue (left), or T_{reg} cells were treated with 1 μM C20 for 30 min, washed, mixed with T_{eff} and proliferation was assayed by carboxyfluorescein diacetate succinimidyl ester (CFSE) (right). (**C**) T_{reg} were treated with 1 μM of C20 for 30 min, washed, and stimulated by anti-CD3, and p65/p50 specific binding to NF-κB consensus sequence was determined by ELISA. O.D., optical density. (**D**) T_{reg} cells were treated with 1 μM of NF-κB and IκB kinase (IKK) inhibitors and mixed with T_{eff}, and IFN-γ secretion was analyzed as in (A) after 48 hours. DMSO, dimethyl sulfoxide. (**E**) T_{reg} were treated with 1 μM of C20, mixed with T_{eff}, and cultured on anti-CD3 with or without neutralizing antibodies against TGF-β RII (20 μg/ml). IFN-γ secretion was analyzed as in (A) after 48 hours. (**F**) T_{reg} were transfected with siRNA targeting PKC-θ or with control siRNA and plated on anti-CD3. After 48 hours, PKC-θ expression was measured by Western blot analysis (top). siRNA-transfected T_{reg} were mixed with $CD4^+$ $CD25^-$ T (T_{eff}) cells at 1:9 ratio and plated on immobilized anti-CD3 mAb. The supernatants were analyzed for IFN-γ after 48 hours.

Fig. 3. Inhibition of PKC-θ rescues and protects T_{reg} function. (**A** and **B**) Freshly purified T_{reg} from healthy donors and RA patients were treated or not with PKC-θ inhibitor C20 for 30 min at 1 μM, washed three times, mixed with $CD4^+CD25^-$ T cells at ratio 1:3, and plated on immobilized anti-CD3. The supernatants were analyzed for IFN-γ after 24 to 48 hours by ELISA. (**C** to **E**) T_{reg} cells from healthy donors were treated with PKC-θ inhibitor C20 [(C) and (E)] or with PKC-θ siRNA (D) as described above and cocultured with $CD4^+$ $CD25^-$ T cells with or without TNF-α (50 ng/ml). IFN-γ secretion was determined after 48 hours by ELISA [(C) and (D)], and proliferation was determined after 96 hours (E). Error bars indicate standard deviation. (**F**) Untreated or TNF-α–treated (50 ng/ml, for 24 hours) T_{reg} were introduced to bilayers with anti-CD3 and ICAM-1, fixed, and imaged by confocal microscopy. Representative images are shown with ICAM-1 (blue), anti-CD3 (red), and PKC-θ (green). Plots show the distribution of endogenous PKC-θ in cells. Each bar shows average of (bottom planes "synapse proximal"/upper planes "synapse distal") ratio of anti-PKCθ intensity per cell. Data points from three independent experiments are included in the analysis.

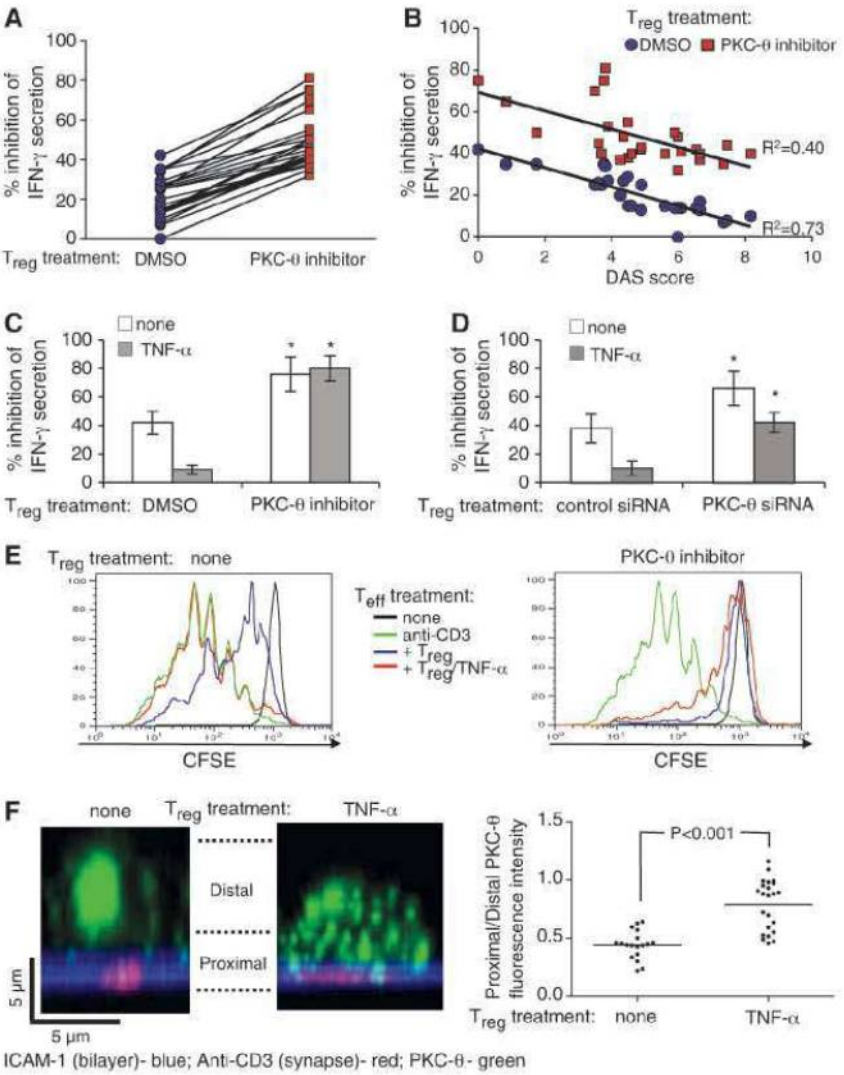

Fig. 4. Treatment with PKC-θ inhibitor up-regulates T_{reg} function in vivo. Colitis was induced in C57BL/10.PL $TCR\alpha^{-/-}$ $\beta^{-/-}$ mice (*31*). Disease progression was monitored by (**A**) body weight loss, (**B**) colitis score, and (**C**) histology. Numbers in parentheses indicate number of mice. Combined data of three independent experiments are presented. *P* values were calculated by *t* test. PBS, phosphate-buffered saline.

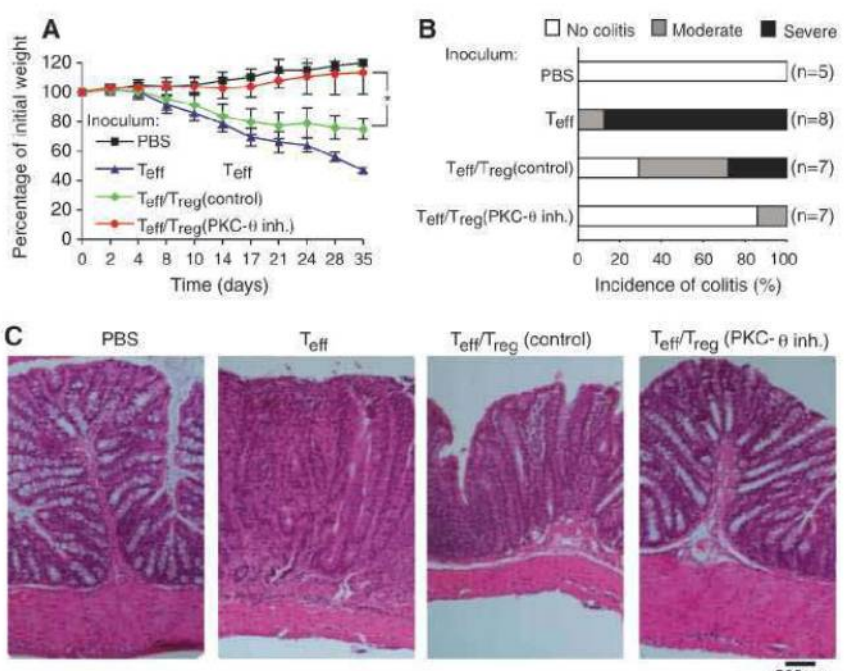

with different severities of disease (fig. S12) and found, despite anergic state and comparable T_{reg} numbers to healthy donors (fig. S13A), that RA T_{reg} demonstrated significantly reduced suppression of IFN-γ from autologous $CD4^+$ $CD25^-$ T_{eff} (fig. S13B). The loss of function was due to defective intrinsic function of T_{reg} from RA patients and not due to increased resistance of T_{eff} (fig. S13C), consistent with previously published results (*5*). Treatment with C20 significantly increased the suppressive function of T_{reg} purified from all 25 RA patients (Fig. 3A) to levels comparable to those of healthy donor-derived T_{reg} (30 to 50% inhibition at a T_{reg}/T_{eff} of 1:3, fig. S13B). Moreover, the defective T_{reg} function in RA patients was inversely correlated with the disease active score (DAS score), and the shift in IFN-γ secretion was similar across the disease score spectrum (Fig. 3B). Thus, inhibition of PKC-θ boosts the suppressive function of T_{reg} isolated from RA patients independent of the severity of disease.

Treatment of T_{reg} cells with TNF-α inhibits their activity and down-regulates expression of the T_{reg} master regulator transcription factor Foxp3 (*5*). We investigated the possibility that elimination of the PKC-θ–mediated negative feedback on T_{reg} function may render T_{reg} resistant to inhibition by TNF-α. As expected, in the presence of TNF-α, T_{reg} displayed significantly reduced inhibition of IFN-γ secretion and proliferation in T_{eff}, and this effect was largely reversed by C20 or PKC-θ–specific siRNA (Fig. 3, C to E, and fig. S14A). Moreover, C20 prevented TNF-α–induced down-regulation of Foxp3 in T_{reg} (fig. S14B). Strikingly, TNF-α treatment induced increased PKC-θ recruitment to IS in T_{reg} by decreasing sequestration at the distal pole (Fig. 3F), consistent with the idea that TCR-activated PKC-θ mediates negative feedback on T_{reg} function that is further enhanced by TNF-α.

Lastly, we determined the ability of C20 to increase T_{reg} function in vivo by using a colitis model in *TCRα*$^{-/-}$ β$^{-/-}$ mice induced by transfer of the $CD4^+$ $CD25^-$ $CD45RB^{high}$ T_{eff} cells (*23*, *24*). Treatment of murine T_{reg} with C20 up-regulated their suppressive function in vitro (fig. S15, A and B). Moreover, C20-treated $CD4^+$ $CD25^+$ T_{reg} cells provided significant protection from colitis, as demonstrated by normal weight gain and normal histology of the distal colon in seven of eight mice (Fig. 4, A to C). C20 treatment increased the number of T_{reg} recovered from mesenteric lymph nodes and the spleen (fig. S15C). This protection was significantly greater than that afforded by T_{reg} left untreated (Fig. 4, A to C). Treatment of $CD4^+$ $CD25^-$ T_{eff} with C20 before transfer with untreated T_{eff} did not protect mice from colitis (fig. S16). Thus, PKC-θ inhibition significantly increased the suppressive effect of T_{reg} in vivo.

T_{reg} function is crucial to prevent autoimmunity in mice and humans. Although T_{reg} numbers in patients suffering from autoimmune diseases are similar to healthy controls, T_{reg} function is defective, probably caused by negative regulation of T_{reg} by the inflammatory milieu (*20*). In the present study, we demonstrate that PKC-θ is sequestered in the distal pole of T_{reg} cells in a manner that reduces its recruitment to the IS. Moreover, inhibition of PKC-θ protects both mouse and human T_{reg} against negative effects of TNF-α, which appears to act in T_{reg} by unleashing PKC-θ from the distal pole. In T_{eff}, PKC-θ is part of a strong positive circuit with free access to TCR signalosomes in the IS, NF-κB activation, increased expression of IL-2, proliferation, and survival (*17*, *25*, *26*). PKC-θ is not sequestered in the distal pole of T_{eff}, although the negative regulators like Csk binding protein are (*27*). In contrast, we noted that T_{reg} display increased IS stability, consistent with decreased PKC-θ activity in the IS and attenuated NF-κB activation. The proposed role of NF-κB in inhibition of T_{reg} function is consistent with the system-wide role of this family of transcription factors in promoting inflammation (*28*). IS stabilization may enhance T_{reg} function on the basis of recent evidence for an important role of IS in T_{reg} effects mediated through dendritic cells (*1*, *29*).

In conclusion, formation of IS induces altered signaling pathways in T_{reg}, which is characterized by reduced recruitment of Src kinases, PKC-θ, and Carma-1 to the IS. Moreover, in T_{reg}, PKC-θ acts as a proinflammatory mediator, and this effect is enhanced by TNF-α. Indeed, T_{reg} treated with C20 displayed enhanced ability to prevent autoimmune colitis and to restore function of T_{reg} from RA patients. Thus, targeting the PKC-θ–mediated negative feedback loop enhances the activity of T_{reg} and makes them resistant to cytokines associated with the inflammatory milieu found in some autoimmune diseases. Thus, inhibition of PKC-θ in T_{reg} may be a valuable component in T_{reg} adoptive immunotherapy to treat autoimmunity and graft versus host disease (*30*).

References and Notes

1. S. Sakaguchi, T. Yamaguchi, T. Nomura, M. Ono, *Cell* **133**, 775 (2008).
2. E. M. Shevach *et al.*, *Immunol. Rev.* **212**, 60 (2006).
3. Y. Zheng, A. Y. Rudensky, *Nat. Immunol.* **8**, 457 (2007).
4. F. Flores-Borja, C. Mauri, M. R. Ehrenstein, *Eur. J. Immunol.* **38**, 934 (2008).
5. X. Valencia *et al.*, *Blood* **108**, 253 (2006).
6. M. R. Ehrenstein *et al.*, *J. Exp. Med.* **200**, 277 (2004).
7. N. K. Crellin, R. V. Garcia, M. K. Levings, *Blood* **109**, 2014 (2007).
8. M. L. Dustin, S. Y. Tseng, R. Varma, G. Campi, *Curr. Opin. Immunol.* **18**, 512 (2006).
9. Q. Tang *et al.*, *Nat. Immunol.* **7**, 83 (2006).
10. D. Q. Tran *et al.*, *J. Immunol.* **182**, 2929 (2009).
11. K. Wing *et al.*, *Science* **322**, 271 (2008).
12. A. Grakoui *et al.*, *Science* **285**, 221 (1999).
13. C. R. Monks, B. A. Freiberg, H. Kupfer, N. Sciaky, A. Kupfer, *Nature* **395**, 82 (1998).
14. T. N. Sims *et al.*, *Cell* **129**, 773 (2007).
15. W. R. Godfrey *et al.*, *Blood* **105**, 750 (2005).
16. G. Campi, R. Varma, M. L. Dustin, *J. Exp. Med.* **202**, 1031 (2005).
17. K. Hayashi, A. Altman, *Pharmacol. Res.* **55**, 537 (2007).
18. D. J. Rawlings, K. Sommer, M. E. Moreno-García, *Nat. Rev. Immunol.* **6**, 799 (2006).
19. C. L. Cywin *et al.*, *Bioorg. Med. Chem. Lett.* **17**, 225 (2007).
20. E. M. Shevach, *Immunity* **30**, 636 (2009).
21. K. K. Srivastava *et al.*, *J. Biol. Chem.* **279**, 29911 (2004).
22. M. Feldmann, *Nat. Rev. Immunol.* **2**, 364 (2002).
23. F. Powrie, J. Carlino, M. W. Leach, S. Mauze, R. L. Coffman, *J. Exp. Med.* **183**, 2669 (1996).
24. Y. Ding, S. Shen, A. C. Lino, M. A. Curotto de Lafaille, J. J. Lafaille, *Nat. Med.* **14**, 162 (2008).
25. C. R. Monks, H. Kupfer, I. Tamir, A. Barlow, A. Kupfer, *Nature* **385**, 83 (1997).
26. Z. Sun *et al.*, *Nature* **404**, 402 (2000).
27. M. H. Shaffer *et al.*, *J. Immunol.* **182**, 1021 (2009).
28. P. J. Barnes, M. Karin, *N. Engl. J. Med.* **336**, 1066 (1997).
29. M. Sarris, K. G. Andersen, F. Randow, L. Mayr, A. G. Betz, *Immunity* **28**, 402 (2008).
30. J. L. Riley, C. H. June, B. R. Blazar, *Immunity* **30**, 656 (2009).
31. Materials and methods are available as supporting material on *Science* Online.

32. This work was funded by NIH through the NIH Roadmap for Medical Research PN2 EY016586 and R01 AI43542 to M.L.D.; a Leukemia and Lymphoma Translational Research grant 6098-09 to B.B. S.K. was supported by the Osaka University Immunology Frontier Research Center. B. Blazer is an ad hoc advisor to Becton Dickinson. Becton Dickinson has purchased licensing rights for the use of T_{reg} cells to prevent alloresponses and autoimmunity. An MTA agreement is required for use of compound 20. M.D. and A.Z.-Z. have applied for patents for the use of compound 20 and RNA interference against PKCθ in adoptive immunotherapy (patent application nos. 61173237 and 61286871).

Supporting Online Material

www.sciencemag.org/cgi/content/full/science.1186068/DC1
Materials and Methods
Figs. S1 to S16
References

16 December 2009; accepted 4 March 2010
Published online 25 March 2010;
10.1126/science.1186068
Include this information when citing this paper.

An Ever-Brighter Future for Fluorescence

New, less toxic fluorescent proteins and tags, and strategies for delivering them, are allowing researchers to watch processes within cells never before observed. Industry and academia are now working to not only detect these processes, but also localize and quantify them. **By Anne Harding**

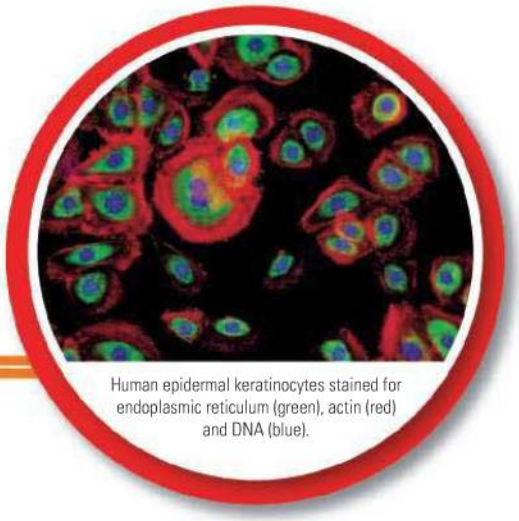

Human epidermal keratinocytes stained for endoplasmic reticulum (green), actin (red) and DNA (blue).

Fluorescent dyes and tags have come a long way since the cloning of green fluorescent protein (GFP) nearly two decades ago. Researchers now have a literal rainbow of products to choose from, in an array of forms from nanoparticles to proteins, and can increasingly multiplex their experiments by using several different colors. "Twenty years ago, people were lucky to be able to detect green fluorescence," says Kathy Free, senior product manager of **Invitrogen,** part of **Life Technologies.** "With the advances in instrumentation, they actually now are comfortable with four or five colors at once."

"Probably since about 2007 there has been a real explosion of new fluorochromes," says Richard Eglen, president of biodiscovery at **PerkinElmer.** "It really is starting to open up the field dramatically."

Roger Tsien, who shared the 2008 Nobel Prize in Chemistry for his work in developing GFP as a tagging tool, developed a series of recombinant fluorescent proteins, including the far-red mPlum and mRaspberry, all derived by directed mutagenesis from a monomeric mutant of DsRed, which itself was derived from a *Discosoma* reef coral fluorescent protein. **Clontech,** a part of the **Takara Bio Group,** which first commercialized GFP technology as a cell biology research tool, back in 1994, also has commercialized these tags as Fruit Fluorescent Proteins.

As always, the makers of fluorescent dyes and tags are aiming for ever-improving brightness and photostability, while the increasingly widespread use of live cells has pushed companies to come up with new ways to illuminate activities within cells without harming them. Progress remains to be made in the development of probes that are spectrally distinct enough in fluorescence and activation to increase multicolor experiment capabilities; meantime, researchers are using photoactivatable and photoswitching proteins to observe biological processes at the molecular scale.

GETTING COLOR INTO THE CELL

Fluorescence is not just about color, of course; it's also about finding new ways to get those colors into the cell. The click chemistry concept introduced by K. Barry Sharpless of the Scripps Research Institute (who shared the 2001 Nobel Prize in Chemistry for this work) is allowing investigators to tag proteins using a much simpler, less toxic process. Invitrogen offers a number of Click-iT labeling kits and reagents based on click chemistry, with reactive probes incorporating the company's Alexa Fluor dyes.

Invitrogen's Click-iT tools use a copper-catalyzed alkyne and azide reaction to join biomolecules. Because the alkyne-azide links use functional groups not found in biological systems, they help investigators avoid nonspecificity and background noise.

"With the advances in instrumentation, researchers actually now are comfortable with four or five colors at once."

Fredika Robertson, a professor at **The University of Texas M.D. Anderson Cancer Center,** uses Invitrogen's Click-iT EdU assay to study the behavior of the tumor-initiating, putative cancer stem cells that give rise to inflammatory breast cancer, a rare and lethal form of the disease that does not respond to chemotherapy or radiation. "The way to enrich for these cells and to study them is to develop three dimensional models in culture," Robertson explains. She and her colleagues culture the cells under low adherence conditions so they spontaneously form tumor spheroids. Robertson has been able to label and track the cells from which these breast cancers emerge using this model.

Initially, Robertson used bromodeoxyuridine (BrdU) to observe replication of these cells. Unlike BrdU, the Click-iT EdU assay does not require extensive pretreatment to visualize the nucleoside label that defines them as "label-retaining cells."

"This is an improvement over BrdU since the quality of the images of the 3D spheroids is improved, allowing quantitation of the label-retaining cells and providing an assay to examine the effect of agents that may target these cancer stem cells," Robertson says.

One limit to the click chemistry approach is the toxicity of copper, Robertson says, although Carolyn Bartozzi, director of the Molecular Foundry at the **Lawrence Berkeley National Laboratory,** and her colleagues are working on a copper-free version. In continued »

UPCOMING FEATURES

Proteomics 1: Mass Spectrometry—May 14

Breakthroughs in Imaging—June 18

Interactomics—July 23

CREDITS: IMAGE COURTESY OF EMELINE RATINEAU, BIOALTERNATIVES, FRANCE; THIS IMAGE WAS OBTAINED USING GE HEALTHCARE'S IN CELL ANALYZER SYSTEM.

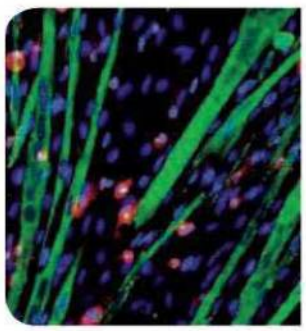

Co-culture of murine macrophages and mesoangioblast stem cells stained for macrophage CD11b (red), mesoangioblast myosin (green) and DNA (blue).

"I think click chemistry has given us the means to view these dynamics in a way that we couldn't do before, but there are innovations coming soon that will make it even better."

January, Bartozzi and her team reported on their use of the copper-free technique to monitor the dynamics of glycans in mice, the first time that click chemistry has been safely used in a living organism.

"I think click chemistry has given us the means to view these dynamics in a way that we couldn't do before," Robertson says. "But there are innovations coming soon that will make it even better."

FOCUSING ON THE RIGHT END OF THE SPECTRUM

Far-red is the hottest end of the spectrum right now for fluorescent dye development, for both microscopy and in vivo imaging, many in the industry say. The instant signal-to-noise ratio advantage that near-infrared fluorescence offers in imaging biological tissues, which do not autofluoresce in this wavelength, allows for seeing more deeply and clearly into samples and animals.

Steve Shifflet, technical product manager for **Thermo Scientific** Pierce Protein Detection Products, says that far-red and near-infrared dyes will continue to be a significant part of his company's efforts. "This will continue to be an area of increasing focus in the life science industry," he said. "This is still a relatively new area that presents lots of opportunities."

In February of this year, Thermo released its DyLight 680B Dye, a brighter version of its DyLight 680. The new dye is significantly brighter than Alexa Fluor 680 Dye, Shifflet says.

Moscow-based **Evrogen** has also made red and far-red fluorescent proteins a focus, says head of product development Ilya Kelmanson. "Now our product line includes four extremely bright red and far-red fluorescent proteins that can be used in different kinds of in vivo imaging applications, including two-photon microscopy and whole body imaging," Kelmanson says.

Evrogen just released a second-generation version of its far-red monomeric fluorescent protein mKate, mKate2, which is three times brighter than its predecessor and 10 times brighter than mPlum, and has a maturation half-time of less than 20 minutes, compared to mCherry's 40 minutes, according to the company.

Clontech also boasts several far-red products designed for in vivo use. "DsRed-Express2 and E2-Crimson were developed and validated specifically for high solubility and use in stem cells and other sensitive cells," says Suvarna Gandlur, product manager at Clontech. "Unlike most far-red fluorescent proteins, E2-Crimson combines a favorable emission wavelength with a bright signal, for easy detection in vivo. Another ideal choice for in vivo imaging is tdTomato, which has been imaged as deep as 1 cm below the surface in SCID [severe combined immunodeficiency] mice." Gandlur said the company is working on developing additional, application-specific fluorescent proteins for in vivo and other uses.

Carestream Health stakes the claim for near-infrared dyes with the biggest Stokes shift. The company's Kodak X-Sight Large Stokes Shift Dyes and LSS Dye Conjugates offer 85 to 98 nanometer separation of excitation and emission peaks within the near-infrared range, the only products now available with such a large, naturally occurring Stokes shift in the near-infrared range, says Seth Gammon, in vivo product manager at Carestream Molecular Imaging.

TARGETING STRUCTURES AND PROCESSES

Fluorescent labels that target specific cell structures and systems for quickly identifying particular processes in cellular metabolism and division are other important areas of growth in the field. Evrogen offers expression vectors for labeling of six subcellular structures and nine key proteins, and a choice of colors is available for most of them. **Active Motif** sells two self-staining kits, one for staining mitochondria, another for staining the cytoskeleton in fixed cells. And Invitrogen's Cellular Lights target six key proteins, while its Organelle Lights target 11 subcellular structures.

Limitations of organelle-specific probes include photobleaching and quenching upon concentration in the target organelle, or only transient association with that organelle, **Enzo Life Sciences** researchers noted in a 2009 report in *FASEB Journal*. In that report, they describe a new "family" of red-emitting, organelle-specific probes—part of their CELLestial product line—that they say are "highly resistant" to these problems.

Cellular processes that can now be studied with "ready to go" fluorescence kits include cellular division, autophagy, apoptosis, and more. Probes produced by Invitrogen and **MBL International** that license work done in the lab of Atsushi Miyawaki at the Brain Science Institute for Physical and Chemical Research (RIKEN) in Tokyo use the fluorescent ubiquitination-based cell cycle (Fucci) to visualize the cell cycle in real time.

Clontech's Lenti-X Actin Dynamics Monitoring Kit allows users to monitor actin filament behavior in live cells. The company also offers Precloned CRE and NFκB DD Reporter Systems, which use Clontech's brightest red, green, and cyan reporters to monitor commonly studied signal transduction pathways.

MAKING SENSE OF SENSORS

One goal companies are reaching for is to make sensors that not only indicate that something is happening, but show where it's happening, quantitatively. "The two strategies are going to be fluorophore/quencher pairs, as well as probes that are actually modified by the chemical they're trying to detect," predicts Carestream's Gammon.

Molecular Devices' FLIPR calcium flux assays, introduced in 1999, employ a calcium-sensing fluorescent dye along with quenching technology, and eliminate the need for cell washing following dye-loading. The company, now a part of **Danaher**, released continued»

CREDIT: MIRIAM ASCAGNI, DIBIT SAN RAFFAELE SCIENTIFIC INSTITUTE, ITALY; THE IMAGE WAS OBTAINED USING GE HEALTHCARE'S IN CELL ANALYZER SYSTEM.

its FLIPR Calcium 5 Kit in June of last year, but expects to keep the original FLIPR Calcium Kit, as well as versions 3 and 4, on the market for as long as its customers need them. "Certain targets respond better to certain versions of the systems," notes applications scientist Carole Crittenden.

Companies are also introducing sensors that use fluorescence resonance energy transfer, or FRET, in which a conformational change brings together two fluorophores attached to the sensor; the excited fluorophore then transfers energy to its unexcited neighbor.

Invitrogen's Molecular Probes Premo Cameleon Calcium sensor uses genetically encoded sensors for FRET-based ratiometric detection for quantitative results, delivered by the company's BacMam system.

Evrogen has two genetically encoded fluorescent sensors for detecting caspase-3 mediated apoptosis in living cells, both FRET-based. The company also sells non-FRET–based sensors, including its HyPer line, the first and only genetically encoded sensor capable of detecting intracellular hydrogen peroxide, and Case12, for detecting intracellular calcium ion changes.

ON AGAIN, OFF AGAIN FLUORESCENCE

Photoactivatable and photoswitchable fluorescent proteins are another key area of innovation, useful for observing dynamic processes within cells and in single molecule–based superresolution protein localization. Photoactivatable fluorescent proteins go from "off" to "on" with exposure to light of a certain wavelength, and will continue to fluoresce until they bleach out. Photoswitchable proteins can be switched from dark to bright or red to green; using light of a different wavelength, they can then be switched back to their original state.

Jennifer Lippincott-Schwartz, who started working with GFP in 1994 and has made major advances in the use of fluorescence in imaging—both at the conventional and molecular levels—has developed a way to use photoswitching and photoactivatable proteins (and even light-activated conventional fluorophores) to watch trafficking within cells at the molecular level. She and her colleagues together with physicists Eric Betzig and Harald Hess first reported on the technique, known as PALM (photoactivated localization microscopy). Xiaowei Zhuang and her colleagues at **Harvard University** have developed a similar technique, STORM (stochastic optical reconstruction microscopy), that uses photoswitchable dyes.

Rather than lighting up ten thousand molecules at once—producing a bunch of overlapping blurry spots—a low amount of activating energy is used to light up just a few at once; this handful of molecules will be far enough apart to be imaged as a spot shape. "That shape, because it has a Gaussian profile, can be fit into an algorithm that allows you to define with very high precision the shape's center, used as the molecule's position," Lippincott-Schwartz explains. Then, thousands of these images are combined to map the total population of molecules. "It's similar to pointillism," she adds. "You're building an image by combining small, distinct spots."

There are over 20 different varieties of photoswitching or photoactivatable proteins available, says Lippincott-Schwartz. "The proliferation of these photoactivatible or photoconvertible fluorescent proteins permits a variety of novel imaging schemes for obtaining new biological insights," she says. "That said, the fluorescent proteins don't give off a huge amount of photons, only about a tenth of the photons that would be produced by a photoswitchable dye."

There has been major interest in trying to develop these sorts of dyes, she adds, with one approach involving caging a dye with a protective group that is destroyed when it's illuminated, permitting the dye to fluoresce. But dyes have their own challenges in that they need to be targeted somehow, for example with antibodies, which carry the risk of nonspecificity and also limit resolution due to their relatively large size. Click chemistry can also be useful, she adds: "Because the protein has been only slightly modified with a cysteine tag or something similar for recruitment of a dye, the protein stays close to its original size and so is more likely to target correctly."

Lippincott-Schwartz and her team are now working on double-labeling two different proteins, and are also collaborating with Hess at **Howard Hughes Medical Institute's Janelia Farm** to look at the three-dimensional distribution of molecules within cells.

According to Lippincott-Schwartz, companies that make imaging equipment have worked closely with researchers in this area to make sure their confocal microscopes and other tools keep up with these types of experimental innovations.

"It's an absolutely amazing synergy between very different groups of people: the physicists who are building the microscopes, the chemists who are working on the probes, and then the biologists who put all of this together to answer biomedically related questions," she says. "All three groups seem to be moving forward. It's pretty neat to see this. It's the right time for all these disparate groups coming together."

Anne Harding is a freelance science writer based near New York City.

DOI: 10.1126/science.opms.p1000043

FEATURED PARTICIPANTS

Active Motif
www.activemotif.com

Carestream Health
www.carestreamhealth.com

Danaher Corporation
www.danaher.com

Enzo Life Sciences
www.enzolifesciences.com

Evrogen
www.evrogen.com

Harvard University
www.harvard.edu

Invitrogen/Life Technologies
www.invitrogen.com

Howard Hughes Medical Institute's Janelia Farm
www.hhmi.org/janelia

Lawrence Berkeley National Laboratory
www.lbl.gov

MBL International
www.mblintl.com

Molecular Devices
www.moleculardevices.com

PerkinElmer
www.perkinelmer.com

Takara Bio Group/Clontech
www.clontech.com

Thermo Scientific
www.thermo.com

The University of Texas M.D. Anderson Cancer Center
www.mdanderson.org

NEW PRODUCTS: FLOURESCENT LABELS

FLUORESCENCE SPECTROMETER

The Lumina is a research-grade, dual-monochromator scanning fluorescence spectrometer that offers a new level of clarity in fluorescence measurement. Designed for both demanding research applications and routine laboratory analyses, the Lumina delivers 0.5 nm spectral bandwidth, high sensitivity, and fast scanning speed. Its ability to provide 0.5 nm spectral bandwidth gives it superior resolving power compared with competitive systems in the same price range. It offers lower limits of detection, less noise, and more consistent baseline measurements. Its powerful xenon lamp, combined with optimized monochromators, allows for the detection of sample concentrations below the parts-per-billion level for heavy metals, polycyclic aromatic hydrocarbons, and more. Its photomultiplier detector offers extended measurement of the near-infrared wavelength, for cutting-edge research in biochemistry and photosynthesis applications.

Thermo Fisher Scientific
For info: 800-532-4752 | www.thermo.com/glows

FLUORESCENCE MICROSCOPES TOOL

The VivaTome for fluorescence microscopes is a tool for developmental and cell biologists to examine the dynamics of living specimens without extensive prior knowledge of optical sectioning. The VivaTome offers ease of use and excellent results in the visualization of fast processes. It is designed for applications in which temporal resolution is a priority. It provides clear, easy-to-interpret and quantifiable results for biological specimens, whether cell structures, tissue sections, or living organisms. Using simple and economical white light illumination, it can achieve frame rates of up to 30 frames a second. It can be used with the entire spectrum of Zeiss objective lenses with consistently high optical section quality.

Carl Zeiss MicroImaging
For info: +49-(0)-3641/64-2770 | www.zeiss.de/vivatome

FLUORESCENT PROTEIN AND TECHNOLOGY CATALOG

The 2010 Evrogen Catalog describes innovative novel fluorescent proteins for biological research and commercial biotechnology applications. The catalog includes basic Tag and Turbo fluorescent proteins, photoactivatable proteins, fluorescent biosensors, and antibodies to detect fluorescent proteins, as well as a panel of nucleic acid research kits. It describes fluorescent proteins ranging from blue to far-red, covering a spectrum of eight colors useful for multicolor labeling of cells, cell organelles, and proteins. It includes a pair of fast-maturing far-red fluorescent proteins for whole body imaging and a set of fluorescent proteins that can be used in fluorescence resonance energy transfer applications as donors and acceptors.

Axxora
For info: 800-550-3033 | www.axxora-usa.com

MICROPLATE READER

The Biochrom Asys UVM 340 is a monochromator-based plate reader that lets the user select the exact wavelength to measure optical density for an application, without compromise. The user can select to measure absorbance at any wavelength between 340 nm and 800 nm at 1 nm intervals. The instrument is suitable for enzyme-linked immunosorbent assays and other absorbance applications with no need to purchase expensive extra filters or to change instruments to perform different assays. The Biochrom Asys UVM 340 is a single-channel microplate reader that can read 12 96-well plates, for greater plate-format flexibility than multichannel systems. It can be integrated into automated systems and features a compact footprint.

Biochrom
For info: +44-(0)-1223-423723 | www.biochrom.co.uk

FLUORESCENT CONJUGATES

Several new DyLight fluorescent conjugates for immunofluorescent staining are available for conjugation to affinity-purified antimouse IgG, antirabbit IgG, and streptavidin. The Dylight fluorescent dyes are direct alternatives to traditional fluorophores such as fluorescein and rhodamine. The dyes currently offered are DyLight 488 (green), Dylight 549 (orange), and DyLight 594 (red). These new conjugates offer brighter fluorescence and greater photostability than other fluorochromes, yet can be used in existing protocols because of their parallel excitation/emission spectra. They are stable over a pH range of 4 to 9. They can be used as single labels or in combination with other fluorophores.

Vector Laboratories
For info: 650-697-3600 | www.vectorlabs.com

NEAR INFRARED FLUORESCENT DYES

The DyLight 680B Dyes for directly labeling proteins and other biomolecules exhibit fluorescence intensity up to 10 times greater than similar dyes. Their applications include enzyme-linked immunosorbent assays, fluorescence microscopy, protein arrays, in vivo imaging, and protein immunoblot analyses. They are available in both amine-reactive and sulfhydryl-reactive chemistries. They exhibit excitation and emission spectra at 679 nm and 698 nm, respectively.

Thermo Fisher Scientific
For info: 815-968-0747 | www.thermofisher.com

Electronically submit your new product description or product literature information! Go to **www.sciencemag.org/products/newproducts.dtl** for more information.

Newly offered instrumentation, apparatus, and laboratory materials of interest to researchers in all disciplines in academic, industrial, and governmental organizations are featured in this space. Emphasis is given to purpose, chief characteristics, and availabilty of products and materials. Endorsement by *Science* or AAAS of any products or materials mentioned is not implied. Additional information may be obtained from the manufacturer or supplier.

Multiply The Power of Science

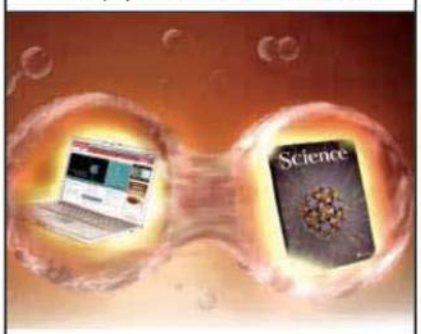

Science Careers
Classified Advertising

For full advertising details, go to ScienceCareers.org and click For Employers, or call one of our representatives.

Tracy Holmes
Worldwide Associate Director
Science Careers
Phone: +44 (0) 1223 326525

UNITED STATES & CANADA

E-mail: advertise@sciencecareers.org
Fax: 202-289-6742

Tina Burks
East Coast/Midwest/Canada
Phone: 202-326-6577

Nicholas Hintibidze
West Coast/South Central
Phone: 202-326-6533

Online Job Posting Questions
Phone: 202-326-6577

EUROPE & REST OF WORLD

E-mail: ads@science-int.co.uk
Fax: +44 (0) 1223 326532

Alex Palmer
Phone: +44 (0) 1223 326527

Dan Pennington
Phone: +44 (0) 1223 326517

Susanne Kharraz Tavakol
Phone: +44 (0) 1223 326529

Lisa Patterson
Phone: +44 (0) 1223 326528

JAPAN

ASCA Corporation
Jie Chin
Phone: +81-3-6802-4616
Fax: +81-3-6802-4615
E-mail: careerads@sciencemag.jp

To subscribe to *Science*:
In US call 866 434-2227
In the rest of the world call +1 202 326-6417

All ads submitted for publication must comply with applicable US and non-US laws. *Science* reserves the right to refuse any advertisement at its sole discretion for any reason, including without limitation for offensive language or inappropriate content, and all advertising is subject to publisher approval. *Science* encourages our readers to alert us to any ads that they feel may be discriminatory or offensive.

Science Careers
From the journal *Science* AAAS

POSITIONS OPEN

TWO TENURE-TRACK POSITIONS in Vector-Borne Disease and Insect Neurophysiology/Toxicology/Pharmacology

The Department of Biochemistry at Virginia Tech seeks applicants for a tenure-track **ASSISTANT PROFESSOR** position in vector-borne disease. Exceptionally qualified applicants for higher ranks will also be considered. Candidates who work on any aspect of vector-borne diseases in a biochemical and/or molecular context will be considered. The successful candidate will build and maintain an internationally recognized, extramurally funded research program, will participate in instruction, and will be open to collaborative research. Competitive startup package will be provided. The successful candidate will join a group of active and collaborative colleagues in vector-borne disease research (**website: http://www.vectorborne.biochem.vt.edu**). Applicants must apply online (**website: http://www.jobs.vt.edu, posting #0100123**) and arrange for three reference letters to be sent electronically, if possible, to one of the **co-chairs of the Vector-Borne Disease Search Committee, Dr. Glenda Gillaspy (e-mail: gillaspy@vt.edu, telephone: 540-231-1850) and Dr. Zhijian Tu (e-mail: jaketu@vt.edu, telephone: 540-231-8062), Department of Biochemistry, Virginia Tech, Blacksburg, VA 24061.**

The Department of Entomology at Virginia Tech seeks applicants for a tenure-track **ASSISTANT PROFESSOR** position in insect neurophysiology/toxicology/pharmacology. Applicants should have a Ph.D. with expertise in insect neurophysiology, toxicology, and/or pharmacology and a demonstrated ability to conduct research, as evidenced by a strong publication record. The successful candidate will be expected to establish and maintain a well-funded, productive research program. The individual should have a strong interest in working with graduate students, demonstrated expertise in teaching, and the ability to work in a team environment. Applicants must apply online (**website: http://www.jobs.vt.edu, posting #090562**) and arrange for three reference letters to be sent electronically, if possible, to the **chair of the Insect Neurophysiology/Toxicology/Pharmacology Search Committee, Dr. Don Mullins (e-mail: mullinsd@vt.edu, telephone: 540-231-5978), Department of Entomology, Virginia Tech, Blacksburg, VA 24061-0319.**

Applications will be reviewed beginning May 1, 2010. However, the positions will remain open until filled. For complete job descriptions and departmental information see **websites: http://www.biochem.vt.edu** and **http://web.ento.vt.edu/ento/**, respectively.

Virginia Tech is an Equal Opportunity/Affirmative Action Institution.

EXECUTIVE DIRECTOR
Society for Conservation Biology

The Society for Conservation Biology, an international professional organization, is seeking an Executive Director. The position serves the global membership of the Society, oversees the operations of its publications (*Conservation Biology*, *Conservation* magazine, and *Conservation Letters*), ensures the successful organization of the biennial global meeting of the membership, supports SCB programs, and represents the mission of SCB to diverse audiences.

The Executive Director reports to the Executive Committee of the elected Board of Governors, supports the activities of the committees of the Board, and manages the SCB executive office in Washington, D.C., and staff located elsewhere.

We seek outstanding candidates who understand the role of science in conservation and have strong managerial and administrative experience, a track record in fund raising and program development, and the ability to respond to the needs of a diverse and global membership.

Applicants should submit electronically a cover letter along with curriculum vitae and names and addresses of three references, addressed to **John G. Robinson, Chair, SCB Executive Director Search Committee, e-mail: edsearch@conbio.org**. For a full job description, visit us at **website: http://www.conbio.org**. Applications should be received by April 30, 2010.

POSITIONS OPEN

Utah State University

ASSISTANT OR ASSOCIATE PROFESSORS in Infectious Disease Animal Modeling and Molecular Biology of Infectious Disease

The Animal, Dairy, and Veterinary Sciences Department at Utah State University is accepting applications for two new faculty members. These are nine-month, tenure-track research and teaching positions funded by the Utah Science, Technology and Research (USTAR) (**website: http://ustar.usu.edu/**). The research focus of the Infectious Disease Animal Modeling position will be to develop and utilize animal models to understand pathogen-host interactions, and for the development of new diagnostics, therapeutics, and vaccines for infectious and immune-mediated diseases. The research focus of the Molecular Biology of Infectious Disease position will be to understand infectious disease mechanisms at the molecular structural or genetic levels of hosts (animal or human) and pathogens, and how such mechanisms determine health and disease. Both positions require an M.D./D.V.M. and/or Ph.D. degree(s) in virology, bacteriology, immunology, cell biology, developmental biology, molecular biology, molecular genetics, or related field plus two years of experience. See **website: http://jobs.usu.edu (requisition ID 052058 and 052059)** for full job description and to apply online. *Affirmative Action/Equal Opportunity Employer.*

TENURE-TRACK FACULTY POSITIONS IN INFLAMMATION
Faculty Excellence Initiative

The Department of Pathology, Microbiology and Immunology, School of Medicine, University of South Carolina (USC), Columbia, invites applications for tenure-track **ASSISTANT PROFESSOR** positions in the broad area of inflammation. Candidates must have a Ph.D. or M.D. or equivalent with postdoctoral research experience. Outstanding applicants working in any area of inflammation complementary to our existing faculty interests (**website: http://pmi.med.sc.edu/default.html**) will be considered. The areas include inflammation as it relates to bacterial and viral infections, cancer, toxicology, and complementary and alternative medicine to treat autoimmune/inflammatory diseases. Candidates are expected to develop a strong, extramurally funded research program using cutting-edge cellular and molecular techniques as well as to participate in the teaching mission of the Department. Investigators who have shown evidence of independence through active grant funding are encouraged to apply. Competitive salary and startup funds are available. Apply with curriculum vitae, statement of research plans, and three letters of recommendation to: **Dr. Mitzi Nagarkatti, Chair, Department of Pathology, Microbiology and Immunology, University of South Carolina School of Medicine, Columbia, SC 29208. Or e-mail: inflammation@uscmed.sc.edu**. The search will start immediately and continue till the position is filled. *USC Columbia is an Equal Opportunity/Affirmative Action Employer and encourages applications from women and minorities.*

ASSISTANT PROFESSOR TENURE-TRACK POSITION

A faculty position in the Department of Plant Pathology, Physiology, and Weed Science at Virginia Tech will focus on understanding the mechanisms that contribute to invasiveness and persistence of weed populations, and may include such issues as weed/crop competition, allelopathy, herbicide resistance, gene flow/introgression, microbial interactions, adaptations to climate change, and risk assessment of novel engineered or biofuel crops. Teaching responsibilities will include training of graduate students and primary responsibility for undergraduate and graduate courses in weed science. Further information and application information are available at **website: https://jobs.vt.edu** under **posting number 0100132.**

Science
AAAS

Senior Editor
Science Translational Medicine

Science and AAAS seek a talented scientist to serve as a Senior Editor for our new interdisciplinary journal, *Science Translational Medicine*.

This position is designed for an individual with broad interests, a lively curiosity, and experience with cutting-edge research in at least one, but preferably more than one, biomedical or clinical research field. To round out our editorial team, we would like our new Senior Editor to have expertise in immunology (vaccines and autoimmune disease especially welcome) or bioengineering (devices, tissue engineering and stem cells are areas of preference).

Responsibilities include, but are not limited to:
- Provide senior leadership for and coordination of encouraging and evaluating original research papers for the journal;
- Supervise the Associate Editors of the journal;
- Judge the scientific value of research;
- Foster relationships and communication with the scientific community through literature reviews, meetings and professional contacts;
- Manage the review, selection, and editing of submitted manuscripts;
- Select reviewers for submitted manuscripts;
- Discuss and make recommendations regarding manuscripts and reviews with other staff, advisers, authors;
- Write summaries of research results for publication;
- Guide authors on manuscript revisions;
- Edit the manuscripts for scientific content and style before and after revisions;
- Follow the manuscript through production process to ensure material is published in a timely manner; and
- Travel to scientific meetings.

The minimum qualifications to be competitive and considered for the position are:
- Mastery of a professional field typically acquired through completion of a doctoral degree in at least one biomedical or clinical research field;
- Five to ten years of postdoctoral research and experience in a broad variety of scientific research topics, including multiple publications and scientific editing experience;
- Experience as a scientific editor and/or equivalent supervisory or management experience in a scientific field;
- Ability to work constructively as a member of a team;
- Experience with cutting-edge research in one of the fields mentioned above;
- Comprehensive knowledge of scientific research methods in order to discuss technical issues with authors; and
- Exceptional writing, communication, and listening skills in order to communicate with authors and reviewers in evaluating, editing and modifying manuscripts.

If you would like to be a member of the AAAS team, please visit our Job Information website at **http://www.aaas.org/careercenter/employmentataaas/** to get more information and to apply online today (**req. #1817**).

AAAS is an Equal Opportunity Employer.

Director, Florida Institute of Oceanography

The University of South Florida (USF) invites applications and nominations for the position of Director of the Florida Institute of Oceanography (FIO). The ideal director will provide the vision to lead coastal oceanographic research in Florida to the forefront of the national and international stage. USF is especially interested in candidates who demonstrate strategic leadership that is visionary, innovative and entrepreneurial. The mission of the FIO is to (1) provide a diverse and collaborative statewide forum addressing problems of concern in coastal oceanographic research and education; (2) leverage and integrate existing physical and intellectual resources within the SUS and throughout Florida; (3) anticipate and plan for future infrastructure needs; (4) facilitate, promote and support collaborative ocean-related research and education statewide; and (5) develop and strengthen networks that enable timely identification of oceanographic research opportunities and distribution of research results and other information to the general public, natural resource management agencies and local, state and national policymakers.

In line with the service mission of the FIO, the Director will be expected to work to provide opportunities for the member institutions and their faculties, to maintain close contact with the member institutions through regular visits and to take advantage of opportunities to serve on state and federal commissions, committees and panels relevant to the FIO mission.

Minimum qualifications: For consideration, candidates must possess a doctoral degree in a discipline related to oceanography or marine science and at least five years of administrative experience that includes facilities operations, program-building, and fund-raising. In addition, candidates must demonstrate a vision for oceanographic research, unquestionable integrity, and a high level of energy. **Preferred qualifications:** The successful candidate will be a recognized leader, both nationally and internationally; will have demonstrated broad and diverse experience to recognize coming trends in oceanography; will demonstrate success in budget planning, financial management, and supervision of personnel; and will possess effective organizational and communications skills.

This is a 12-month full-time administrative appointment. A faculty appointment may be considered for an appointee with appropriate academic credentials and accomplishments. The anticipated appointment date is August 1, 2010. The salary will be internationally competitive with excellent fringe benefits. USF values campus diversity and encourages members of historically underrepresented groups to apply.

A full position announcement and application instructions may be accessed at: https://employment.usf.edu.

USF is an EO/AA/EA Institution. For disability accommodations contact Ms. Desiree Woroner at dworoner@usf.edu at least five working days in advance of need.

USF UNIVERSITY OF SOUTH FLORIDA

• TAMPA • ST. PETERSBURG
• SARASOTA - MANATEE • POLYTECHNIC

UNIVERSITY OF DELAWARE

Howard E. Cosgrove Chair in Environment

One of the oldest institutions of higher education in this country, the University of Delaware today combines tradition and innovation, offering students a rich heritage along with the latest in instructional and research technology. The University of Delaware is a Land-Grant, Sea-Grant, and Space-Grant institution with its main campus in Newark, DE, located halfway between Washington, DC and New York City. Please visit our website at **www.udel.edu**.

We seek an internationally renowned scholar in environmental science, engineering, policy, or economics to further enhance the prominence of the university's environmental interdepartmental teaching and research programs, and to assist in building the Delaware Environmental Institute (DENIN) to a position of national and international prominence. To complement the Cosgrove Chair, we anticipate additional faculty hires in a number of environmental areas including: biogeochemistry, aerosol science, environmental toxicology, ecology, environmental economics, and social behavior and policy. The Cosgrove Chair is a university-wide position, with potential appointments in multiple departments.The University of Delaware provides an outstanding environmental research base through existing strengths in a number of areas including biogeochemistry, soil and environmental chemistry, environmental engineering, environmental microbiology, environmental genomics and bioinformatics, geomicrobiology, land/coastal dynamics, land use, nutrient management, environmental modeling, hydrology, environmental forecasting and restoration, ecosystem health and sustainability, and environmental policy and economics. These activities are carried out across the University's seven colleges and in a number of well regarded institutes and centers of excellence, including the Center for Climate and Land-Surface Change, Center for Energy and Environmental Policy, Center for Remote Sensing, Delaware Geological Survey, Delaware Water Resources Center, Disaster Research Center, University of Delaware Energy Institute, Institute of Soil and Environmental Quality, and Water Resources Agency, among others. More details on our environmental programs can be found at www.environmental-portal.udel.edu/ . The need to utilize the strengths in the colleges, institutes, and centers, and to foster collaboration and enhance competitiveness in attracting outstanding faculty and students, led to the creation of the Delaware Environmental Institute. DENIN's goals are to initiate interdisciplinary research projects, support interdisciplinary academic programs, forge partnerships among government agencies, nonprofits, industry, policymakers, and the public to address environmental challenges and coordinate and sponsor University-based interdisciplinary initiatives. DENIN will strive to translate cutting-edge discovery research to applications that will benefit the state and nation and help create sound environmental policies while working with government and the private sector to create and promote green jobs and green technology. More details on DENIN can be found at www.udel.edu/denin

Candidates for the position are expected to hold a Ph.D or equivalent degree and have a demonstrated record of accomplishments and leadership in environmental research and scholarship commensurate with appointment to a senior faculty position in one or more departments of the university. Nominations and applications should be submitted electronically to **als@udel.edu** or sent to Environmental Chair Search Committee, University of Delaware, Delaware Technology Park, 15 Innovation Way, Suite 103, Newark, DE 19711. Application materials should include a statement of interest, curriculum vitae, description of research and teaching interests and accomplishments, and the names and contact information of at least four references. Review of applications will begin immediately, and will continue until the position is filled.

The UNIVERSITY OF DELAWARE is an Equal Opportunity Employer which encourages applications from Minority Group Members and Women.

NIDA NATIONAL INSTITUTE ON DRUG ABUSE

Supervisory Medical Officer GS-602-15
Clinical/Medical Branch
Division of Pharmacotherapies and Medical Consequences of Drug Abuse
National Institute on Drug Abuse
National Institutes of Health (NIH)
Department of Health and Human Services

The National Institute on Drug Abuse (NIDA) at the National Institutes of Health (NIH) is seeking a senior-level medical officer with expertise in medications development and the conduct of clinical trials who will bring significant experience to operate in an intellectually challenging Federal biomedical research institution engaged in a program to develop novel pharmacotherapies to treat drug addictions.

This is a Supervisory, GS-15 level position that offers a unique and challenging opportunity for the right individual to direct an extramural scientific program of national and international scope within the National Institute on Drug Abuse.
Successful candidates will have a knowledge of neuropsychopharmacology and clinical research, and have experience in medications development. The candidate should also possess knowledge of addiction medicine and the neuroscience of addiction. Managerial experience in medications development in the biotech or pharmaceutical sectors, or Federal service for at least 5 years is highly desirable. The individual must also have demonstrated ability to manage personnel, budgets, and timelines across multiple fiscal years.

Salary is commensurate with experience at the GS-15 level and a full package of Federal benefits is available including retirement, health and life insurance, long term care insurance, leave and savings plan (401 K equivalent). Physicians Comparability Allowance of up to $30,000 per annum may be paid based on the selected physician's assignment, qualifications, experience, and duration of a negotiated service agreement

Application Process: This announcement will be open from April 8 through May 11, 2010. For additional information about this opportunity as supervisory Medical Officer at NIDA, please visit www.usajobs.gov where detailed information may be found under Announcement HHS/NIH-2010-1601. Supplemental documentation must be submitted to Jean Coleman, Human Resources Specialist, NIH, Office of Human Resources @ Jean.Coleman@nih.gov, or faxed to (301) 451-5688.

The NIH encourages the application and nomination of qualified women, minorities and individuals with disabilities.

National Institute on Aging

Department of Health and Human Services
National Institutes of Health
National Institute on Aging
Intramural Research Program

Staff Scientist - Animal Program Director

The National Institute on Aging (NIA), a major research component of the National Institutes of Health (NIH) and Department of Health and Human Services (DHHS), is recruiting for a Staff Scientist-Facility Head who will serve as the Animal Program Director for the NIA Intramural Research Program (IRP).

The Animal Program Director (APD) will work closely with the Chief of the Comparative Medicine Section, and will serve as the Attending Veterinarian for the NIA Animal Care and Use Committee. The APD will provide support for the animal research programs in the Institute, studying animal models of development and aging, and interventions to prevent or alleviate aging-related deficits. The supervisory and regulatory responsibilities of this position require the applicant to hold a veterinary degree (D.V.M., V.M.D., or equivalent degree) with certification or eligibility for board certification in laboratory animal medicine or veterinary pathology.

The APD will be responsible for the clinical and regulatory aspects of the animal program including continued accreditation by AAALAC. The APD will provide veterinary expertise (e.g., clinical, surgical, pathology) and training to investigators, animal care, and technical staff in the form of formal instruction and ongoing guidance. The incumbent will perform animal surgery and teach appropriate procedures to animal care and technical staff. Familiarity with re-derivation and cryopreservation techniques as well as diagnostic testing is desired. The incumbent will take primary responsibility for the clinical aspects of the animal program and will oversee animal health surveillance and maintain both a barrier facility and a quarantine area. Applicants must have a proven record of management of an animal research program and demonstrated experience with the regulatory aspects of animal welfare. The expertise and experience should include, but not be limited to interaction and cooperation with scientific staff in a manner that promotes and facilitates their scientific programs.

Salary is commensurate with experience and accomplishments. The salary range for Staff Scientists is $89,033 - $173,826. A full Civil Service package of benefits (including retirement, health, life and long term care insurance, Thrift Savings Plan, etc.) is available. Additional information regarding the NIA, IRP and the RRB is available at the following websites: http://www.grc.nia.nih.gov and http://grc.nia.nih.gov/branches/rrb/rrb.htm . To apply: Please send a cover letter, curriculum vitae, bibliography, statement of research interests, and three letters of recommendation to: Peggy Grothe, Intramural Program Specialist; Office of the Scientific Director; National Institute on Aging, 251 Bayview Boulevard, Suite 100-Room 04C232, Baltimore, MD 21224-6825. Position will remain open until filled; however, application reviews will begin May 1, 2010. Please include the following vacancy number in all correspondence: Vacancy # NIA-IRP-10-02. If additional information is needed, please call 410-558-8012 or email: grothep@mail.nih.gov.

Weill Cornell Medical College

Cancer Computational Biology Faculty Position
Department of Pathology and Laboratory Medicine and the Institute for Computational Biomedicine

The Department of Pathology and Laboratory Medicine at Weill Cornell Medical College is seeking a full-time faculty member at the Assistant Professor level for Cancer Computational Biology. The successful candidate will develop an independent academic research program within the Department of Pathology and the Institute for Computational Biomedicine, pursuing innovative computational and statistical approaches for integrative analysis of cancer genomic data (e.g., from deep sequencing, proteomics, etc.) to elucidate cancers in terms of DNA alterations, RNA profiles, proteomic signatures, and functional responses. The candidate will interface with well-established cancer research teams in the areas of prostate cancer and lymphoma/leukemia that provide an exceptional collaborative environment. An outstanding track record of publication in cancer research, genomics, and computational biology is required for this position.

Interested applicants should forward curriculum vitae, statement of interests, and the names and contact information for three references to: **Mark A. Rubin, MD, Vice Chair for Experimental Pathology, Department of Pathology and Laboratory Medicine, Weill Cornell Medical College, 1300 York Ave., C-410A, New York, New York 10065, email: rubinma@med.cornell.edu**.

Weill Cornell Medical College is an Affirmative Action/Equal Opportunity Employer.

THE UNIVERSITY OF HONG KONG

Post-doctoral Fellows and Research Assistant Professors for the Area of Excellence Project (Ref.: 20100118)

Applications are invited for appointments as Post-doctoral Fellows (PDF) and Research Assistant Professors (RAP) in Emerging Electronics for the AoE Project, from as soon as possible for one to three years, with the possibility of renewal.

Applicants should possess a doctoral degree in Physics, Chemistry or Electric Engineering, with strong experience in Computational Science and Engineering. Successful candidates will join a multi-institutional interdisciplinary project on modeling and simulation of emerging electronics in Hong Kong to develop a suite of multi-scale electronic devices and automation software tools. Details can be found at http://www.physics.hku.hk/~fczhang/AoE/AoE.html.

Applicants who have responded to the previous advertisement (Ref.: RF-2009/2010-435) need not re-apply.

A highly competitive salary commensurate with qualifications and experience will be offered. Annual leave and medical/dental benefits will be provided. The appointments of RAPs for two years or more will attract a contract-end gratuity and University contribution to a retirement benefits scheme, totalling up to 15% of basic salary.

Interested candidates should send a cover letter, C.V. and 3 recommendation letters to Ms. Anna Wong (**e-mail**: annaylw@hkucc.hku.hk). **Review of applications will continue until the posts are filled.** Candidates who are not contacted within 3 months from the date of their applications may consider their applications unsuccessful.

The University is an equal opportunity employer and is committed to a No-Smoking Policy

TEXAS TECH UNIVERSITY
Edward E. Whitacre Jr. College of Engineering

The Maddox Chairs *in Energy* at Texas Tech University

The Edward E. Whitacre Jr. College of Engineering at Texas Tech University is committed to leveraging these **two exceptionally large endowed chairs at over $7 million each**, to become one of the nation's leaders in finding solutions to the world's energy challenges. The college is seeking world-class researchers in solar and sustainable energy as candidates for the Maddox Chairs.

Donovan Maddox Distinguished Engineering Chair *in Solar Energy*

Candidates are expected to have national and international reputation in solar energy based on research publications. In addition, a record of acquiring external resources to support research, team building, and mentoring of associates and graduate and undergraduate students is necessary. The holder of the Donovan Maddox Chair will be expected to not only bring his or her own research activities to the Whitacre College of Engineering, but also to build a collaborative community of scholars at Texas Tech dedicated to solar energy research, thereby building a world-class research program. The appointment will be as a full professor in the Whitacre College of Engineering.

Jack Maddox Distinguished Engineering Chair *in Sustainable Energy*

Candidates with exceptional and diverse backgrounds in energy sciences and engineering are sought for this endowed position. The successful candidate will demonstrate a national and international reputation for contributions to the solution or advancement of the state of the art on a variety of research issues in the sustainable energy fields including energy efficiency, biofuels, wind power, tidal power, geothermal, and energy storage. The successful candidate, along with the Donavan Maddox Chair in Solar Energy, will set the tone, vision, and the path in order to build a nationally and internationally recognized program at Texas Tech University in sustainable energy research. The appointment will be as a full professor in the Whitacre College of Engineering.

Screening will begin upon the receipt of applications and will continue until the position is filled. Candidates names will not be made public until the final stages of the search. Curriculum vitae and the names and contact information of at least four references should be submitted at www.coe.ttu.edu/maddox. To nominate a colleague for these chairs, visit www.coe.ttu.edu/maddox. Nominations can be made anonymously.

Questions about the Jack Maddox or Donovan Maddox Chairs should be directed to:
Jack Maddox and Donovan Maddox Search Committees
Texas Tech University | Whitacre College of Engineering
Box 43103 | Lubbock, Texas 79409-3013 | engineeringdean.coe@ttu.edu | 1.800.528.5583

Texas Tech University | Whitacre College of Engineering
1.800.528.5583 | www.coe.ttu.edu/maddox

Huazhong Agricultural University Recruits Professor

Huazhong Agricultural University (HZAU) seeks candidates for multiple positions of full-time professors in following fields: Crop Cultivation and Farming System, Crop Genetics and Breeding, Pomology, Vegetable Science, Microbiology, Biochemistry and Molecular Biology, Aquaculture Science, Animal Genetics, Breeding and Reproduction Science, Agriculture Economics, etc. We are interested in candidates with oversea education/research experience, good publication records in their field and promising research programs.

HZAU is a National Key university of the Project 211 and a leading agriculture university in China, located at Wuhan City of Hubei province. The University celebrated its 110th anniversary in 2008 and has several world famous research programs, especially in agriculture sciences. The beautiful campus is one of the largest in China (4.9 km^2), surrounded by natural lakes. The campus is also neighboring many famous universities and research institutes, shopping centers, excellent schools and kindergarten, making it an ideal place for education, scientific research and living.

Depending on the candidates' qualification and experience, we will provide each candidate 100,000-5,000,000 RMB for start-fund and settling-in allowance, research assistants and lab space, offer a new on-campus apartment of 150 m^2, campus job for spouse and school/kindergarten for children.

The university also welcomes applications for part-time professors for above positions. The university will provide temporary housing during the candidate's work time in the university. Part-time professors may have research assistant and lab space depending on qualification.

Qualified candidates can directly contact with the Department of Personnel of Huazhong Agricultural University.

Contactor: Miss Deng Mr. Zhang
Contact E-mail: rcjlzx@mail.hzau.edu.cn
Contact phone number: 86-27-87280957
Related Web Site: http://www.hzau.edu.cn

VIB is a non-profit life sciences centre of excellence located in Flanders, Belgium. About 1,200 scientists and technicians conduct basic research on the molecular mechanisms that are responsible for the functioning of the human body, plants, and microorganisms. Through a close partnership with four Flemish universities - UGent, K.U.Leuven, University of Antwerp, and Vrije Universiteit Brussel - and a solid funding program, VIB unites the forces of 72 research groups clustered in 8 research departments. The corner stone of VIB's policy is excellence, as well in science as in tech transfer. The goal of the research is to move forward the boundaries of our knowledge of life profoundly. Through its technology transfer activities, VIB wants to convert research results into products for the benefit of consumers and patients. VIB develops and disseminates a wide range of scientifically substantiated information about biotechnology. More information: **www.vib.be**

VIB

www.vib.be

VIB is currently seeking outstanding candidates (m/f) for the position of **directors**

Department director VIB-Department of Medical Protein Research

(UGent)

The VIB-department of Medical Protein Research (91 staff) has an outstanding track record in proteomics, interactomics, biochemistry, molecular biology and protein chemistry. The focus of the department is geared towards unraveling biological processes, by enriching this technology base with cell biology, genetics and bioinformatics approaches. The ambition of VIB is to move the frontline of science in this department by combining proteomics, interactomics and experimental approaches with computational approaches to dissect the structure and function of macromolecular complexes and their dynamic composition to elucidate their functions in cells, tissues, organs and the human body. The VIB-department is also part of the Faculty of Medicine at UGent.

The director will provide vision and leadership to the department, with responsibility for:

- developing the departmental research strategy and its future mission
- creating a stimulating environment and dialectic culture, which fosters talent and triggers excellence
- organizing and managing the department in terms of science, tech transfer, logistics, finance and human talent

It is expected that the director will maintain active research interest in leading an independent research lab (significant long term support will be provided to do so). The director will be a member of the VIB management committee in which he/she has co-responsibility for the overall success of VIB. .

Requirements for the position:

VIB is in search for a dynamic, internationally recognized leader to inspire and lead the department.

The selected candidate will be appointed as department director at VIB and will have a tenure faculty appointment as full professor at UGent.

Department director VIB-Department of Systems Structural Biology Brussels

(Vrije Universiteit Brussel)

VIB is starting up a new research department in structural biology, focused on solving important biological questions, using structural insight in macromolecular complexes. The department will be located in Brussels at the campus of the Vrije Universiteit Brussel and will be composed of a selection of existing structural biology groups from our current Department of Molecular & Cellular Interactions, meeting the standards of VIB and the new director and some new groups, to be hired by the new director. The new department can build on existing expertise and infrastructure in genetic engineering, protein purification, enzymology, calorimetry, fluorimetry, crystallography, surface plasmon resonance, atomic force microscopy and protein NMR capacity.

The director will provide vision and leadership to the department, with responsibility for:

- developing the departmental research strategy and its future mission
- creating a stimulating environment and dialectic culture, which fosters talent and triggers excellence
- organizing and managing the department in terms of science, tech transfer, logistics, finance and human talent

It is expected that the director will maintain active research interest in leading an independent research lab (significant long term support will be provided to do so). The director will be a member of the VIB management committee in which he/she has co-responsibility for the overall success of VIB.

Requirements for the position:

VIB is in search for a dynamic, internationally recognized structural biologist, willing to accept the challenge of building an exciting centre of excellence in structural biology in Brussels, Belgium.

The selected candidate will be appointed as department director at VIB and will have a tenure faculty appointment as full professor at Vrije Universiteit Brussel.

The successful candidates for both positions:

- have a Ph.D degree and are expected to be experienced visionary scientists, widely recognized in their academic field, who have demonstrated a strong record of scientific publications in leading scientific journals. They will continue their own research program at VIB.
- rank as full professor with - preferentially - a track record of management in universities or research institutions.
- have an extensive international network with a wide scope of research collaborations.
- have excellent communication and negotiating skills and have a strong will for developing a common vision and purpose for VIB and their own department.
- by preference, have experience with technology transfer and science policy.

The total package consists of:

(a) personal: • a competitive salary commensurate with experience • total social security, including pension scheme and health care program
(b) own research group: • start-up package • funding of your own research group with 5-10 positions • access to the VIB core facilities: (deep)sequencing, antibody and protein production, transcriptomics, proteomics, compound screening, bio-informatics training facility (see www.vib.be)
(c) departmental grant: • solid funding of the department subject to excellent performance with quinquennial reviews.

Candidates who are interested in this position are asked to send a complete CV and publication list and 3 letters of reference to marijke.lein@vib.be. Further information can be obtained from Marijke Lein, HR director of VIB +32 92446611. Closing date for applications is 31 May 2010.

KATHOLIEKE UNIVERSITEIT LEUVEN

UNIVERSITEIT GENT

Universiteit Antwerpen

Vrije Universiteit Brussel

Science Careers

is the forum that answers questions.

Visit our ENHANCED WEBSITE!

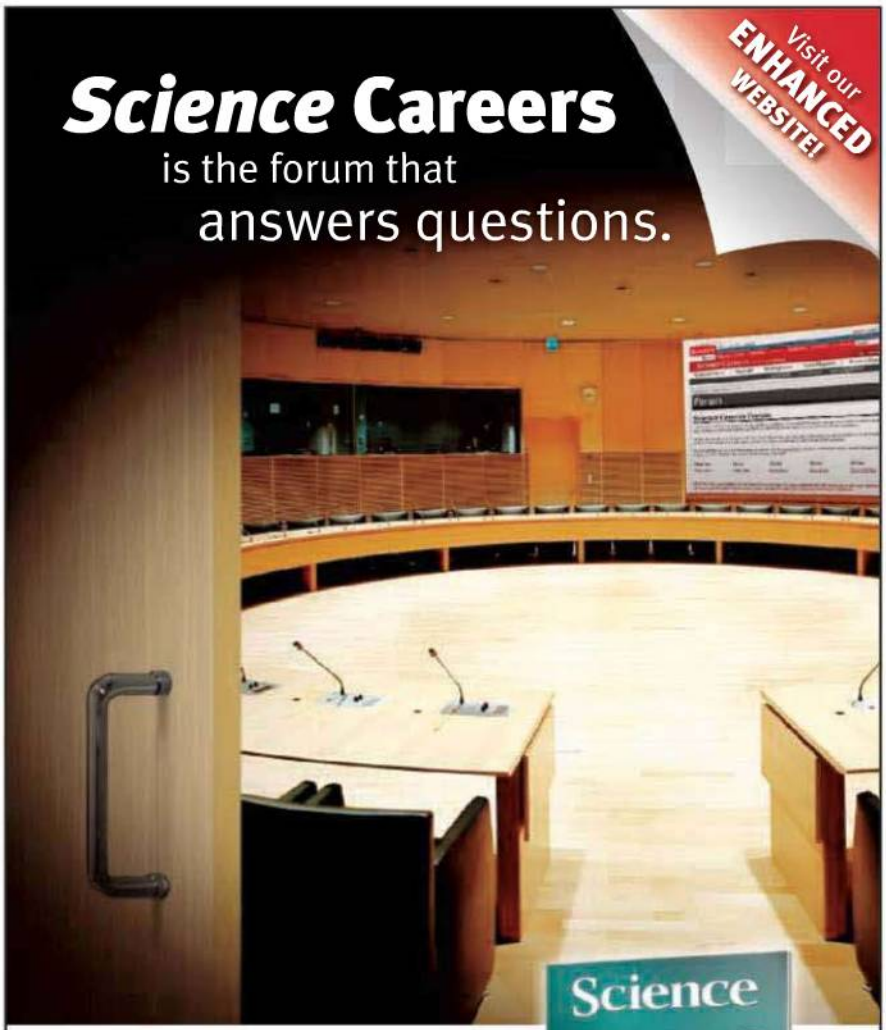

Science Careers is dedicated to opening new doors and answering questions on career topics that matter to you. We're the go-to career site for connecting with top employers, industry experts, and your peers. We're the source for the latest and most relevant career information across the globe.

With community feedback and a professional atmosphere, our careers forum allows you to connect with colleagues and associates to get the advice and guidance you seek.

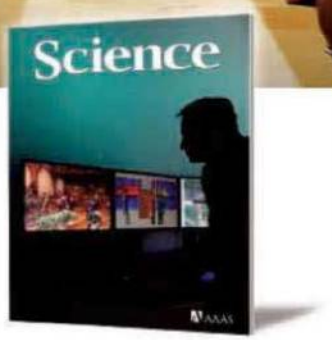

Your Future Awaits.

***Science* Careers Forum:**

- » Relevant Career Topics
- » Advice and Answers
- » Community, Connections, and More!

Visit the forum and get your questions answered today!

Science Careers
From the journal *Science* AAAS
ScienceCareers.org

Sr. Research Scientist - Cardiovascular/Calcium Imaging

Our Pharmacology Biology Group is seeking a Ph.D. scientist who has extensive experience in calcium imaging of cardiac cells/tissues using fluorescent dyes. The main focus of the work for this position is to study calcium signaling in heart cells and isolated hearts with experimental approaches including the use of fluorescent Ca2+ indicators and electrophysiological techniques. The incumbent will develop imaging-based screening platforms to support our current drug discovery projects for cardiovascular indications and our research on the regulation and function of cardiac ion channels, kinases and molecular mechanisms underlying the development of cardiac hypertrophy, heart failure, and arrhythmias. The incumbent will be a member of project teams and interact with other scientists in cardiovascular drug discovery. Experience with confocal microscopy, Ca2+ signaling pathways, patch clamp electrophysiology is a plus. The ideal candidate will have a PhD with a minimum of 5 years cardiovascular research in arrhythmia and heart failure. Pharmaceutical and/or biotech industry experience highly desired. Gilead Sciences, Inc. is a research-based biopharmaceutical company that discovers, develops and commercializes innovative medicines in areas of unmet need. With each new discovery and experimental drug candidate, we seek to improve the care of patients suffering from life-threatening diseases. Our Palo Alto site is engaged in the discovery, development and commercialization of small molecule therapeutics for the treatment of cardiovascular disorders. To apply, please submit resume through our website at **www.gilead.com**, Req. **#4044**.

Gilead is an Equal Opportunity Employer.

Want to search more job postings?

www.sciencecareers.org

Search thousands of job postings —updated daily— all for free.

Science Careers
From the journal *Science* AAAS

Universität Hamburg

The Department of Geosciences in the **Faculty of Mathematics, Informatics and Natural Sciences** at the University of Hamburg is now seeking applicants for a

FULL PROFESSORSHIP (W 3)

for **Dynamic Meteorology**

Reference number: 2088/W3

The University aims to increase the number of women in research and teaching and specifically encourages women to apply. Qualified female applicants will receive preference in accordance with the "Hamburgisches Hochschulgesetz" (Hamburg Higher Education Law).

Description:
The Faculty is seeking applicants who can conduct research in dynamic meteorology and who have a prolific research profile, a strong record of leadership, peer-reviewed publications, external research funding, significant national recognition or an international reputation in their field and outstanding teaching and mentoring skills.

The successful candidate will head the Dynamic Meteorology Division (Theoretische Meteorologie) of the Meteorological Institute in the Department of Geosciences. Experience and outstanding ability in at least one of the following research areas is desirable: Fundamental Dynamical Meteorology, conceptual models and models of intermediate complexity of atmospheric circulation and of the climate system, feedback processes in the climate system, advanced diagnostics of climate variability. The applicant is expected to play an active role in the excellence cluster CliSAP (Integrated Climate System Analysis and Prediction) and the KlimaCampus.

The successful candidate will be expected to teach dynamic meteorology courses at both undergraduate and graduate level and to supervise undergraduate and graduate student research projects. He/She will play a leading role in the further development of the BSc/MSc programme in "Meteorology" and the MSc programme in "Integrated Climate System Sciences".

Requirements:
According to § 15 of the Hamburg Higher Education Act.

The University of Hamburg places special value on the quality of teaching.

We therefore ask applicants to describe both their teaching experience and their teaching approaches.

Qualified disabled applicants receive preference over non-disabled applicants.

Applications which include a curriculum vitae, a list of publications, a list of teaching activities as well as a statement of teaching interests and ideas should be submitted no later than **May 15th, 2010** to the office of the "Präsident der Universität Hamburg, Referat Organisation & Personalentwicklung, **Reference number: 2088/W3**, Moorweidenstraße 18, 20148 Hamburg, Germany".

TOR ZUR WELT DER WISSENSCHAFT

UNIVERSITY OF CALIFORNIA
UC RIVERSIDE

Health ▪ Sustainability ▪ Technology

LIVING THE PROMISE

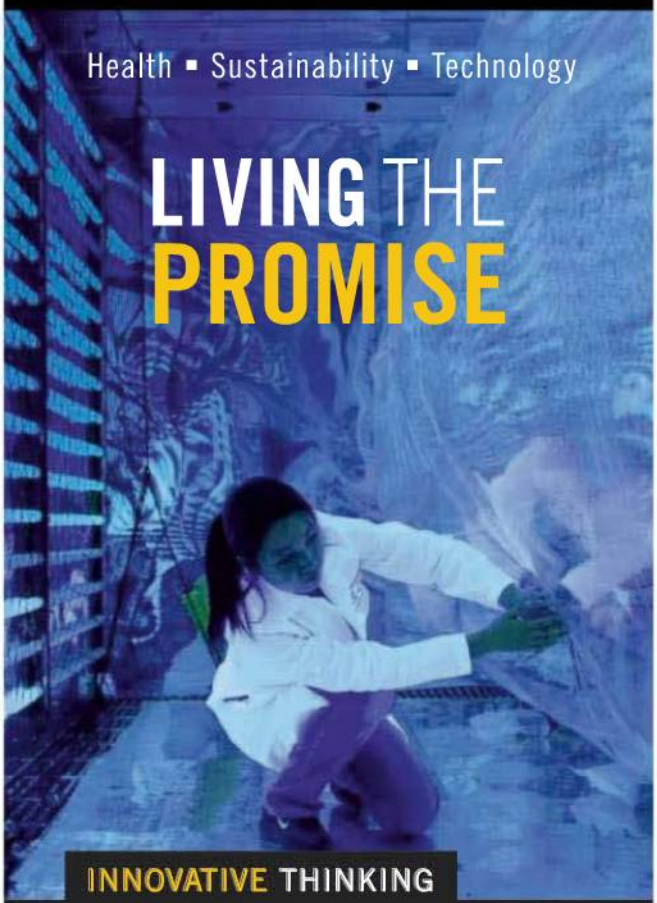

INNOVATIVE THINKING
BREAKTHROUGH RESEARCH
REAL-WORLD SOLUTIONS

HEALTH

- Improving Air Quality
- Combating Insect-Borne Viruses
- Revolutionizing Wound Care
- Preventing Third-World Hunger
- Launching California's Newest School of Medicine

Explore more solutions:
promise.ucr.edu

Science Careers online @sciencecareers.org

Science Digital

With the ability to access anywhere in the world, *Science* Digital is the electronic version of *Science* magazine supporting our ongoing strides towards an eco-friendly future. At just $99 for professionals and $50* for students and postdocs, *Science* Digital is currently available at a discounted rate offering our readers the very latest in groundbreaking scientific news and discoveries. And this is just one of the ways that AAAS is committed to advancing science to support a healthy and prosperous world. Join us. Together we can make a difference. promo.aaas.org/show

AAAS + U = Δ

*Plus 5% VAT where applicable (all EU countries)

UNIVERSITÄT BASEL

The Faculty of Science (Philosophisch-Naturwissenschaftliche Fakultät) of the University of Basel invites applications for the position of

Annetta and Gustav E. Grisard Professor of Molecular Bionics

The successful candidate is expected to establish an outstanding research program in chemical approaches capitalizing the potential of sustainable, natural resources. Innovative research approaches focusing on wood or wood products as a sustainable resource or model for new materials and molecular systems are of particular interest. Initially the professorship is limited to a period of 5 years.

The successful person will participate in teaching chemistry and nanosciences at all levels of the BSc-, MSc- and PhD programmes. The chemistry degree programme at the University of Basel can lead to both the BSc and MSc level and covers all aspects of chemical science. The University of Basel pioneered one of the first BSc and MSc programmes in Nanosciences worldwide. The teaching of chemistry is critical to the succes of these courses and constitutes about one third of the curriculum. Depending on the experience of the successful candidate, appointments at all levels will be considered.

The Department of Chemistry is located near the centre of Basel, a town which provides a stimulating and attractive environment for interdisciplinary research due to the concentration of science institutes as well as the chemical and pharmaceutical industry. The Swiss Nanoscience Institute is based in Basel and provides a platform for multidisiplinary research in the Nanosciences, primarily across the Departments of Chemistry and Physics and the Biozentrum.

For further information about the Department of Chemistry, see http://www.chemie.unibas.ch

The successful candidate is expected to commence the appointment in fall 2010. Applications received by 15th May 2010 will be guaranteed full consideration. The University of Basel is an equal opportunity employer. Applications from female candidates are particularly encouraged. Applications, including a curriculum vitae, list of publications, names of four referees, outline of current and future research plans should be addressed to Prof. Dr. Eberhard Parlow, Dean, Faculty of Science, University of Basel, Klingelbergstrasse 50, 4056 Basel, Switzerland, and also be provided in electronic form (pdf or zip) to Dekanat-Philnat@unibas.ch.

For further information please contact: Prof. Dr. Wolfgang Meier, Head, Department of Chemistry, Tel: +41 61 267 38 02, E-mail: wolfgang.meier@unibas.ch

UNI BASEL

550 JAHRE WISSEN BEWEGT UNS

Download your free copy.

ScienceCareers.org/booklets

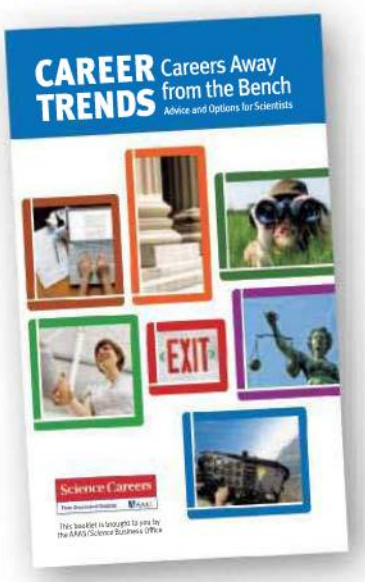

Science Careers
From the Journal *Science* AAAS

复旦大学脑科学研究院

The Institutes of Brain Science, Fudan University

Principal Investigator Positions

The Institutes of Brain Science, Fudan University, Shanghai, China, a newly established research institution supported by the National "985" Program of the Ministry of Education, is currently recruiting principal investigators in the fields of basic and applied research of neuroscience and neurological disorders.

Applicants must have a Ph.D. or M.D. degree with over 2-year postdoctoral experience; an impressive research record with important papers published in international journals of high reputation as a corresponding or the first author; and the capacity to develop a vigorous and independent research program. The successful candidates will be expected to work in Fudan University full-time, when appointed.

Interested individuals should send a package including CV, publication list, reprints of 3-5 representative papers, a one page summary of the research accomplishments, and a 1-2 page research proposal, and arrange to have 3 letters of reference sent to: Ms. Rong Chen, Institutes of Brain Science, Mail Box 295, Fudan University, 138 Yixueyuan Road, Shanghai 200032, China. **ibs@fudan.edu.cn**.

For more information, please visit
http://iobs.fudan.edu.cn

Science Careers online @sciencecareers.org

Your career is our cause.

Get help from the experts.

www.sciencecareers.org

- Job Postings
- Job Alerts
- Resume/CV Database
- Career Advice
- Career Forum
- Graduate Programs
- Meetings and Announcements

Science Careers
From the journal Science AAAS

POSITIONS OPEN

ASSOCIATE/FULL PROFESSOR
Periodontology Vacancy Announcement
Position #00025507

The Department of Periodontology is seeking applications for a full-time, tenure-track **CLINICIAN/TRANSLATIONAL SCIENTIST** at the rank of Associate or Full Professor. Applicants should have expertise in the areas of immunology, microbiology, inflammation, pathology, cell biology, and/or endocrinology. The incumbent will be expected to work closely with college faculty in several departments on basic and clinical/translational research associated with the relationships of oral disease and systemic health, such as the effects of chronic periodontal inflammatory diseases on the control of diabetes, cardiovascular, or other associated chronic diseases. Collaborations with other groups across campus, including the Center on Aging, diabetes researchers, Clinical and Translational Science Institute, or the Genetics Institute will be expected. This position will conduct research to more efficiently and effectively attack the issues that stem from the interrelationships of chronic oral inflammatory diseases and systemic diseases. Minimum requirements include a D.D.S., D.M.D., M.D., Ph.D., or equivalent degree and at least five years of related experience. Clinical experience in periodontology is desirable, but not required. Preference will be given to candidates who have a history of external funding. Salary and academic rank are commensurate with credentials and experience. Anticipated start date is September 2010.

Review of applications is currently under way and will continue until an applicant pool is identified. Applicants should send curriculum vitae, a cover letter describing their interest in the position, referencing **requisition #0804201,** and a list of three references to:

Prof. Edward K.L. Chan,
Search Committee Chair
c/o Ms. Mary Bennett
P.O. Box 100405
Gainesville, FL 32610-0405

Or the information can be sent electronically to **e-mail: mbennett@dental.ufl.edu**. Any questions regarding the position may be directed to **Dr. Chan, e-mail: echan@dental.ufl.edu**.

The University of Florida is an Equal Opportunity Institution dedicated to building a culturally diverse and inclusive faculty and staff. The selection process will be conducted in accord with the provisions of Florida's "Government in the Sunshine" and Public Records Laws. Search committee meetings and interviews will be open to the public, and all applications, resumes, and other documents related to the search will be available for public inspection.

POSTDOCTORAL POSITION will be available in July 2010 in the Department of Neurology at The University of Chicago for candidates with M.D. or Ph.D. to study (1) cellular and molecular mechanisms in mouse models of demyelinating diseases (central nervous system and peripheral nervous system); and (2) B lymphocyte function in autoimmunity. There is superb opportunity to collaborate with other immunologists and neuroscientists. Prior experience and publications in neuroimmunology and/or glial cell biology are essential. Please electronically send curriculum vitae, statement of interest, and names of three references with contact information to **Betty Soliven, M.D., e-mail: bsoliven@neurology.bsd.uchicago.edu**. *The University of Chicago is an Affirmative Action/Equal Opportunity Employer.*

A **POSTDOCTORAL POSITION** is available to investigate G-protein mediated signaling pathways involved in the regulation of cancer cell growth and metastasis (see *Oncogene* **26:**3122, 2007; **27:**6245, 2008). Applications are encouraged from individuals with strong interest and experience in the area of molecular biology, cell biology, or signal transduction research. Send curriculum vitae and names of three references to: **Danny N. Dhanasekaran, Ph.D., Oklahoma University Cancer Institute, University of Oklahoma Health Sciences Center, Oklahoma City, OK 73104. E-mail: danny-dhanasekaran@ouhsc.edu**. *The University of Oklahoma is an Equal Opportunity Employer.*

POSITIONS OPEN

CaridianBCT

CaridianBCT is the leading global provider of innovative technologies and services specializing in automated blood collections, therapeutic apheresis and cell therapy systems, whole blood processes, and pathogen reduction technologies. The company provides technology, products, and services to blood centers, hospitals, and scientific, clinical, and biotech researchers.

CaridianBCT is currently developing an automated cell expansion system for mesenchymal stem cells and other cell types. To support launch preparation and system evaluation work for the new system, CaridianBCT is currently recruiting for product support and training roles in the United States and in Europe as well as a U.S.-based marketing role. Ideal candidates will have solid experience in the stem cell therapy field, enjoy working in a team environment, and thrive when faced with complex tasks.

The **SENIOR PRODUCT SUPPORT AND TRAINING SPECIALIST** will work within a regional/global/customer environment to provide process support and development as well as product training. Ideal candidates will have a Ph.D. (preferred but not required) in a relevant field, and experience from stem cell therapy work, cell culture, and flow cytometry. CaridianBCT is looking to fill both U.S.- and European Union–based positions. The **MARKETING MANAGER** will analyze and translate customer needs into a compelling product offering, while developing and managing global marketing strategies. Ideal candidates will have a marketing degree and several years of experience in relevant fields, preferably stem cell therapies. The position will be United States based.

Please visit CaridianBCT's candidate portal at **website: https://careersintheusa.caridianbct.com/index.html** to apply.

POSTDOCTORAL FELLOW
Virology/Cancer Biology
University of Wisconsin-Madison

Two Postdoctoral positions are available in the laboratory of **Robert F. Kalejta** in the Institute for Molecular Virology and the McArdle Laboratory for Cancer Research at the University of Wisconsin-Madison. The Kalejta laboratory is interested in human cytomegalovirus replication and pathogenesis, and focuses specifically on viral latency and modulation of the cell cycle (search Google or PubMed for more information). Projects are available in each of these areas, but new directions that expand the scope of the laboratory and fit with the interests and abilities of the applicant are always welcome. UW-Madison has the facilities and expertise to support high-level productivity, and is located in one of the most beautiful and livable small cities in the United States. Applicants should have or be nearing a Ph.D. in a relevant discipline with a record of productivity. Please forward a cover letter briefly describing your past research, future goals, and preferred starting date, along with curriculum vitae containing the names and e-mail addresses of three references to **e-mail: rfkalejta@wisc.edu**. *UW-Madison is an Equal Opportunity Employer.*

MARKETPLACE

Promab Biotechnologies Inc.
Custom Monoclonal Antibody $4,200
>3,000 CLONES WILL BE SCREENED
1-866-339-0871
www.promab.com info@promab.com

AAAS is here – bringing scientific expertise to policy making.

Good science policy is the result of politicians understanding science and scientists understanding policy. Toward this end, AAAS manages the Science & Technology Policy Fellowships program, which embeds scientists and engineers in the federal government for up to two years. From Congress to the State Department, each class of Fellows contributes to the policy-making process while getting hands-on experience at the intersection of science and policy. As a AAAS member your dues support these efforts. If you're not yet a AAAS member, join us. Together we can make a difference.

To learn more, visit **aaas.org/plusyou/fellows**.

AAAS + U = Δ

A Portfolio of Real-Time Possibilities. Just for Me.

Only Applied Biosystems delivers superior end-to-end workflow solutions for all your real-time PCR applications.
Finding a line of real-time PCR solutions to advance your experiments from start to finish is all about knowing where to look. Applied Biosystems offers a range of quality real-time PCR instruments, reagents, assays, service, and support to help accelerate your research at every step—saving you time and money along the way. When you want a real-time portfolio that can take you from sample prep to proven results, talk to us. We have a growing range of affordable real-time PCR solutions optimized just for you!

As Flexible as You Want to Be.

applied biosystems
part of life technologies

Real-time PCR solutions optimized just for you at
www.appliedbiosystems.com/realtimesystems

FOR RESEARCH USE ONLY. NOT INTENDED FOR ANY ANIMAL OR HUMAN THERAPEUTIC OR DIAGNOSTIC USE, UNLESS OTHERWISE STATED. © 2010 Life Technologies Corporation. All rights reserved. Trademarks of Life Technologies Corporation and its affiliated companies: Applied Biosystems™ and AB Logo™. All other trademarks are the sole property of their respective owners.